UNIVERSIDADE FEDERAL DE SÃO CARLOS
CENTRO DE CIÊNCIAS EXATAS E DE TECNOLOGIA
PROGRAMA DE PÓS-GRADUAÇÃO EM ENGENHARIA QUÍMICA

Felipe Fernando Furlan

METODOLOGIA PARA GUIAR O DESENVOLVIMENTO E IMPLEMENTAÇÃO INDUSTRIAL DE NOVAS TECNOLOGIAS UNINDO ENGENHARIA ECONÔMICA E ENGENHARIA DE (BIO)PROCESSOS E SISTEMAS:

APLICAÇÃO À PRODUÇÃO DE ETANOL DE SEGUNDA GERAÇÃO

São Carlos

Março, 2016

Felipe Fernando Furlan

Metodologia para guiar o desenvolvimento e implementação industrial de novas tecnologias unindo engenharia econômica e Engenharia de (bio)processos e sistemas:

Aplicação à produção de etanol de segunda geração

Tese apresentada ao Programa de Pós-Graduação em Engenharia Química da Universidade Federal de São Carlos, como parte dos requisitos para a obtenção do título de Doutor em Engenharia Química.

Universidade Federal de São Carlos

Orientador:	Prof. Dr. Roberto de Campos Giordano
Coorientadores:	Profa. Dra. Caliane Bastos Borba Costa
	Prof. Dr. Argimiro Resende Secchi
Colaborador:	Prof. Dr. John M. Woodley

São Carlos

Março, 2016

Ficha catalográfica elaborada pelo DePT da Biblioteca Comunitária UFSCar
Processamento Técnico
com os dados fornecidos pelo(a) autor(a)

F985m

Furlan, Felipe Fernando
Metodologia para guiar o desenvolvimento e implementação industrial de novas tecnologias unindo engenharia econômica e Engenharia de (bio)processos e sistemas : Aplicação à produção de etanol de segunda geração / Felipe Fernando Furlan. -- São Carlos : UFSCar, 2016.
222 p.

Tese (Doutorado) -- Universidade Federal de São Carlos, 2016.

1. Bioetanol de cana-de-açúcar. 2. Simuladores orientados a equações. 3. Análise tecno-econômica de bioprocessos. 4. Engenharia de bioprocessos e sistemas. 5. Etanol de primeira e segunda geração. I. Título.

MEMBROS DA BANCA EXAMINADORA DA DEFESA DE TESE DE FELIPE FERNANDO FURLAN APRESENTADA AO PROGRAMA DE PÓS-GRADUAÇÃO EM ENGENHARIA QUÍMICA DA UNIVERSIDADE FEDERAL DE SÃO CARLOS, EM 18 DE MARÇO DE 2016.

BANCA EXAMINADORA:

Roberto de Campos Giordano
Orientador, UFSCar

Argimiro Resende Secchi
Coorientador, UFRJ

Charles Dayan Farias de Jesus
CTBE

Guilherme José Maximo
UNICAMP

Ruy de Sousa Júnior
UFSCar

Agradecimentos

Agradeço primeiramente ao meu pai, João (*in memorian*), minha mãe, Cecília e minhas irmãs, Tatiana e Luciana, o apoio, incentivo e respeito às minhas escolhas durante toda minha vida.

Ao professor Roberto de Campos Giordano a orientação, o incentivo, a empolgação e principalmente a confiança demonstrada cada vez que eu aparecia com ideias novas. Pretendo levar seus ensinamentos até o fim de minha carreira.

Aos professores Caliane Bastos Borba Costa e Argimiro Resende Secchi a orientação, os bons conselhos e sugestões durante esses quatro anos.

Ao professor John Woodley a orientação e acolhimento durante meu doutorado sanduíche.

Ao Anderson, companheiro nos dias e noites de trabalho no Kyatera, agradeço a ajuda e as discussões úteis e interessantes durante esses últimos dois anos.

Ao colegas do CTBE, Antonio Bonomi, Charles Jesus, Isabelle Sampaio, Marcos Watanabe, Mateus Chagas, Moisés Alves e Tássia Junqueira por toda a ajuda no desenvolvimento deste trabalho.

Ao Alonso Constante Escobar "Seu Tino", Fábio Henrique Paschoal Bianchi Pinto e Renato Tonon Filho toda a informação gentilmente disponibilizada.

Ao Adalberto, grande amigo, as boas conversas, as discussões profundas e também as não tão profundas.

À Patrícia o incentivo, ajuda e paciência nesse período final do meu doutorado.

Aos meus (ainda pequenos) sobrinhos, Luiza, Letícia e Bruno, por conseguirem me descontrair e tirar um pouco a minha cabeça do doutorado.

Aos amigos da Dinamarca, Peam, Dasha, Carolina, Simone, Miriam, Estelle, Catarina, Teresa, Mafalda, Inês, Francesco, João, Larissa, Seyed e Tanaz o acolhimento caloroso naquelas terras frias.

A todos os colegas e amigos, Vitor, Karina, Andreza, Harminder, Cássia, Gui-

lhermina, Gabriel, Erich, Agnes, Renata, Cláudia, Luciano, Gislene, Úrsula, Carlos e todos os demais que também fizeram parte da minha vida durante estes quatro anos.

À CAPES e CNPq o apoio financiamento.

Por fim, agradeço a todos que de alguma forma contribuíram para a concretização deste trabalho.

"I've already got the prize. The prize is the pleasure
of finding the thing out, the kick in the discovery,
the observation other people use it.
Those are the real things."
Richand Feynman

Resumo

A produção de etanol lignocelulósico, o chamado etanol de segunda geração, é uma alternativa promissora para diminuir a dependência energética global dos combustíveis fósseis. Entretanto, um desenvolvimento maior de seu processo de produção ainda é necessário para sua efetiva implementação industrial. Apesar do grande esforço experimental na área, ainda não existem informações claras sobre os valores limites a serem alcançados nas diversas etapas de processo para que esse se torne economicamente viável. Nesse contexto, o objetivo deste trabalho foi construir uma metodologia para avaliação econômica de processos em estágio inicial de desenvolvimento, como é o caso do etanol de segunda geração, indicando à área de P&D direções a serem seguidas para sua viável implementação industrial. Tal procedimento sistemático integra ferramentas de engenharia de bioprocessos e sistemas e engenharia econômica para realizar uma análise tecno-econômica "reversa", que permite obter as variáveis que mais influenciam a viabilidade do processo, bem como seus valores limites para que tal viabilidade seja alcançada. Inicialmente, a metodologia proposta foi testada em um estudo de caso envolvendo o processo de produção de ácido succínico a partir da sacarose por rota fermentativa. Nesse processo, a metodologia conseguiu eliminar uma das variáveis inicialmente consideradas (a conversão da sacarose), devido a sua baixa influência. Além disso, foram obtidos valores mínimos para a concentração de ácido succínico no fermentador em função da seletividade e da produtividade específica (as variáveis de processo escolhidas). Em seguida, considerou-se a produção integrada de etanol a partir do caldo e do bagaço de cana-de-açúcar, etanol de primeira e segunda geração, respectivamente. As três variáveis com maior impacto na viabilidade econômica do processo foram: o rendimento do biocatalisador, a conversão da celulose no reator de hidrólise e a fração de sólidos nesse reator. A produtividade do reator, por outro lado apresentou baixo impacto na viabilidade, além de os resultados experimentais já estarem no patamar necessário para essa variável. De modo geral, a metodologia foi aplicada com sucesso aos estudos de caso escolhidos, produzindo dados importantes quanto às melhorias necessárias para que os processos alcancem a viabilidade econômica. Apesar de ter sido aplicada a bioprocessos, a metodologia é geral, sendo adequada ao estudo econômico de qualquer processo químico.

Palavras-chave: Bioetanol de cana-de-açúcar, Simuladores orientados a equações, Análise tecno-econômica de bioprocessos, Engenharia de bioprocessos e sistemas, Etanol de primeira e segunda geração, Valores-alvo para métricas de (bio)processos.

Abstract

Lignocellulosic ethanol, also called second generation ethanol, is a promising alternative for decreasing fossil fuel dependency globally. Nevertheless, its production process still needs further improvements in order to achieve industrial feasibility. Despite the massive experimental effort in this area, threshold values to be pursued in order to attain an economically feasible process are still missing. In this context, this study focused on constructing a methodology for economic evaluation of early-stage developing processes, such as second generation ethanol, aiming to show the R&D area directions to be followed for a successful industrial implementation of the process. The systematic procedure integrates bioprocess systems engineering (PSE) and economic engineering tools to perform a "retro" tecno-economic analysis. This analysis is able to identify the main process variables that influence the economic feasibility of the process and their target values. Initially, the methodology was tested on a case study involving the production of succinic acid from sucrose by fermentation. The methodology was able to eliminate one of the variables initially considered (sucrose conversion), due to its low influence on the process feasibility. Additionally, target values were obtained for the succinic acid concentration in the fermenter as a function of the selectivity and the specific productivity (the process variables chosen). Finally, the integrated production of ethanol from sugarcane juice and bagasse (first and second generation ethanol, respectively) was assessed. The three variables with the highest effect on the economic feasibility of the process were: the biocatalyst yield, the sucrose conversion and the solid mass fraction, both in the hydrolysis reactor. The reactor productivity, on the other hand, had little impact on the process feasibility. Besides, the experimental results already achieved the values needed for this variable. In general, the methodology was able to yield important information about both case studies required improvements for achieving economic feasibility. Although used in biochemical processes, the methodology is general, applying to all types of chemical processes.

Keywords: Sugarcane bioethanol, Equation-oriented simulators, Bioprocess techno-economic analysis, Bioprocess systems engineering, First and Second generation ethanol production, Bioprocess metrics target values.

Sumário

1 Introdução

1.1 Contextualização e motivação

Existe uma tendência mundial nas últimas décadas na direção do aumento da participação de energias renováveis na matriz energética. Isso se deve em partes à pressão pública visando diminuir o impacto ambiental causado pelo uso de combustíveis não renováveis. Entretanto, existe principalmente a preocupação governamental com a segurança energética, ainda altamente dependente do mercado externo de petróleo, que é dominado por um pequeno conjunto de países (CHERUBINI; STRØMMAN, 2010; NG, 2010). Isso impulsiona a pesquisa e desenvolvimento de novos processos químicos e, especialmente, bioquímicos para obtenção de combustíveis. Nesse contexto, o etanol se apresenta como bom candidato, já sendo amplamente utilizado em alguns países, como Brasil e EUA, e tendo grande potencial de expansão (HAHN-HÄGERDAL et al., 2006). A opção com melhor possibilidade de expansão é sua obtenção a partir de materiais lignocelulósicos, o que amplia o conjunto de matérias-primas que podem ser utilizadas para sua produção (NG, 2010). Entretanto, esse processo ainda é bastante novo, com poucas aplicações industriais até o momento. No contexto do Brasil, até o presente momento, existem três sítios industriais produzindo etanol a partir de material lignocelulósico (bagaço e/ou palha da cana-de-açúcar, MILANEZ et al., 2015).

A avaliação preliminar da viabilidade das diversas rotas de produção de etanol a partir de materiais lignocelulósicos é essencial para o desenvolvimento eficiente da tecnologia. Através de análises desse tipo, pode-se avaliar qual rota apresenta maiores chances de alcançar a viabilidade econômica e, com isso, guiar o foco das pesquisas. Várias opções existem para realizar tais análises. A opção escolhida inicialmente para o presente trabalho de doutorado foi a otimização superestrutural. Nesta, desenvolve-se uma superestrutura capaz de representar todas as alternativas de processo a serem estudadas (YEOMANS; GROSSMANN, 1999). Uma vez criado o problema de otimização a partir da superestrutura, diversos algoritmos de otimização inteira-mista não-linear (MINLP) podem ser aplicados, dependendo da estrutura do problema matemático obtido (FLOUDAS, 1995; GROSSMANN, 2002). Durante a otimização, tanto a rota quanto as condições de operação são otimizadas. Entretanto, para que o problema de otimização gerado a partir da superestrutura proposta seja tratável, em geral é necessário o uso de modelos simplificados (lineares) para as operações unitárias envolvidas (GROSSMANN, 2002). Quando modelos simplificados são empregados torna-se essen-

cial a utilização de valores embasados em dados experimentais ou simulações rigorosas para as conversões e eficiências dos equipamentos. Além disso, as eficiências em uma determinada etapa do processo normalmente dependem do processo que a precedeu, e como esse varia durante a resolução do problema de otimização, há muita incerteza sobre a representatividade desses parâmetros de processo. Pode-se realizar uma análise de incertezas nos parâmetros e verificar se o resultado (layout do processo) é afetado por essas incertezas (QUAGLIA et al., 2013; GROSSMANN et al., 2015).

De uma forma geral, a otimização superestrutural demanda um amplo conjunto de dados tanto sobre o processo quanto dados econômicos sobre cada rota testada. No caso do uso de algumas biomassas, particularmente a palha de milho, isso está disponível especialmente devido ao trabalho do Laboratório Nacional de Energia Renovável (*National Renewable Energy Laboratory* - NREL), nos Estados Unidos (KAZI et al., 2010; HUMBIRD et al., 2011), o que permite a construção e avaliação da superestrutura (CHEALI; GERNAEY; SIN, 2013). Porém, esse não é o caso para o uso do bagaço de cana-de-açúcar, foco do presente estudo. Nesse caso, seria necessária a análise tecno-econômica das rotas particulares antes da construção efetiva da superestrutura. Tal fato desestimulou o uso dessa abordagem e, nesse período, uma outra opção, bastante interessante, já se apresentava. Esse foi o período de doutorado sanduíche, realizado no grupo de pesquisa do Centro de Engenharia de Processos e Tecnologia (*Center for Process Engineering and Technology*), da Universidade Técnica da Dinamarca (DTU), sob a supervisão do professor John Woodley. No grupo, um outro procedimento é utilizado, principalmente para desenvolvimento de novos processos bioquímicos (TUFVESSON et al., 2013). Seu foco está em permitir uma avaliação sistemática das alternativas de processo, passando pela síntese das rotas (bio)químicas, projeto conceitual do processo e avaliação de opções. Desta forma, é possível descartar as rotas menos viáveis, desviando os esforços para as mais promissoras; isso com o mínimo de informação disponível. Porém, essa metodologia utiliza valores médios para as métricas mais importantes do processo, dependendo do tipo de produto (produtos químicos de base, de especialidades, de química fina ou farmacêuticos) (TUFVESSON et al., 2011; RAMOS; TUFVESSON; WOODLEY, 2014), para construir (quando possível) janelas de operação nas quais a operação do processo é factível e, provavelmente, economicamente viável. Por utilizar valores médios, ela não consegue capturar as características específicas de cada processo. Assim, encontrou-se uma oportunidade de fazer uma contribuição original à área. Aliando-se ferramentas de engenharia econômica e engenharia de (bio)processos e sistemas em um simulador orientado a equações, é possível calcular diretamente os valores para as métricas de processo necessários para que um determinado processo se torne economicamente viável. Tal metodologia foi denominada "Análise Tecno-Econômica Reversa" (ATER). Desta forma, é possível capturar as parti-

cularidades do processo e construir as janelas de operação específicas para o processo em questão.

De um modo geral, a análise econômica é aliada a simulação de processo para auxiliar na compreensão e verificação da viabilidade econômica de novos processos. Além disso, ela pode ser aliada à outras ferramentas como otimização de processos, estudos de caso e análises de sensibilidade para verificar diferentes cenários e possibilidades para um mesmo processo. Essas aplicações partem de condições operacionais específicas, baseadas em dados experimentais ou hipóteses sobre o funcionamento do processo para avaliar sua viabilidade econômica e comparar as diversas opções. A Análise Tecno-Econômica Reversa, proposta aqui, faz o caminho oposto. Ao fixar um desempenho econômico mínimo para o processo, as condições de processo necessárias para que este seja alcançado são obtidas. Como o número de variáveis que influenciam na viabilidade deste é normalmente grande (sendo, em último caso, igual ao número de especificações do processo) foi necessário criar um critério para a escolha das variáveis mais importantes. Valores mínimos para as variáveis de processo escolhidas são obtidos, bem como a correlação entre elas, na forma de diagramas.

A ATER só se torna eficiente quando implementada em simuladores orientados a equações, por não necessitar de um loop externo de convergência (MORTON, 2003). Entretanto, esses simuladores não permitem a implementação de estratégias específicas para a resolução de problemas locais de convergência. Isso torna imprescindível a correta inicialização das variáveis quando modelos não-lineares são utilizados. Porém, essa solução é inviável quando se pretende realizar simulações globais em diversas condições de processos. A solução normalmente utilizada é a aproximação dos modelos não-lineares por modelos simplificados (*surrogate models*), o que leva a uma perda de acuracidade. A proposta utilizada, entretanto, faz uso de interpoladores multilineares. Interpoladores multilineares têm uma ampla utilização, com aplicações em controle de processos, processamento de imagens, entre outros, principalmente nas áreas de ciências da computação e engenharias (WAN; KOTHARE, 2003; MOBLEY et al., 2005). Porém, não existe na literatura aplicação de interpoladores multilineares na aproximação de modelos complexos para sua efetiva solução em simuladores orientados a equações, de modo que uma metodologia foi proposta para esse fim. Assim, uma metodologia foi proposta para a construção da tabela de inspeção utilizada pelo interpolador multilinear, envolvendo a escolha do espaçamento entre os pontos desta.

Em paralelo aos trabalhos do doutorado, foi desenvolvido também um estudo com o aluno de iniciação científica Leonardo Calabrez Gloeden Gonçales sobre otimização multiobjetivo (JAIMES; COELLO, 2009) utilizando algoritmo não-determinístico (PSO - *Particle Swarm Optimization*, KENNEDY; EBERHART, 1995). Tal trabalho re-

sultou no artigo intitulado *Implementation of Pareto Multi-objective Particle Swarm Optimization* publicado nos anais do 3^{th} *International Conference on Engineering Optimization* - EngOpt 2012. Neste trabalho, a otimização multiobjetivo foi aplicada a um processo clássico de produção de amônia e utilizado para obter uma curva de pontos ótimos sem recorrer à análise econômica do mesmo. Em decorrência deste trabalho, estudou-se a possibilidade de inclusão de otimização multiobjetivo, aliada à análise de impacto ambiental, no estudo da produção de etanol 2G. Essa decisão ocorreu antes que a otimização superestrutural fosse abandonada e, portanto, não foi continuada quando isso ocorreu. Porém, após o desenvolvimento completo da metodologia da ATER, ficou evidente que seria possível incorporar também a análise ambiental, o que foi sugerido para trabalhos futuros.

1.2 Objetivo

O objetivo desta tese é desenvolver uma metodologia de análise econômica de processos em estágios iniciais de desenvolvimento que promova um *feedback* para as áreas de P&D, auxiliando o desenvolvimento desse processo, bem como sua implementação industrial. Dentre os objetivos específicos, destacam-se:

- Desenvolvimento de uma metodologia de análise tecno-econômica "reversa", que permite a obtenção de valores mínimos a serem alcançados para a implementação viável do processo;
- Construir uma metodologia para aproximação de modelos cuja não-linearidadedificulte sua utilização em simuladores orientados a equações;
- Desenvolvimento de uma biblioteca de modelos que permita a simulação de biorrefinarias de cana-de-açúcar em diversas situações;
- Avaliação da metodologia, suas limitações e vantagens através de sua aplicação em estudos de caso, em particular, na produção de etanol de segunda geração a partir do bagaço de cana-de-açúcar.

1.3 Organização da tese

Ao iniciar o desenvolvimento dos modelos para simulação de biorrefinarias de cana-de-açúcar, foi detectada uma limitação do simulador escolhido (que utiliza a abordagem orientada a equações). Por não empregar rotinas específicas para resolver cada modelo, a simulação de modelos complexos se torna bastante difícil, sendo altamente dependente da inicialização das variáveis. Isso pode tornar impraticável

a utilização destes modelos complexos de forma integrada em uma simulação global (do processo completo). Assim, o Capítulo 2 apresenta uma metodologia desenvolvida para aproximar tais modelos empregando tabelas de inspeção multidimensionais para facilitar sua inclusão em simulações globais. Tal abordagem permitiu o desenvolvimento do presente trabalho, sem perdas consideráveis na acurácia da resposta, o que normalmente é ocasionado quando modelos simplificados são utilizados. Uma aplicação da metodologia incorporada à otimização do processo também é apresentada nesse capítulo.

A análise tecno-econômica detalhada da biorrefinaria é considerada no Capítulo 3. Como estudo de caso, considera-se a viabilidade de uma biorrefinaria flexível, nos mesmos moldes normalmente encontrados em usinas de açúcar e etanol, que apresentam certa flexibilidade quanto à proporção entre seus dois produtos principais.

A partir das considerações levantadas no capítulo anterior, uma nova metodologia é desenvolvida no Capítulo 4. Tal metodologia utiliza conceitos de engenharia de (bio)processos e sistemas e engenharia econômica, como é o caso das análises econômicas clássicas. Porém, esses conceitos são utilizados não para avaliar a viabilidade econômica de um processo (empregando dados obtidos em escala de laboratório ou piloto) mas para obter as principais variáveis de processo que influenciam na viabilidade do processo, seus valores mínimos para que o mesmo seja viável e a correlação entre elas. Dessa forma, tais conceitos são utilizados para derivar diretrizes e objetivos a serem alcançados experimentalmente.

No Capítulo 5 a metodologia desenvolvida é aplicada ao processo de produção de etanol de segunda geração (2G) a partir do bagaço de cana-de-açúcar. Um conjunto de diretrizes e objetivos a serem alcançados experimentalmente é levantado, podendo servir de base para a elaboração de futuros experimentos visando a viabilidade econômica desse processo.

Por fim, o Capítulo 6 apresenta as principais conclusões desse trabalho e sugestões para trabalhos futuros.

2 Aproximação de modelos complexos por interpoladores multilineares e aplicação em simuladores orientados a equações

O simulador EMSO (*Environment for Modeling, Simulation and Optimization*), que é um simulador orientado a equações, foi escolhido como plataforma das simulações deste trabalho. Esse simulador apresenta uma linguagem de modelagem que pode ser utilizada pelo usuário para desenvolver novos modelos e/ou estender os modelos já existentes na biblioteca. Além disso, o simulador também possui uma interface para adicionar bibliotecas dinâmicas como *plug-ins* ou *solvers*, implementando novas funcionalidades a ele. Essas características são fundamentais para a implementação de novos processos, os quais podem incluir equipamentos cujos modelos não estão representados nas bibliotecas padrão de simuladores. Além disso, a abordagem orientada a equações se provou essencial para que a metodologia proposta no Capítulo 4 fosse implementada com sucesso.

Entretanto, diferente dos simuladores sequenciais modulares, os orientados a equações não empregam uma ordem específica para a solução dos modelos, impedindo a implementação de estratégias particulares para resolver problemas locais de convergência. Essa é, provavelmente, a maior desvantagem de simuladores orientados a equações. Para contornar tal limitação, normalmente são utilizados modelos simplificados (*surrogate models*) para descrever as etapas de difícil convergência. Esses modelos envolvem superfícies de resposta (THOMBRE; PREISIG; ADDIS, 2015; IPSITABANERJEE; PAL; MAITI, 2010), redes neurais (HOSKINS; HIMMELBLAU, 1988; GRACIANO; ROUX, 2013), entre outros. Esses modelos se baseiam em otimizar a distância entre a resposta real e a fornecida pelo modelo. Uma etapa de otimização (ou treinamento) prévia a sua utilização é necessária, e esta deve ser repetida caso novos dados fiquem disponíveis, tornando tais modelos pouco flexíveis. Além disso, tal abordagem apresenta um compromisso entre a complexidade dos modelos utilizados e a acurácia da aproximação. Assim, estes modelos podem apresentar altos desvios com relação aos modelos rigorosos e/ou a realidade, além de pouca flexibilidade operacional (MORTON, 2003).

A proposta apresentada neste capítulo faz uso de interpoladores multilineares (NELLES, 2001) para aproximar dados de equipamentos obtidos em separado por modelos rigorosos ou experimentalmente. Uma descrição detalhada do funcionamento do interpolador bem como sua implementação na forma de *plug-in* é apresentada em Furlan (2012). A sintaxe utilizada para a construção da tabela de inspeção é apresentada na subseção A.7.1. Nessa abordagem, a complexidade do sistema é substituída pelo aumento no número de pontos na tabela de inspeção utilizada, que permite o controle da acurácia da aproximação. Além disso, o uso de interpoladores é mais flexível, pois novos experimentos podem ser inseridos diretamente na tabela de inspeção, sem a necessidade de uma nova etapa de otimização ou treinamento.

Para avaliar a metodologia proposta, esta foi aplicada a duas seções da produção de etanol de segunda geração: a purificação do etanol, consistindo em dois trens de colunas de destilação, e a hidrólise do bagaço, constituída por um conjunto de reatores operando em batelada. A primeira aplicação é um exemplo típico de um modelo não-linear complexo, que geralmente apresenta grandes problemas de convergência em simuladores orientados a equações e, portanto, é normalmente foco de simplificações. Neste caso, os trens de colunas foram simulados em separado no simulador *Aspen Plus*® (um simulador sequencial modular), usando modelo rigoroso de coluna de destilação (radfrac) e seus dados alimentados ao interpolador. Por sua vez, a hidrólise da celulose é um processo descontínuo (batelada) e sua inclusão em simulações estacionárias normalmente requer a solução analítica das equações diferenciais ou a resolução numérica das mesmas. Neste caso, a simulação dinâmica foi realizada no próprio EMSO e as conversões em função do tempo inseridas no interpolador, representando o desempenho do reator caso a batelada fosse interrompida naquele período.

A descrição detalhada da metodologia desenvolvida bem como os principais resultados obtidos no estudo de caso descrito são apresentados a seguir, no artigo intitulado *A simple approach to improve the robustness of equation-oriented simulators: Multilinear look-up table interpolators*, publicado no periódico *Computers and Chemical Engineering* (v. 86, p. 1–4, 2016).

Os resultados apresentados no artigo mostram que a metodologia desenvolvida consegue representar de forma acurada modelos rigorosos, sem as desvantagens decorrentes de modelos não-lineares. Além disso, a metodologia inclui um critério simples e quantitativo para decidir sobre o número mínimo de pontos utilizado na construção das tabelas de inspeção usadas pelo interpolador.

Apesar da aproximação do modelo de hidrólise em batelada pelo interpolador apresentar uma baixa acurácia em algumas regiões, tais regiões são de pouco interesse

prático, por apresentarem baixas conversões. Como desenvolvimento futuro da metodologia, é possível expandir a abordagem para interpoladores com passo variável, o que permitiria um refinamento da malha no início da batelada. Desta forma, o comportamento não-linear apresentado nesse período seria melhor representado.

Uma segunda aplicação mostra o potencial da metodologia proposta. Os modelos de colunas de destilação para a produção de etanol hidratado são utilizados em uma otimização do processo de produção de etanol empregando tanto a cana-de-açúcar quanto o bagaço (etanol de segunda geração). Essa aplicação é apresentada no artigo intitulado *Assessing the production of first and second generation bioethanol from sugarcane through the integration of global optimization and process detailed modeling*, publicado no periódico *Computers and Chemical Engineering* (v. 43, p. 1–9, 2012). O artigo é reproduzido no Anexo A. O processo foi otimizado utilizando o algoritmo *particle Swarm* (PSO) e empregando a abordagem por caminho viável (*feasible path*) no qual o otimizador atua somente nas variáveis de escolha enquanto a resolução do sistema de equações fica a cargo de algoritmos especializados (BIEGLER; GROSSMANN; WESTERBERG, 1997). Devido ao fato de ser utilizado um otimizador global e a abordagem de caminho viável, o sistema é simulado em um grande conjunto de condições operacionais. A partir dos resultados obtidos, verifica-se que a modelagem se mostrou robusta o suficiente dentro destas condições. Verificou-se também a necessidade de refinar a análise econômica da planta, bastante simplificada neste caso.

Os modelos de destilação e desidratação do etanol desenvolvidos nessa etapa usando o interpolador multilinear foram empregados nos demais trabalhos realizados, com exceção do apresentado no capítulo Capítulo 4. Por outro lado, o modelo de hidrólise foi substituído por um modelo de reator estequiométrico, pois as análises posteriores não poderiam ficar restritas às condições experimentais utilizadas no desenvolvimento do modelo rigoroso utilizado.

Computers and Chemical Engineering 86 (2016) 1–4

Contents lists available at ScienceDirect

Computers and Chemical Engineering

journal homepage: www.elsevier.com/locate/compchemeng

Note

A simple approach to improve the robustness of equation-oriented simulators: Multilinear look-up table interpolators

Felipe Fernando Furlan[a], Anderson Rodrigo de Andrade Lino[b], Karina Matugi[a], Antonio José Gonçalves Cruz[a,b], Argimiro Resende Secchi[c], Roberto de Campos Giordano[a,b,*]

[a] Chemical Engineering Graduate Program, Universidade Federal de São Carlos (UFSCar), Rodovia Washington Luís (SP-310), km 235, São Carlos, SP, CEP: 13565-905, Brazil
[b] Chemical Engineering Department/UFSCar, Universidade Federal de São Carlos (UFSCar), Rodovia Washington Luís (SP-310), km 235, São Carlos, SP, CEP: 13565-905, Brazil
[c] Chemical Engineering Graduate Program, COPPE, Universidade Federal de Rio de Janeiro, UFRJ, Cidade Univesitária, Rio de Janeiro, RJ, CEP: 21941-972, Brazil

ARTICLE INFO

Article history:
Received 6 November 2015
Received in revised form 7 December 2015
Accepted 21 December 2015
Available online 29 December 2015

Keywords:
Robustness of equation-oriented simulators
Multilinear look-up table interpolators
1G–2G bioethanol production
Particle swarm optimization

ABSTRACT

Equation-oriented simulators have some advantages over the modular sequential ones, but improvements are still necessary to deal with nonlinearities, while preserving the robustness of the solver. Linear approximations and/or surrogate models can be used in place of nonlinear models, but the loss of predictive accuracy may be a drawback. An alternative to circumvent this problem is the use of grid-based look-up tables for interpolating responses from rigorous models. This methodology was integrated in an equation-oriented simulator (EMSO). A case study involving the production of bioethanol from sugarcane is used to demonstrate the robustness of this approach. Look-up tables replaced the models of two distillation column trains and of the cellulose hydrolysis reactor. These models were included into the global process and an optimization problem aiming at the maximum production of ethanol was successfully solved by a PSO algorithm varying the solid mass fraction in the hydrolysis reactor.

1. Introduction

Equation-oriented process simulators solve the system of equations simultaneously. Although useful when the number of recycle streams in the process is large, this approach prevents the implementation of strategies for circumventing local convergence problems (i.e., including ad hoc algorithms within the models of specific process units, the "modules" of the sequential modular simulators). According to Morton (2003), processes with awkward nonlinearity and high recycle complexity should be solved by equation-oriented simulators, provided their robustness undergoes some improvements. Nevertheless, while such generically robust solver is not available, some strategies can be developed to circumvent this bottleneck. As a general case, these strategies rely on simplifications of the models that constitute the chemical plant. However, these simplifications generally imply loss of accuracy and operational flexibility (Morton, 2003).

Here, an alternative approach is presented: using grid-based look-up tables to interpolate the results of previous offline simulations, for the process unit models whose nonlinearity was hindering the convergence of the simulations of the overall industrial plant. With this simple strategy, the accuracy of the simplified model (the interpolator) can be tuned, while still requiring low computational power (Nelles, 2001). As a proof of concept, an integrated first and second generation ethanol biorefinery was modeled, using both sugarcane and sugarcane leaves as feedstock. Two process sections, chosen for their characteristically nonlinear behavior, were used for testing the methodology: the distillation columns trains, which were simulated in steady-state, and the enzymatic hydrolysis reactor, which was simulated dynamically, with the results at the end of the batch run being considered in the global process simulations. In both cases, results obtained with this methodology were compared to the ones generated by the original phenomenological models. The look-up table interpolators were then coupled

* Corresponding author at: Chemical Engineering Graduate Program, Universidade Federal de São Carlos (UFSCar), Rodovia Washington Luís (SP-310), km 235, São Carlos, SP, CEP: 13565-905, Brazil. Tel.: +55 16 3351 8708; fax: +55 16 3351 8266.
E-mail addresses: felipef.furlan@gmail.com (F.F. Furlan), andersonlyno@gmail.com (A.R. de Andrade Lino), karinamatugi@gmail.com (K. Matugi), ajgcruz@ufscar.br (A.J.G. Cruz), arge@peq.coppe.ufrj.br (A.R. Secchi), roberto@ufscar.br (R. de Campos Giordano).

http://dx.doi.org/10.1016/j.compchemeng.2015.12.014
0098-1354/

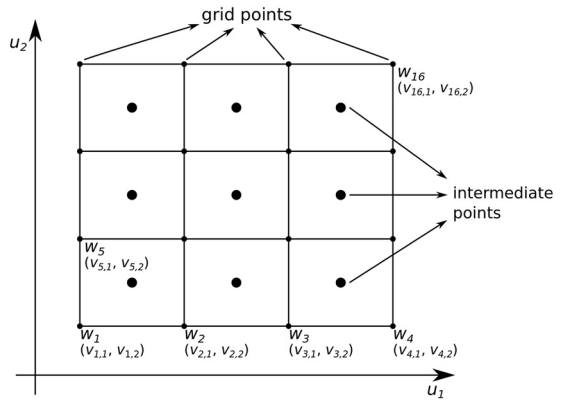

Fig. 1. Example of a two-dimensional grid with the intermediate points used to test the grid accuracy. w is the output variable (a scalar) and v the input variables vector (here, two-dimensional) at the grid nodes. u is a new input vector to be interpolated.

to the global process flowsheet, in order to evaluate the robustness of the approach.

2. Methodology

2.1. Simulator

The simulator EMSO™ (Environment for Modeling Simulation and Optimization), used in this work, is equation-oriented. This simulator has an internal object-oriented modeling language that allows insertion of new models into its internal library. Moreover, it is possible to add plug-ins for running calculations which are not suitable for the equation-oriented approach; and new solvers may be linked as dynamic libraries as well (Soares and Secchi, 2003).

2.2. Grid-based look-up tables

Grid based look-up tables consist of a set of data points positioned in a multi-dimensional grid. The scalar values w_i in the grid are the estimates (or the actual values) of the nonlinear function for a given vector of n input variables $v_{i,k}$, (v is a matrix where each column corresponds to a point in the grid and each row to one element of the input variables vector, Vogt et al., 2004). Fig. 1 illustrates the two-dimensional case ($n=2$). The output of the interpolator is determined by considering the smallest n-cube or n-parallelepiped (C) defined by the grid points v_i, columns of the matrix v which enclose a new input vector u (i.e., the input variables whose corresponding model output, $\hat{y}$, is required to be calculated). The interpolated output ($\hat{y}$, a scalar) is a weighted average of the output values (w_i) at each vertex of C (whose coordinates are given by the i-column of v, v_i), with weights Φ_i, Equation (1). These weights (Φ_i) are the ratios between the volume of each n-cube whose longer n-diagonal is defined by u and the vertex v_j of C that is opposed to v_i (i.e. the coordinates v_i and v_j define a longer diagonal of C), divided by the total volume of C (Nelles, 2001):

$$\hat{y} = \sum_{i=1}^{M} w_i \Phi_i(u, v) \tag{1}$$

According to this definition, the closer each column of v (v_i, corresponding to a set of input variables) is from u, the higher will be its weight. Eq. (1) is a basis function formulation for $\hat{y}$. Hence, the value of Φ_i is actually defined for the whole interpolation region (defined by the M interpolation points), being zero for all n-cubes' vertices except for the ones of the n-cube C, which encloses u (Eq. (2)), with M being obtained by Eq. (3).

$$\phi_i(u, v) = \begin{cases} \dfrac{\prod_{k=1}^{n} |u_k - v_{j,k}|}{\prod_{k=1}^{n} |v_{i.k} - v_{j,k}|}, & \text{when} i \text{ is a vertex of C} \\ 0, & \text{when} i \text{ is not a vertex of C} \end{cases} \tag{2}$$

$$M = \prod_{k=1}^{n} M_k \tag{3}$$

where M_k is the number of points in the grid for the input variable k and n is the number of input variables.

Many applications of look-up tables implement uniformly distributed input variables. This choice allows fast access to the neighboring points (C) by address computation. However, it also restricts the flexibility of the look-up table since the spacing cannot be adjusted to increase accuracy where it is needed (Nelles, 2001). In the present study, only look-up tables with uniformly distributed grids were implemented. Accuracy evaluations were performed to determine the minimum number of points in the grid for each variable. A maximum relative error of 5% was considered in this analysis for absolute values greater than one, while the absolute error (with a maximum of 0.05) was considered for absolute values smaller than one. Intermediate points in the center of the most refined grid were used as test for the accuracy of the grids (Fig. 1). The interpolated points for each look-up table were compared with the "exact" values (provided by phenomenological models).

Table 1
Input variables and process specifications for the simulations of the hydrous ethanol distillation columns train.

	Description	Value
Input variables	Input stream temperature (K)	348.15–378.15
	Input stream ethanol mass fraction	0.065–0.105
Process specifications	Ethanol mass fraction in hydrous ethanol	0.935
	Ethanol mass fraction in vinasse	0.002
	Ethanol mass fraction in Phlegmasse	0.002
	Ethanol recovered in the vapor phlegm stream	76%

2.3. Distillation columns

Distillation columns for bioethanol purification were configured according to Dias (2008). In a conventional configuration, two columns are used and saturated vapor of hydrous ethanol is obtained with ethanol mass fraction of 0.935 (w/w).

Column trains were simulated in ASPEN PLUS® using RADFRAC model. The liquid phase was described by Wilson model, while the vapor phase was assumed to be ideal. It was considered that the wine was composed only by ethanol and water. Temperature and ethanol mass fraction of the feed stream were elected as input variables for the look-up tables (Table 1). The output variables were the heat duties of columns' reboilers and condensers, the molar fraction of ethanol at the top of the first column, the molar flowrates of first column bottom (vinasse), first column top (second grade ethanol), second column bottom (flegmass) and second column top (hydrous ethanol). Except for the molar fraction of ethanol at the top of the first column, all output variables were divided by the mass flowrate of the first column feed in order to obtain an intensive value, independent of the inlet flowrate. Three look-up tables with 15, 45 and 153 points and constant intervals were generated.

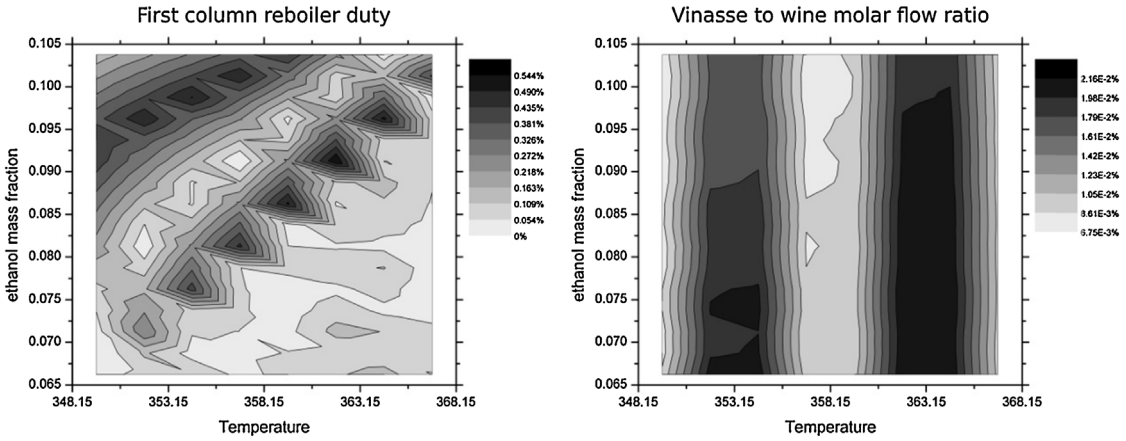

Fig. 2. Two examples of the error distributions as function of the input variables for the hydrous ethanol distillation column train. The look-up table had 15 grid points.

The look-up tables, to be included in EMSO for simulating the complete biorefinery, were chosen based on their size and the number of violations of the restriction on the maximum error (5%). In this sense, the smallest look-up table with the smallest number of restriction violations was chosen.

2.4. Enzymatic hydrolysis

The enzymatic hydrolysis reactor was simulated using the kinetic model described by Angarita et al. (2015). Three input variables were chosen to build the look-up table: solid mass fraction in the reactor, enzymatic load and hydrolysis reaction time. The output variables were the conversions of cellulose and hemicellulose.

2.5. Global process

In order to assess the robustness of the methodology, look-up tables were used in the simulations of an integrated first (1G) and second (2G) generation ethanol-from-sugarcane plant. The process also includes electric energy cogeneration, based on a Rankine cycle, burning sugarcane residual biomass to meet the process energy demands. A detailed description of the process can be found in Furlan et al. (2013). A third look-up table was used to approximate a second train of distillation columns, delivering anhydrous ethanol. The ratio between the entrainer (monoethylene glycol) and the hydrous ethanol mass flow was the input variable in this case.

3. Results and discussion

Based on the accuracy criteria described in Section 2.2, a grid with 15 points (three inlet temperatures and five ethanol mass fractions) was used for approximating the behavior of the hydrous ethanol distillation column train. Fig. 2 presents the error distribution as a function of the two input variables (wine temperature and molar fraction of ethanol). Two output variables were selected as examples of the error distribution: the heat duty in the first column reboiler (the main energy consumption) and vinasse specific production (the main environmental impact in this step). As it can be seen, no common pattern is apparent in the error distribution (and the same is valid for the other output variables, not shown here). The relative average deviation and the standard deviation of all output variables are in Table 2. The same analysis was performed for the dehydration train, and a look-up table with 26 points was chosen.

The error distribution for the hydrolysis reactor presented a strong influence of the reaction time. The error in the first hours of the hydrolysis was at least one order of magnitude higher than the ones after these initial hours. Since three input variables were chosen for this look-up table, the error plots were presented for two different hydrolysis times. The error distributions for the cellulose conversion, shown in Fig. 3, are for a look-up table with 2409 points (73 for the hydrolysis time, eleven for the enzyme load, and three for the solid mass fraction). Table 3 shows the relative average deviation and the standard deviation of all output variables. None of the fixed-grid look-up tables tested here was able to meet the maximum error requirements for all range of time. These errors were concentrated in the initial hours of the hydrolysis in the batch reactor, when the Michaelis–Menten reaction rates change more drastically. Nevertheless, probably no industrial biorefinery would operate with a conversion below 45% in this reactor, the threshold above which the accuracy meets the criteria described in Section 2.2. If the initial hours of the hydrolysis were used in the global simulation, a look-up table with variable grid stepsize should be considered.

To show the power of the present methodology, the look-up tables presented for both columns and for the hydrolysis reactor were incorporated in an optimization problem, aiming at maximizing the ethanol production by varying the solid mass fraction

Table 2
Relative average deviation $|(\hat{y} - y)/y|$ and standard deviation of the output variables of the distillation column look-up table with 15 grid points.

	Relative average deviation	Standard deviation
First column reboiler duty	1.64E−3	1.42E−3
Second column reboiler duty	1.50E−3	1.20E−3
First column condenser duty	1.65E−3	1.12E−3
Second column condenser duty	1.95E−3	1.19E−3
Ethanol molar fraction in the first column top	6.56E−5	6.71E−5
First column bottom to feed ratio	1.42E−4	5.65E−5
First column top to feed ratio	8.22E−4	4.00E−4
Second column bottom to feed ratio[a]	1.62E−3	6.52E−4
Second column top to feed ratio[a]	4.75E−6	2.94E−6

[a] The first column feed is considered in this ratio.

Table 3
Relative average deviation $|(\hat{y} - y)/y|$ and standard deviation of the output variables of the hydrolysis reactor look-up table with 2409 grid points.

	Relative average deviation	Standard deviation
Cellulose conversion	8.00E−3	3.59E−2
Hemicellulose conversion	7.79E−3	3.77E−2

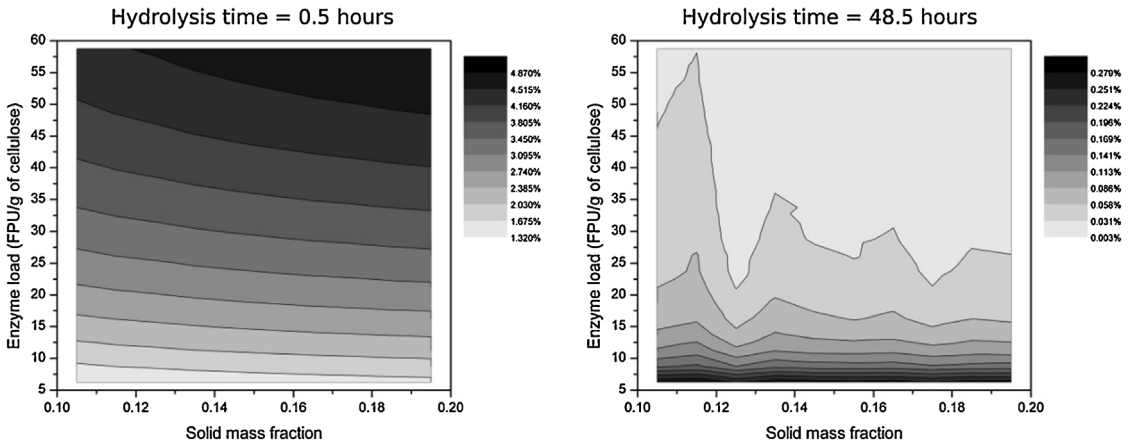

Fig. 3. Error distribution of cellulose conversion in the hydrolysis reactor as function of the solid mass fraction and enzyme load for two different hydrolysis times (at the beginning and at the end of the hydrolysis). The look-up table had 2409 grid points.

in the hydrolysis reactor. This 1G–2G biorefinery comprised 26,502 process variables.

The global optimization used the non-deterministic algorithm PSO (particle swarm optimization, Kennedy and Eberhart, 1995) with the feasible path approach, as described in Biegler et al. (1997). This approach allows the optimization algorithm to deal only with the decision variables, while an efficient solver should deal with the nonlinear system (Furlan et al., 2012). As a general case, the feasible path approach using non-deterministic algorithms is more robust in terms of finding at least a good candidate for (sub-)optimal solution of the problem. Nevertheless, since the nonlinear system is solved for each particle at each iteration, this approach is usually slower than the infeasible one when solving in sequential computer.

Processing time for solving the optimization problem, for a swarm with 20 particles and 20 iterations in a two-core virtual machine running Ubuntu 12.04 with 1.5 GB of RAM in a quad-core AMD Phenon II X4 955 computer, with 4 GB of RAM, was app. 475 min. The simulation of one steady state of the biorefinery took app. 120 s in the same computer.

The algorithm, using the proposed methodology, was able to find a (sub-)optimum in the search space, with a specific ethanol production of 102.3 l/t of sugarcane, an increase of 19% relative to the 1G process.

4. Conclusions

In this work, a methodology involving the use of grid-based look-up tables in equation-oriented simulators was developed. The methodology allowed the construction of simplified models that approximate nonlinear phenomenological models with a controllable accuracy, without the impairments in convergence caused by the rigorous models. As a demonstration of the capabilities of the methodology, an integrated first and second generation (1G–2G) ethanol production process (with 26,502 process variables solved simultaneously) was considered for optimization (maximizing ethanol production), with EMSO^{TM} simulator. Phenomenological models for the distillation column trains and for the cellulose hydrolysis reactor were used to provide the basis for the look-up tables. The non-deterministic optimization algorithm PSO (particle swarm optimization) with a feasible path approach was employed to find a (sub-)optimal solution that represented a 19% increase in the specific ethanol production, relative to an equivalent autonomous distillery. Thus, the proposed methodology performed well for robustness.

Acknowledgements

This work was financially supported by CAPES, CNPq and FAPESP (Proc. 09/13325-0 and 08/56246-0).

References

Angarita JD, Souza RBA, Cruz AJG, Biscaia EC, Secchi AR. Kinetic modeling for enzymatic hydrolysis of pretreated sugarcane straw. Biochem Eng J 2015;104:10–9.
Biegler LT, Grossmann IE, Westerberg AW. Systematic methods of chemical process design. Old Tappan: Prentice Hall; 1997.
Dias MOS. (Master thesis) Simulation of ethanol production process from sugar and sugarcane bagasse aiming at process integration and energy production maximization (Master thesis). Universidade Estadual de Campinas; 2008 (in Portuguese).
Furlan FF, Costa CBB, Fonseca GC, Soares RP, Secchi AR, Cruz AJG, Giordano RC. Assessing the production of first and second generation bioethanol from sugarcane through the integration of global optimization and process detailed modeling. Comput Chem Eng 2012;43:1–9.
Furlan FF, Tonon Filho R, Pinto FHPB, Costa CBB, Cruz AJG, Giordano RLC, Giordano RC. Bioelectricity versus bioethanol from sugarcane bagasse: is it worth being flexible? Biotechnol Biofuels 2013;6:142.
Kennedy J, Eberhart RC. Particle swarm optimization. In: IEEE International Conference on Neural Networks (ICNN); 1995. p. 1942–8.
Morton M. Equation-oriented simulation and optimization. Proc Indian Natl Sci Acad 2003;69:317–58.
Nelles O. Linear, polynomial, and look-up table models. In: Nonlinear System Identification. 2nd ed. Berlin: Springer; 2001. p. 219–38.
Soares RP, Secchi AREMSO. A new environment for modelling, simulation and optimisation. Comput Aided Chem Eng 2003;14:947–52.
Vogt M, Müller N, Isermann R. On-line adaptation of grid-based look-up tables using a fast linear regression technique. J Dyn Syst 2004;126:732–9.

3 Análise econômica da biorrefinaria

Dentro do contexto da avaliação econômica da biorrefinaria, a primeira questão que se coloca é se a produção de etanol de segunda geração (utilizando o bagaço da cana-de-açúcar) pode competir economicamente com o atual uso deste subproduto da produção de etanol (e açúcar): a produção de energia elétrica. Além dessa resposta ser altamente dependente do contexto econômico considerado, deve-se também levar em consideração a sazonalidade dos preços da energia elétrica e do etanol (causados pelos períodos de chuva e seca - entressafra e colheita na região sudeste, respectivamente). Esse fato indica a possibilidade de existência de uma biorrefinaria flexível, nos mesmos moldes das usinas de açúcar e álcool, que podem alterar a fração de matéria-prima desviada para cada finalidade. Tal biorrefinaria teria a capacidade de aumentar sua produção de energia elétrica quando os preços do mercado estivessem favoráveis, ou aumentar a produção de etanol através do etanol 2G, quando o preço deste estivesse mais atrativo.

Esta foi a questão desenvolvida no artigo intitulado *Bioelectricity versus bioethanol from sugarcane bagasse: is it worth being flexible?* publicado no periódico *Biotechnology for Biofuels* (v. 6, n. 142, 2013). Neste, compara-se três biorrefinarias alternativas: a primeira produzindo etanol de primeira geração e utilizando todo o bagaço para produção de excedente de energia elétrica, a segunda desviando a quantidade máxima de bagaço para produção de etanol 2G (a planta ainda deve ser autossuficiente) e a terceira flexível, permitindo uma decisão mensal entre as duas abordagens, dependendo dos preços dos dois produtos, etanol e energia elétrica.

Dentre os resultados obtidos, destaca-se o fato do investimento superior da biorrefinaria flexível não ser sustentado pelos níveis de oscilações sazonais apresentados tanto pelo etanol quanto pela energia elétrica. Além disso, nenhuma das opções consideradas apresentou viabilidade econômica no contexto considerado. Porém, vale ressaltar que não foram considerados diferentes perfis de financiamento como, por exemplo, o plano conjunto BNDES-Finep de apoio à inovação tecnológica industrial dos setores sucroenergético e sucroquímico – PAISS (MILANEZ et al., 2015). Sem dúvida, uma linha de crédito especial para o desenvolvimento dessa tecnologia, com baixas taxas de juros, terá forte impacto na viabilidade do processo. Isso seria equivalente, nas análises realizadas, a diminuir a taxa mínima de atratividade considerada. Porém, a análise de diferentes cenários econômicos não era o foco deste trabalho. Ao contrário, coloca-se uma segunda questão: sem depender de variações de origem econômica,

quais condições e desempenhos de processo tornariam o etanol 2G viável?

Essa questão levou a um novo estudo, no qual empregou-se o conceito de preço mínimo de venda do etanol (para o qual o valor presente líquido da planta se torna zero) e estudou-se o efeito de alguns parâmetros de processo nesse preço mínimo. Um novo processo foi utilizado, por apresentar resultados experimentais aparentemente mais promissores e as hipóteses sobre os custos de investimento e preço da celulase foram atualizados, para representar melhor o processo. Esse trabalho, intitulado *Process Alternatives for Second Generation Ethanol Production from Sugarcane Bagasse*, foi publicado nos anais do PSE2015/ESCAPE25 - *12th International Symposium on Process Systems Engineering and 25th European Symposium on Computer Aided Process Engineering* (v.37B, p. 1349-1354, 2015). Neste, verificou-se que o etanol 2G ainda apresenta um preço mínimo de venda superior ao do etanol 1G e também ao preço de venda atualmente praticado no Brasil. Além disso, verificou-se uma forte influência tanto da conversão obtida no reator de hidrólise quanto da carga de sólidos neste mesmo reator no preço mínimo de venda do etanol 2G. Uma terceira questão então se coloca: existe um conjunto de parâmetros de processo (alcançáveis ou não experimentalmente) para o qual o processo seja economicamente viável?

A abordagem utilizando o preço mínimo de venda, porém, ainda não é suficiente para avaliar tal questão. Para respondê-la de forma mais completa, é necessária uma inversão da ordem em que as análises tecno-econômicas são normalmente construídas. Ao invés realizar a avaliação tecno-econômica de cenários fixos, com os parâmetros de processo já definidos, deve-se estipular um desempenho econômico mínimo a ser alcançado e a partir disso calcular o conjunto de condições operacionais que permitem alcançar tal desempenho, unindo modelagem matemática do processo e econômica. A metodologia necessária para responder essa pergunta de forma sistemática é abordada no capítulo Capítulo 4 e a mesma é utilizada para obter uma possível resposta a essa pergunta no Capítulo 5

Furlan *et al. Biotechnology for Biofuels* 2013, **6**:142
http://www.biotechnologyforbiofuels.com/content/6/1/142

Biotechnology for Biofuels

RESEARCH Open Access

Bioelectricity versus bioethanol from sugarcane bagasse: is it worth being flexible?

Felipe F Furlan[1], Renato Tonon Filho[1], Fabio HPB Pinto[1], Caliane BB Costa[1,2], Antonio JG Cruz[1,2], Raquel LC Giordano[1,2] and Roberto C Giordano[1,2*]

Abstract

Background: Sugarcane is the most efficient crop for production of (1G) ethanol. Additionally, sugarcane bagasse can be used to produce (2G) ethanol. However, the manufacture of 2G ethanol in large scale is not a consolidated process yet. Thus, a detailed economic analysis, based on consistent simulations of the process, is worthwhile. Moreover, both ethanol and electric energy markets have been extremely volatile in Brazil, which suggests that a flexible biorefinery, able to switch between 2G ethanol and electric energy production, could be an option to absorb fluctuations in relative prices. Simulations of three cases were run using the software EMSO: production of 1G ethanol + electric energy, of 1G + 2G ethanol and a flexible biorefinery. Bagasse for 2G ethanol was pretreated with a weak acid solution, followed by enzymatic hydrolysis, while 50% of sugarcane trash (mostly leaves) was used as surplus fuel.

Results: With maximum diversion of bagasse to 2G ethanol (74% of the total), an increase of 25.8% in ethanol production (reaching 115.2 L/tonne of sugarcane) was achieved. An increase of 21.1% in the current ethanol price would be enough to make all three biorefineries economically viable (11.5% for the 1G + 2G dedicated biorefinery). For 2012 prices, the flexible biorefinery presented a lower Internal Rate of Return (IRR) than the 1G + 2G dedicated biorefinery. The impact of electric energy prices (auction and spot market) and of enzyme costs on the IRR was not as significant as it would be expected.

Conclusions: For current market prices in Brazil, not even production of 1G bioethanol is economically feasible. However, the 1G + 2G dedicated biorefinery is closer to feasibility than the conventional 1G + electric energy industrial plant. Besides, the IRR of the 1G + 2G biorefinery is more sensitive with respect to the price of ethanol, and an increase of 11.5% in this value would be enough to achieve feasibility. The ability of the flexible biorefinery to take advantage of seasonal fluctuations does not make up for its higher investment cost, in the present scenario.

Keywords: Second generation ethanol production, Techno-economic evaluation, Lignocellulose, Sugarcane, Bagasse, Process simulation

Background

It is already a consensus that a shift of the global energy matrix towards renewable sources is mandatory. Yet, the role that each specific alternative will play, say, at the year 2050, will be defined along the road, depending on technological developments, political options by stakeholders, economical and social demands. Anyway, in this scenario ethanol will certainly be an important biofuel.

Sugarcane is known to be the most efficient crop for 1G ethanol production, with an energy balance of 9.3 produced/consumed tonne of oil equivalent (toe) [1]. During the 1970's the Brazilian government initiated the National Ethanol Program (PROALCOOL, in Portuguese, [2]) to decrease national dependence on oil. Since then, the use of 1G ethanol as a vehicle fuel has been consolidated, and presently 86% of the cars sold in this country are flex-fuel, running with any mixture of ethanol and gasoline [3]. In modern facilities, ethanol production is a highly integrated process, with sugarcane bagasse burnt in boilers to supply the industrial plant energy demands, further exporting the surplus of electric energy to the grid.

*Correspondence: roberto@ufscar.br
[1]Chemical Engineering Graduate Program, Federal University of São Carlos, PPGEQ/UFSCar Via Washington Luis, km 235, São Carlos, SP, Brazil
[2]Department of Chemical Engineering, Federal University of São Carlos, DEQ/UFSCar Via Washington Luis, km 235, São Carlos, SP, Brazil

One of the alternatives for the industrial production of 2G ethanol is the biochemical route, i.e., acid or enzymatic hydrolysis of the biomass followed by fermentation of the resulting sugars. Logistics and transportation of the lignocellulosic raw material may be a bottleneck for 2G ethanol [4]. From this point of view, sugarcane bagasse has an important advantage, since it has already been collected and processed for the extraction of the juice, being immediately available at the plant site. Moreover, sugarcane trash (mostly the leaves) can be transported with the stalk, after small adaptations of the mechanical harvesting – although part of this biomass must be left for covering the fields [5]. Since the process must be energetically self-sufficient, the addition of sugarcane trash as boiler fuel can increase the amount of bagasse available for hydrolysis, therefore enhancing ethanol yields.

Industrial production of 2G ethanol is still not consolidated in large scale. Therefore, an economic analysis is important to indicate if it is the most interesting alternative, specially when compared to selling electric energy (bioelectricity). Nevertheless, this answer is not unique, given the volatility of relative prices: biomass electricity prices in public auctions in Brazil ranged from 85.35 USD/MWh to 53.02 USD/MWh in the last two auctions (Aug/2010 and Aug/2011) [6], a -37.9% variation. The spot market (that buys surplus power, beyond the amount contracted during the auctions) presented an even higher range of prices, between 3.26 USD/MWh and 341.13 USD/MWh over the last nine years (Jan/2003 - Dez/2012) [7]. Ethanol prices are equally volatile, changing from 0.258 USD/L to 0.818 USD/L (for the hydrated fuel) over the same period of nine years [8]. All prices above, used in this study, were calculated in Brazilian reais, brought to December/2012 value (to take into account the inflation in the period), and converted to US dollars using the exchange rate value of 2.077 BRL/USD (dez/2012).

Sugarcane biorefineries have been intensively studied by the recent literature. Seabra *et al.* (2011) [9] presented economic and environmental analyses of a sugarcane biorefinery. The authors concluded that, although electric energy presented a better economic feasibility, its environmental impact was greater than the one for second generation ethanol. An economic analysis comparing 2G ethanol production with electric energy was also done by Dias *et al.* (2011) [10]. The authors concluded that, although for the present technology electric energy is a better option, 2G ethanol can compete with it if sugarcane trash is used, provided that new technologies could increase yields. On the other hand, Macrelli *et al.* (2012) [11] presented results for several sugarcane biorefineries configurations and concluded that 2G ethanol from sugarcane is already competitive with 1G starch-based ethanol in Europe. The advantages of the integrated production of 1G and 2G ethanol production based on sugarcane was highlighted by Dias *et al.* (2012) [12]. The integrated biorefinery presented higher ethanol production rates, and better economic and environmental performance, when compared to a stand-alone 2G ethanol-from-sugarcane bagasse plant.

The 2G biorefinery could be flexible, just as the industry that employs current 1G technology already is, shifting between sugar and ethanol production. This new flexible biorefinery might be able to choose between electric energy and 2G ethanol production. The present study focuses on assessing the economic feasibility of a flexible biorefinery, for an autonomous distillery (not considering the manufacture of sugar), and comparing it to the dedicated 1G + electric energy and 1G + 2G ethanol biorefineries. The process chosen as case study uses enzymatic hydrolysis of the biomass (sugarcane bagasse) and ethanolic fermentation of hexoses and pentoses. Specifically, this study presents a computational applicative that may be a useful tool for the process scheduling of future cane-based biorefineries but, beyond that scope, that may also support decision-making concerning national energy policies. Such computationally robust tool was developed within an equation-oriented simulator (EMSO) [13] and is based on phenomenological modelling, at least for the most important unit operations and reactors that are present in the process.

Results and discussion

Process simulation

Two boundary process configurations were considered and compared: an industry producing 1G ethanol and burning all sugarcane bagasse and 50% of the trash produced in the field for power generation in a Rankine cicle (BioEE) and another one using all bagasse surplus (the biorefinery must be energetically self-sufficient) for 2G ethanol production, integrated to the 1G facility (BioEth). The most important information for BioEE and BioEth streams (as enumerated in Figure 1 and Figure 2) is presented in Table 1 and Table 2. 74% of the bagasse could be diverted to 2G ethanol in BioEth. This accounted for an increase in ethanol production of 25.8% when compared to BioEE. At this condition, a specific production yield for 2G ethanol of 120.7 L/tonne of bagasse was obtained, which is a conservative estimate based on current yields (158 L/tonne of lignocellulosic material [12]). The increase in steam consumption for 2G ethanol was entirely fulfilled by the burning of lignin and of non-hydrolyzed cellulose. Since 65% of the cellulose was hydrolyzed, 35% of the material was still able to be separated and used as fuel. Table 3 shows ethanol production (total and specific) for both cases.

As shown in Table 4, the steam demand increased by 56.3% from BioEE to BioEth. This represented a steam

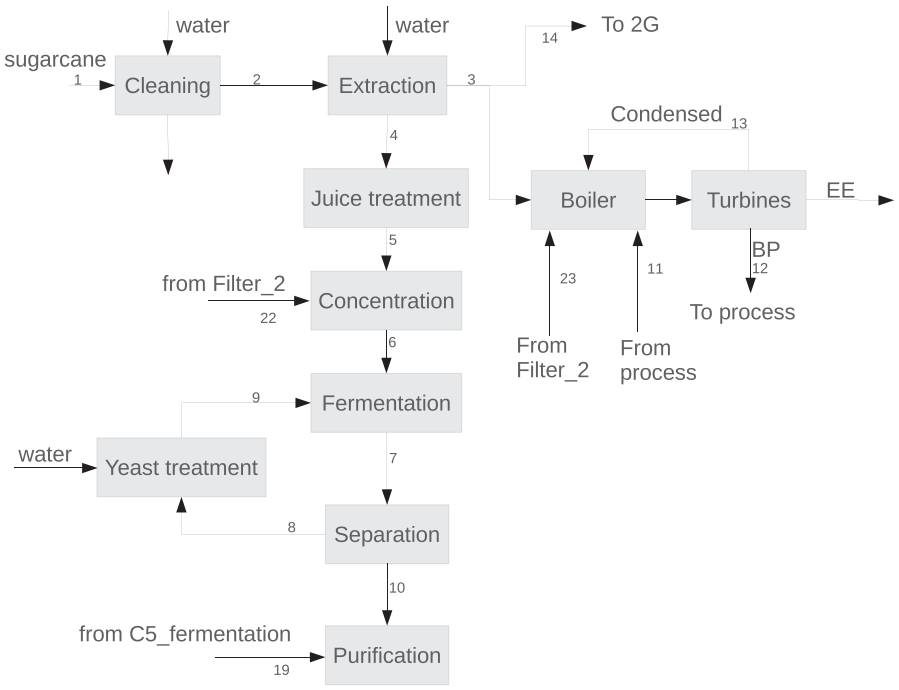

Figure 1 Process diagram for first generation ethanol production.

consumption of 8.8 kg of steam/L of 2G ethanol, compared to 4.0 kg of steam/L of 1G ethanol. This higher consumption was mainly caused by the low concentration of both glucose in the hydrolyzed liquor (9 wt% compared to 17.7 wt% for sugarcane juice) and of ethanol in the C5 wine (21.3 g/L compared to 78.8 g/L for C6 wine). Nevertheless, the higher energy demand of 2G ethanol was diluted by the 1G's, and the overall specific steam consumption was 5.0 kg of steam/L of ethanol (1G + 2G).

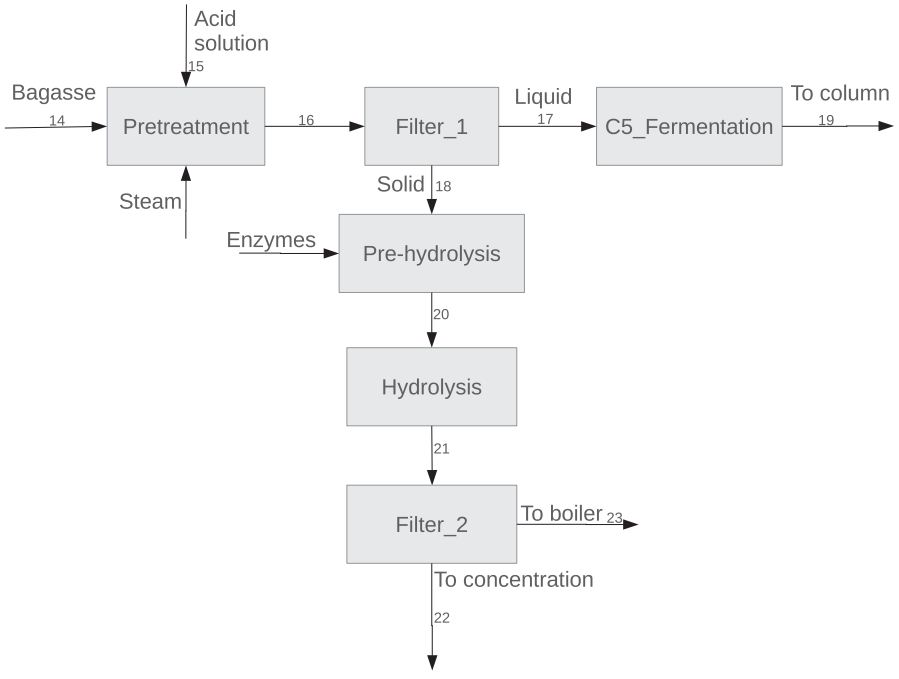

Figure 2 Process diagram for second generation ethanol production.

Table 1 Main streams for 1G + Cogeneration biorefinery (BioEE)

Stream n°	Mass flow (kg/h)	Temperature (°C)	Pressure (bar)	Fraction of sugars
1	500000	30	1	0.145
2	495675	30	1	0.144
3	131791	30	1	0.02
4	512584	30	1	0.134
5	513565	90	1	0.133
6	389697	111.7	1	0.177
7	578699	31	1	0
8	90016	31	1	0
9	189003	30	1	0
10	488683	31	1	0
11	299182	110.5	2.5	0
12	293196	189.3	2.5	0
13	193026	55.7	0.1	0

Table 5 presents the energy demand by plant sector. Since not all electric power produced was consumed in BioEth, it delivered electric energy to the grid, too. It is clear that the impact of the production of 2G ethanol on the overall energy demand was low. The major impact, in fact, was on the condensing turbine, since all bagasse surplus was diverted to 2G ethanol production. Therefore, this turbine was absent in the BioEth plant.

Economic analysis

An economic analysis was performed for both process configurations described above (BioEE and BioEth). Besides, a flexible biorefinery (Flex), which can switch between cogeneration and 2G ethanol, was also considered. This option might enable a better exploitation of the seasonality of both ethanol and electric energy prices (Table 6).

Since the condensing turbine is not necessary for BioEth and, moreover, steam production in this case was lower than in BioEE, the investment in the combined heat and power plant decreased from BioEE to BioEth. On the other hand, an increase in costs for fermentation, distillation and tankage was necessary in BioEth to account for the higher ethanol production. For the flexible biorefinery, it must be suitable for both maximum ethanol and maximum electric energy production, which makes its investment costs the highest. Table 7 presents the investment costs for the cases considered.

The flexible biorefinery (Flex) allows the decision (considered here to be in a monthly basis) to operate between the two boundary cases represented by BioEE and BioEth. Table 8 shows the chosen option (between electric energy or 2G ethanol) over the whole period considered. It is worth mentioning that both earnings and costs were equally distributed through the year for the flexible biorefinery. Therefore, ethanol and/or bagasse must be stocked to assure the selling during the off-season period. As reported by Agblevor et al. [14], bagasse composition is not greatly affected by storage period, even when it is exposed to weather conditions. The authors verified that only the upper third and the outer region of the dry interior were attacked by micro-organisms and had their composition changed in a period of 26 weeks.

Table 2 Main streams for 1G + 2G biorefinery (BioEth)

Stream n°	Mass flow (kg/h)	Temperature (°C)	Pressure (bar)	Fraction of sugars
1	500000	30	1	0.145
2	495675	30	1	0.144
3	131791	30	1	0.02
4	512584	30	1	0.134
5	513565	90	1	0.133
6	332396	111.7	1	0.206
7	493607	31	1	0
8	76920.5	31	1	0
9	161212	30	1	0
10	416687	31	1	0
11	196577	110.5	2.5	0
12	188785	189.3	2.5	0
13	0	55.7	0.1	0
14	97613.3	30	1	0.02
15	174018	30	1	0
16	271631	120	2	0.02
17	201087	100	1	0.02
18	70544	100	1	0.01
19	201045	27	1	0.02
20	153036	50	1	0.02
21	153036	50	1	0.08
22	104925	50	1	0.09
23	48111	50	1	0.05

Table 3 First and second generation ethanol production rates

	BioEE	BioEth
Ethanol production (L/h)	45796.6	57580.8
Specific ethanol production (1G + 2G) (L/tonne of sugarcane (TC))	91.6	115.2
2G ethanol production (L/h)	0	11784.2
Specific 2G ethanol production (L/tonne of bagasse (TB))	0	120.7

Plant capacity: 500 tonnes of sugarcane per hour.

Table 4 Steam consumption (total and specific)

Sector	Steam consumption (total (kg/h) / specific (kg/TC))	
	BioEE	BioEth
Juice treatment	51971/103.9[a]	51971/103.9[a]
Concentration	185240/370.5	241210/482.6
Distillation	121775/243.5[a]	188455/376.9[b]
Pretreatment*	0	38493/394.3
Total	**185240/370.5**	**289550/579.1**

*Steam specific consumption in kg/TB.
[a]Uses steam from concentration step.
[b]Uses both steam from concentration step and from the back pressure turbine (5.2% of the latter).
Plant capacity: 500 tonnes of sugarcane per hour.

The results of the economic analysis are presented in Table 7. Both IRR and Net Present Value (NPV) showed similar results, with BioEth being the best option, followed by the flexible biorefinery. As it can be seen, none of the options presented a positive NPV or, equivalently, an IRR higher than the Minimum Acceptable Rate of Return (MARR), assumed to be 11%/yr, when the present market prices for ethanol and electric energy in Brazil are considered. Nevertheless, as it will be shown later in the sensitivity analysis, an increase in ethanol price of 21.1% can turn all options feasible. Besides, specifically for the BioEth biorefinery, an increase of only 11.5% in this price would assure feasibility.

Unfortunately, a direct comparison of the obtained result with the ones from literature is not a straightforward task. There is a large variability in the economic premisses and in the technical solutions for the biorefineries that can be considered in a techno-economic study. For example, Seabra and Macedo (2011) [9] considered a 2G biorefinery adjacent to the 1G industrial plant (i.e., not sharing utilities and equipment, just importing bagasse), while Dias et al. (2011) [10] and Macrelli et al. (2012) [11] considered that 1G and 2G production plants were integrated (in different degrees). Even when similar processes are considered, the results can be quite different: while the autonomous 1G industrial plant in Dias et al. (2011) [10] obtained an IRR of 15.9 %, in Macrelli et al. (2012) [11] a similar plant obtained an IRR of 32.1 %.

Table 5 Power consumption divided by sector (positive values for produced energy and negative for consumed)

Sector	Power demand/production (kW)	
	BioEE	BioEth
Mills	-6368.7	-6368.7
Pretreatment	0	-62.0
Hydrolysis	0	-246.4
Centrifuges	-380.9	-599.6
Pumps	-1389.8	-1055.9
Back pressure turbine	+32106.7	+49863.9
Condensing turbine	+48051.6	0
Total	**+72019**	**+41531.3**

Table 6 Ethanol and electric energy average seasonality over the period 2003-2012

Month	Ethanol (%)	Electric energy (spot market) (%)
January	11.19%	22.97%
February	7.64%	-24.71%
March	9.29%	-27.39%
April	5.76%	-31.52%
May	-8.90%	-26.25%
June	-12.61%	-16.08%
July	-8.79%	-5.77%
August	-6.53%	-11.77%
September	-5.37%	20.39%
October	-1.11%	40.86%
November	2.81%	41.92%
December	6.60%	17.36%

Percentage variation from the average mean.

Sensitivity analysis

Since ethanol prices presented an approximately normal distribution, its standard deviation was calculated and a variation equivalent to one standard deviation (20.5%) was used for the sensitivity analysis. On the other hand, electric energy price (spot market) did not present a normal distribution and its influence was better seen when the double of its current price was considered. Therefore, for

Table 7 Investment costs by sector of the biorefinery, internal rate of return and net present value

Sector	Cost (10^6 USD)		
	BioEE	BioEth	Flex
Sugarcane reception, preparation and milling	38.5	38.5	38.5
Combined heat and power plant	50.2	42.9	50.2
Fermentation, distillation and tankage	30.8	35.4	35.4
Sugarcane juice treatment	23.1	23.1	23.1
Piping, general tankage and valves	15.4	15.4	15.4
Licenses, project and ground leveling	7.7	7.7	7.7
2G (pre-treatment, hydrolysis and C5 fermentation)	0	9.6	9.6
Total	**165.8**	**172.7**	**180.0**
IRR*	**7.6%**	**8.3%**	**8.0%**
NPV (10^6 USD)*	**-34.5**	**-30.0**	**-41.8**

*for an ethanol price of 513.7 USD/m^3.

Table 8 Chosen option between electric energy surplus (EE) and 2G ethanol production (2G) for the flexible biorefinery

Month	1st to 8th year	9th to 13th year	14th to 25th year
January	2G	2G	2G
February	2G	2G	2G
March	2G	2G	2G
April	2G	2G	2G
May	2G	2G	2G
June	2G	2G	2G
July	2G	2G	2G
August	2G	2G	2G
September	EE	2G	2G
October	EE	EE	2G
November	EE	2G	2G
December	2G	2G	2G

The numbers in the first row are the interval of years for which the behavior of the flexible biorefinery remained constant. Spot energy price assumed to be equal to twice its current value (80.2 USD/MWh).

this case a variation of 40% was considered and, for the other ones that had only punctual data available, a variation of 20% was chosen, thus assuming a percent variation similar to the one in ethanol prices. For Flex sensitivity analysis, the variations described were applied before the simulation of the seasonality effect on the prices.

Figure 3 presents the sensitivity analysis of electric energy selling prices in public auctions on the IRR. As expected, the influence was higher for BioEE, since it has the higher amount of electric energy being sold in public auctions. BioEth and Flex produced the same amount of electric energy to be sold in the auction market. Therefore, both were equally influenced by the variation in auction prices. As it can be seen, the effect of the electric energy price on the biorefineries economic performance was not strong enough to make them feasible. The cash flow provided by the selling of electric energy was one order of magnitude smaller than the one for ethanol.

Electric energy prices in the spot market only influenced Flex's IRR (Figure 4). The sensitivity to this parameter was quite small, though. As seen in Table 8, only a few months were dedicated to electric energy production, even when the spot market price was assumed equal to twice its current value. The income from electric energy sold in the spot market was small, compared to the one coming from public auctions. It should be mentioned that an increase in both auction and spot prices can be expected in the near future in Brazil. Thermoelectric plants using natural gas currently complement the production of hydroelectric energy during the dry period, and this is hardly sustainable, both in economic and environmental perspectives. Therefore, an increase in these prices, associated with improvements in the distribution grid, could stimulate investments in cogeneration.

It is worth noticing that while Flex could reproduce almost perfectly the behaviour of BioEth (except for the higher investment cost), the same was not true for BioEE. This is due to the fact that the latter sold all its available electric energy in the auction market, which pays higher prices (in general), while the flexible biorefinery would not do this.

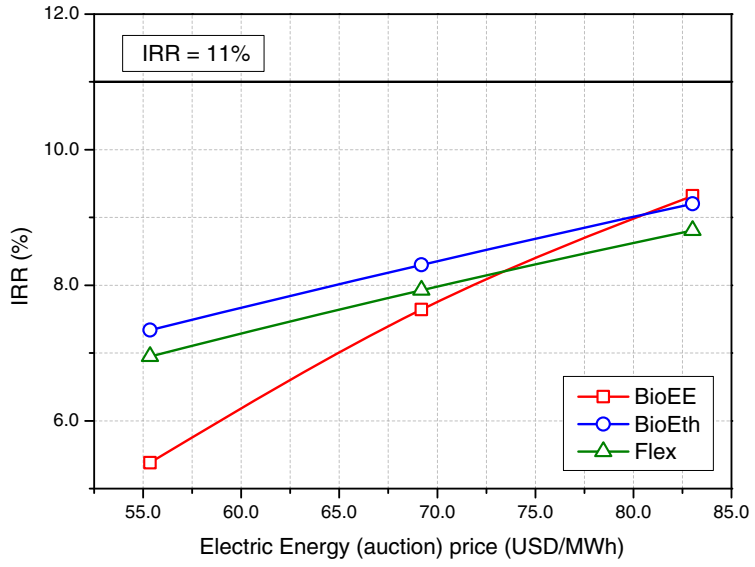

Figure 3 Impact of electric energy selling prices (annual auctions) on the internal rate of return. All other prices kept unchanged.

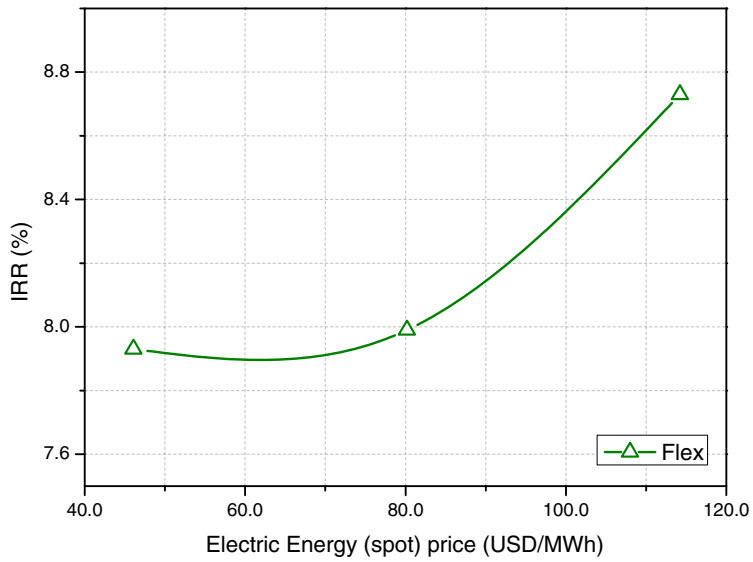

Figure 4 Impact of electric energy selling prices (spot market) on the internal rate of return. The central point corresponds to a price (80.2 USD/MWh) equal to twice the current value. All other prices kept unchanged.

The sensitivity with respect to enzyme prices was not as significant as initially expected (Figure 5). Although enzyme costs played a major role in composing 2G ethanol prices (75% of the total cost), this influence was diluted by the 1G ethanol costs. Therefore, the overall ethanol costs (1G + 2G) changed from 416.3 USD/m^3 (for an enzyme price of 2.02 USD/kg) to 392.6 USD/m^3 (for an enzyme price of 1.35 USD/kg), a variation of 5.9%, for a 40% reduction in enzyme price.

Figure 6 shows the impact of ethanol selling prices on the IRR for the current price for electric energy in spot market (a) and for a price equal to twice its current value (b). It is clear that ethanol price presented the higher influence for all biorefineries. In fact, it was the only factor strong enough to make the biorefineries economically feasible, within the range spanned in this study. Accordingly, BioEE, BioEth and Flex became feasible for an ethanol price of 622.1 USD/m^3, 572.8 USD/m^3 and 583.1 USD/m^3, respectively. This means an increase

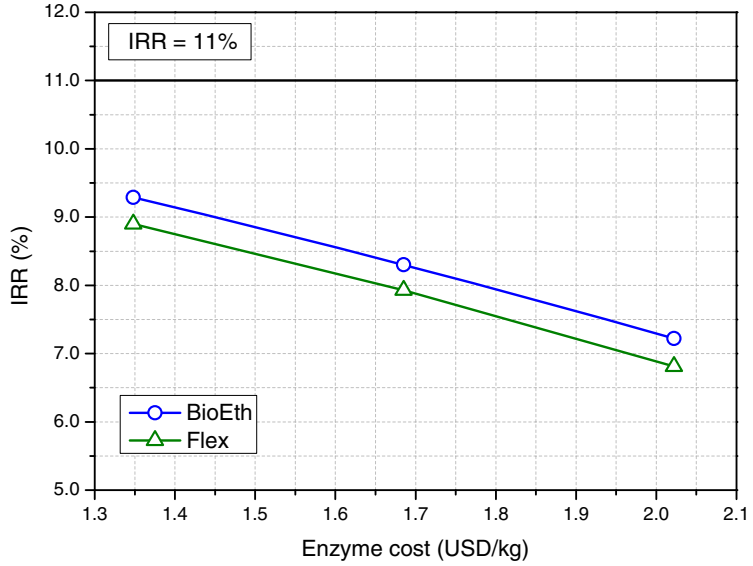

Figure 5 Impact of enzyme costs on the internal rate of return. All other prices kept unchanged.

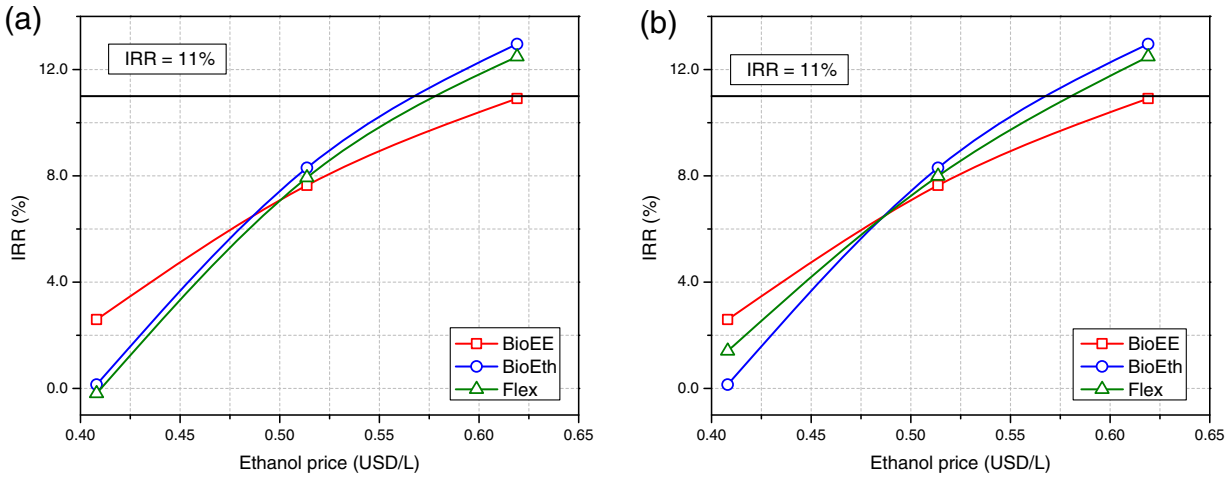

Figure 6 Impact of ethanol selling prices on the internal rate of return. In **(a)**, the current spot energy price (40.1 USD/MWh) is considered, while in **(b)** a spot energy price of twice this value (80.2 USD/MWh) is used. All other prices kept unchanged.

in ethanol price of 21.1%, 11.5% and 13.5%, respectively. While in Figure 6 (a) it is clear that BioEth was always superior to the flexible biorefinery, when a higher price in the spot market was considered (Figure 6 (b)) the flexible biorefinery became less influenced by negative variations of the ethanol price. The switch towards electric energy production for the flexible biorefinery is clear in this case. If the current ethanol price were considered, no extra electric energy was produced in any month for the whole period considered (25 years). On the other hand, when ethanol price is on its lower value, the flexible biorefinery switched to electric energy production during 30% of the months, becoming superior to BioEth.

The non-linear behaviour of the system becomes evident in Figure 6. This is mostly caused by the fact that both tax rates and dividends only apply when there is profit. Therefore, the positive influence of an increase in ethanol prices on the IRR is attenuated by both of them and the second derivative of these curves is negative.

Since there are many uncertainties regarding the investment costs on the second generation ethanol production process, a sensitivity analysis was also performed for this parameter. Maximum and minimum values of twice and

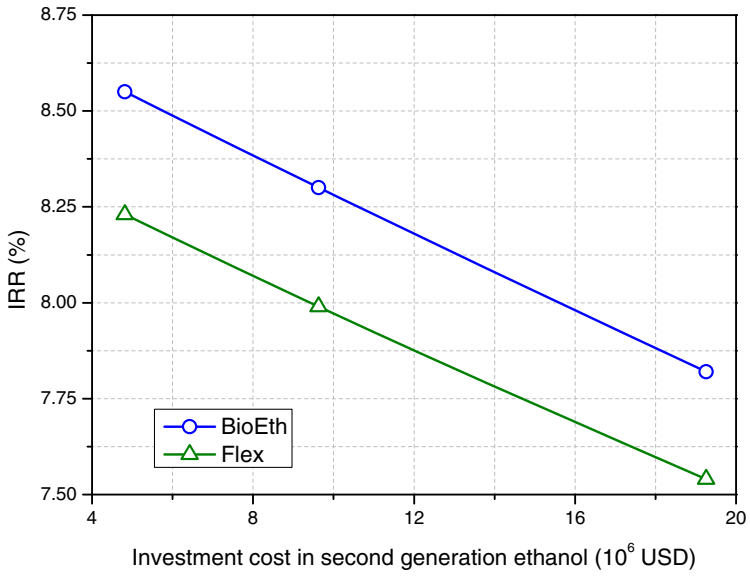

Figure 7 Impact of the investment cost on second generation ethanol on the internal rate of return. All other prices kept unchanged.

Table 9 Main data for first generation ethanol production

Input	Value	Unit
Sugarcane flow	500	tonne/h
Sugarcane TRS (Total Reducing Sugars)	15.86	% w/w
Cleaning section		
Sugar losses	1.5	%
Cleaning efficiency	70	%
Water flow	1	kg/kg of sugarcane
Sugar extraction section		
Sugarcane bagasse humidity	50	% w/w
Sugar recovery (first mill)	70	%
Sugar recovery (total)	96	%
Duty	16	kWh/tonne of fiber
Water flow	30	% w/w
Sugarcane juice treatment section		
CaO flow	2	kg/tonne of juice
CaO concentration	10	% w/w
Heating final temperature	105	°C
Steam used	53698	kg/h
Water losses in flash	6495.5	kg/h
Polymer	3534	kg/h
Polymer concentration	0.05	% w/w
Sugar losses (decanter)	6.8	%
Sludge humidity	50	% w/w
Clarifier temperature (after decanter)	92	°C
Sugar losses (filter)	5.6	%
Filter cake humidity	70	% w/w
Water flow (filter)	116	%
Sugarcane juice concentration section		
Evaporators area	8000	m^2
Outlet sugar concentration	21.4	% w/w
Steam consumption	190584	kg/h
Steam produced	181657	kg/h
Pressure of steam produced	2.5	bar
Fermentation section		
Fermentation yield	89	%
Yeast concentration (wine)	14	% w/w
Wine ethanol concentration	9	°GL
Yeast concentration (after separation)	70	% w/w
Ration of yeast rich stream / sugar solution	33	% w/w
Ethanol purification section		
Specific steam consumption (1G)	2.7	kg/L of ethanol
Specific ethanol production (1G)	91.6	L/tonne of sugarcane
Specific vinasse + phlegm production (1G)	10.1	kg/L of ethanol

half the base investment cost for the 2G ethanol process were considered. As seen in Figure 7, the impact of the investment cost on the IRR is small. The decrease in IRR between the maximum and minimum investment costs was only of -0.72% and -0.68% for BioEth and Flex, respectively. Therefore, it is expected that the uncertainty of this value will not invalidate the analyses performed.

It is worth highlighting that the 2G process is coupled to the 1G process, which is responsible for the low investment cost of the former, when compared to literature [15], because costs of fermentation, distillation and combined heat and power stages are included in our 1G cost, which is scaled proportionally to the combined process flows.

Conclusions

A flexible sugarcane biorefinery (Flex) was simulated and compared to dedicated first generation + cogeneration (BioEE) and first + second generation ethanol (BioEth) biorefineries. The flexible one presented an inferior economic performance in all cases for 2012 market prices. Nevertheless, if an increase in electric energy prices in the spot market were considered, the flexible biorefinery could be the best option.

In general, all biorefineries were not economically feasible for 2012 selling prices and costs. This conclusion was actually validated in practice by recent governmental actions (April/2013) which aimed to improve the competitiveness of the ethanol industry. Additionally, of all parameters considered in the sensitivity analysis, ethanol prices were the only ones that could make the biorefineries economically viable, within the studied range of values. In fact, an increase in ethanol price of 21.1% would be sufficient to make feasible all biorefineries. Particularly for BioEth, a 11.5% increase in ethanol prices would be enough for viability.

Enzyme prices, on the other hand, were less significant than it could be expected. This is due to the fact that 2G ethanol costs were diluted by 1G ethanol's, produced

Table 10 Main data for the cogeneration system

Parameter	Value	Unit
Cellulose LHV[a]	15997.1	kJ/kg
Hemicellulose LHV[a]	16443.3	kJ/kg
Lignin LHV [a]	24170	kJ/kg
Boiler outlet vapor pressure	65.7	bar
Boiler outlet vapor temperature	520	°C
Boiler efficiency	92	%
Back-pressure turbine outlet pressure	2.5	bar
Back-pressure turbine efficiency	68	%
Condensing turbine efficiency	70	%

[a] Lower Heating Value (LHV) calculated using data from Wooley and Putsche [18].

in higher volumetric rates. Therefore, the overall ethanol production cost in the integrated plant was not greatly influenced by enzyme prices.

Finally, it is obvious that the quantitative results presented here are dependent on the economic scenario proposed and on the assumed process yields and energy demands, but the presented methodology is general.

Methods

Process implemented

The 1G ethanol production process was simulated based on a typical industrial plant. Figure 1 shows the main required operations. First, sugarcane is cleaned with water to remove dirt carried during harvesting. Next, the sugars are extracted by mechanical pressure. The solution containing the extracted sucrose (juice) follows a series of steps in order to remove impurities which could decrease fermentation yields. The solution is concentrated and fermented by *Saccharomyces cerevisiae*, producing an alcoholic solution which is purified in distillation columns, producing hydrous ethanol. Table 9 shows the main parameters used in the simulations. A rigorous description of the main models used in this study can be found in Furlan *et al.* [16].

The cogeneration system was also considered in the simulations. It uses sugarcane bagasse, sugarcane trash, and alternatively, non-hydrolyzed cellulose and lignin, as fuel and produces steam and electric energy to supply process demands using a Rankine cicle. It was considered that 50% of sugarcane trash is brought from the field to be burnt in the boiler. Since around 140 kg of trash (dry basis) is produced per tonne of sugarcane [9,17], it was considered that a flow of 35 tonnes of sugarcane trash/h was fed to the boiler. If there is a surplus of electric energy, it can be sold to the grid. The cogeneration system includes a boiler, a back-pressure turbine and a condensing one. Table 10 presents the main data used in the simulation of the cogeneration system.

2G ethanol was produced via the biochemical route, using weak acid pretreatment and enzymatic hydrolysis. The main steps can be seen in Figure 2. First, bagasse is pretreated with a solution of H_2SO_4 (3 wt% at 120°C and 2 bar of pressure). At this point, most hemicellulose is hydrolyzed, increasing cellulose accessibility. A filter (Filter_1) is used to separate the solid fraction from the liquid. The solid fraction is pre-hydrolyzed in

Table 11 Main data for second generation ethanol production

Main data used in the simulation	Value	Unit
Pretreatment		
Pressure	2	Bar
Temperature	121	°C
Cellulose to glucose conversion	8.0	%
Hemicellulose to xylose conversion	74.0	%
Solid/liquid ratio	0.2	
Acid solution concentration	3	wt%
Volumetric power (mixing)[a]	342	W/m^3
Space-time	40	min
Reactor volume	182	m^3
Pre-hydrolysis		
Cellulose to glucose yield	20	%
Solid/liquid ratio	0.2	
Enzyme/Cellulose ratio	67.34 (20)	g/kg (FPU/g)
Space-time	18	h
Temperature	50	°C
Hydrolysis		
Cellulose to glucose yield	65	%, w/w
Solid/liquid ratio	0.178	
Volumetric power (mixing)[a]	302.5	W/m^3
Enzyme/Cellulose ratio	67.34 (20)	g/kg (FPU/g)
Space-time	54	h
Temperature	50	°C
C5 Fermentation		
Xylose to ethanol yield	70	%, w/w
Temperature	30	°C
Space-time	9	h

[a]Calculated using data from Pereira et al. [20].

Table 12 Economic data, base case used as reference

Process and economic data	Value
Time usage	80%
Days of operation	210 days/year
Ethanol direct/indirect costs (1G)	94.75 USD/m^3
Sugarcane costs (1G)	314.78 USD/m^3
Ethanol production cost(2G, extra cost)	290.1 USD/m^3
Electric energy production cost	38.9 USD/MWh
Ethanol transportation cost	28.9 USD/L
Administrative and general costs	1.1 USD/TC
Ethanol selling price	513.7 USD/m^3
Electric energy selling price (public auction)	69.2 USD/MWh
Electric energy selling price (spot market)	40.1 USD/MWh
Enzymes	1.68 USD/kg
Depreciation	10%(p.y.)
Minimum acceptable rate of return	11%(p.y.)
Decrease in production cost due to learning curve*	0.3(1)%(p.y.)
Tax rate (income and social contributions)	34%

*for 1G(2G).

a horizontal reactor, in order to decrease mixing power demands and water usage. The second hydrolysis is carried out in a stirred reactor without any further addition of water or enzymes. The solid fraction (non-hydrolyzed cellulose + lignin) is separated from the glucose solution in a filter and sent to the boiler to increase steam production. On the other hand, the liquid fraction is directed to the concentration step, being mixed to the 1G juice. The liquid fraction from Filter_1 is sent to a (SIF) reactor, where the xylose in the solution is transformed to xylulose and fermented by *Saccharomices cerevisiae* [19]. The resulting alcoholic solution is sent to the distillation columns with the wine from hexose fermentation. The parameters used for this section are shown in Table 11.

EMSO Software

EMSO [13] was the software chosen as the platform for the simulations in this study. It is an equation-oriented, general purpose process simulator with its own modelling language [21]. Besides the several models for the main process pieces of equipments, the software also allows the user to implement his/hers own models. The software has several numeric solvers for solution of algebraic and differential-algebraic systems, and users can plug in their own numerical routines (in C/C++ or FORTRAN). Physical and thermodynamic properties can be added to the package database by the user whenever needed.

Economic analysis

Table 12 shows the main economic premisses. Except for 2G ethanol costs, all process costs were obtained from industry (at Dez/2012). 2G ethanol cost is composed by enzyme prices plus all other costs, which are assumed equivalent to 1G's, due to the lack of industrial information on this topic. Ethanol and electric energy (spot market) selling prices were considered as the mean value over the period between Jan/2003 and Dez/2012. All values were adjusted for inflation in Brazil in the period and converted to US dollars using the exchange rate of 2.077 BRL/USD (dez/2012). For the flexible biorefinery, the economic analysis was made in a monthly basis and, for this case, both ethanol and electric energy price variations due to seasonality were considered (Table 6).

Abbreviations

1G: First generation; 2G: Second generation; BioEE: First generation biorefinery using all sugarcane bagasse (and trash) to produce electricity in a Rankine cicle; BioEth: First generation biorefinery using sugarcane bagasse surplus to produce second generation ethanol; EE: Electric energy; EMSO: Environment for Modeling Simulation and Optimization; Flex: Flexible biorefinery capable of operating as both BioEE and BioEth; IRR: Internal Rate of Return; MARR: Minimum Acceptable Rate of Return; NPV: Net Present Value; SIF: Simultaneous Isomerization and Fermentation; TB: Tonne of bagasse; TC: Tonne of sugarcane; TOE: Tonne of oil equivalent.

Competing interests

The authors declare that they have no competing interests.

Authors' contributions

FF did the process simulations in EMSO, the 2G sector economic analysis and the sensitivity tests. RT provided the economic analysis tools and did the economic analysis in the base case, for the 1G sector. FP provided the basic configuration of the 1G plant and helped with the economic analysis. RLG helped defining the technological options for the 2G process configuration (pretreatment, hexoses and pentose fermentation). CC, AC and RG worked in process integration (1G + 2G + EE). RG coordinated the work and supervised all other tasks. All authors read and approved the final manuscript.

Acknowledgements

The authors would like to thank the FAPESP BIOEN Program and the Brazilian National Council for Scientific and Technological Development (CNPq) for the financial support. The authors would also like to thank Mr. Alonso Constante Escobar (Tino), Mr. Carlos Henrique Manfredi and Mr. Marcelo Nishida for all technical information about 1G ethanol production and electric energy selling auctions.

Received: 1 May 2013 Accepted: 24 September 2013
Published: 3 October 2013

References

1. Macedo IC, Seabra JEA, Silva JEAR: **Green house gases emissions in the production and use of ethanol from sugarcane in Brazil: The 2005/2006 averages and a prediction for 2020.** *Biomass Bioenergy* 2008, **32:**582–595.
2. Zanin GM, Santana CC, Bon EPS, Giordano RLC, Moraes FF, Andrietta SR, Neto CCC, Macedo IC, Fo DL, Ramos LP, Fontana J: **Brazilian bioethanol program.** *Appl Biochem Biotechnol* 2000, **84:**1147–1163.
3. National Association of Motor Vehicles (ANFAVEA): **Brazilian automotive industry yearbook.** Tech. rep., São Paulo, 2012.
4. Gnansounou E: **Production and use of lignocellulosic bioethanol in Europe: Current situation and perspectives.** *Bioresour Technol* 2010, **101:**4842–4850.
5. Hassuani SJ, Leal MRLV, Macedo IC: *Biomass power generation: Sugarcane bagasse and trash*. Piracicaba: United Nations Development Programme and Sugarcane Technology Centre; 2005.
6. **Electric Energy National Agency – ANEEL (in portuguese).** http://www.aneel.gov.br.
7. **Electric Energy Commercialization Chamber – CCEE (acronym in portuguese).** http://www.ccee.org.br/.
8. **Center of Advanced Studies in Applied Economy – CEPEA/ESALQ/USP (in portuguese).** http://www.cepea.esalq.usp.br.
9. Seabra JE, Macedo IC: **Comparative analysis for power generation and ethanol production from sugarcane residual biomass in Brazil.** *Energy Policy* 2011, **39:**421–428. http://www.sciencedirect.com/science/article/pii/S0301421510007706.
10. Dias MO, Cunha MP, Jesus CD, Rocha GJ, Pradella JGC, Rossell CE, Maciel Filho R, Bonomi A: **Second generation ethanol in Brazil: Can it compete with electricity production?** *Bioresour Technol* 2011, **102**(19):8964–8971.
11. Macrelli S, Mogensen J, Zacchi G, et al: **Techno-economic evaluation of 2 nd generation bioethanol production from sugar cane bagasse and leaves integrated with the sugar-based ethanol process.** *Biotechnol Biofuels* 2012, **5:**22.
12. Dias M, Junqueira T, Cavalett O, Cunha MP, Jesus C, Rossell C, Filho R, Bonomi A: **Integrated versus stand-alone second generation ethanol production from sugarcane bagasse and trash.** *Bioresour Technol* 2012, **103:**152–161.
13. Soares RP, Secchi AR: **EMSO: A new environment for modelling, simulation and optimisation.** *Comput Aided Chem Eng* 2003, **14:**947–952.
14. Agblevor F, Rejai B, Wang D, Wiselogel A, Chum H: **blueInfluence of storage conditions on the production of hydrocarbons from herbaceous biomass.** *Biomass Bioenergy* 1994, **7:**213–222.

15. Eggeman T, Elander RT: **Process and economic analysis of pretreatment technologies.** *Bioresource Technol* 2005, **96**(18):2019–2025.
16. Furlan FF, Costa CBB, Fonseca GC, Soares RP, Secchi AR, Cruz AJG, Giordano RC: **Assessing the production of first and second generation bioethanol from sugarcane through the integration of global optimization and process detailed modeling.** *Comput Chem Eng* 2012, **43:**1–9.
17. Canilha L, Chandel AK, Suzane dos Santos Milessi T, Antunes FAF, Luiz da Costa Freitas W, das Graças Almeida Felipe M, da Silva SS: **Bioconversion of sugarcane biomass into ethanol: An overview about composition, pretreatment methods, detoxification of hydrolysates, enzymatic saccharification, and ethanol fermentation.** *J Biomed Biotechnol* 2012, **2012:**1–15.
18. Wooley R, Putsche V: **Development of an ASPEN PLUS physical property database for biofuels components.** *NREL,* Tech. rep., Report MP-425-20685 1996, 38.
19. Silva C, Zangirolami T, Rodrigues J, Matugi K, Giordano R, Giordano R: **An innovative biocatalyst for production of ethanol from xylose in a continuous bioreactor.** *Enzyme Microb Technol* 2012, **50:**35–42.
20. Pereira LTC, Pereira LTC, Teixeira RSS, Bon EPS, Freitas SP: **Sugarcane bagasse enzymatic hydrolysis: rheological data as criteria for impeller selection.** *J Ind Microbiol Biotechnol* 2011, **38**(8):901–907.
21. Rodrigues R, Soares RP, Secchi AR: **Teaching chemical reaction engineering using EMSO simulator.** *Comput Appl Eng Educ* 2010, **18**(4):607–618.

doi:10.1186/1754-6834-6-142
Cite this article as: Furlan *et al.*: Bioelectricity versus bioethanol from sugarcane bagasse: is it worth being flexible? *Biotechnology for Biofuels* 2013 **6**:142.

Krist V. Gernaey, Jakob K. Huusom and Rafiqul Gani (Eds.), 12th International Symposium on Process Systems Engineering and 25th European Symposium on Computer Aided Process Engineering.
31 May - 4 June 2015, Copenhagen, Denmark.

Process Alternatives for Second Generation Ethanol Production from Sugarcane Bagasse

Felipe F. Furlan[a], Roberto C. Giordano[a], Caliane B. B. Costa[a], Argimiro R. Secchi[b] and John M. Woodley[c]

[a]*Chemical Engineering Graduate Program, Universidade Federal de São Carlos, PPGEQ/UFSCar, Via Washington Luiz, km 235, São Carlos, SP, 13565-905, Brazil*
[b]*Chemical Engineering Program, COPPE, Universidade Federal do Rio de Janeiro, Av. Horácio Macedo, 2030, Rio de Janeiro, RJ, 21941-972, Brazil*
[c]*Department of Chemical and Biochemical Engineering, Technical University of Denmark, Building 229, DK-2800. Lyngby, Denmark*
felipef.furlan@gmail.com

Abstract

In ethanol production from sugarcane juice, sugarcane bagasse is used as fuel for the boiler, to meet the steam and electric energy demand of the process. However, a surplus of bagasse is common, which can be used either to increase electric energy or ethanol production. While the first option uses already established processes, there are still many uncertainties about the techno-economic feasibility of the second option. In this study, some key parameters of the second generation ethanol production process were analyzed and their influence in the process feasibility assessed. The simulated process includes the enzymatic hydrolysis of sugarcane bagasse pretreated with liquid hot water, and the analyzed parameters were the solid consistency in the hydrolysis and pretreatment reactors and the hydrolysis reaction time. The solid consistency in the hydrolysis reactor had the highest influence on the economic feasibility of the process. For the economic scenario considered in this study, using bagasse to increase ethanol production yielded higher ethanol production costs compared to using bagasse for electric energy production, showing that further improvements in the process are still necessary.

Keywords: Bioethanol, sugarcane, techno-economic analysis, process simulation

1. Introduction

The production of ethanol from sugarcane juice is well established in Brazil. In this process, sugarcane juice is extracted and used to produce ethanol, while sugarcane bagasse is sent to boilers, producing steam and electric energy to meet the process demands. However, a surplus of bagasse is frequently possible and this opens opportunities to produce and sell electric energy to the grid or alternatively to increase ethanol yields through second generation (2G) ethanol production. It is expected that these processes would be integrated to the already existing first generation (1G) ethanol process, taking advantage of the economy of scale and decreasing transportation costs. This system will be a highly integrated one with the steam and electric energy demands being met by the burning of by-products of ethanol production. Therefore, it is not a trivial task to infer the effect of some process parameters on the overall process economic performance. In this sense, process systems engineering (PSE) tools can be applied to assess these effects for some key parameters in order to provide insights about the process. Additionally, it will allow

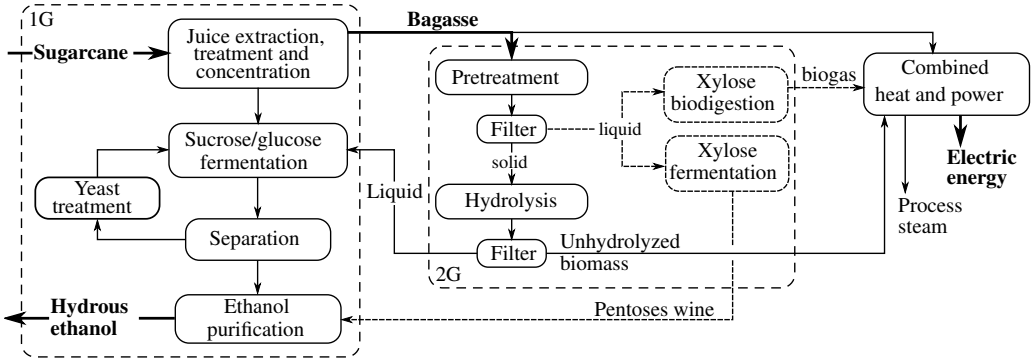

Figure 1: First and second generation ethanol production process. 1G stands for the first generation process, adapted to the integrated process, while 2G stands for the specific second generation process.

new experimental datasets to be quickly evaluated from the whole process perspective and search directions to be derived.

In this study, second generation ethanol production following the biochemical route is considered, including the enzymatic hydrolysis of sugarcane bagasse, pretreated with liquid hot water. The influence of key process parameters on the economic feasibility of the integrated process (first and second generation ethanol) was assessed. The solid consistency in the pretreatment unity and in the hydrolysis reactor were considered, along with the hydrolysis reaction time. Additionally, both fermentation and biodigestion of the pentoses produced in the pretreatment stage are studied.

2. Methodology

The process considered in this study uses liquid hot water for pretreatment of the sugarcane bagasse. The solid fraction from the pretreatment stage is hydrolyzed and the glucose solution is subsequently fermented by *Saccharomyces cerevisiae* along with the treated sugarcane juice. The liquid fraction, consisting mainly of xylose from the hemicellulose hydrolysis, can also be fermented or, alternatively, it can be anaerobically digested to produce biogas. The ethanol solution is sent to the purification stage and hydrous ethanol is produced. Unhydrolyzed cellulose and remaining lignin are separated from the liquid fraction after the hydrolysis reactor and sent to the boiler. The process steam and electric energy demands are still met by the burning of bagasse (in addition to biogas and the solid fraction from the hydrolysis reactor), which limits the amount of bagasse that can be diverted to 2G ethanol production. Therefore, the amount of bagasse diverted to this process varies for each case studied. Figure 1 shows the second generation process and how it is integrated to the (1G) ethanol process: bagasse is diverted to the 2G process, glucose liquor from cellulose hydrolysis is fermented with sugarcane juice and xylose wine is purified with 1G ethanol.

Minimum ethanol selling price (MESP) was determined as the ethanol price that yields a zero net present value. The investment costs for the first generation process were derived from Pinto (2010) and adapted to represent the integrated process. The investment in the combined heat and power stage was based on Dantas (2013) and the investment for the xylose biodigestion system was based on Procknor (2009). Finally, the investment cost of the second generation stage was based on the technical report from the National Renewable Energy Laboratory (Humbird et al., 2011). Other parameters used for the economic analysis are described in Furlan et al. (2013), while the enzyme price was updated to 10.14 USD/kg of enzyme, as reported by Klein-Marcuschamer et al. (2012)

and represents the baseline production cost for the enzyme. Additionally, since sugarcane bagasse does not have an established market price, to assess the feasibility of the process, its opportunity cost regarding electric energy production was considered. This was accomplished by comparing the surplus of electric energy produced with a base case were all bagasse is burnt.

The software EMSO (Environment for Modeling, Simulation and Optimization, Soares and Secchi (2003)) was chosen as the platform for the simulations. This is an equation-oriented simulator with its own modelling language enabling the user to add models to the ones already present in the software. EMSO has several numerical packages for solving algebraic and differential-algebraic systems and also a thermodynamic package, where the user can add compounds and properties as needed.

3. Results and Discussion

Three process parameters were considered in this study: solid consistency (solid mass fraction) in the pretreatment reactor, in the hydrolysis reactor and the hydrolysis reaction time. Table 1 shows the range considered for each parameter. The effect of the parameters were analyzed for three levels of conversion in the hydrolysis reactor: 45, 60 and 75% of the theoretical, i. e., for each set of solid consistencies in the hydrolysis reactor, in the pretreatment reactor and reaction time, three levels of conversion were evaluated.

Table 1: Ranges considered for the parameters studied. Underlined values were used as standard for each parameter when the values of the other parameters were varied.

	Solid fraction in hydrolysis reactor	Solid fraction in pretreatment reactor	Hydrolysis reaction time
Range	10, <u>20</u>,30 and 40%	10, <u>20</u> and 30%	48, <u>72</u> and 96h

As a general case, the biodigestion of xylose allowed a higher amount of bagasse to be diverted to 2G ethanol, resulting in higher ethanol production (23.0 % increase (biodigestion) vs. 21.5 % (fermentation), for the highest increase). However, it also increases investment costs, due to the biodigestors and bigger boilers. Consequently, the MESP of the biodigestion option was on average 46 USD/m^3 higher than the fermentation one. Table 2 shows the cases with the lowest MESP for the xylose fermentation and biodigestion and compares it to 1G base case, with all bagasse being burnt and electric energy surplus being produced. The use of biogas as fuel for steam production allowed 61.9 % of the bagasse to be diverted to 2G production in the biodigestion case. In this case, 50.8 % of the steam demand is met by burning the biogas and the unhydrolyzed fraction of bagasse. At the same time, the higher sugar concentration decreased the specific steam demand (kg of steam/l of ethanol) in 4.4 % compared to the 1G ethanol process. It is worth noticing that this study does not consider the use of sugarcane trash as fuel for the boiler.

As it can be seen in Table 2 the MESP for the best 1G+2G ethanol process with xylose fermentation is 6.3 % higher than the base case, although only 3.1 % higher than the ethanol selling price considered (513.7 USD/m^3, relative to the average price between Jan/2003 and Dez/2012 in Brazil). This shows that second generation ethanol still needs further development in order to compete with electric energy production, at least for the electricity prices used in this study (80.8 USD/MWh), which correspond to the average value of auctions in Brazil in the period 2005-2011.

Among the parameters considered in this study, the solid consistency in the hydrolysis reactor had the most significant effect on the economic feasibility of the process, as it can be seen in Figure 2 for the xylose fermenting case, while the other parameters had only marginal effect on the MESP. Interestingly, 2G MESP is not monotonic with respect to the solid consistency in the hydrolysis reactor, which can be related to a decrease in glucose recovery in the separation step after the

Table 2: Base case (1G burning all bagasse) and best cases (lowest 2G MESP) for the 1G+2G process, for xylose biodigestion and fermentation. Hydrolysis reaction time was 72h for the last two cases.

	1G	1G+2G (xylose biodigestion)	1G+2G (xylose fermentation)
Solid consistency (hydrolysis)	–	20 %	20 %
Solid consistency (pretreatment)	–	10 %	30 %
Hydrolysis reaction yield	–	75 %	75 %
Bagasse fraction burnt	100 %	38.1 %	48.3 %
Increase in ethanol production	–	17.6 %	20.4 %
1G+2G MESP (USD/m^3)	498.4	565.2	529.6
2G MESP (USD/m^3)	–	943.9	682.0
Steam produced (kg/TC)	522.9	404.6	380.4
Contribution to steam production (bagasse /unhydrolyzed biomass/ biogas)	100 % / 0 % / 0 %	49.2 % / 37.4 % / 13.4 %	66.4 % / 33.6 % / 0 %

hydrolysis. This suggests the importance of a washing step to increase sugar recovery when high solid consistencies are used, although in this case there will be a trade-off between sugar recovery and its final concentration in the stream.

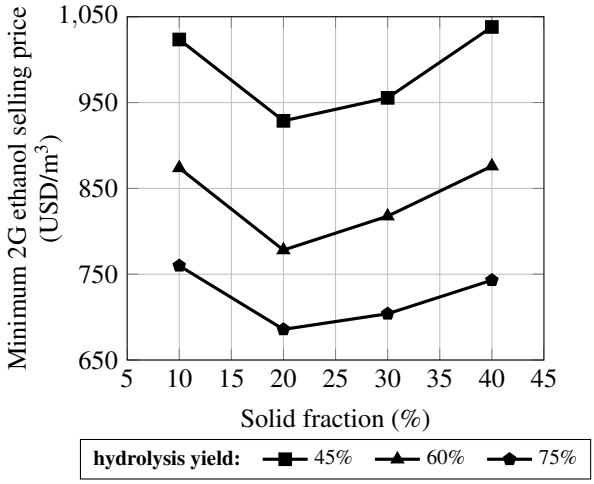

Figure 2: Influence of the solid consistency in the hydrolysis reactor on the minimum 2G ethanol selling price when xylose is fermented.

For the overall cost of ethanol (1G + 2G), sugarcane cost clearly dominated the contribution, followed by capital expenditures (CAPEX) and other operating expenses (OPEX) related to 2G production (enzyme cost, electric energy opportunity cost and other raw material costs), as shown in Figure 3a. The specific 2G cost, on the other hand, is highly dominated by the enzyme costs which is on average 42 % of the total production costs, while the CAPEX cost (second higher) accounts for 23 % of the total cost. The solid consistency in the hydrolysis reactor has a clear effect on the enzyme and CAPEX cost contributions while its effect on the other components of 2G ethanol costs are much weaker, as shown in Figure 3b. Also, it can be inferred that the effect of solid consistency on MESP decreases for higher yields. Since more ethanol is produced for higher yields, the influence of the parameter is softened.

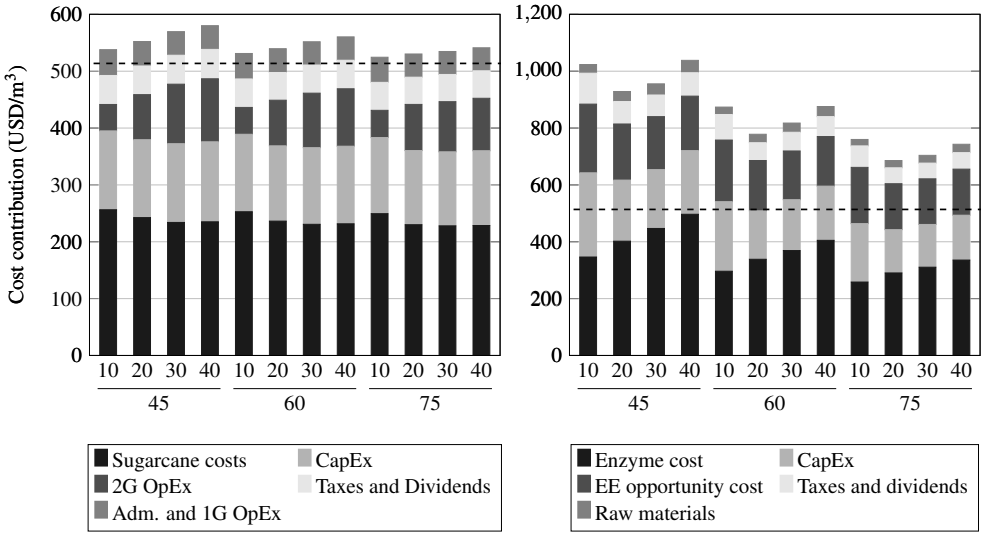

(a) Overall production cost of ethanol. (b) production cost of 2G ethanol.

Figure 3: Influence of the solid consistency in the hydrolysis reactor (10–40% m/m) and of the hydrolysis yield (45–75% of the theoretical) on the overall production cost of ethanol (a) and on 2G ethanol (b) when xylose is fermented. The dashed line represents the current selling price for ethanol.

To assess the current state of the technology and its feasibility, the yields reported by Souza et al. (2014) for the enzymatic hydrolysis of sugarcane bagasse pretreated with liquid hot water were used. Based on these data, Figure 4 shows the 2G MESP obtained, for the process with xylose fermentation to ethanol. It can be seen that 2G MESP generally decreased for the whole time range considered in the study, showing that the negative effect of the reaction time on 2G MESP is in general lower than the positive effect of the increase in the yield. Only for the higher solid consistency (20%), an increase in 2G MESP is seen in the final hours of reaction. If results similar to the best experimental ones (solid consistency of 15 % and 72 hour of hydrolysis reaction) could be obtained in industrial scale, an increase in ethanol production of 13.9%, with a MESP of 540.3 USD/m^3 (841.9 USD/m^3 for the 2G MESP) could be expected.

4. Conclusions

An integrated first and second generation ethanol industrial plant based on the enzymatic hydrolysis of sugarcane bagasse pretreated with liquid hot water was simulated, and its economic feasibility assessed. In general, for the economic scenario considered, the second generation ethanol cost was higher than the first generation one, even when high solid consistencies in the reactors was considered. This shows that the process still needs further developments in order to compete with electric energy production. Xylose fermentation to ethanol yielded lower MESPs than its biodigestion, although the latter option allowed a higher ethanol production. Among the process parameters considered, the solid consistency in the hydrolysis reactor showed the strongest influence on 2G MESP: the lowest prices were between 20 and 30% of solids, with a slight increase after that. Additionally, simulations based on experimental yields reported in the literature showed that, for the time range considered for the hydrolysis reaction, its negative effect on the 2G MESP was lower than the positive effect of the increase in the yield. For the experimental data considered, a MESP of 540.3 USD/m^3 could be reached if similar results were to be achieved in industrial scale. This is 5.2% higher than the prices in Brazil in the period 2002-2012, but 8.4%

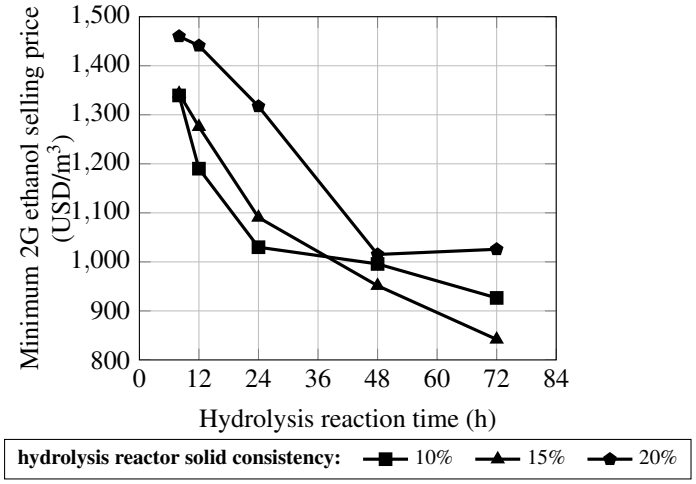

Figure 4: Minimum ethanol selling price considering experimental data reported by Souza et al. (2014) and xylose fermentation.

higher than the MESP for the stand alone 1G process.

5. Acknowledgements

The authors would like to thank CAPES (fellowship process n° 2608/14-6) for the financial support.

References

Dantas, G. A., 2013. Investment alternatives for the sugarenergetic sector for exploitation of sugarcane bagasse and straw. PhD thesis, Universidade Federal do Rio de Janeiro, Rio de Janeiro, in Portuguese.

Furlan, F. F., Filho, R. T., Pinto, F. H. P. B., Costa, C. B. B., Cruz, A. J. G., Giordano, R. L. C., Giordano, R. C., 2013. Bioelectricity versus bioethanol from sugarcane bagasse: is it worth being flexible? Biotechnology for Biofuels 6 (142), 1–12.

Humbird, D., Davis, R., Tao, L., Kinchin, C., Hsu, D., Aden, A., Schoen, P., Lukas, J., Olthof, B., Worley, M., Sexton, D., Dudgeon, D., 2011. Process design and economics for biochemical conversion of lignocellulosic biomass to ethanol. Tech. rep., National Renewable Energy Laboratory.

Klein-Marcuschamer, D., Oleskowicz-Popiel, P., Simmons, B. A., Blanch, H. W., 2012. The challenge of enzyme cost in the production of lignocellulosic biofuels. Biotechnology and bioengineering 109 (4), 1083–1087.

Pinto, F. H. P. B., 2010. Cellulosic ethanol: a study of economic and financial viability. Masters thesis, Universidade de São Paulo, São Paulo, in Portuguese.

Procknor, C., 2009. Electric energy from vinasse. In Portuguese. http://www.unica.com.br/convidados/2564115692037715081/energia-eletrica-a-partir-da-vinhaca/.

Soares, R. P., Secchi, A. R., 2003. Emso: A new environment for modelling, simulation and optimisation. Computer Aided Chemical Engineering 14, 947–952.

Souza, R. B. A., Corrêa, L. J., Suarez, C. A. G., Cruz, A. J. G., 2014. Evaluation of the effect of the solid consistency in the enzymatic hydrolysis of sugarcane bagasse and comparisson between different comercial enzymatic mixtures. In: Brazilian Congress in Chemical Engineering. pp. 1–8, in Portuguese.

4 Reversão da análise econômica: metodologia e estudo de caso

Como descrito no capítulo anterior, a questão que se coloca quando um novo processo está sendo desenvolvido é se tal processo em questão pode vir a se tornar economicamente viável (considerando um contexto econômico) e qual o desempenho necessário para que isso ocorra. Vários métodos se preocupam em eliminar as rotas menos promissoras, seja utilizando métodos heurísticos de síntese de processos, seja utilizando métodos mais sistemáticos, como otimização super-estrutural (HARMSEN, 2004). Outros métodos utilizam valores mínimos para as métricas de processo para avaliar a viabilidade de processos em estágios iniciais de desenvolvimento sem para isso recorrer diretamente à análise econômica dos mesmos (TUFVESSON et al., 2011; RAMOS, 2013; TUFVESSON et al., 2013). Faixas de valores são utilizados para essas métricas nesses métodos, o que os tornam insensíveis às especificidades de cada processo. Assim, nenhuma dessas abordagens faz a ligação entre as áreas de engenharia de (bio)processos e sistemas e engenharia econômica para derivar valores mínimos de desempenho para que o processo seja viável. Um agravante advém do fato de que o número de variáveis que afetam o desempenho econômico do processo é normalmente grande. Isso faz necessário um tratamento sistemático, para eliminar as menos influentes e focar nas que apresentam maior efeito. A Análise Tecno-Econômica Reversa (ATER) apresentada neste capítulo tem exatamente esse objetivo: apresentar uma forma sistemática de determinar as variáveis que mais afetam o desempenho econômico do processo e a partir disso derivar seus valores mínimos necessários para isso e a correlação entre estas.

Para que esse objetivo seja alcançado, é imprescindível que as equações empregadas na análise econômica sejam inseridas no próprio simulador. Desta forma, o resultado da análise econômica pode ser obtido em tempo de simulação e a reversão da análise tecno-econômica se torna possível sem recorrer a um processo iterativo externo ao simulador. Interessante notar que o conjunto de equações necessárias para o cálculo do desempenho econômico da planta é bastante simples e sua adição ao sistema de equações não acarreta problemas de convergência na análise tecno-econômica clássica, onde as variáveis de processo são especificadas e o desempenho econômico é calculado. Por outro lado, ao fixar a variável de desempenho econômico ao invés de uma das variáveis de processo abre-se a possibilidade para problemas de convergência que derivam dessa variável (ou outra dependente dessa) cruzar um de seus limites

físicos. Por exemplo, uma conversão ser superior a 100 % para que o desempenho econômico seja alcançado. A metodologia deve ser capaz de prevenir que tal problema ocorra, e isso é de fato atingido pela escolha cuidadosa das variáveis analisadas.

A descrição detalhada da metodologia desenvolvida bem como os principais resultados obtidos no estudo de caso descrito são apresenados a seguir, no artigo *Retro-Techno-Economic Analysis (RTEA): using (bio)process systems engineering tools to attain process target values*, submetido à revista indexada em fevereiro de 2016. Ademais, o material complementar do artigo apresenta todas as equações utilizadas tanto na modelagem do processo quanto do desempenho econômico do mesmo.

Uma limitação da metodologia foi observada ao testá-la no estudo de caso proposto. Por causa da reversão do problema, problemas de convergência podem ocorrer causados por descontinuidades na modelagem do processo. Tal problema surgiria caso a função que descreve a relação entre a variável do desempenho econômico e a variável de processo seja descontínua exatamente no ponto de interesse, ou seja, no valor especificado de desempenho econômico. Desta forma, não existiria um conjunto de variáveis de processo que resultariam no desempenho especificado, impedindo a resolução do sistema. Caso esse tipo de problema ocorra, deve-se partir para uma aproximação contínua do processo. Isso é particularmente importante na determinação do custo de investimento da planta, no qual usualmente se calcula o número de equipamentos necessário em cada etapa do processo.

A metodologia desenvolvida foi primeiramente testada em um sistema simples, sem o nível de integração presente na biorrefinaria. O processo escolhido foi o da produção de ácido succínico a partir da sacarose por rota fermentativa. O trabalho apresentado por Efe, Wielen e Straathof (2013) foi escolhido como base para o estudo de caso por apresentar uma descrição completa do processo, bem como todos os dados necessários para replicar o trabalho. Além disso, os autores gentilmente enviaram as planilhas utilizadas para o cálculo, o que permitiu verificar com mais clareza as hipóteses utilizadas. Verificou-se que a modelagem realizada foi bastante simples, o que foi replicado no estudo de caso.

Aplicada ao processo, a metodologia foi capaz de avaliar a influência das variáveis de processo na viabilidade da planta, descartando uma das variáveis previamente consideradas (a conversão da sacarose no fermentador). Ademais, foi possível construir diagramas representando a correlação entre as demais variáveis consideradas, apresentando os valores mínimos necessários para que o desempenho econômico imposto fosse alcançado. Esse tipo de informação é fundamental no processo de desenvolvimento e implementação de novos processos, indicando as métricas cujos valores

já são suficientes e quais ainda devem ser desenvolvidos futuramente.

Retro-Techno-Economic Analysis (RTEA): using (bio)process systems engineering tools to attain process target values

Felipe F Furlan[a], Caliane B B Costa[b], Argimiro R Secchi[c], John M Woodley[d], Roberto C Giordano[a]*

[a]Chemical Engineering Graduate Program, Universidade Federal de São Carlos (UFSCar), Rodovia Washington Luís (SP-310), km 235, São Carlos - SP – Brazil, CEP: 13565-905

[b]Chemical Engineering Department, Universidade Estadual de Maringá (UEM), Avenida Colombo, 5790, Maringá, Paraná, Brazil, CEP: 87020-900

[c]Chemical Engineering Graduate Program, COPPE, Universidade Federal de Rio de Janeiro, UFRJ, Cidade Univesitária, Rio de Janeiro, RJ, Brazil, CEP: 21941-972

[d]Department of Chemical and Biochemical Engineering, Technical University of Denmark, DK-2800 Kgs. Lyngby, Denmark

*E-mail of corresponding author: roberto@ufscar.br

Abstract:

Economic analysis allied to process systems engineering (PSE) tools can provide useful insights about the techno-economic feasibility of specific process conditions. More interestingly, rather than being used to evaluate specific conditions, this techno-economic analysis can be turned upside down to obtain target values for the main process metrics, providing feedback to the R&D team and setting goals for experimental studies. The present study proposes a methodology for performing such a “retro” techno-economic analysis (RTEA). It consists of choosing the most important variables

of the process, finding their threshold values and the correlation between them. In order to demonstrate the capabilities of the methodology, the production of succinic acid from sucrose was assessed. Through the use of this methodology an infeasible region was identified and threshold values for the process variables obtained. Although applied to a biochemical process, the methodology is general, and should be applicable to all types of chemical process.

1. Introduction

Economic analysis is an important field in (bio)process engineering, since it supports decisions concerning process improvements (Edgar et al., 2001). When allied to process systems engineering (PSE) tools, economic analysis can be useful to verify and understand the techno-economic feasibility of new processes. Its ultimate use can be quite comprehensive: assessing the effects of local variables on the global process responses (sensitivity analysis, Kazi et al., 2010; Patel et al., 2010), assessing the effect of process optimization on the plant feasibility (Martín and Grossmann, 2011) or comparing different process layouts (Cheali et al., 2013; Macrelli et al., 2012). These applications have in common the fact that they usually consider specific operational conditions, mostly based on reliable experimental data.

As a general rule, it is not a trivial task to infer the effects that process conditions and process metrics have on the overall process economic performance. Similarly, when designing experiments, it is usually not trivial to deduce the effect of process conditions on process metrics. Even if a qualitative inference is possible, a quantitative one is often unreliable. This is especially true for biochemical processes, for which data extrapolation can be difficult. Therefore, even though techno-economic analysis (TEA)

provides useful information about the specific process conditions that are being tested, in the present state of the art little information can be derived from TEA to guide new experiments, which would otherwise provide a valuable feedback during R&D stages for implementation of new technologies.

Some studies already addressed part of this problem by integrating process simulation for the design of experiments. Tufvesson et al. (2013) proposed a systematic methodology including chemical route synthesis, conceptual design and evaluation of alternative options to improve the efficiency of process development. The methodology aims at efficiently eliminating infeasible routes, thus focusing on the most promising options. To achieve this, the authors proposed some general target values (Tufvesson et al., 2013; Lima-Ramos et al., 2014) for important process metrics to ease the evaluation of the overall process and to construct an operating window (when possible). However, since these studies start with already given process metrics, they cannot capture specific characteristics of the process.

In this work, a new approach for this problem is presented. The essential concept is to turn the techno-economic analysis upside down: rather than being used to evaluate specific conditions, it is used to obtain target values for the main process metrics, thus indicating goals to be pursued, to be fed back to the R&D team and set targets to be attained in the experimental studies. For this to be possible, the economic analysis expressions must be inserted in the process simulator, alongside the usual equations that are included in these simulators: mass and energy balances, black box models of process units, thermodynamics and kinetic relationships that are part of phenomenological models, and so forth. Next, a threshold value for the economic metric

must be specified, while a specified process variable is freed, thus keeping the problem well posed, with zero degrees of freedom. Without relying on an external iterative loop (simulator-TEA-simulator-…), this approach is only possible using equation-oriented simulators, where no order is imposed for the resolution of the system of equations (Morton, 2002).

The proposed methodology, described in Section 2, starts by choosing the most important metrics for a given process, then finding their threshold values and the correlation between them. As a proof of concept, in Section 3, a process for the production of succinic acid from sucrose is analyzed, and the results are presented and discussed in Section 4.

2. Retro-Techno-Economic Analysis

The retro-techno-economic analysis (RTEA) consists in obtaining diagrams of the main process variables, for a fixed value of the economic metric (e.g., a zero net present value, NPV = 0). Since they represent a constant economic performance, these curves are here termed “isoeconomic”. The main steps to build these diagrams are presented in Figure 1. Initially, process and economic data are collected, as well as the necessary process models. A traditional techno-economic analysis is constructed, which will be the basis for the retro one. It is important to draw attention to the fact that no discontinuous function should be used in this analysis.

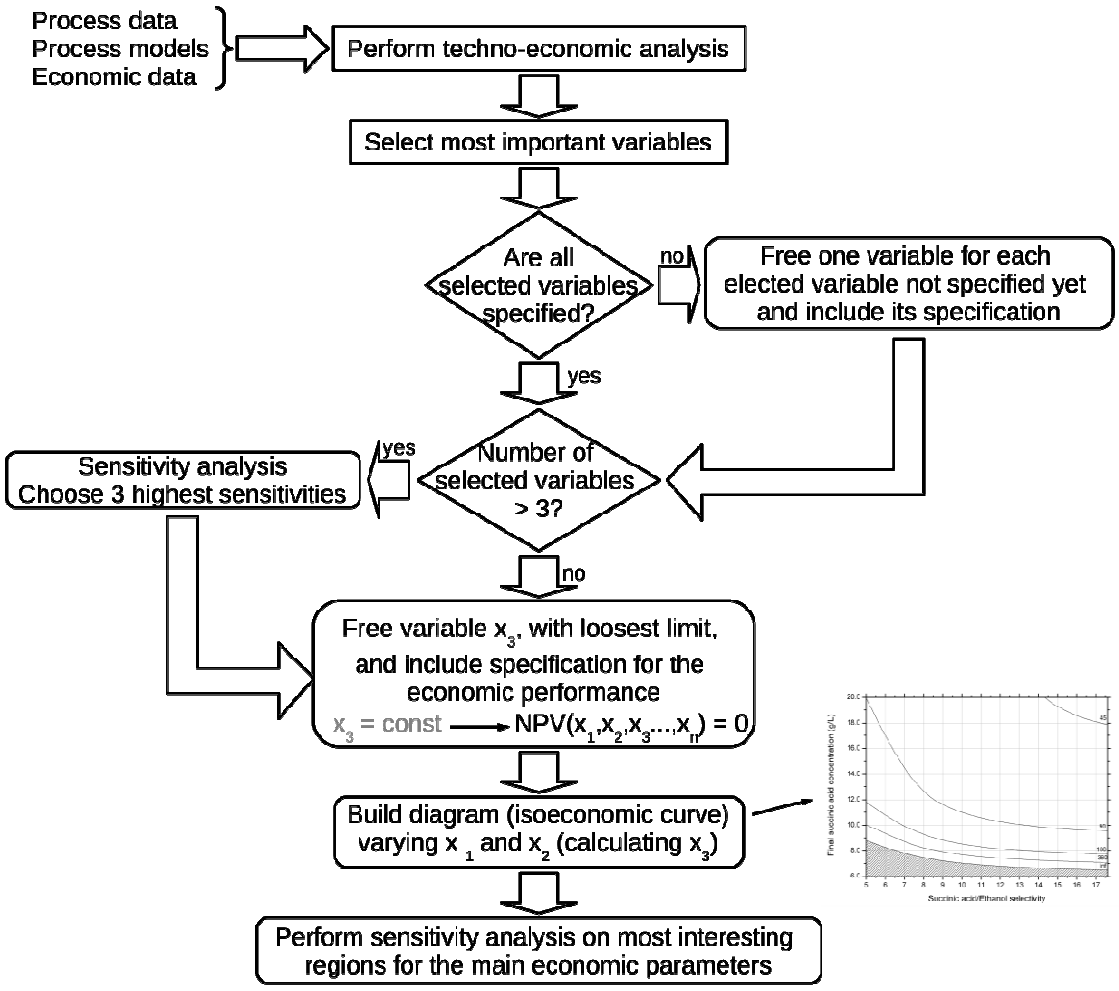

Figure 1: Main steps performed in the retro-techno-economic analysis (RTEA), to construct the isoeconomic surface and its contour plots. The net present value (NPV) is used as an example of an economic performance metric.

Of course, the metric chosen to represent the economic performance of the process is affected by many of the specified variables. Since it would be impractical to visualize more than three variables in the diagrams, prior knowledge and/or statistical methods should be used to select the most influential ones. One possible option is to use prior knowledge to select a broad range of variables and subsequently use a sensitivity analysis to eliminate the least influential ones until only three remain. It is fundamental that the variables chosen for the analysis are the specified ones, i.e., their values are

specified in the simulation, rather than calculated by the system of equations. If that is not the case, another variable should be freed and the chosen variable specified.

The RTEA is obtained by swapping the specification of one of the chosen variables for a threshold value of the economic metric. The threshold value represents the economic feasibility limit for the process, i.e. zero net present value (NPV = 0). The variable chosen to have its specification swapped should be the one with the largest physically feasible region, since its limiting value for the process economic feasibility will be calculated. If its physical feasible region is narrow (relative to the usual expected values) convergence problems may arise, with the variable crossing the bounds of the constraint. The other two variables will have their values varied to construct the diagrams. Some prior knowledge can also be used to choose which variable will be parameterized and which one will be the abscissa of the diagram. Preference should be given to controllable variables for the abscissa. On the other hand, the variable with clear constraints (e.g., conversion, split fractions, etc.) should be the one parameterized, since this can be used to divide the diagram into a feasible and an infeasible region. Finally, a sensitivity analysis can be performed on the main economic parameters.

3. Case Study

In order to demonstrate the potential of the described methodology, a case study was analyzed which implements the production of succinic acid from sucrose by fermentation. It was based on a process described by Efe et al. (2013), see Figure 2.

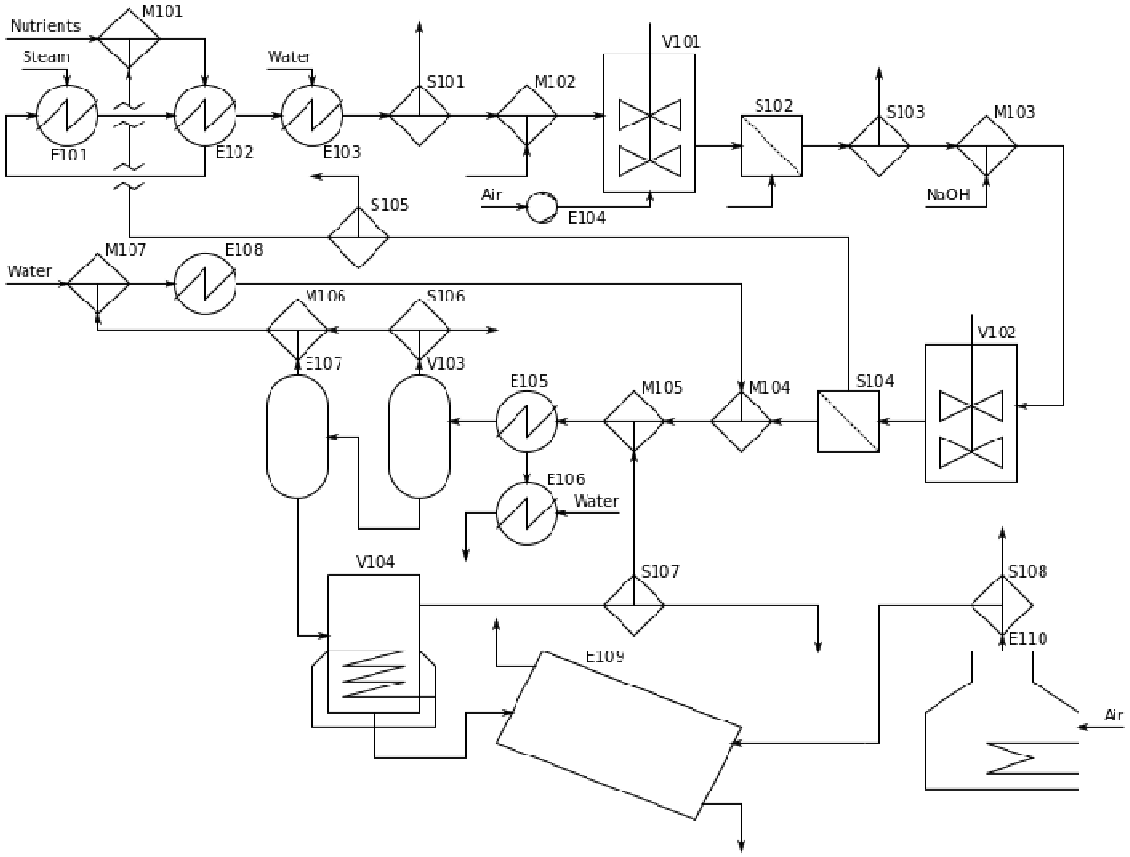

Figure 2: Process flow diagram for the production of succinic acid. Adapted from Efe et al (2013).

First, the sucrose solution, with a partial recycle, is sterilized and cooled in a sequence of heat exchangers (E101 – E103). The stream is then sent to the fermenters (V101 and V102), with yeast recycle. Once a week, all yeast is discarded and substituted, dragging part of the succinic acid produced with it, and implying a loss of part of the sucrose used for growth of the microorganism. The output of the fermenters is centrifuged (S102) and the solution sent to an adsorption column (S104 and M104), where succinic acid is adsorbed along with some of the byproducts. The effluent is recycled to the sucrose feed stream and the adsorbed compounds are desorbed with hot water. The output undergoes a pressure drop in a flash vessel (V103) and is further concentrated in an evaporator (E107). The concentrated solution is crystallized (V104) and the crystals

are dried in a rotary drier (E109). Finally, the steam and hot air demands are met by a furnace (E110).

Some modifications were necessary to adapt the process to the approach used in this work. First, the fermentation and the adsorption operations, both discontinuous, were modified to be represented continuously. In the fermentation stage, two purges were inserted, to represent the loss of sugars for yeast growth (S101 in Figure 2) and product loss due to yeast substitution (S103). Also, a mixer (M103) was added, representing the addition of sodium hydroxide in the first batch with new yeast. The adsorption step was represented by a separator (S104) and a mixer (M104). Additionally, two purges were added in both recycles of the process (S105 and S107) to prevent the byproduct concentrations increase (building-up).

As a general case, the models used in the simulation comprised only mass balances, with energy balances being added when necessary. Additionally, extra equations and variables were added to allow the cost calculation. A comprehensive description of all the models used in the simulations, as well as the ones used in the economic analysis is presented in the supplementary information. The second reactor (V102) is responsible for partly converting the acids produced into their salts, a reaction that occurs in parallel to the fermentation in the first reactor. Therefore, only the first one was used in the investment cost calculation. A specified productivity was used to determine the reactor residence time, volume and cost. The flash drum (V103) and the evaporator (E107) used the latent heat and the heat capacity of water as approximations. The crystallizer considered the overall crystal growth rate to determine the tank residence time necessary to achieve the specified average crystal size. Finally, the hot air flow demand

in the rotary drier was calculated based on both the heat necessary to evaporate all water in the crystals and the saturation humidity of the air at the outlet temperature.

Fixed and operating costs were calculated based on the same assumptions listed in the original base case study (Efe et al., 2013). The economic analysis equations were inserted in the simulator as well, so that the NPV (the economic metric used in this study) could be obtained in simulation time. This is an essential feature to enable the present methodology. As a simplification of the problem, the labor cost was considered constant in the simulations, while all other cost values were calculated based on operational data. It is important to point out that the equipment cost was described by continuous equations. Therefore, the number of pieces of equipment for each unit operation was disregarded and the total value for the sizing factor was used instead. The exponential factors used to scale the pieces of equipment were adjusted to represent the overall cost and not a single unit. Since the focus here was not on the final values obtained for this specific process, but rather on a proof of concept of the proposed methodology, the economic parameters were kept in the original values described by the authors (Efe et al., 2013) for 2010. In the original study, the authors did not use a fixed price for succinic acid, but instead calculated its minimum selling price. In the present study, a price of 2.00 USD/kg was assumed (www.alibaba.com).

4. Results and Discussion

The simulation software used in this study was EMSO^{TM} (Environment for Modeling Simulation and Optimization). It is an equation-oriented simulator with a particular modeling language, which allows users to implement their own models, besides using the ones already available in the software library. Moreover, EMSO has an interface

mechanism to add new plug-ins and solvers as dynamic libraries, thus extending its capabilities (Soares and Secchi, 2003). All model equations and economic analysis, described in the supplementary information, were implemented in this simulator.

4.1. Base case

The first step of the methodology is to perform a techno-economic analysis of the process. All data necessary for this step was obtained from the base case (Efe et al., 2013). Table I shows the main results of the TEA of the original study and the present one.

Table I: Main process and economic results of the techno-economic analysis of the original study (Efe et al., 2013) and of the present one.

Parameter	Original study	Present study
Sucrose flow (kt/year)	49.1	51.3
Electricity (GWh/year)	38.7	39.1
Natural gas (GJ/year)	1.14×10^6	1.44×10^6
Equipment purchase cost (US$\times10^6$)	36.9	36.4
Total capital investment (US$\times10^6$)	146.6	144.7
Annual operating costs (US$\times10^6$/year)	36.0	38.1
Minimum succinic acid selling price (US$)	2.26	2.29

Essentially, the results were replicated with just minor differences. The exception is the natural gas consumption, which was due to a difference in the energy balance of the adsorption column. The authors of the base case study disregarded the heat capacity of the soluble compounds in the outlet stream of the adsorption column (during desorption). By contrast, in the present study the heat capacity of the overall solution

was approximated by the water heat capacity. This difference propagates to the economic analysis along with the difference in sucrose consumption. However, their combined effect is small; the annual operating cost obtained was only 5.8% higher than the original study while the succinic acid minimum selling price was 1.3% higher. Since the results were reasonably close to the original study, the simulation was considered adequate and the adaptations described in Section 3 were performed.

4.2. Selection of variables

A breakdown of the investment and operating costs of the process shows that the fermentation stage is responsible for 80% of the former and 50% of the latter. It is expected that the economic performance of the process will be mostly affected by the process variables in this stage. Therefore, the sucrose conversion, the specific productivity (g of succinic acid/kg of yeast/h), the final succinic acid concentration in the fermentation and the selectivity (succinic acid/ethanol) of the reaction were chosen for the retro-techno-economic analysis. Since more than three variables were chosen, a sensitivity analysis was performed to exclude the one with the weakest effect on the process NPV, the economic metric chosen. The process sensitivity was evaluated at the operating point described in the original study, but using a succinic acid price of US$ 2.00/kg. Table II shows the specific sensitivities of the NPV relative to the four variables chosen.

Table II: Specific sensitivity of the process net present value, relative to four selected process variables.

Variable	unit	Specific sensitivity	Value
X_{sucr} (conversion) = (sucrose consumed)/(sucrose fed)	none	$\frac{dln(NPV)}{dln(X_{sucr})}$	0.0281
S (Selectivity) = (succinic acid produced)/(ethanol produced)	none	$\frac{dln(NPV)}{dln(S)}$	0.2568
Pr (specific productivity) = (succinic acid produced)/(mass of yeast)/reaction time	g/kg/h	$\frac{dln(NPV)}{dln(Pr)}$	1.2330
C_{sa} (Succinic acid concentration)	g/L	$\frac{dln(NPV)}{dln(C_{sa})}$	3.3891

As can be clearly seen, the effect of the sucrose conversion on the process NPV is the smallest. This is mainly due to the hypothesis that sucrose has no interaction with the zeolite in the adsorption column, being recycled to the start of the process. Also, since sucrose is available in crystal form, the concentration in the input stream can be adjusted. Therefore, no increased dilution of the raw material arises from the increasing recycle flow and the reactor volume necessary to carry out the fermentation remains almost constant. The only effect of sucrose conversion is on its loss in the purge, since the byproducts concentration must be controlled.

4.3. Retro-Techno-Economic Analysis

At this point, sucrose conversion could be disregarded and the next step of the methodology could be carried on. Nevertheless, the effect of this variable will be further explored to show another approach for eliminating variables. Table III shows the ranges considered for all four variables in the construction of the feasibility diagrams.

Table III: Ranges of the process variables used for constructing the isoeconomic surface (NPV = 0). The infinite productivity is obtained by eliminating the reaction time (filling, emptying and cleaning times remained constant).

Process metrics	Lower bound	Upper bound
Sucrose conversion	0.5	1.0
Succinic acid to Ethanol selectivity	5.0	17.6
Productivity (g/kg/h)	45	Infinite
Succinic acid concentration in the end of the fermentation (g/L)	5	22

Two diagrams were built, with the specific productivity being chosen to vary between them. The lower and upper bounds showed in Table III are represented in the diagrams. The sucrose conversion was chosen as the abscissa while the selectivity was considered for the contour plots, since it has an upper limit value of 17.6. Finally, the succinic acid concentration in the end of the fermentation is the ordinate, since its bounds are the loosest. The two diagrams are presented in Figure 3. As it can be seen, except for low selectivities, the effect of sucrose conversion was small, both for small and high specific productivities. Therefore, the choice of disregarding this variable in further analysis is assumed to be correct.

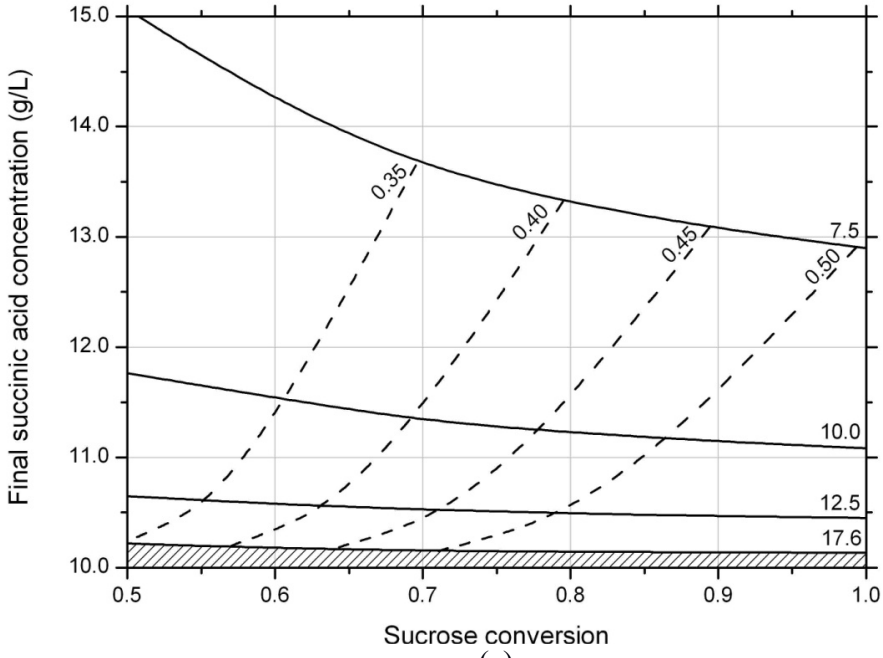

(a)

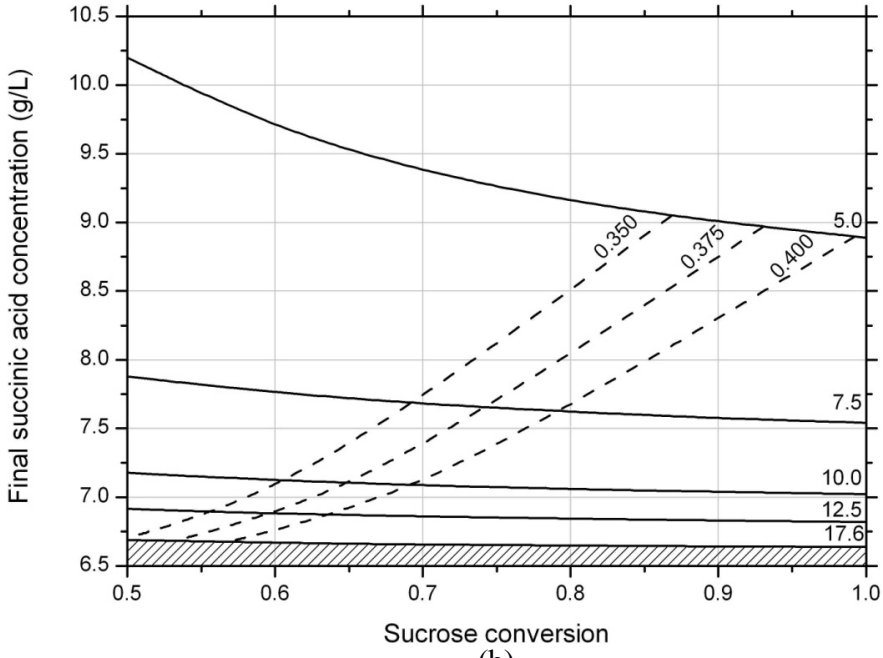

(b)

Figure 3: Final succinic acid concentration in the fermenter as a function of the sucrose conversion with (a) specific productivity of 90 g/kg/h and (b) infinite productivity – reaction time equal zero. The continuous lines are contour plots of the isoeconomic surface (NPV = 0) for constant selectivity (considering succinic acid and ethanol), while the dashed lines are contour plots for constant succinic acid efficiency (actual yield/theoretical yield, numbers above the lines). Economically feasible region: above the contour plots. Hatched area is infeasible due to the process physical constraints.

With the new set of variables (without sucrose conversion), a new arrangement is necessary. The specific productivity is chosen for the contour plots, since it has a clear upper limit (infinite productivity), while the selectivity is chosen for the abscissa. The succinic acid concentration remains as the ordinate. It is clear from the new diagram (Figure 4) that the effect of the specific productivity is much more important at low selectivities. On the other hand, the distance between the contour curves quickly decreases as the selectivity increases (a 3 g/L difference between the specific productivity of 90 g/kg/h and the limit case). On the other hand, if intermediate selectivities are already achievable, say 10, there may be no reason to further increase it (using genetic engineering) if the yeast can handle succinic acid (and the equivalent byproducts) concentrations above 12 g/L. As it becomes clear, lab experiments can be quickly evaluated, and a new search direction derived, by using these diagrams.

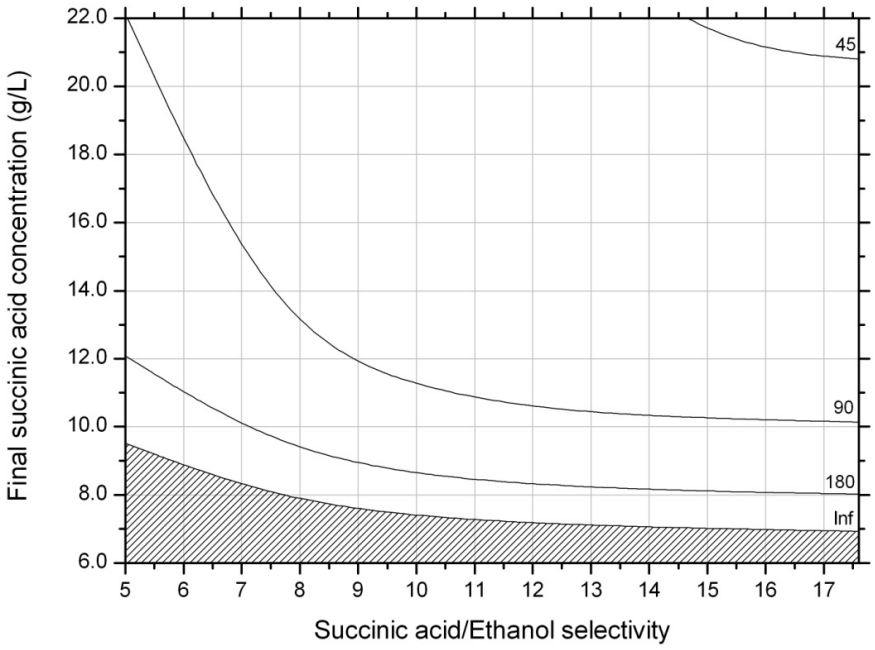

Figure 4: Final succinic acid concentration in the fermenter for different specific productivities as a function of the reaction selectivity (succinic acid/ethanol, keeping sucrose conversion constant at 100%). The numbers above the contour curves of the isoeconomic surface (i.e., where NPV = 0) are the specific productivities (obtained by varying the reaction time).The economic feasible region is above the curves. Hatched area is infeasible due to process physical constraints. The infinite specific productivity was obtained by eliminating the reaction time (filling, emptying and cleaning times remained constant).

4.4. Sensitivity Analysis

As a final step, a sensitivity analysis is carried out to evaluate the influence of economic parameters on the isoeconomic surface. This analysis is shown in Figure 5, for the influence of succinic acid prices.

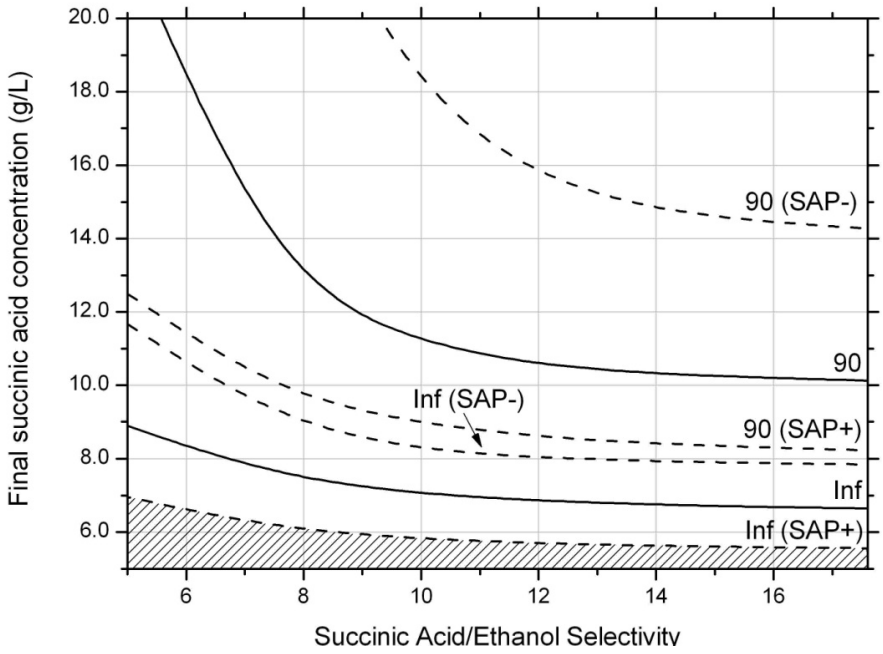

Figure 5: Sensitivity analysis of the succinic acid selling price over the isoeconomic surface. The continuous lines are contour curves for fixed specific productivities for the current price, while the dashed lines represent variations of ± 0.25 USD/kg. The numbers above the curves are the specific productivities and the succinic acid price (SAP + or -). The infinite specific productivity was obtained by eliminating the reaction time (filling, emptying and cleaning times remained constant).

The effect of this price on increasing or decreasing the economically feasible region is strong and becomes stronger as the specific productivity drops. This can be used to anticipate some market changes and develop processes for these high variations, for example, a process that can deal with 19 g/L of succinic acid in the reactor (using the previous example assumptions).

5. Conclusion

In this work, a methodology was developed which uses techno-economic analyses to derive goals for process metrics values to be pursued experimentally. The methodology,

called Retro-Techno-Economic Analysis (RTEA), is able to identify the main process variables that influence the process economic feasibility, their threshold values and also their relations. As a demonstration of the capabilities of the methodology, the production of succinic acid from sucrose was used as a case study. The methodology was able to identify the main process metrics (Succinic acid/ethanol selectivity, specific productivity and final succinic acid concentration). Based on the analyses, infeasible regions were derived, as well as threshold values for the three variables depending on operating conditions. With this information in hand, new directions for process development can be quickly evaluated and experiments designed to improve the process. Although used in a biochemical process, the methodology is general, applying to all types of chemical processes.

Acknowledgments

Special thanks to Adrie Straathof for kindly providing the spreadsheets used in their paper “Techno-economic analysis of succinic acid production using adsorption from fermentation medium”, the case study considered here. The present study was financially supported by CAPES (Proc. 2608/14-6) and CNPq (Proc. 140762/2012-4).

References

Cheali P, Gernaey KV, Sin G. 2013. Toward a Computer-Aided Synthesis and Design of Biorefinery Networks: Data Collection and Management Using a Generic Modeling Approach. ACS Sustain Chem Eng 2:19-29.

Edgar TF, Himmelblau DM, Lasdon L. 2001. Optimization of chemical processes. New York:McGraw-Hill. 650 p.

Efe Ç, van der Wielen LAM, Straathof AJJ. 2013. Techno-economic analysis of

succinic acid production using adsorption from fermentation medium. Biomass Bioenergy 56:479-492.

Kazi KF, Fortman J, Anex R, Kothandaraman G, Hsu D, Aden A, Dutta A. 2010. Techno-Economic Analysis of Biochemical Scenarios for Production of Cellulosic Ethanol. Denver: National Renewable Energy Laboratory. 102 p.

Lima-Ramos J, Tufvesson P, Woodley JM. 2014. Application of environmental and economic metrics to guide the development of biocatalytic processes. Green Process Synth 3:195-213.

Macrelli S, Mogensen J, Zacchi G. 2012. Techno-economic evaluation of 2nd generation bioethanol production from sugar cane bagasse and leaves integrated with the sugar-based ethanol process. Biotechnol Biofuels 5:22.

Manufacturers, Suppliers, Exporters & Importers from the world's largest online B2B marketplace-Alibaba.com. Date of access: 06/01/16 <www.alibaba.com>

Martín M, Grossmann IE. 2011. Process Optimization of FT-Diesel Production from Lignocellulosic Switchgrass. Ind Eng Chem Res 50:13485-13499.

Morton W. 2002. Equation-oriented simulation and optimization. Proc Indian National Science Academy Part A 69:317-358.

Patel AD, Serrano-Ruiz JC, Dumesic JA, Anex RP. 2010. Techno-economic analysis of 5-nonanone production from levulinic acid. Chem Eng J 160:311-321.

Soares RP, Secchi AR. 2003. EMSO: A new environment for modelling, simulation and optimisation. Computer Aided Chemical Engineering 14:947-952.

Tufvesson P, Lima-Ramos J, Haque NA, Gernaey KV, Woodley JM. 2013. Advances in the process development of biocatalytic processes. Org Process Res Dev 17:1233-1238.

Tufvesson P, Lima-Ramos J, Nordblad M, Woodley JM. 2011. Guidelines and Cost Analysis for Catalyst Production in Biocatalytic Processes. Org Process Res Dev

15:266-274.

Mathematical modeling

All the operations in the succinic acid production were modeled as short-cut models, with mass and energy balances and design correlations. The basic stream, used to connect the different pieces of equipment, is constituted by the total mass flow (*F*), component mass fractions (*z*) and temperature (*T*). The modeling language of EMSO implements aspects of object-oriented languages. Therefore, the temperature of the inlet stream of unit1, for example, is described as *unit1.inlet.T*. This language will be used in the models description below.

1. Models description

1.1. Mixer

The mixer was modeled with two inlets and one outlet stream. The global mass balance and component mass balance are shown in equations 1 and 2. As a simplification, the energy balance was not performed in this model, with the outlet temperature being specified.

$$Inlet1.F + Inlet2.F = Outlet.F \quad (1)$$

$$Inlet1.F \times Inlet1.z[i] + Inlet2.F \times Inlet2.z[i] = Outlet.F \times Outlet.z[i] \quad (2)$$

1.2. Splitter

The splitter was modeled with one inlet and two outlets. A split fraction (*f*) is defined, which represents the mass flow of the inlet that is diverted to the first outlet (eq. 3). The global mass balance is also calculated (eq. 4) and both outlets composition is supposed to be equal to the inlet one (eq. 5). Finally, thermal equilibrium is supposed between all streams (eq. 6).

$$Outlet1.F = f \times Inlet.F \quad (3)$$

$$Inlet.F = Outlet1.F + Outlet2.F \quad (4)$$

$$Inlet.z[i] = Outlet1.z[i] = Outlet2.z[i] \quad (5)$$

$$Inlet.T = Outlet1.T = Outlet2.T \quad (6)$$

1.3. Heat Exchanger

Since there is no mixture between the hot and cold streams in the heat exchanger both the global and component mass balances are trivial (eqs. 7 – 10). The heat exchanged between the streams is given by equations 11 and 12, for the hot and cold sides, respectively. The heat exchanger area is calculated using the global heat transfer coefficient (eq. 13). An approximation for the logarithmic mean temperature difference described by Chen (1987) is used to facilitate the system convergence (eqs. 14 – 16).

$$InletHot.F = OutletHot.F \quad (7)$$

$$InletCold.F = OutletCold.F \quad (8)$$

$$InletHot.z[i] = OutletHot.z[i] \quad (9)$$

$$InletCold.z[i] = OutletCold.z[i] \quad (10)$$

$$Q = Cp_{Hot} \times InletHot.F \times (InletHot.T - OutletHot.T) \quad (11)$$

$$Q = Cp_{Cold} \times InletCold.F \times (OutletCold.T - InletCold.T) \quad (12)$$

$$Q = U \times A \times DT_{lm} \quad (13)$$

$$DT_{lm}{}^{0.3275} = DT_1{}^{0.3275} + DT_2{}^{0.3275} \quad (14)$$

$$DT_1 = InletHot.T - OutletCold.T \quad (15)$$

$$DT_2 = OutletHot.T - InletCold.T \quad (16)$$

1.4. Flash

The flash model was used to simulate both the flash and the evaporator in the succinic acid production process. The model comprises an inlet stream, a vapor outlet and a liquid outlet. The global and component mass balances are shown in equations 17 and 18, respectively. The actual phase equilibrium was not calculated. Instead, all compounds with boiling points lower than the water were supposed to leave the equipment on the vapor stream along with part of the water. All other compounds leave the flash on the liquid stream (eq. 19). This is accomplished by specifying the variable *f* between zero and one. Also, equation 20 specifies that the sum of mass fractions in the vapor and liquid streams are equal, which, together with equations 17 to 19, guarantees that both sums are equal to one. The energy balance (eq. 21) is based on the heat capacity and latent heat of water, since the other compounds are present in low concentrations. Finally, thermal equilibrium is supposed (eq. 22).

$$Inlet.F = OutletV.F + OutletL.F \quad (17)$$

$$Inlet.F \times Inlet.z[i] = OutletV.F \times OutletV.z[i] + OutletL.F \times OutletL.z[i] \quad (18)$$

$$OutletV.F \times OutletV.z[i] = Inlet.F \times Inlet.z[i] \times f[i] \quad (19)$$

$$\sum_i OutletV.z[i] = \sum_i OutletL.z[i] \quad (20)$$

$$Inlet.F \times Cp \times Inlet.T + Q = OutletL.F \times Cp \times OutletL.T + OutletV.F \times (Cp \times OutletV.T + VapHeat) \quad (21)$$

$$OutletV.T = OutletL.T \quad (22)$$

1.5. Fermenter

The fermenter model comprises two inlets (substrate and air) and two outlets (succinic acid solution and fermentation gases). Besides the global mass balance (eq. 23), the component mass balance takes into account the consumed raw material and formed products based on the stoichiometric coefficients of the reactions and a conversion relative to the limiting reagent (eqs. 24 and 25). To calculate the total volume necessary to carry the fermentation (eq. 26), the total batch time must be obtained from the duration of the four steps: filling, reaction, emptying and cleaning (eq. 27).

$$Inlet.F + Air.F = Outlet.F + Gases.F \quad (23)$$

$$Inlet.F \times Inlet.z[i] + Air.F \times Air.z[i] + \sum_j (r[j] \times stoic[j,i]) \times M[i] = Gases.F \times Gases.z[i] \quad (24)$$

$$r[j] \times M[l[j]] = (Inlet.F \times Inlet.z[l[j]] + Air.F \times Air.z[l[j]] \times conv \quad (25)$$

$$V_{total} \times workingVolume \times \rho \times ReactorUsage = Inlet.F \times T_{total} \quad (26)$$

$$T_{total} = T_{filling} + T_{emptying} + T_{cleaning} + T_{reaction} \quad (27)$$

The mass of cells that needs to be re-grown each week should be calculated based on the number of reactors that are full or emptying at a giving time. Nevertheless, as explained in section 2, the methodology does not allow the models to have discontinuous functions. Therefore, a continuous approximation of the function was used (eq. 28).

$$M_{cells} = \frac{(T_{filling} + T_{reaction})}{T_{total}} \times V_{total} \times workingVolume \times C_{cells} \quad (28)$$

The productivity of the yeast (a specific productivity, mass of succinic acid/mass of cells/h) was calculated considering the amount of sucrose that is converted to succinic acid (eq. 29). Also, the power consumption for the reactor mixing is also calculated taking the reactors total volume (eq. 30).

$$Pr \times C_{cells} \times T_{reaction} = Inlet.z[1] \times conv[1] \times stoic[1,3] \times \frac{M[3]}{M[1]} \times \rho_{reactor} \quad (29)$$

$$P_{mix} \times T_{total} = V_{total} \times P_{specMix} \times T_{reaction} \quad (30)$$

The maximum volume of the reactor (400 m³) was used to calculate the reactor diameter (using an aspect ratio of 3, eq. 31), the mass of steel in each reactor (eq. 32) and consequently the steam required to heat the reactor to the sterilization temperature (121 ºC) and the water to cool it back to the fermentation temperature (eqs. 33 – 35).

$$V_{max} = \frac{3 \times \pi \times D_{reactor}^3}{4} \quad (31)$$

$$M_{steel} = \frac{21}{4} \times \pi \times D_{reactor}^2 \times Thickness \times \rho_{steel} \quad (32)$$

$$Q_{ster} \times T_{total} = Cp_{steel} \times (T_{steam} - Inlet.T) \times M_{steel} \times \frac{V_{total}}{V_{max}} \quad (33)$$

$$F_{steam} \times L_{steam} = Q_{ster} \quad (34)$$

$$F_{water} \times Cp_{water} \times \Delta T = Q_{ster} \quad (35)$$

1.6. Crystallizer

In the crystallizer, besides the usual global and component mass balances (eqs. 36 and 37), the initial and final crystal volumes (eqs. 38 and 39) are used to calculated the crystal growth and residence time, using a specified overall crystal growth rate (eq. 40).

Therefore, the crystallizer volume is calculated taking into account the space-time, the average density (eq. 41) and the working volume (85%, eq. 42). Finally, thermal equilibrium is assumed (eq. 43).

$$Inlet.F = OutletS.F + OutletL.F \quad (36)$$

$$Inlet.F \times Inlet.z[i] = OutletL.F \times OutletL.z[i] + OutletS.F \times OutletS.z[i] \quad (37)$$

$$V_i = \frac{4 \times \pi \times r_i^3}{3} \quad (38)$$

$$V_f = \frac{4 \times \pi \times r_f^3}{3} \quad (39)$$

$$\tau = \frac{r_{average} \times \rho_{crystal}}{4 \times Rg} \quad (40)$$

$$\frac{1}{\rho_L} = \frac{Inlet.z(SA)}{\rho_{crystal}} + \frac{1 - Inlet.z(SA)}{1000\ kg/m^3} \quad (41)$$

$$V_{reactor} = \frac{Inlet.F \times \tau}{\rho_L \times 0.85} \quad (42)$$

$$OutletL.T = OutletS.T \quad (43)$$

1.7. Dryer

The amount of evaporated water, the inlet and outlet air streams were not represented by the basic stream defined here. They were represented as mass flows only, since there was no need for knowing their composition. The global mass balance is simplified, since it is supposed that no air is absorbed by the drying solid (eq. 44). Also, all water is evaporated (eq. 45). The amount of air needed in the dryer is calculated by two limiting factors, the equilibrium humidity at the outlet temperature (eq. 46) and the minimum

heat transferred to the solid to evaporate all the water (eq. 47). The maximum value between these two is considered to be the real air flow (eq. 48), with the real outlet temperature and humidity of the air being calculated by equations 49 and 50. Numbers in equations 47 and 50 are the heat capacity constants for the air. Finally, the dryer area is obtained by the amount of water evaporated and a specified mean evaporation rate (r_e, eq. 51).

$$Inlet.F = Outlet.F + F_{evap} \quad (44)$$

$$F_{evap} = Inlet.F \times Inlet.z[water] \quad (45)$$

$$F'_{air} \times (H_{out} - InletAir.H) = F_{evap} \quad (46)$$

$$F''_{air} \times \left(0.96 \times (InletAir.T - T_{out}) + \frac{7.5 \times (InletAir.T^2 - T_{out}^2)}{100000}\right) = F_{evap} * L_{evap} \quad (47)$$

$$OutletAir.F = \max\ (F'_{air}, F''_{air}) \quad (48)$$

$$OutletAir.F \times (OutletAir.H - InletAir.H) = F_{evap} \quad (49)$$

$$OutletAir.F \times \left(0.96 \times (InletAir.T - OutletAir.T) + \frac{7.5 \times (InletAir.T^2 - OutletAir.T^2)}{100000}\right) = F_{evap} \times L_{evap} \quad (50)$$

$$A \times r_e = F_{evap} \quad (51)$$

2. Economic Analysis

In order to perform the economic analysis of the process, both capital expenditures (CapEx) and operating expenditures (OpEx) were calculated. CapEx direct costs were based on the equipment purchase cost (*EPC*, eq. 52) and the equipment installed cost

(*EIC*, eq. 53), with all other direct costs being based on these two, as show in Table 1. Equipment costing uses the scaling factor (*SF*) considering the equipment sizing factor (S_{actual}), a base size (S_{base}), price ($\$_{base}$) and an installation factor (*IF*).

$$EPC = \sum \left(\frac{S_{actual}}{S_{base}}\right)^{SF} \times \$_{base} \quad (52)$$

$$EIC = \sum IF \times \left(\frac{S_{final}}{S_{base}}\right)^{SF} \times \$_{base} \quad (53)$$

Table 1: Direct and Indirect costs of CapEx.

Direct costs	**Value**
Piping	31% of EPC
Instrumentation and control	18% of EPC
Electrical equipment and materials	10% of EPC
Buildings	38% of EPC
Service facilities	40% of EPC
Yard improvement	10% of EPC
Land	6% of EPC
Indirect costs (IC)	
Engineering and supervision	8% of TDC
Construction expenses	10% of TDC
Contractors fee	5% of TDC
Contingency	8% of TDC

Therefore, the total direct costs (*TDC*) can be calculated from this two values (eq. 54), while the indirect costs (*IC*) were based on the *TDC* (Table 1, eq. 55).

$$TDC = IEC + 1.53 \times EPC \quad (54)$$

$$IC = 0.31 \times TDC \quad (55)$$

The fixed capital investment (*FCI*) is the sum of the direct and indirect costs of CapEx (eq. 56). Also, the working capital (*WC*) is based on the indirect costs, being fixed at 10% of the IC (eq. 57). Finally, the total capital investment (*TCI*) is the sum of *FCI* and *WC* (eq. 58).

$$FCI = TDC + IC \quad (56)$$

$$WC = 0.1 \times IC \quad (57)$$

$$TCI = FCI + WC \quad (58)$$

The plant OpEx was calculated considering fixed costs, direct costs, raw materials and utilities costs. The raw materials (*RM*) comprise sucrose, sodium hydroxide, water, ammonia and zeolite. Total RM costs were calculated (eq. 59) from the mass flow (F_i) and price per mass unit ($\$_i$) for each raw material i for one operating time (*OT*, considered equal to 330 days). The raw materials and utilities costs were kept equal to the original study (Efe, van der Wielen and Straathof, 2013, Table 2). The utilities costs (*U*) were calculated from the electric energy (*EE*), cooling water (*CW*) and natural gas (*NG*) consumptions (eq. 60). The EE was calculated from the main pieces of equipment consumption and increased in 50% to account for the auxiliary equipments.

$$RM = OT \times (\$_{Suc} \times F_{Suc} + \$_{NaOH} \times F_{NaOH} + \$_W \times F_W + \$_{Am} \times F_{Am} + \$_z \times F_z) \quad (59)$$

$$U = OT \times (\$_{EE} \times EE \times 1.5 + \$_{CW} \times CW + \$_{NG} \times NG) \quad (60)$$

Table 2: Raw material and utilities price per unit.

Item	Price
Sucrose	212 US$/tonne
NaOH	200 US$/tonne
Process water	0.27 US$/m³
Ammonia	310 US$/tonne
Zeolite	33000 US$/tonne
Electric energy	0.07 US$/MWh
Cooling water	0.014 US$/m³
Natural gas	4.1 US$/GJ

OpEx direct costs (*ODC*) comprise operating labor (*OperLabor*), supervision (*superv*), laboratory charges (*LabChar*), maintenance and repair (*Maint*) and operating supplies

(*OperSupplies*) – eq. 61. The Operating labor was considered constant as a simplification of the process and both supervision and laboratory charges were based on its value (both 15% of it). The maintenance cost was taken as 5% of the fixed capital investment and operating supplies 15% of maintenance cost.

$$ODC = OperSupplies + LabChar + Maint + Superv + OperLabor \quad (61)$$

The OpEx fixed costs (*OFC*) were based on the insurance (*Insur*), administrative costs (*AdmCosts*), distribution and marketing (*Mark*) and plant overhead (*PlantOverhead*) – eq. 62. The plant overhead was taken as 50 % of the maintenance, operating labor and supervision costs. The administrative cost was considered to be 20% of operating labor, insurance as 3% of *FCI* and marketing and distribution as 2% of total operating costs (*OC*, eq. 63).

$$OFC = Insur + AdmCosts + PlantOverhead + Mark \quad (62)$$

$$OC = OFC + ODC + RM + U \quad (63)$$

For the cash flow (*CF*) calculation, it was considered one year of design (when only the *IC* was expend), two years of construction (with half of the *TDC* being expend each year) and ten years of operation (eqs. 64a-e). The only source of revenue was the selling of succinic acid (eq. 65).

$$CF[1] = -IC \quad (64a)$$

$$CF[2:3] = \frac{-TDC}{2} \quad (64b)$$

$$CF[4] = Revenue - OC - Tax[1] - WC \quad (64c)$$

$$CF[5:12] = Revenue - OC - Tax[2] \quad (64d)$$

$$CF[13] = Revenue - OC - Tax[3] + WC \quad (64e)$$

$$Revenue = \$_{SA} \times \dot{M}_{SA} \times OT \quad (65)$$

The taxes were calculated based on equations 66a-c, with a linear depreciation over the 10 years of operation.

$$Tax[1] = (Revenue - OC - Depreciat - WC) \times 0.34 \quad (66a)$$

$$Tax[2] = (Revenue - OC - Depreciat) \times 0.34 \quad (66b)$$

$$Tax[3] = (Revenue - OC - Depreciat + WC) \times 0.34 \quad (66c)$$

Finally, the discounted cash flow (*DCF*) is calculated (eq. 67) which is used to calculate the *NPV* of the process (eq. 68)

$$DCF = \frac{CF}{(1+r)^i} \quad (67)$$

$$NPV = \sum_{i=0}^{12} DCF\,[i+1] \quad (68)$$

3. References

Chen, JJJ. 1987. Comments on improvements on a replacement for the logarithmic mean. Chemical Engineering Science 42(10):2488-2489.

5 Aplicação da análise econômica reversa à biorrefinaria

Finalmente, a metodologia desenvolvida no capítulo anterior é aplicada ao processo integrado de produção de etanol 1G e 2G a partir da cana-de-açúcar e do bagaço. Esse processo apresenta alto grau de complexidade, principalmente causada pelo sistema de cogeração que atende às demandas de vapor (em três pressões) e energia elétrica da planta. Além disso, a variação de algumas variáveis de processo causam modificações estruturais no processo como, por exemplo: a eliminação de evaporadores quando a concentração de entrada já está na especificação; a substituição de um aquecedor por um refervedor quando a temperatura de entrada passa a superar a especificação, etc. Felizmente, tais modificações puderam ser tratadas pontualmente, sem que tal descontinuidade afetasse a metodologia. Os resultados são apresentados no artigo intitulado *Attaining process target metrics through retro-techno-economic analysis: the ethanol from sugarcane bagasse case*, a ser submetido à revista indexada.

O processo de produção de etanol de primeira geração está bastante consolidado, com os parâmetros de processo envolvidos em sua produção já próximos ao ótimo. Assim, as variáveis de processo cujos valores ainda carregam incertezas se concentram na etapa de produção de etanol de segunda geração, em especial, na etapa de hidrólise. Por esse motivo, a análise se concentrou nas variáveis dessa etapa, escolhendo para tal as seguintes variáveis: o rendimento do biocatalisador, a conversão da celulose no reator de hidrólise, a fração de sólidos e a produtividade nesse mesmo reator. Um resultado que se destaca é o baixo impacto da produtividade do reator de hidrólise na viabilidade da planta, que se deve, principalmente, ao baixo custo do reator de hidrólise considerado, bem como seu baixo gasto energético com agitação, baseado no descrito por Kazi et al. (2010). Verifica-se que os resultados experimentais já se apresentam nesse patamar (SOUZA et al., 2014; SILVA, 2015; SILVA, 2009). A produtividade do biocatalisador, por outro lado, tem forte influência na viabilidade do processo e os resultados experimentais reportam valores inferiores aos obtidos pela ATER, mostrando um possível gargalo de processo. Obviamente, os resultados apresentados nesse trabalho são dependentes do processo e das hipóteses (de processo e econômicas) realizadas. Entretanto, é possível ver que os resultados apresentados permitem avaliar rapidamente dados experimentais obtidos para o pré-tratamento descrito e indicar uma nova direção de busca, por exemplo, dando menos ênfase à produtividade, que apresentou pouco impacto na viabilidade do processo.

Attaining process target metrics through detailed techno-economic analysis: the ethanol from sugarcane bagasse case

Felipe F. Furlan[a], Anderson Rodrigo de Andrade Lino[b], Argimiro R. Secchi[c], Caliane B. B. Costa[d], John M. Woodley[e], Roberto C. Giordano[a,b]

[a]Chemical Engineering Graduate Program, Universidade Federal de São Carlos (UFSCar), Rodovia Washington Luís (SP-310), km 235, São Carlos – SP – Brazil, CEP: 13565-905

[b]Department of Chemical Engineering, Universidade Federal de São Carlos (UFSCar), Rodovia Washington Luís (SP-310), km 235, São Carlos – SP – Brazil, CEP: 13565-905

[c]Chemical Engineering Graduate Program, COPPE, Universidade Federal de Rio de Janeiro, UFRJ, Cidade Univesitária, Rio de Janeiro, RJ, Brazil, CEP: 21941-972

[d]Chemical Engineering Department, Universidade Estadual de Maringá (UEM), Avenida Colombo, 5790, Maringá, Paraná, Brazil, CEP: 87020-900

[e]Department of Chemical and Biochemical Engineering, Technical University of Denmark, DK-2800 Kgs. Lyngby, Denmark

Abstract:

The production of ethanol from lignocellulosic materials is a promising alternative for decreasing the dependence on fossil fuel, although the process needs more development for achieving industrial feasibility. Despite the massive experimental effort in this area, thresholds values to be pursued in order to attain a feasible process are still missing,

which impairs the research. Meanwhile, simulation studies focus essentially on analyzing the techno-economic feasibility of a specific process. Alternatively, the present study uses a new approach for this problem, within a framework that promotes detailed techno-economic analyses embedded in process systems engineering simulation tools. In this way, general targets for process parameters, identified as process bottlenecks, can be drawn. This information would be a valuable feedback for the experimental studies. A case study consisting of a second generation ethanol process, integrated to a first generation one, using both sugarcane juice and bagasse as feedstock is considered. The process includes liquid hot water pretreatment and enzymatic hydrolysis of the cellulose. Additionally, the pentoses were also fermented. The methodology was able to find a feasible region for the case study and to outline regions to be further explored experimentally. The main effect on process feasibility came from the biocatalyst yield (kg of product / kg of catalyst).

Keywords: Bioethanol, Sugarcane, Techno-economic analysis, Process metrics thresholds.

1 Introduction

There is a clear tendency in the last decades in global politics towards increasing the participation of renewable energies in the overall energetic matrix. This is caused both by a public pressure to decrease environmental burdens caused by non-renewable fuels, and by the governments' concern about energy security, aiming at decreasing the influence of the external market on this strategic area (Cherubini and Strømman, 2010, Ng, 2010). In this scenario, ethanol is known to play an important role as an automotive fuel (Hahn-Hägerdal et al., 2006). In the case of Brazil, this tendency started in the

1970's, due to the two consecutive oil crises. In response, the government initiated the National Ethanol Program (PROALCOOL, in Portuguese, Zanin et al., 2000) to decrease national dependence on fossil oil. The program aimed to develop ethanol-based cars and to promote ethanol production from sugarcane.

The production of ethanol from sugarcane and corn are both called first generation (1G) ethanol production processes. For the former process, sugarcane is crushed in order to extract its juice (essentially a sucrose solution with impurities). The impurities are eliminated through a series of chemical and physical processes and the stream is concentrated. The concentrated juice undergoes ethanolic fermentation by *Saccharomyces cerevisiae* and the ethanol produced in this step is separated (as hydrous or anhydrous ethanol) in a train of distillation columns. Sugarcane bagasse, which is a lignocellulosic by-product of this process, is separated in the extraction step and used as fuel in boilers, producing process steam and electric energy to meet the process demands. If high pressure boilers are employed, a surplus of electric energy can be produced, which can be sold to the grid (Dias et al., 2011). In the specific case of bulk chemicals (fuels), the gap between the raw material costs and the profitable product cost is usually low (Ramos, 2013). Therefore, using the whole raw material efficiently is mandatory and process energy efficiency becomes important, to increase the surplus of electric energy. Alternatively, a surplus of bagasse can be sought in order to increase ethanol production through the so called second generation (2G) ethanol production process (Alvira et al., 2010, Cardona and Sánchez, 2007).

Additionally, for the specific case of sugarcane bagasse, there are three possible

approaches for integrating the 2G ethanol production process with the existing infrastructure of industries and with the already mature market. The most straightforward approach would be to retrofit an existing 1G ethanol production plant, taking advantage of the existing structure. In this scenario, the 1G process would not be altered and bagasse would be used for ethanol production aiming to decrease the input of sugarcane. Therefore, the industrial plant would produce the same amount of ethanol from a smaller amount of sugarcane. Nevertheless, most of the existing industrial units would need improvements in the process energetic efficiency in order to have a surplus of bagasse. These improvements, which probably include the purchase of high pressure boilers, would most likely have a negative impact on the 2G process economic feasibility.

The second option would be a standalone 2G ethanol production plant. This would buy sugarcane bagasse from other industries and use it to produce ethanol in a completely separated process. Nevertheless, as it was shown by Dias et al. (2012), a standalone 2G process would present a worse economic performance when compared to an integrated first and second generation process. This is mostly due to a 30 % difference between the investment cost of the integrated 1G and 2G unit and the combined prices of the 1G and the standalone 2G unit. Additionally, this process would be more prone to uncertainties on the operating costs. In particular, the impact of uncertainties concerning the enzyme price would be higher, since the damping of this cost by the selling of 1G ethanol would not occur.

The third option is an integrated first and second generation process starting from

scratch. In this approach, the capital costs involved in adapting the industrial unit to produce 2G ethanol (mainly the high pressure boiler) would be diluted in both 1G and 2G ethanol costs, increasing 2G feasibility. The same would be true for the uncertainties about 2G operating costs. Therefore, most studies in the literature consider this option in the economic analysis (Dias et al., 2013, Macrelli et al., 2012, Seabra et al., 2010, Walter and Ensinas, 2010).

Many experimental studies focus on optimizing specific process conditions usually employing design of experiments (Rabelo et al., 2013). Given that the information provided by these experiments is not easily extrapolated, it is most beneficial if the conditions approach the ones most likely to be used industrially. Otherwise, any techno-economic analysis based on the experimental data will be highly impaired. Nevertheless, it is not always easy to infer beforehand which conditions will be adopted in industry.

2G ethanol production process still is in early stage of development, and the fact that it will most probably be integrated to the 1G process adds challenges to the already existing ones for the clear understanding of the overall process. For this reason, it is not evident what level of performance should be pursued for the process metrics involved when running experimental studies. In this context, Retro-Techno-Economic Analysis (RTEA - Furlan et al., 2016) can be used to explore the influence of process parameters on the economic feasibility of the process and set minimum performances for the several process metrics, to be achieved experimentally. In the present study, RTEA is

applied to an integrated 1G and 2G ethanol production process to set minimum performance levels for the main process metrics. The process chosen as case study uses enzymatic hydrolysis of bagasse previously pretreated with liquid hot water. Both the pentoses and hexoses released are separately fermented and the purification step is integrated to the first generation process. The integrated process is compared to a base case where only 1G ethanol is produced and all bagasse is burned to yield a surplus of electric energy, sold to the grid.

2 Methodology

2.1 Process

The 1G ethanol production process was simulated based on a typical industrial unit. This will be the base case, representing the current technology. The process includes a washing step, to remove dirt carried during harvesting, followed by an extraction step, where the juice is separated from bagasse. In this step, water is added in counter-current to increase sugar recovery. The juice is sent to a series of physical and chemical processes in order to eliminate most of the impurities that were carried during the extraction step. The purified juice is then concentrated and fermented in a fed-batch process with recirculation of yeast. Finally, the resulting ethanolic solution is distilled and hydrous ethanol is obtained. Bagasse, on the other hand, is sent to the boiler to produce steam and electric energy in a Rankine cycle, to meet the process demand and to be sold to the grid. Table 1 shows the main data used for the 1G ethanol process.

Table 1: Main process parameters used in the simulation of 1G ethanol production.

Parameter	**Value**
Sugarcane bagasse humidity	50 wt.%
Sugar recovery (extraction step)	96 %
Mill energy demand	15.5 kWh/tonne
Fermentation efficiency (theoretical conversion = 100%)	90.5 %
Hydrous ethanol purity	93.5 wt.%
100 bar boiler efficiency - LHV basis	86 %
100 bar steam temperature	530 °C
Turbines isentropic efficiency	80 %
Generator efficiency	95.8 %
Exhaust steam pressure	2.5 bar

The integrated 2G ethanol plant diverts the maximum available amount of bagasse towards the production of biofuel (the process steam and electric demands are still completely fulfilled by burning bagasse and by-products of the biomass hydrolysis – mostly lignin and non-hydrolyzed cellulose). The bagasse will undergo a liquid hot water pretreatment, followed by a flash tank to release the high pressure. The acids produced in this step are neutralized with ammonia and the mixture is sent to a belt filter. The liquid fraction, rich in xylose, is fermented in a continuous bioreactor, as described in (Giordano et al., 2014), to produce ethanol which is sent to the distillation columns along with the 1G ethanol. Xylose biodigestion is also an explored possibility, although previous preliminary studies in the literature show that for the integrated process this option presents worse economic performance (Furlan et al., 2015, Macrelli et al., 2014). The solid fraction, on the other hand, is sent for enzymatic hydrolysis, and the final mixture undergoes another solid/liquid separation. The resulting solid fraction, composed mainly by lignin and non-hydrolyzed cellulose, is sent to the boiler. The

liquid fraction, with glucose as the main solute, is sent to the fermenter along with sugarcane juice. To sustain a fixed sugar concentration in the fermenter feed, the juice is further concentrated to make up for the lower glucose concentration in the hydrolysis outlet. Figure 1 shows the overall process, with the integration streams highlighted, while Table 2 shows the main data used in the 2G ethanol process. It should be noticed that in the present case study the use of sugarcane trash (straw and leaves, mostly) as fuel for the boiler was not considered. One possible scenario would be to collect part (for instance, 50 %) of this material from the field, which would imply in a transportation cost.

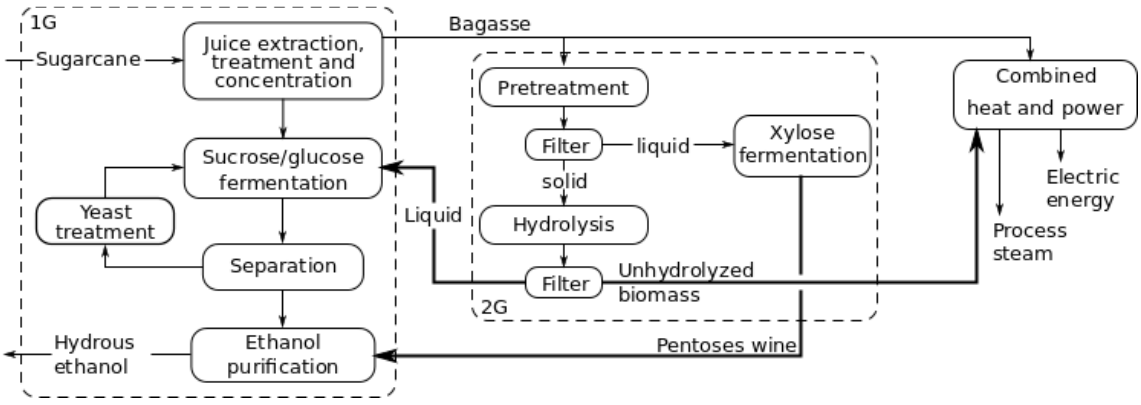

Figure 1: Integrated first and second generation ethanol production process with a combined heat and power stage. The bold lines show the streams that integrate both processes. 1G stands for the first generation process, adapted to the integrated process, while 2G stands for the specific second generation process.

Table 2: Main process parameters used in the simulation of 2G ethanol production.

Parameter	**Value**
Cellulose fraction in sugarcane bagasse	45.2 wt.%
Hemicellulose fraction in sugarcane bagasse	26.0 wt.%
Lignin fraction in sugarcane bagasse	26.6 wt.%
Ash fraction in sugarcane bagasse	2.2 wt.%
Pretreatment - hemicellulose to xylose conversion	46.5 %
Pretreatment - cellulose to glucose conversion	8.1 %
Pretreatment - temperature	195 °C
Pretreatment - reaction time	10 min
Pretreatment - solid mass fraction	20 wt.%
Hydrolysis - cellulose to glucose conversion	75 %
Hydrolysis - reaction time	72 h
Hydrolysis - solid mass fraction	20 wt.%
Hydrolysis - enzyme load	20 mg of enzyme/g of cellulose (10 FPU/g of cellulose)
Pentoses fermentation efficiency (theoretical conversion = 100%)	66.5 %
Filters - solid humidity	50 wt.%

2.2 Software

The software used for process simulation was EMSO (Soares, Secchi, 2003) which is an equation-oriented, general purpose process simulator with an embedded modeling language. Besides using the standard models that already exist in EMSO for most of the main pieces of equipment of the process, the user can also implement in-house models. The software also has several numeric solvers for solution of algebraic and differential-algebraic systems, and optimization of processes. Users can still plug in their own numerical routines (in C/C++ or FORTRAN). Additionally, the VRTherm (VRTech, 2005) thermodynamic package can be plugged in the software for prediction of thermodynamic properties.

2.3 Assumptions

The investment cost for the first generation ethanol production unit was based on Pinto (2010), adapted to the current process and currency basis (December/2012). The same was done for the combined heat and power stage (Dantas, 2013). For the 2G ethanol production process, the investment cost was obtained by calculating the main equipment costs using data from the literature (Humbird et al., 2011) and online equipment cost estimators (Matches, 2015), using scaling factors when necessary. The operating cost was based on the raw materials cost, shown in Table 3, and on personal contacts with the industry. The enzyme prices were based on the study by Klein-Marcuschamer et al. (2011) and, therefore, do not represent any commercial enzymatic complex.

Table 3: Prices of chemicals, raw materials and products.

Chemical/Raw material	**Cost (US$/tonne)**
Sugarcane[a]	23.59
Water	0.0143
Ammonia (99.9 % ammonia)	600
H_2SO_4 (98 %)	51.9
KH_2PO_4 (98 %)	400
Ureia (99 %)	200
$CaCl_2$ (94 %)	100
Kamoran (antibiotics)	109800
NaOH (99 %)	310
H_3PO_4 (85 %)	700
$MgSO_4$ (99 %)	80
Enzyme (150 g of enzyme/L)[b]	1520
Ethanol (US$/m³)[c]	513.7
Electric energy (US$/MWh)[d]	80.8

[a] Average sugarcane price between Jan/2001 and Dec/2012 in São Paulo state (UDOP, 2015).

[b] Klein-Marrcuschamer et al. (2011).

[c] Cepea (2015).

[d] Dantas (2010).

The economic analysis was carried out assuming the parameters displayed in Table 4. The minimum ethanol selling price (MESP) for both the base case and the combined production (1G + 2G) corresponds to a zero net present value for the enterprise. In this sense, the MESP not only accounts for the direct costs, but also for the indirect ones: taxes, shareholders payout and return over the investment. It is important to point out that the electric energy is accounted for as an opportunity cost. In this sense, it is negative for the 1G process, as well as for the combined 1G + 2G, while it is positive

for the 2G process, since in the later, the total electric energy production is decreased. The main cost contributions for the MESP were also calculated both for the combined (1G + 2G) and for the 2G ethanol alone. The later was obtained by subtracting the costs for the base case (1G) using Equation (1), as described by Macrelli et al. (2012).

$$P_{2G}^{i} = \frac{F_{1G+2G} \times P_{1G+2G}^{i} - F_{1G} \times P_{1G}^{i}}{F_{1G+2G} - F_{1G}} \quad (1)$$

where P^{i}_{j} is the cost contribution of item i in the j process and F_j is the ethanol flow in the j process. Therefore, the cost contribution for the 2G ethanol is given by the weighted ratio between the difference in the cost contribution of item i in the combined process (1G + 2G) and in 1G ethanol single production.

Table 4: Main economic premises.

Parameter	**Value**
Internal rate of return after tax and above inflation	11 %
Project lifetime	25 years
Tax rate	34 %
Tax-deductible linear depreciation	10 %/year
Plant scrap value	None
Project construction time	1 year
Currency basis	2012 US$
Shareholder rate after taxes	20 %

Tufvesson et al. (2013) described general target values for the main process metrics involved in a bioprocess, depending on the type of product and on the production scale. The same metrics were considered as the base for the present study, except for the product concentration, which was replaced by a process parameter, the solid mass fraction in the reactor and the space-time yield (or productivity), which was included in the analysis. This is actually a different perspective for the problem, although using the

same approach: ethanol concentration in the industrial fermenters output stream actually spans a narrow range, which is already optimized taking into account mostly the cost of energy for distillation. Thus, the concentration of the main product (ethanol) is not the most appropriate metric. On the other hand, since the present case study focus on an integrated 1G-2G process, the streams coming from 1G and 2G sections are mixed before fermentation (i.e., sucrose and glucose are simultaneously fermented to ethanol), and concentrated to meet the necessary specification. So, in this particular case, it seems more reasonable to choose for process metrics a few operating parameters of the 2G process that impact capital and operating costs, and that are not still established in industrial practice.

Thus, based on the general methodology described by Furlan et al. (2016), target values for the process metrics (reaction yield, space-time yield, biocatalyst yield and solid mass fraction in the reactor) were obtained for the process described. The targets for the process metrics were attained based on Equation 2, which defines economic feasibility of the process. Since the equation includes four variables, in order to facilitate the visualization of the feasible regions, one of them was fixed while two other were varied, to obtain the value of the last one at the boundary of the economic feasible region.

NPV(solid mass fraction, reaction yield, biocatalyst yield, space-time yield) = 0 (2)

3 Results and discussion

The chosen base case represents a medium size industrial unit in Brazil, processing two million tonnes of sugarcane per year, or 500 tonnes/h. This is converted to 42.6 m^3/h of hydrous ethanol or 85.2 liters/tonne of sugarcane. Additionally, an electric energy

production of 57.4 MW is achieved, which corresponds to a surplus of 41.6 MW, after supplying the process demands. This setup is comparable to other results in the literature, with some small differences related to the process assumptions made in each study.

These results are translated to a MESP of 498.4 USD/m³. As expected, the biggest contribution for the cost of 1G ethanol is the main raw material, sugarcane, followed by the capital costs (CapEx cost), as shown in Figure 2.

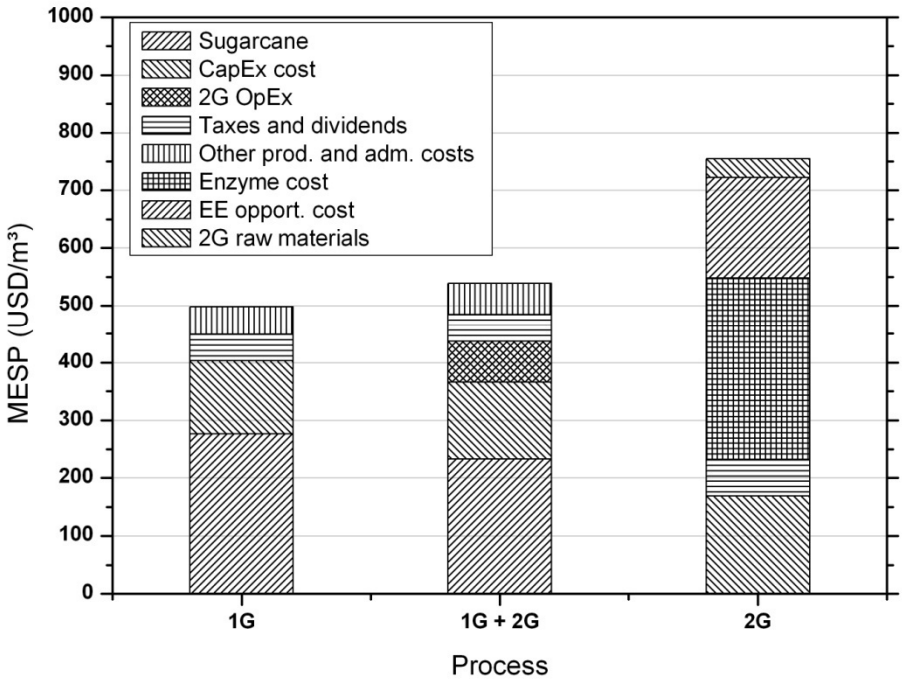

Figure 2: Cost contribution for the base case, the integrated 1G and 2G ethanol and for the 2G ethanol production, isolated from the rest of the plant.

For the integrated 1G and 2G ethanol production process, keeping the same input of

sugarcane, it was possible to increase the production in 18.8 %, equivalent to 101.2 liters/tonne of sugarcane. In this case, 51 % of bagasse was diverted from the steam production to the 2G process, which led to a decrease in electric energy surplus of 52.6 %. The high fraction of bagasse diverted to 2G ethanol was possible due to the high solid mass fractions in the main steps (pretreatment and hydrolysis) and the use of by-products (mainly lignin) as fuel to the boiler. The combined MESP obtained in this case was 539.1 USD/m³. The cost contribution of sugarcane remains the main one for the combined 1G and 2G production. Nevertheless, if only the 2G ethanol is considered, the enzyme cost contribution clearly dominates, followed by the capital cost and the electric energy opportunity cost, as shown in Figure 2.

3.1 Process metrics

Each process metric was evaluated as described in the Methodology section. Feasibility curves are plotted, all of them as a function of the solid mass fraction in the hydrolysis reactor. Figure 3 shows the feasibility curves for the biocatalyst yield for different reaction yields and a fixed space- time yield of 2.5 $gL^{-1}h^{-1}$. There is a visible minimum point for all feasible boundaries that dislocates from around 14 % solid mass fraction in the hydrolysis reactor (for high hydrolysis yields) to around 22 % (for low yields). This is due to the trade-off between the final glucose concentration, which increases with the solid mass fraction, and the sugar recovery in the filter, which decreases with it. Maximum sizes were imposed to all pieces of equipments in this study. The hills visible in the feasibility curves in Figure 3 (the most visible one between 18 and 22 % solid mass fraction for a 70 % reaction yield) are caused by increases in the number of

equipments. Also, the figure shows that the correlation between the biocatalyst yield and the solid mass fraction decreases for high reaction yields but becomes very important for low ones. Finally, the hatched area represents the infeasible area, i. e., for biocatalyst yields below 60 g of glucose/g of enzyme, no feasible process can be achieved.

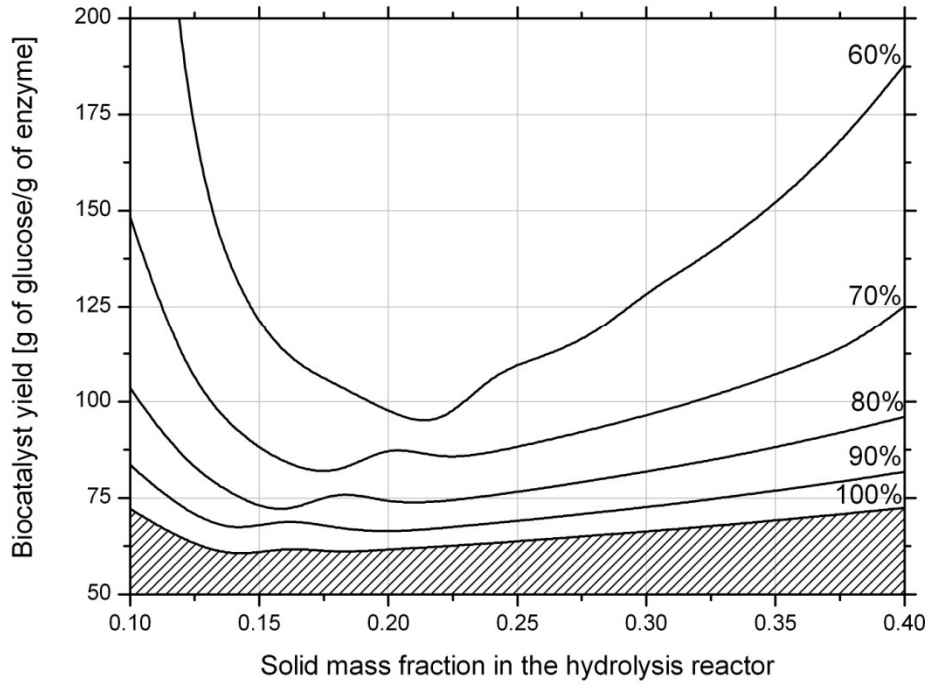

Figure 3: Feasibility line for the biocatalyst yield for different reaction yields as a function of the solid mass fraction in the hydrolysis reactor (space-time yield = 2.5 g L^{-1} h^{-1}). Feasible region: above the curves (boundaries of the feasibility regions). Hatched area is infeasible. The numbers above the feasibility lines are the reaction yields.

The opposite plot (reaction yield vs. solid mass fraction for different biocatalyst yields) is presented in Figure 4 and shows more clearly the relation between the two metrics.

As it can be seen, the influence of the biocatalyst yield in the reaction yield is strong, but quickly decreases above 150 g of glucose/g of enzyme. Nevertheless, this value is already around four times the average biocatalyst yield for the hydrolysis reaction (for a 10 FPU/g of cellulose load). For the usual enzyme load, no feasible reaction yield can be obtained for the system studied and the economic scenario considered. This shows the importance of increasing the enzyme activity in order to increase the biocatalyst yield or of decreasing the cost of production for the enzyme. These two alternatives would appear as equivalents in the present analysis, since both would result in a decrease in the final cost contribution of the enzyme on MESP, increasing the feasible area for this metric. Also, it is important to bear in mind that the pretreatment has a great influence on both yields. This influence, however, is not straightforward since both capital and operating costs of the pretreatment and the amount of lost sugar during it must be carefully assessed.

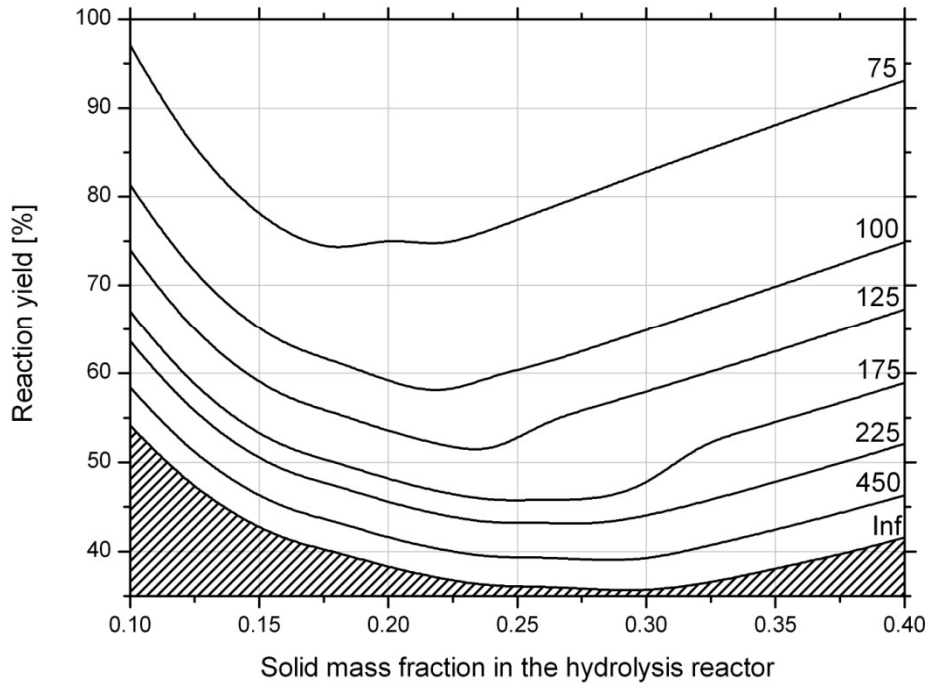

Figure 4: Feasibility line for the reaction yield for different biocatalyst yield as a function of the solid mass fraction in the hydrolysis reactor (space-time yield = 2.5 g L^{-1} h^{-1}). Feasible region: above the curves (boundaries of the feasibility regions). Hatched area is infeasible. The numbers above the feasibility lines are the biocatalyst yields. The infinite biocatalyst yield was obtained by eliminating the enzyme cost.

It is worth to recall that the enzyme complex considered in this study is not a commercial one. Therefore, the biocatalyst yield cannot be easily converted to the one expected for a commercial complex. Nevertheless, by keeping the ratio between the enzyme activity and its cost fixed, the biocatalyst yield can be presented in an activity base. In this case, values around 0.12 g of glucose/FPU (60 g of glucose/g of enzyme, for a conversion of 100 %) would be necessary. This implies a limit of 9.2 FPU/g of cellulose as the initial enzyme load.

The space-time yield, on the other hand, showed a small influence on the overall process feasibility, as it can be seen in Figure 5. This metric only becomes important for low reaction yields, as its feasibility curves are more influenced by the solid mass fraction. . It is interesting to note that the experimental space-time yields are usually above the presented threshold, showing that this metric is not as important as initially expected. This is mostly due to the low cost of the reactor considered in the present study, and to the low agitation power that it demands (Humbird, 2011), which decreases the impact of this metric on the overall process feasibility.

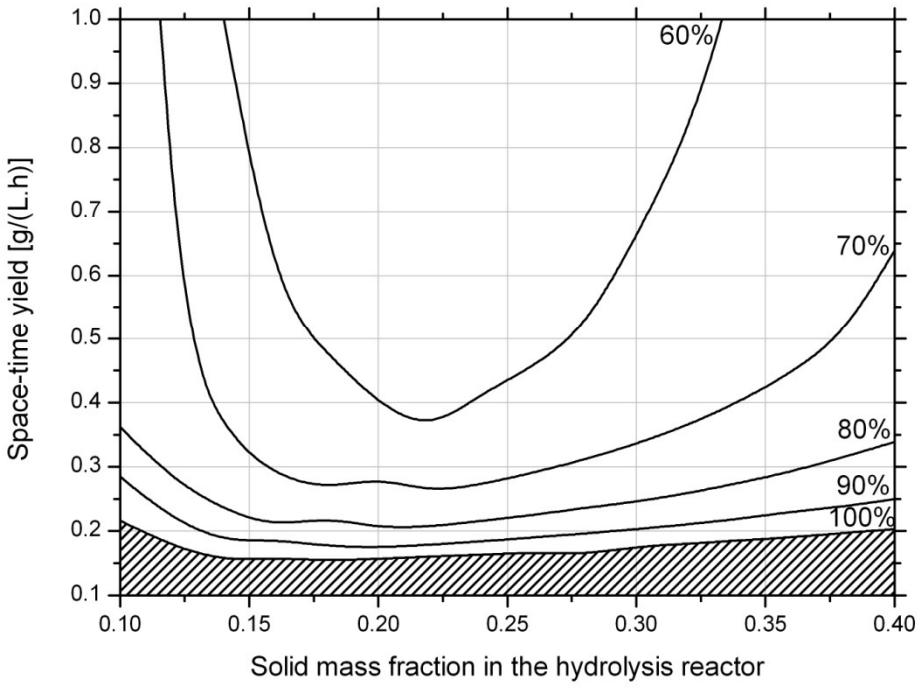

Figure 5: Feasibility line for the space-time yield for different reaction yields as a function of the solid mass fraction in the hydrolysis reactor (biocatalyst yield = 150 g of glucose/g of enzyme). Feasible region: above the curves (boundaries of the feasibility regions). Hatched area is infeasible. The numbers above the feasibility lines are the

reaction yields.

4 Conclusion

The production process of 2G ethanol from sugarcane bagasse presents some peculiarities. For this reason, the targets normally considered for bioprocesses cannot be directly applied for this case. The methodology described can provide a useful approach to obtain these target values and guide future developments in the area. For the case study considered, for example, it was possible to verify that the space-time yield is not as important as initially expected. Additionally, a limit value for the enzyme load could be derived, which will probably demand future improvements in enzyme production.

Acknowledgements

The authors would like to thank the FAPESP BIOEN Program, the Brazilian National Council for Scientific and Technological Development (CNPq) and CAPES (Fellowship Process # 2608/14-6) for the financial support.

References

Alvira, P., Tomás-Pejó, E., Ballesteros, M., Negro, M.J. 2010. Pretreatment technologies for an efficient bioethanol production process based on ezymatic hydrolysis: A review. Bioresour Technol. 101, 4851-4861.

Cardona, C.A., Sánchez, O.J. 2007. Fuel ethanol production: Process design trends and integration opportunities. Bioresour Technol. 98, 2415-2457.

Cepea - Center of Advanced Studies in Applied Economy. 2015. Ethanol prices <http://cepea.esalq.usp.br/etanol/> (retrieved in 17/02/2015).

Cherubini, F., Strømman, A.H. 2010. Production of Biofuels and Biochemicals from Lignocellulosic Biomass: Estimation of Maximum Theoretical Yields and Efficiencies Using Matrix Algebra. Energy Fuels. 24, 2657-2666.

Dantas, G.A. 2013. Investment alternatives for the sugar-energetic sector for exploitation of sugarcane bagasse and straw. PhD thesis, Universidade Federal do Rio de Janeiro, Rio de Janeiro, in Portuguese

Dias, M.O.S., Cunha, M.P., Jesus, C.D.F, Rocha, G.J.M., Pradella, J.G.C., Rossell, C.E.V., Maciel Filho, R., Bonomi, A. 2011. Second generation ethanol in Brazil: Can it compete with electricity production? Bioresour Technol. 102, 8964-8971.

Dias, M.O.S., Junqueira, T.L., Cavalett, O., Cunha, M.P., Jesus, C.D.F., Rossell, C.E.V., Maciel Filho, R., Bonomi, A. 2012. Integrated versus stand-alone second generation ethanol production from sugarcane bagasse and trash. Bioresour Technol. 103, 152-161.

Dias, M.O.S., Junqueira, T.L., Cavalett, Pavanello, L.G., Cunha, M.P., Jesus, C.D.F., Maciel Filho, R., Bonomi, A. 2013. Biorefineries for the production of first and second generation ethanol and electricity from sugarcane. Appl Energy. 109, 72-78.

Furlan, F. F., Costa, B. B. C., Secchi, A. R., Woodley, J. M., Giordano, R. C. Retro-Techno-Economic Analysis (RTEA): using (bio)process systems engineering tools to attain process target values. Submitted.

Furlan, F.F., Giordano, R.C., Costa, C.B.B., Secchi, A.R., Woodley, J.M. 2015. Process Alternatives for Second Generation Ethanol Production from Sugarcane Bagasse, in: 12th International Symposium on Process Systems Engineering and 25th European Symposium on Computer Aided Process Engineering, Denmark.

Giordano, R. L. C. *et al*. 2014. Catalytic system and process for obtaining 2G bioethanol

from xylane / xylose olygomers". INPI Patent application, BR1020140233946, Brazil, in Portuguese.

Hahn-Hägerdal, B., Galbe, M., Gorwa-Grauslund, M., Liden, G., Zacchi, G. 2006. Bioethanol-the fuel of tomorrow from the residues of today. Trends Biotechnol. 24, 549-556.Humbird, D., Davis, R., Tao, L., Kinchin, C., Hsu, D., Aden, A., Schoen, P., Lukas, J., Olthof, B., Worley, M., Sexton, D., Dudgeon, D. 2011. Process Design and Economics for Biochemical Conversion of Lignocellulosic Biomass to Ethanol: Dilute-Acid Pretreatment and Enzymatic Hydrolysis of Corn Stover. NREL/TP-5100-47764. Golden, CO. National Renewable Energy Laboratory.

Klein-Marcuschamer, D., Oleskowicz-Popiel, P., Simmons, B.A., Blanch, H.W. 2011. The Challenge of Enzyme Cost in the Production of Lignocellulosic Biofuels. Biotechnol Bioeng. 109, 1083-1087.

Macrelli, S., Galbe, M., Wallberg, O. 2014. Effects of production and market factors on ethanol profitability for an integrated first and second generation ethanol plant using the whole sugarcane as feedstock. Biotechnol Biofuels. 7, 26.

Macrelli, S., Mogensen, J., Zacchi, G. 2012. Techno-economic evaluation of 2nd generation bioethanol production from sugar cane bagasse and leaves integrated with the sugar-based ethanol process. Biotechnol Biofuels. 5, 22.

Matches' 275 Equipment Cost Estimates. 2015. <http://www.matche.com/equipcost/Default.html> (retrieved in 15/01/2015).Ng, D.K.S. 2010. Automated targeting for the synthesis of an integrated biorefinery. Chem Eng J. 162, 67-74.

Pinto, F.H.P.B. 2010. Cellulosic ethanol: a study of economic and financial viability. Masters thesis, Universidade de São Paulo, São Paulo, in Portuguese.

Rabelo, S.C., Maciel Filho, R., Costa, A.C. 2013. Lime Pretreatment and Fermentation of Enzymatically Hydrolyed Sugarcane Bagasse. Appl Biochem Biotechnol. 169, 1696-1712.

Ramos, J.A.L. 2013. A methodology for development of biocatalytic processes. PhD thesis, Technical University of Denmark, Lyngby.

Seabra, J.E.A, Tao, L., Chum, H.L., Macedo, I.C. 2010. A techno-economic evaluation of the effects of centralized cellulosic ethanol and co-products refinery options with sugarcane mill clustering. Biomass Bioenergy. 34, 1065-1078.

Soares, R.P., Secchi, A.R. 2003. EMSO: A new environment for modelling, simulation and optimisation. Comput Aided Chem Eng. 14, 947-952.

Tufvesson, P., Lima-Ramos, J., Al Haque, N., Gernaey, K.V., Woodley, J.M. 2013. Advances in the Process Development of Biocatalytic Processes. Org Process Res Dev. 17, 1233-1238.

UDOP - Union Of Biofuel Producers, 2015. Sugarcane prices. <http://udop.com.br/cana/tabela_consecana_saopaulo.pdf> (retrieved 17/02/2015).

VRTech. 2005. www.vrtech.com.br.

Walter, A., Ensinas, A.V. 2010. Combined production of second-generation biofuels and electricity from sugarcane residues. Energy. 35, 874-879.

Zanin, G.M., Santana, C.C., Bon, E.P.S., Giordano, R.L.C., Moraes, F.F., Andrieta, S.R., Carvalho Neto, C.C., Macedo, I.C., Fo, D.L., Ramos, L.P., Fontana, J.D. 2000. Brazilian bioethanol program. Appl Biochem Biotechonol. 84, 1147-1163.

6 Conclusões e sugestões de trabalhos futuros

6.1 Conclusões

O presente trabalho apresentou inicialmente uma metodologia para aproximação de modelos não-lineares. Esses modelos apresentam difícil convergência em simuladores orientados a equações, o que inviabiliza sua utilização em simulações de processos completos, onde uma correta inicialização de suas variáveis é pouco prática. A metodologia desenvolvida, que utiliza interpolador baseado em tabelas de inspeção multilineares, se mostrou bastante robusta. Ademais, a acurácia da aproximação pôde ser controlada através do número de pontos utilizados para construir a tabela de inspeção. Isso permitiu a simulação do processo completo de produção de etanol 1G/2G sem recorrer a modelos simplificados de colunas de destilação, cujo modelo mais rigoroso foi de difícil convergência e, por isso, não foi utilizado. O interpolador foi particularmente apto a aproximar o comportamento das colunas, apresentando boa acurácia em toda a região estudada.

A análise econômica que se seguiu permitiu abordar a questão da viabilidade de um processo flexível, no qual o bagaço da cana-de-açúcar pudesse ser desviado tanto para a produção de energia elétrica quanto para a produção de etanol. Analisou-se também a influência tanto de parâmetros econômicos quanto de processo na viabilidade econômica do processo 1G/2G integrado. Tais análises, apesar de produzirem resultados interessantes são insuficientes quando se considera processos (bio)químicos em estágios iniciais de desenvolvimento. Nesses casos, são imprescindíveis informações que ajudem a guiar o desenvolvimento do processo, indicando as melhorias que impactariam de forma mais significativa a viabilidade do processo.

Não foi encontrada na literatura uma metodologia sistemática para obter essas informações baseada em modelagem rigorosa do processo aliada à análise econômica do mesmo. Essa limitação observada na literatura motivou o desenvolvimento de uma metodologia original e de utilização geral que permitisse avaliar qual conjunto de variáveis de processo tem maior influência no desempenho econômico do processo, obter seus valores mínimos para que a viabilidade do processo fosse alcançada e também a correlação entre essas variáveis. A aplicação da metodologia em dois estudos de caso mostrou sua flexibilidade e capacidade de fornecer informações fundamentais para guiar futuros experimentos visando alcançar condições que viabilizem o processo. Em

particular, para o processo de produção de etanol 1G/2G, as variáveis mais importantes foram o rendimento do biocatalisador, a conversão da celulose e a carga de sólidos no reator de hidrólise.

6.2 Sugestões de trabalhos futuros

O desenvolvimento deste trabalho de doutorado levantou algumas possibilidades de extensão das metodologias apresentadas. Essas são apresentadas a seguir:

O interpolador construído e testado neste trabalho apresentou algumas limitações causadas pela escolha por passo fixo das variáveis. Apesar de facilitar a localização dos pontos utilizados na interpolação dos resultados, essa escolha impossibilita o refino da malha em regiões com gradientes acentuados. Assim, uma possível expansão da metodologia seria considerar o espaçamento variável da malha e a necessária adaptação do critério para escolha desse espaçamento.

Dentro do contexto da metodologia da análise econômica reversa, há a possibilidade de investigação de métodos para a escolha das variáveis mais significativas na viabilidade econômica do processo. Uma análise de sensibilidade foi utilizada para auxiliar nessa decisão. Porém, tal método é local e pode ser interessante incluir uma análise estatística da influência de todas as variáveis dentro das regiões estudadas.

Concernente ao processo 1G/2G utilizado nas análises econômicas, vale ressaltar que este não foi otimizado. Duas variáveis não utilizadas no presente estudo são claramente foco de uma otimização, sendo estas as duas adições de água usadas para lavar as tortas dos filtros após o pré-tratamento do bagaço e após a etapa de hidrólise. Tais variáveis afetam a recuperação dos açúcares nessas etapas, ao mesmo tempo em que diluem a solução. São portanto candidatadas claras a uma otimização. Porém, é importante frisar que o ponto de ótimo para estas variáveis sofre influências das variáveis de processo consideradas na análise econômica reversa. Ao mesmo tempo, a realização da otimização destas variáveis combinada à análise econômica reversa demandaria bastante tempo computacional. Pode-se portanto, avaliar a possibilidade de utilizar um ponto sub-ótimo para essas variáveis, que seja pouco sensível a variações das variáveis utilizadas na análise tecno-econômica reversa.

Finalmente, como era de se esperar, a análise tecno-econômica reversa somente leva em consideração o critério econômico para construção dos diagramas. A inclusão de outros critérios, principalmente os de caráter ambiental, pode trazer uma grande contribuição à metodologia. Utilizando o mesmo conceito de desempenho mínimo para cada indicador ambiental, seria possível incluí-los no mesmo diagrama. Isso pos-

sivelmente criará janelas de operação, nas quais tanto as metas econômicas quanto ambientais serão atendidas.

Referências

AGBLEVOR, F. A.; REJAI, B.; WANG, D.; WISELOGEL, A.; CHUM, H. L. Influence of storage conditions on the production of hydrocarbons from herbaceous biomass. *Biomass and Bioenergy*, v. 7, n. 1, p. 213–222, 1994.

Agência nacional de energia elétrica – ANEEL. 2012. Disponível em: <http://www.aneel.gov.br>. Acesso em: Jan. 2013.

FUNDAÇÃO UNIVERSIDADE FEDERAL DE SÃO CARLOS. R L C Giordano et al. *Sistema catalítico e processo de obtenção de bioetanol 2G a partir de derivados de xilana/oligômeros de xilose*. 2015. IPNI BR 10 2014 023395-4.

ALVIRA, P.; TOMÁS-PEJÓ, E.; BALLESTEROS, M.; NEGRO, M. J. Pretreatment technologies for an efficient bioethanol production process based on enzymatic hydrolysis: a review. *Bioresource technology*, v. 101, n. 13, p. 4851–4861, 2010.

ANGARITA, J. D.; SOUZA, R. B. A.; CRUZ, A. J. G.; SECCHI, E. C. B. A. R. Kinetic modeling for enzymatic hydrolysis of pretreated sugarcane straw. *Biochemical Engineering Journal*, v. 104, p. 10–19, 2015.

BIEGLER, L. T.; GROSSMANN, I. E.; WESTERBERG, A. W. *Systematic methods of chemical process design*. Nova Jérsia: Prentice Hall, Old Tappan, NJ (United States), 1997. 796 p.

Brazilian Automotive Industry Association – ANFAVEA (ACRONYM IN PORTUGUESE). *Brazilian Automotive Industry Yearbook*. São Paulo, 2012.

Câmara de Comercialização de Energia Elétrica – CCEE. 2013. Disponível em: <http://http://www.ccee.org.br/>. Acesso em: Jan. 2013.

CANILHA, L.; CHANDEL, A. K.; MILESSI, T. S. dos S.; ANTUNES, F. A. F.; FREITAS, W. L. da C.; FELIPE, M. das G. A.; SILVA, S. S. da. Bioconversion of sugarcane biomass into ethanol: An overview about composition, pretreatment methods, detoxification of hydrolysates, enzymatic saccharification, and ethanol fermentation. *Journal of Biomedicine and Biotechnology*, v. 2012, p. 1–15, 2012.

CARDONA, C. A.; SÁNCHEZ, Ó. J. Fuel ethanol production: process design trends and integration opportunities. *Bioresource technology*, v. 98, n. 12, p. 2415–2457, 2007.

Centro de Estudos Avançados em Economia Aplicada – CEPEA/ESALQ/USP. 2013. Disponível em: <http://www.cepea.esalq.usp.br>. Acesso em: Jan. 2013, Fev. 2015.

CHEALI, P.; GERNAEY, K. V.; SIN, G. Toward a computer-aided synthesis and design of biorefinery networks: data collection and management using a generic modeling approach. *ACS Sustainable Chemistry & Engineering*, v. 2, n. 1, p. 19–29, 2013.

CHEN, J. Comments on improvements on a replacement for the logarithmic mean. *Chemical Engineering Science*, v. 42, n. 10, p. 2488–2489, 1987.

CHERUBINI, F.; STRØMMAN, A. H. Production of biofuels and biochemicals from lignocellulosic biomass: Estimation of maximum theoretical yields and efficiencies using matrix algebra. *Energy & Fuels*, v. 24, n. 4, p. 2657–2666, 2010.

DANTAS, G. de A. *Alternativas de investimento do setor sucroenergético brasileiro para aproveitamento de bagaço e de palha*. 2013. 202 p. Tese (Doutorado em planejamento energético) — Instituto Alberto Luiz Coimbra de pós-graduação e pesquisa de engenharia, Universidade Federal do Rio de Janeiro, Rio de Janeiro, 2013.

DIAS, M. O. S. *Simulation of ethanol production process from sugar and sugarcane bagasse aiming at process integration and energy production maximization (Simulação do processo de produção de etanol a partir do açúcar e do bagaço, visando a integração do processo e a maximização da produção de energia e excedentes do bagaço)*. 2008. 282 p. Dissertação (Mestrado em Engenharia Química) — Faculdade de Engenharia Química, Universidade Estadual de Campinas, Campinas, SP, 2008.

DIAS, M. O. S.; CUNHA, M. P.; JESUS, C. D. F.; ROCHA, G. J. M.; PRADELLA, J. G. C.; ROSSELL, C. E. V.; FILHO, R. M.; BONOMI, A. Second generation ethanol in brazil: Can it compete with electricity production? *Bioresource technology*, v. 102, n. 19, p. 8964–8971, 2011.

DIAS, M. O. S.; JUNQUEIRA, T. L.; CAVALETT, O.; CUNHA, M. P.; JESUS, C. D. F.; ROSSELL, C. E. V.; FILHO, R. M.; BONOMI, A. Integrated versus stand-alone second generation ethanol production from sugarcane bagasse and trash. *Bioresource Technology*, v. 103, n. 1, p. 152–161, 2012.

DIAS, M. O. S.; JUNQUEIRA, T. L.; CAVALETT, O.; PAVANELLO, L. G.; CUNHA, M. P.; JESUS, C. D. F.; FILHO, R. M.; BONOMI, A. Biorefineries for the production of first and second generation ethanol and electricity from sugarcane. *Applied Energy*, v. 109, p. 72–78, 2013.

EDGAR, T. F.; HIMMELBLAU, D. M.; LASDON, L. *Optimization of chemical processes*. 2° edição. ed. Nova Iorque: McGraw-Hill, 2001. 650 p.

EFE, Ç.; WIELEN, L. A. M. van der; STRAATHOF, A. J. J. Techno-economic analysis of succinic acid production using adsorption from fermentation medium. *Biomass and Bioenergy*, v. 56, p. 479–492, 2013.

EGGEMAN, T.; ELANDER, R. T. Process and economic analysis of pretreatment technologies. *Bioresource technology*, v. 96, n. 18, p. 2019–2025, 2005.

FLOUDAS, C. A. *Nonlinear and Mixed-Integer Optimization: Fundamentals and Applications*. Nova Iorque: Oxford University Press, 1995. 462 p.

FURLAN, F. F. *Desenvolvimento de ambiente integrado para simulação e otimização estática da produção de etanol a partir de bagaço de cana-de-açúcar por rota bioquímica*. 2012. 108 p. Dissertação (Mestrado em Engenharia Química) — Departamento de Engenharia Química, Universidade Federal de São Carlos, São Carlos, 2012.

FURLAN, F. F.; COSTA, C. B. B.; FONSECA, G. de C.; SOARES, R. de P.; SECCHI, A. R.; CRUZ, A. J. G. da; GIORDANO, R. de C. Assessing the production of first and second generation bioethanol from sugarcane through the integration of global optimization and process detailed modeling. *Computers & Chemical Engineering*, v. 43, p. 1–9, 2012.

FURLAN, F. F.; FILHO, R. T.; PINTO, F. H.; COSTA, C. B.; CRUZ, A. J.; GIORDANO, R. L.; GIORDANO, R. C. Bioelectricity versus bioethanol from sugarcane bagasse: is it worth being flexible? *Biotechnology for biofuels*, v. 6, p. 142, 2013.

FURLAN, F. F.; GIORDANO, R. C.; COSTA, C. B. B.; SECCHI, A. R.; WOODLEY, J. M. Process alternatives for second generation ethanol production from sugarcane bagasse. In: GERNAEY, K. V.; HUUSOM, J. K.; GANI, R. (Ed.). *12^{TH} International Symposium on Process Systems Engineering and 25^{TH} European Symposium on Computer Aided Process Engineering*. Lyngby: Elsevier, 2015. p. 1349–1354.

GNANSOUNOU, E. Production and use of lignocellulosic bioethanol in europe: Current situation and perspectives. *Bioresource Technology*, v. 101, p. 4842–4850, 2010.

GRACIANO, J.; ROUX, G. L. Improvements in surrogate models for process synthesis. application to water network system design. *Computers & Chemical Engineering*, v. 59, p. 197–210, 2013.

GROSSMANN, I. Review of nonlinear mixed-integer and disjunctive programming techniques. *Optimization and Engineering*, v. 3, n. 3, p. 227–252, 2002.

GROSSMANN, I. E.; APAP, R. M.; CALFA, B. A.; GARCIA-HERREROS, P.; ZHANG, Q. Recent advances in mathematical programming techniques for the optimization of process systems under uncertainty. In: GERNAEY, K. V.; HUUSOM, J. K.; GANI, R. (Ed.). *12^{TH} International Symposium on Process Systems Engineering and 25^{TH} European Symposium on Computer Aided Process Engineering*. Lyngby: Elsevier, 2015. p. 641–646.

HAHN-HÄGERDAL, B.; GALBE, M.; GORWA-GRAUSLUND, M. F.; LIDÉN, G.; ZACCHI, G. Bio-ethanol–the fuel of tomorrow from the residues of today. *Trends in biotechnology*, v. 24, n. 12, p. 549–556, 2006.

HARMSEN, G. J. Industrial best practices of conceptual process design. *Chemical Engineering and Processing*, v. 43, p. 677–681, 2004.

HASSUANI, S. J.; LEAL, M. R. L. V.; MACEDO, I. C. *Biomass power generation: Sugarcane bagasse and trash*. Piracicaba: United Nations Development Programme and Sugarcane Technology Centre, 2005. 217 p.

HOSKINS, J. C.; HIMMELBLAU, D. Artificial neural network models of knowledge representation in chemical engineering. *Computers & Chemical Engineering*, v. 12, n. 9, p. 881–890, 1988.

HSIEH, C. wen C.; CANNELLA, D.; JØRGENSEN, H.; FELBY, C.; THYGESEN, L. G. Cellulase inhibition by high concentrations of monosaccharides. *Journal of agricultural and food chemistry*, v. 62, n. 17, p. 3800–3805, 2014.

HUMBIRD, D.; DAVIS, R.; TAO, L.; KINCHIN, C.; HSU, D.; ADEN, A.; SCHOEN, P.; LUKAS, J.; OLTHOF, B.; WORLEY, M.; SEXTON, D.; DUDGEON, D. *Process Design and Economics for Biochemical Conversion of Lignocellulosic Biomass to Ethanol: Dilute-Acid Pretreatment and Enzymatic Hydrolysis of Corn Stover*. Golden, Colorado, 2011. 147 p.

IPSITABANERJEE; PAL, S.; MAITI, S. Computationally efficient black-box modeling for feasibility analysis. *Computers & chemical engineering*, v. 34, n. 9, p. 1515–1521, 2010.

JAIMES, A. L.; COELLO, C. A. C. Multi-objective evolutionary algorithms: A review of the state-of-the-art and some of their applications in chemical engineering. In: *Multi-Objective Optimization: Techniques and Applications in Chemical Engineering*. Singapura: World Scientific, 2009. p. 61–86.

KAZI, F. K.; FORTMAN, J.; ANEX, R.; KOTHANDARAMAN, G.; HSU, D.; ADEN, A.; DUTTA, A. NREL/TP-6A2-46588. *Techno-economic analysis of biochemical scenarios for production of cellulosic ethanol*. Golden, Colorado: National Renewable Energy Laboratory - NREL, 2010. 102 p.

KENNEDY, J.; EBERHART, R. Particle swarm optimization. In: *Proceedings of IEEE International Conference on Neural Networks*. Perth: Institute of Electrical & Electronics Enginee - IEEE, 1995. p. 1942–1948.

KLEIN-MARCUSCHAMER, D.; OLESKOWICZ-POPIEL, P.; SIMMONS, B. A.; BLANCH, H. W. The challenge of enzyme cost in the production of lignocellulosic biofuels. *Biotechnology and Bioengineering*, v. 109, n. 4, p. 1083–1087, 2012.

MACEDO, I. C.; SEABRA, J. E. A.; SILVA, J. E. A. R. Green house gases emissions in the production and use of ethanol from sugarcane in brazil: The 2005/2006 averages and a prediction for 2020. *Biomass and Bioenergy*, v. 32, p. 582–595, 2008.

MACRELLI, S.; GALBE, M.; WALLBERG, O. Effects of production and market factors on ethanol profitability for an integrated first and second generation ethanol plant using the whole sugarcane as feedstock. *Biotechnology for biofuels*, v. 7, p. 26, 2014.

MACRELLI, S.; MOGENSEN, J.; ZACCHI, G. Techno-economic evaluation of 2^{nd} generation bioethanol production from sugar cane bagasse and leaves integrated with the sugar-based ethanol process. *Biotechnology for biofuels*, v. 5, p. 22, 2012.

MARTÍN, M.; GROSSMANN, I. E. Process optimization of ft-diesel production from lignocellulosic switchgrass. *Industrial & Engineering Chemistry Research*, v. 50, n. 23, p. 13485–13499, 2011.

MILANEZ, A. Y.; NYKO, D.; VALENTE, M. S.; SOUSA, L. C.; BONOMI, A.; JESUS, C. D. F.; WATANABE, M. D. B.; CHAGAS, M. F.; REZENDE, M. C. A. F.; CALALETT, O.; JUNQUEIRA, T. L.; GOUVÊIA, V. L. R. De promessa a realidade: como o etanol celulósico pode revolucionar a indústria da cana-de-açúcar – uma avaliação do potencial competitivo e sugestões de política pública. *BNDES setorial*, v. 41, p. 237–294, 2015.

MILLIGAN, D.; MILLIGAN, J. *Matches' 275 Equipment Cost Estimates*. 2015. Disponível em: <http://www.matche.com/equipcost/Default.html>. Acesso em: Jan. 2015.

MOBLEY, C. D.; SUNDMAN, L. K.; DAVIS, C. O.; BOWLES, J. H.; DOWNES, T. V.; LEATHERS, R. A.; MONTES, M. J.; BISSETT, W. P.; KOHLER, D. D.; REID, R. P. et al. Interpretation of hyperspectral remote-sensing imagery by spectrum matching and look-up tables. *Applied Optics*, v. 44, n. 17, p. 3576–3592, 2005.

MORTON, W. Equation-oriented simulation and optimization. *PROCEEDINGS-INDIAN NATIONAL SCIENCE ACADEMY PART A*, v. 69, n. 3&4, p. 317–357, 2003.

NAIK, S. N.; GOUD, V. V.; ROUT, P. K.; DALAI, A. K. Production of first and second generation biofuels: a comprehensive review. *Renewable and Sustainable Energy Reviews*, v. 14, n. 2, p. 578–597, 2010.

NELLES, O. Linear, polynomial, and look-up table models. In: *Nonlinear System Identification*. Nova Iorque: Springer, 2001. p. 219–238.

NG, D. K. S. Automated targeting for the synthesis of an integrated biorefinery. *Chemical Engineering Journal*, v. 162, n. 1, p. 67–74, 2010.

PATEL, A. D.; SERRANO-RUIZ, J. C.; DUMESIC, J. A.; ANEX, R. P. Techno-economic analysis of 5-nonanone production from levulinic acid. *Chemical Engineering Journal*, v. 160, n. 1, p. 311–321, 2010.

PEREIRA, L. T. C.; PEREIRA, L. T. C.; TEIXEIRA, R. S. S.; BON, E. P. S.; FREITAS, S. P. Sugarcane bagasse enzymatic hydrolysis: rheological data as criteria for impeller selection. *J Ind Microbiol Biotechnol*, v. 38, n. 8, p. 901–907, 2011.

PINTO, F. H. P. B. *Etanol celulósico: um estudo de viabilidade econômico-financeira*. 2010. 78 p. Dissertação (Mestre em Agroenergia) — Escola de Economia de São Paulo-FGV-EESP, Empresa Brasileira de Pesquisa Agropecuária EMBRAPA e Escola Superior de Agricultura "Luis de Queiroz"-ESALQ/USP, São Paulo, 2010.

QUAGLIA, A.; SARUP, B.; SIN, G.; GANI, R. A systematic framework for enterprise-wide optimization: Synthesis and design of processing networks under uncertainty. *Computers & Chemical Engineering*, v. 59, n. 5, p. 47–62, 2013.

RABELO, S. C.; FILHO, R. M.; COSTA, A. C. Lime pretreatment and fermentation of enzymatically hydrolyzed sugarcane bagasse. *Applied biochemistry and biotechnology*, v. 169, n. 5, p. 1696–1712, 2013.

RAMOS, J. A. L. *A methodology for development of biocatalytic processes*. 2013. 281 p. Tese (Doutorado em Engenharia) — Department of chemical and biochemical engineering, Technical University of Denmark, Lyngby, 2013.

RAMOS, J. L.; TUFVESSON, P.; WOODLEY, J. M. Application of environmental and economic metrics to guide the development of biocatalytic processes. *Green Processing and Synthesis*, v. 3, p. 195–213, 2014.

RODRIGUES, R.; SOARES, R. P.; SECCHI, A. R. Teaching chemical reaction engineering using emso simulator. *Computer Applications in Engineering Education*, Wiley Online Library, v. 18, n. 4, p. 607–618, 2010.

SEABRA, J. E. A.; MACEDO, I. C. Comparative analysis for power generation and ethanol production from sugarcane residual biomass in brazil. *Energy Policy*, v. 39, n. 1, p. 421 – 428, 2011.

SEABRA, J. E. A.; TAO, L.; CHUM, H. L.; CMACEDO, I. A techno-economic evaluation of the effects of centralized cellulosic ethanol and co-products refinery options with sugarcane mill clustering. *Biomass and Bioenergy*, v. 34, n. 8, p. 1065–1078, 2010.

SILVA, C. R.; ZANGIROLAMI, T. C.; RODRIGUES, J. P.; MATUGI, K.; GIORDANO, R. C.; GIORDANO, R. L. C. An innovative biocatalyst for production of ethanol from xylose in a continuous bioreactor. *Enzyme and Microbial Technology*, v. 50, n. 1, p. 35 – 42, 2012.

SILVA, G. M. da. *Avaliação de diferentes configurações de hidrólise enzimática e fermentação utilizando bagaço de cana-de-açúcar para a produção de etanol 2G*. 2015. 125 p. Dissertação (Doutorado em Engenharia Química) — Departamento de Engenharia Química, Universidade Federal de São Carlos, São Carlos, 2015.

SILVA, V. F. N. da. *Estudos de pré-tratamento e sacarificação enzimática de resíduos agroindustriais como etapas no processo de obtenção de etanol celulósico*. 2009. 116 p. Dissertação (Mestrado em Ciências) — Escola de Engenharia de Lorena, Universidade de São Paulo, Lorena, 2009.

SOARES, R. de P.; SECCHI, A. R. Emso: A new environment for modelling, simulation and optimisation. *Computer Aided Chemical Engineering*, v. 14, p. 947–952, 2003.

SOUZA, R. B. A.; CORRÊA, L. J.; SUAREZ, C. A. G.; CRUZ, A. J. G. Avaliação do efeito da carga de sólidos sobre a hidrólise enzimática do bagaço de cana-de-açúcar e comparação entre complexos enzimáticos comerciais. In: *Anais do XX Congresso Brasileiro de Engenharia Química*. Florianópolis: Editora Cubo, 2014. p. 1–7.

THOMBRE, M. N.; PREISIG, H. A.; ADDIS, M. B. Developing surrogate models via computer based experiments. In: GERNAEY, K. V.; HUUSOM, J. K.; GANI, R. (Ed.). *12^{TH} International Symposium on Process Systems Engineering and 25^{TH} European Symposium on Computer Aided Process Engineering*. Lyngby: Elsevier, 2015. p. 641–646.

TUFVESSON, P.; LIMA-RAMOS, J.; HAQUE, N. A.; GERNAEY, K. V.; WOODLEY, J. M. Advances in the process development of biocatalytic processes. *Organic Process Research & Development*, v. 17, n. 10, p. 1233–1238, 2013.

TUFVESSON, P.; LIMA-RAMOS, J.; NORDBLAD, M.; WOODLEY, J. M. Guidelines and cost analysis for catalyst production in biocatalytic processes. *Organic Process Research & Development*, v. 15, n. 1, p. 266–274, 2011.

União dos produtores de bioenergia – UDOP. *Tabela consecana São Paulo*. 2015. Disponível em: <http://udop.com.br/cana/tabela_consecana_saopaulo.pdf>. Acesso em: Fev. 2015.

VOGT, M.; MÜLLER, N.; ISERMANN, R. On-line adaptation of grid-based look-up tables using a fast linear regression technique. *Journal of dynamic systems, measurement, and control*, v. 126, n. 4, p. 732–739, 2004.

VRTech. *Portal VRTech*. Disponível em: <www.vrtech.com.br>.

WALTER, A.; ENSINAS, A. V. Combined production of second-generation biofuels and electricity from sugarcane residues. *Energy*, v. 35, n. 2, p. 874–879, 2010.

WAN, Z.; KOTHARE, M. V. An efficient off-line formulation of robust model predictive control using linear matrix inequalities. *Automatica*, v. 39, n. 5, p. 837–846, 2003.

WOOLEY, R. J.; PUTSCHE, V. *Development of an ASPEN PLUS physical property database for biofuels components*. Golden, Colorado, 1996. 36 p.

YEOMANS, H.; GROSSMANN, I. E. A systematic modeling framework of superstructure optimization in process synthesis. *Computers & Chemical Engineering*, v. 23, n. 6, p. 709–731, 1999.

ZANIN, G. M.; SANTANA, C. C.; BON, E. P. S.; GIORDANO, R. L. C.; MORAES, F. F.; ANDRIETTA, S. R.; NETO, C. C. C.; MACEDO, I. C.; FO, D. L.; RAMOS, L. P.; FONTANA, J. Brazilian bioethanol program. *Applied Biochemistry and Biotechnology*, v. 84, p. 1147–1163, 2000.

APÊNDICE A – Modelagem matemática da biorrefinaria

Neste capítulo são apresentados os modelos matemáticos utilizados nas simulações apresentadas no Capítulo 5. Eles estão divididos em sete áreas:

Correntes básicas seção A.1

Trocadores de calor seção A.2

Misturadores e separadores seção A.3

Bombas e turbinas seção A.4

Reatores seção A.5

Separadores seção A.6

Plug-ins seção A.7

A.1 Correntes básicas

A.1.1 Corrente de calor – *heatStream*

Essa corrente é usada para transferir calor entre os equipamentos do processo.

Variáveis

W Potência [kW]

A.1.2 Fonte de calor – *heatSource*

Fonte de calor.

Variáveis

OutletQ heatStream

A.1.3 Corrente de trabalho – *workStream*

Essa corrente é usada para transferir trabalho entre os equipamentos do processo.

Variáveis

W Potência [kW]

A.1.4 Fonte de trabalho – *workSource*

Fonte de trabalho.

Variáveis

OutletW workStream

A.1.5 Corrente Sólida – *solidStream*

Essa corrente deve ser utilizada quando sólidos insolúveis estão presentes. A corrente é dividida em duas fases: fluida e sólida. A fase fluida herda do modelo *streams* da biblioteca de modelos do EMSO (*eml*). Ambas as fases possuem variáveis para as vazões molares e mássicas, entalpia molar e frações mássicas e molares. Além disso, a vazão total e as frações totais (ambas mássicas e molares) são calculadas. Note que a entalpia da fase sólida é calculada com uma chamada para o método "VapourEnthalpy" do VRTherm.

Esse modelo não considera o equilíbrio entre as fases sólida e fluida (ambas líquida e vapor). Assim, quando houver uma transição de fase envolvendo a fase sólida, essa deve ser representada como uma reação química. Vale ressaltar que para a transição de fase ser representada, os componentes envolvidos devem estar presentes tanto na fase sólida quanto na fluida.

Parâmetros

Além do parâmetro *NComp* herdado do modelo *streams*, a corrente material ainda possui os seguintes parâmetros:

***outer* PP** Chamada para o plugin externo *VRTherm* que calcula as propriedades físicas da fase fluida

***outer* PPS** Chamada para o plugin externo *VRTherm* que calcula as propriedades físicas da fase sólida

***outer* NCompS** Número de compostos na fase sólida

M(NComp) Vetor de tamanho "NComp" contendo os pesos moleculares dos compostos da fase fluida [kg/kmol]

MS(NCompS) Vetor de tamanho "NCompS" contendo os pesos moleculares dos compostos da fase sólida [kg/kmol]

Variáveis

Além das variáveis F, z, T, P e h herdadas do modelo *streams* a corrente material ainda possui as seguintes variáveis:

$\mathbf{F_{sol}}$ Vazão molar da fase sólida [kmol/h]

$\mathbf{F_{total}}$ Vazão molar total (fases sólida e fluida juntas) [kmol/h]

$\mathbf{F_{mass}}$ Vazão mássica da fase fluida [kg/h]

$\mathbf{F_{sol\_mass}}$ Vazão mássica da fase sólida [kg/h]

$\mathbf{F_{total\_mass}}$ Vazão mássica total (fases sólida e fluida juntas) [kg/h]

$\mathbf{z_{sol}}$**(NCompS)** Vetor de tamanho "NCompS" com as frações molares dos compostos da fase sólida

$\mathbf{z_{total}}$**(NComp+NCompS)** Vetor de tamanho "NComp+NCompS" com as frações molares dos compostos das fases fluida e sólida combinadas

$\mathbf{z_{mass}}$**(NComp)** Vetor de tamanho "NComp" com as frações mássicas dos compostos da fase fluida

$\mathbf{z_{sol\_mass}}$**(NCompS)** Vetor de tamanho "NCompS" com as frações mássicas dos compostos da fase sólida

$\mathbf{z_{total\_mass}}$**(NCompS)** Vetor de tamanho "NComp+NCompS" com as frações mássicas dos compostos das fases fluida e sólida combinadas

$\mathbf{h_{sol}}$ Entalpia específica molar da fase sólida [kJ/kmol]

Mw Massa molar média da fase fluida [kg/kmol]

$\mathbf{Mw_{sol}}$ Massa molar média da fase sólida [kg/kmol]

Equações

As seguintes equações são implementadas no modelo:

Cálculo do peso molecular médio da fase fluida

$$Mw = \sum_{i=1}^{NComp} z(i) \times M(i) \tag{A.1}$$

Conversão entre fração mássica e fração molar para a fase fluida

$$z_{mass}(i) \times Mw = z(i) \times M(i) \times \sum_{i=1}^{NComp} z(i) \tag{A.2}$$

Conversão entre vazão mássica e molar para a fase fluida

$$F_{mass} = F \times Mw \tag{A.3}$$

Cálculo do peso molecular médio da fase sólida

$$Mw_{sol} = \sum_{i=1}^{NCompS} z_{sol}(i) \times MS(i) \tag{A.4}$$

Conversão entre fração mássica e fração molar para a fase sólida

$$z_{sol\_mass}(i) \times Mw_{sol} = z_{sol}(i) \times MS(i) \times \sum_{i=1}^{NCompS} z_{sol}(i) \tag{A.5}$$

Conversão entre vazão mássica e molar para a fase fluida

$$F_{sol\_mass} = F_{sol} \times Mw_{sol} \tag{A.6}$$

Cálculo da vazão mássica total

$$F_{total\_mass} = F_{mass} + F_{sol\_mass} \tag{A.7}$$

Cálculo da fração mássica total para a fase fluida ($i \leq NComp$)

$$z(i)_{total\_mass} \times F_{total\_mass} = z(i)_{mass} \times F_{mass} \tag{A.8}$$

Cálculo da fração mássica total para a fase fluida ($NComp < i \leq NCompS$)

$$z(i)_{total\_mass} \times F_{total\_mass} = z(i - NComp)_{sol\_mass} \times F_{sol\_mass} \tag{A.9}$$

Cálculo da vazão molar total

$$F_{total} = F + F_{sol} \tag{A.10}$$

Cálculo da fração molar total para a fase fluida ($i \leq NComp$)

$$z(i)_{total} \times F_{total} = z(i) \times F \tag{A.11}$$

Cálculo da fração molar total para a fase fluida ($NComp < i \leq NCompS$)

$$z(i)_{total} \times F_{total} = z(i - NComp)_{sol} \times F_{sol} \tag{A.12}$$

A.1.6 *solidStreamPH*

Esse modelo extende as funcionalidades da corrente solidStream para calcular o estado físico da corrente (vapor, líquido ou equilíbrio entre os dois). Esse modelo deve ser utilizado quando a fração de vaporização é desconhecida. As equações para o cálculo de flash determina o estado da corrente como uma função da composição global (líquida e vapor, z), da pressão (P) e da entalpia (h). Adicionalmente, a composição das fases líquida (x) e vapor (y) são calculadas.

Variáveis

x Fração molar da fase líquida

y Fração molar da fase vapor

Equações

Cálculo flash

$$[v, x, y] = PP.FlashPH(P, h, z) \tag{A.13}$$

Cálculo da entalpia molar da fase líquida

$$h = (1 - v) \times PP.LiquidEnthalpy(T, P, x) + v \times PP.VapourEnthalpy(T, P, y) \tag{A.14}$$

Cálculo da entalpia molar da fase vapor

$$h_{sol} = PP.VapourEnthalpy(T, P, z_{sol}) \tag{A.15}$$

A.1.7 *solidStreamEq*

Esse modelo estende as funcionalidades da corrente solidStream, permitindo que o usuário especifique o estado físico da corrente (vapor, líquido ou equilíbrio entre os dois). Essa corrente deve ser utilizada quando o estado da corrente é conhecido: Líquido ou vapor. Isso irá determinar o método do VRTherm que será utilizado para calcular a entalpia da fase fluida.

Parâmetros

Phase Estado físico da corrente para o cálculo da entalpia. Estados válidos = [“*Liquid*”,“*Vapour*”]

Equações

Cálculo da entalpia molar da fase sólida

$$h_{sol} = PP.VapourEnthalpy(T, P, z_{sol}) \tag{A.16}$$

Phase = “*Liquid*”:

$$h = PP.LiquidEnthalpy(T, P, z) \tag{A.17a}$$
$$v = 0 \tag{A.17b}$$

Phase = “*Vapour*”:

$$h = PP.VapourEnthalpy(T, P, z) \tag{A.18a}$$
$$v = 1 \tag{A.18b}$$

A.1.8 *solidSource*

Fonte da corrente *solidStream*. Esse modelo deve ser utilizado para correntes de entrada do processo. De modo geral, essas correntes são conhecidas e provém de outras unidades de processo.

Deve-se especificar:

- A vazão molar ou mássica tanto da corrente fluida quando da sólida;
- A temperatura;
- A pressão;

- A composição mássica ou molar tanto da corrente fluida quando da sólida.

O modelo fornece as seguintes informações adicionais:

- Densidade mássica da corrente fluida;
- As vazões mássicas e molares de ambas as correntes;
- As composições mássicas e molares de ambas as correntes;
- O volume específico;
- A fração de vapor;
- A vazão volumétrica;
- As composições da fase líquida e vapor da corrente fluida.

Parâmetros

***outer* PP** Chamada para o plugin externo *VRTherm* que calcula as propriedades físicas da fase fluida

***outer* PPS** Chamada para o plugin externo *VRTherm* que calcula as propriedades físicas da fase sólida

***outer* NCompS** Número de compostos na fase sólida

M(NComp) Vetor de tamanho "NComp" contendo os pesos moleculares dos compostos da fase fluida [kg/kmol]

MS(NCompS) Vetor de tamanho "NCompS" contendo os pesos moleculares dos compostos da fase sólida [kg/kmol]

ValidPhases Estado físico da corrente para o cálculo da entalpia. Estados válidos = ["*Vapour-Liquid*","*Liquid-Only*","*Vapour-Only*"]

CompositionBasis Base usada para a especificação das frações. Estados válidos = ["*Mass*","*Molar*"]

Variáveis

out Outlet solidSource

Composition Frações (mássica ou molar) da fase fluida

SumOfComposition Soma das frações (mássica ou molar) da fase fluida

CompositionSolid Frações (mássica ou molar) da fase sólida

SumOfCompositionSolid Soma das frações (mássica ou molar) da fase sólida

F Vazão molar da fase fluida [kmol/h]

$\mathbf{F_{sol}}$ Vazão molar da fase sólida [kmol/h]

$\mathbf{F_{w}}$ Vazão mássica da fase fluida [kg/h]

$\mathbf{F_{solw}}$ Vazão mássica da fase sólida [kg/h]

$\mathbf{F_{vol}}$ Vazão volumétrica da fase fluida [m^3/h]

T Temperatura da corrente [K]

$\mathbf{T_{Cdeg}}$ Temperatura da corrente [°C]

P Pressão da corrente [atm]

x Fração molar da fase líquida

y Fração molar da fase vapor

vm Volume molar da fase fluida [m^3/mol]

rho Densidade mássica da fase fluida [kg/m^3]

rhom Densidade molar da fase fluida [kmol/m^3]

Equações

Soma das frações (mássica ou molar) da fase fluida

$$SumOfComposition = \sum_{i=1}^{NComp} Composition \tag{A.19}$$

Soma das frações (mássica ou molar) da fase sólida

$$SumOfCompositionSolid = \sum_{i=1}^{NCompS} CompositionSolid \tag{A.20}$$

Cálculo da entalpia molar da fase sólida

$$h_{sol}^{Outlet} = PPS.VapourEnthalpy(T^{Outlet}, P^{Outlet}, z_{sol}^{Outlet}) \tag{A.21}$$

Densidade da fase fluida

$$rhom \times vm = 1 \tag{A.22}$$

Conversão entre densidade mássica e molar

$$rhom \times Mw^{Outlet} = rho \tag{A.23}$$

Vazão mássica da fase fluida

$$Fw = F_{mass}^{Outlet} \tag{A.24}$$

Vazão mássica da fase sólida

$$F_{solw} = F_{sol\_mass}^{Outlet} \tag{A.25}$$

Vazão volumétrica da fase fluida

$$F_{vol} = F^{Outlet} \times vm \tag{A.26}$$

Conversão de temperatura entre Kelvin e grau Celsius

$$T_{Cdeg} = T^{Outlet} - 273.15 \tag{A.27}$$

Vazão molar da fase fluida

$$F^{Outlet} = F \tag{A.28}$$

Vazão molar da fase sólida

$$F_{sol}^{Outlet} = F_{sol} \tag{A.29}$$

Pressão da corrente

$$P^{Outlet} = P \tag{A.30}$$

Temperatura da corrente

$$T^{Outlet} = T \tag{A.31}$$

CompositionBasis = "Molar"

$$z^{Outlet} = \frac{Composition}{\sum_{i=1}^{NComp} Composition} \tag{A.32a}$$

$$z_{sol}^{Outlet} = \frac{CompositionSolid}{\sum_{i=1}^{NComp} CompositionSolid} \tag{A.32b}$$

CompositionBasis = "Mass"

$$z_{mass}^{Outlet} = \frac{Composition}{\sum_{i=1}^{NComp} Composition} \tag{A.33a}$$

$$z_{sol\_mass}^{Outlet} = \frac{CompositionSolid}{\sum_{i=1}^{NComp} CompositionSolid} \tag{A.33b}$$

ValidPhases="Liquid-Only"

$$v^{Outlet} = 0 \tag{A.34a}$$

$$x = z^{Outlet} \tag{A.34b}$$

$$y = z^{Outlet} \tag{A.34c}$$

$$h^{Outlet} = PP.LiquidEnthalpy(T^{Outlet}, P^{Outlet}, z^{Outlet}) \tag{A.34d}$$

$$vm = PP.LiquidVolume(T^{Outlet}, P^{Outlet}, z^{Outlet}) \tag{A.34e}$$

ValidPhases="Vapour-Only"

$$v^{Outlet} = 1 \tag{A.35a}$$

$$x = z^{Outlet} \tag{A.35b}$$

$$y = z^{Outlet} \tag{A.35c}$$

$$h^{Outlet} = PP.VapourEnthalpy(T^{Outlet}, P^{Outlet}, z^{Outlet}) \tag{A.35d}$$

$$vm = PP.VapourVolume(T^{Outlet}, P^{Outlet}, z^{Outlet}) \tag{A.35e}$$

ValidPhases="Liquid-Only"

$$[v^{Outlet}, x, y] = PP.Flash(T^{Outlet}, P^{Outlet}, z^{Outlet}) \tag{A.36a}$$

$$\begin{aligned} h^{Outlet} = {} & (1 - v^{Outlet}) \times PP.LiquidEnthalpy(T^{Outlet}, P^{Outlet}, x) \\ & + v^{Outlet} \times PP.VapourEnthalpy(T^{Outlet}, P^{Outlet}, y) \end{aligned} \tag{A.36b}$$

$$\begin{aligned} vm = {} & (1 - v^{Outlet}) \times PP.LiquidVolume(T^{Outlet}, P^{Outlet}, x) \\ & + v^{Outlet} \times PP.VapourVolume(T^{Outlet}, P^{Outlet}, y) \end{aligned} \tag{A.36c}$$

A.1.9 Corrente de água – *waterStream*

Esse modelo implementa uma corrente de água pura para integração energética da planta.

Variáveis

F Vazão mássica [kg/h]

P Pressão [atm]

T Temperatura [K]

S Entropia mássica [kJ/kg/K]

H Entalpia mássica [kJ/kg]

v Título

A.1.10 *waterStreamVapFrac*

Esse modelo de corrente extende as funcionalidades do modelo waterStream, incluindo o cálculo do título. Essa corrente deve ser utilizada quando a fração de vapor é desconhecida. A fração de vapor é determinada por comparação da entalpia da corrente com as entalpias da água e do vapor saturados.

Parâmetros

propterm *Plug-in* que calcula as propriedades físicas da água pura.

Variáveis

Hl Entalpia específica mássica da água líquida saturada na pressão especificada [kJ/kg]

Hv Entalpia específica mássica do vapor saturado na pressão especificada [kJ/kg]

Sl Entropia específica mássica da água líquida saturada na pressão especificada [kJ/kg/K]

Sv Entropia específica mássica do vapor saturado na pressão especificada [kJ/kg/K]

Equações

Cálculo da entropia e entalpia mássicas para o líquido saturado na pressão especificada

$$[Sv, Hv] = propterm.propPTv(P, propterm.Tsat(P)) \tag{A.37}$$

Cálculo da entropia e entalpia mássicas para o vapor saturado na pressão especificada

$$[Sv, Hv] = propterm.propPTv(P, propterm.Tsat(P)) \tag{A.38}$$

A.1.11 *waterStreamEq*

Esse modelo extende as funcionalidades da corrente waterStream. Essa corrente deve ser usada quando o estado da água é conhecida: água subresfriada, vapor superaquecido ou equilíbrio entre água e vapor. Quando os estados de água subresfriada ou vapor superaquecido são escolhidos, deve-se especificar a pressão e a temperatura. Quando o estado de equilíbrio entre água e vapor é escolhido, deve-se especificar a fração de vapor e a temperatura ou a pressão.

Parâmetros

propterm *Plug-in* que calcula as propriedades físicas da água pura

ValidPhases Estado físico da corrente para o cálculo da entalpia. Estados válidos = [*"Vapour-Liquid"*,*"Liquid-Only"*,*"Vapour-Only"*]

Variáveis

Hl Entalpia específica mássica da água líquida saturada na pressão especificada [kJ/kg]

Hv Entalpia específica mássica do vapor saturado na pressão especificada [kJ/kg]

Sl Entropia específica mássica da água líquida saturada na pressão especificada [kJ/kg/K]

Sv Entropia específica mássica do vapor saturado na pressão especificada [kJ/kg/K]

Equações

Cálculo da entropia e entalpia mássicas para o líquido saturado na pressão especificada

$$[Sv, Hv] = propterm.propPTv(P, propterm.Tsat(P)) \tag{A.39}$$

Cálculo da entropia e entalpia mássicas para o vapor saturado na pressão especificada

$$[Sv, Hv] = propterm.propPTv(P, propterm.Tsat(P)) \tag{A.40}$$

ValidPhases = *"Vapour-Only"*:

$$[S, H] = propterm.propPTv(P, T) \tag{A.41a}$$

$$v = 1 \tag{A.41b}$$

ValidPhases = *"Liquid-Only"*:

$$[S, H] = propterm.propPTl(P, T) \tag{A.42a}$$

$$v = 0 \tag{A.42b}$$

ValidPhases = *"Vapour-Liquid"*:

$$T = propterm.Tsat(P) \tag{A.43a}$$

$$S = Sl + v \times (Sv - Sl) \tag{A.43b}$$

$$H = Hl + v \times (Hv - Hl) \tag{A.43c}$$

A.1.12 Fonte de água – *waterSource*

Fonte da corrente waterStream. Esse modelo deve ser utilizado para correntes de entrada do processo. De modo geral, essas correntes são conhecidas e provém de outras unidades de processo. Deve-se especificar o estado da corrente: água subresfriada, vapor superaquecido ou equilíbrio entre água e vapor. Quando os estados de água subresfriada ou vapor superaquecido são escolhidos, deve-se especificar a pressão e a temperatura. Quando o estado de equilíbrio entre água e vapor é escolhido, deve-se especificar a fração de vapor e a temperatura ou a pressão.

Deve-se especificar:

- Se for água subresfrida ou vapor superaquecido: pressão e temperatura;
- Se for água e vapor em equilíbrio: fração de vapor e temperatura ou pressão;
- Em ambos os casos: Vazão mássica.

O modelo fornece as seguintes informações adicionais:

- Entalpia mássica;
- Entropia mássica.

Parâmetros

propterm *Plug-in* que calcula as propriedades físicas da água pura.

ValidPhases Estado físico da corrente para o cálculo da entalpia. Estados válidos = [“*Vapour-Liquid*”,“*Liquid-Only*”,“*Vapour-Only*”]

Variáveis

Outlet waterStream

F Vazão mássica [kg/h]

P Pressão [atm]

T Temperatura [K]

v Título

Hl Entalpia específica mássica da água líquida saturada na pressão especificada [kJ/kg]

Hv Entalpia específica mássica do vapor saturado na pressão especificada [kJ/kg]

Sl Entropia específica mássica da água líquida saturada na pressão especificada [kJ/kg/K]

Sv Entropia específica mássica do vapor saturado na pressão especificada [kJ/kg/K]

Equações

Cálculo da entropia e entalpia mássicas para o líquido saturado na pressão especificada

$$[Sv, Hv] = propterm.propPTv(P, propterm.Tsat(P)) \tag{A.44}$$

Cálculo da entropia e entalpia mássicas para o vapor saturado na pressão especificada

$$[Sv, Hv] = propterm.propPTv(P, propterm.Tsat(P)) \tag{A.45}$$

$$P = P^{Outlet} \tag{A.46}$$

$$T = T^{Outlet} \tag{A.47}$$

$$F = F^{Outlet} \tag{A.48}$$

$$v = v^{Outlet} \tag{A.49}$$

ValidPhases = *"Vapour-Only"*:

$$[S^{Outlet}, H^{Outlet}] = propterm.propPTv(P, T) \tag{A.50a}$$
$$v^{Outlet} = 1 \tag{A.50b}$$

ValidPhases = *"Liquid-Only"*:

$$[S^{Outlet}, H^{Outlet}] = propterm.propPTl(P, T) \tag{A.51a}$$
$$v^{Outlet} = 0 \tag{A.51b}$$

ValidPhases = *"Vapour-Liquid"*:

$$T^{Outlet} = propterm.Tsat(P) \tag{A.52a}$$
$$S^{Outlet} = Sl + v \times (Sv - Sl) \tag{A.52b}$$
$$H^{Outlet} = Hl + v \times (Hv - Hl) \tag{A.52c}$$

A.2 Trocadores de calor

A.2.1 *heatExchanger*

Modelo de um trocador de calor simplificado em que calor é fornecido ou retirado da corrente solidStream. O modelo também inclui o cálculo do custo do equipamento usando a regra dos 6/10.

Hipóteses:

- Operação em estado estacionário;
- Sem perda de calor para o ambiente;
- O custo do equipamento é baseado no custo do equipamento de certo tamanho e considerando um fator de escala.

Deve-se especificar:

- A corrente de entrada;
- A temperatura de saída;
- A queda de pressão ou a pressão de saída.

Deve-se definir os seguintes parâmetros:

- Se o custo do equipamento deverá ser calculado ou não;
- O fator de escala;
- O fator de instalação;
- A área que servirá de base para o cálculo do custo;
- O custo base do equipamento;
- A área máxima que o trocador poderá ter.

Variáveis

in Inlet solidStream

out Outlet solidStream

Q Calor trocado [kW]

Pdrop Perda de carga no trocador [kPa]

lmtd Diferença de temperatura média logarítmica [K]

U Coeficiente global de transferência de calor [kJ/K/m^2]

A Área de troca [m^2]

Equações

Balanço de energia

$$Q = F^{Inlet} \times (h^{Outlet} - h^{Inlet}) + F_{sol}^{Inlet} \times (h_{sol}^{Outlet} - h_{sol}^{Inlet}) \tag{A.53}$$

Balanço de massa

$$F^{Inlet} = F^{Outlet} \tag{A.54a}$$

$$F_{sol}^{Inlet} = F_{sol}^{Outlet} \tag{A.54b}$$

Balanço de massa por componente

$$z^{Inlet} = z^{Outlet} \tag{A.55a}$$

$$z_{sol}^{Inlet} = z_{sol}^{Outlet} \tag{A.55b}$$

Perda de carga no trocador de calor

$$P^{Outlet} = P^{Inlet} - \Delta P \tag{A.56}$$

A.2.2 Aquecedor – *heater*

Esse modelo estende as funcionalidades do modelo heatExchanger, definindo o sentido da troca de calor. Deve-se especificar (ou incluir no fluxograma uma equação para calcular) a diferença de temperatura média logarítmica (*lmtd*).

Variáveis

InletQ heatStream

Equações

$$Q^{InletQ} = Q \tag{A.57}$$

$$Q^{InletQ} = U \times A \times lmtd \tag{A.58}$$

A.2.3 Resfriador – *cooler*

Esse modelo estende as funcionalidades do modelo heatExchanger, definindo o sentido da troca de calor. Deve-se especificar (ou incluir no fluxograma uma equação para calcular) a diferença de temperatura média logarítmica (*lmtd*).

Variáveis

OutletQ heatStream

Equações

$$Q^{OutletQ} = -Q \tag{A.59}$$

$$Q^{OutletQ} = U \times A \times lmtd \tag{A.60}$$

A.2.4 *WheatExchanger*

Modelo de um trocador de calor simplificado em que calor é fornecido ou retirado da corrente waterStream. O modelo também inclui o cálculo do custo do equipamento usando a regra dos 6/10.

Hipóteses:

- Operação em estado estacionário;
- Sem perda de calor para o ambiente;
- O custo do equipamento é baseado no custo do equipamento de certo tamanho e considerando um fator de escala.

Deve-se especificar:

- A corrente de entrada;
- A temperatura de saída;
- A queda de pressão ou a pressão de saída.

Parâmetros

propterm *Plug-in* que calcula as propriedades físicas da água pura.

Variáveis

in Inlet waterStream

out Outlet waterStream

Q Calor trocado [kW]

Pdrop Perda de carga no trocador [kPa]

lmtd Diferença de temperatura média logarítmica [K]

U Coeficiente global de transferência de calor [kJ/K/m^2]

A Área de troca [m^2]

Equações

Balanço de energia

$$Q = F^{Inlet} \times (H^{Outlet} - H^{Inlet}) \tag{A.61}$$

Balanço de massa

$$F^{Inlet} = F^{Outlet} \tag{A.62}$$

Perda de carga no trocador de calor

$$P^{Outlet} = P^{Inlet} - \Delta P \tag{A.63}$$

A.2.5 Aquecedor de água – *Wheater*

Esse modelo estende as funcionalidades do modelo heatExchanger, definindo o sentido da troca de calor. Deve-se especificar (ou incluir no fluxograma uma equação para calcular) a diferença de temperatura média logarítmica (*lmtd*).

Variáveis

InletQ heatStream

Equações

$$Q^{InletQ} = Q \tag{A.64}$$

$$Q^{InletQ} = U \times A \times lmtd \tag{A.65}$$

A.2.6 Resfriador de Água – *Wcooler*

Esse modelo estende as funcionalidades do modelo heatExchanger, definindo o sentido da troca de calor. Deve-se especificar (ou incluir no fluxograma uma equação para calcular) a diferença de temperatura média logarítmica (*lmtd*).

Variáveis

OutletQ heatStream

Equações

$$Q^{OutletQ} = -Q \tag{A.66}$$

$$Q^{OutletQ} = U \times A \times lmtd \tag{A.67}$$

A.2.7 Trocador de calor entre correntes sólidas – *MMheatex*

Modelo de um trocador de calor com duas correntes. O modelo realiza os balanços de massa e energia para as duas correntes e também calcula a troca de calor utilizando uma equação simplificada para a diferença de temperatura média logarítmica (CHEN, 1987). A aproximação é dada por $\theta_{CM2}^{0.3275} = 0.5 \times (\theta_1^{0.3275} + \theta_2^{0.3275})$. Onde θ_{CM2} é a aproximação para o *lmtd*, θ_1 e θ_2 são as diferenças de temperatura entre as duas correntes na entrada e na saída do trocador. Tanto a operação em contra-corrente quanto em concorrente são possíveis nesse modelo. O modelo também inclui o cálculo do custo do equipamento usando a regra dos 6/10.

Hipóteses:

- Operação em estado estacionário;
- Sem perda de calor para o ambiente;
- O custo do equipamento é baseado no custo do equipamento de certo tamanho e considerando um fator de escala.

Deve-se especificar:

- As correntes de entrada;

- A temperatura de uma das correntes de saída;
- As quedas de pressão ou pressões das correntes de saída;
- A área de troca ou o coeficiente de troca térmica.

Deve-se definir os seguintes parâmetros:

- O tipo de operação do trocador de calor: paralelo ou contra-corrente;
- Se o custo do equipamento deverá ser calculado ou não;
- O fator de escala;
- O fator de instalação;
- A área que servirá de base para o cálculo do custo;
- O custo base do equipamento;
- A área máxima que o trocador poderá ter.

Parâmetros

ExchangerType Tipo de trocador de calor: paralelo ou contracorrente. Estados válidos = [*"Counter flow"*,*"Cocurrent flow"*].

Variáveis

in InletHot solidStream

in InletCold solidStream

out OutletHot solidStreamPH

out OutletCold solidStreamPH

Q Calor trocado [kW]

THot Temperatura de saída da corrente quente

TCold Temperatura de saída da corrente fria

U Coeficiente global de transferência de calor [kJ/K/m^2]

A Área de troca [m^2]

θ**1** Média aritmética das temperaturas [K]

θ2 Média aritmética das temperaturas [K]

$\theta_{\mathbf{CM2}}$ Aproximação da diferença de temperatura média logarítmica [K] (CHEN, 1987).

$\mathbf{\Delta P^{Hot}}$ Perda de carga no trocador para a corrente quente [kPa]

$\mathbf{\Delta P^{Cold}}$ Perda de carga no trocador para a corrente fria [kPa]

Equações

Balanço de energia para o lado quente

$$Q = F^{InletHot} \times (h^{InletHot} - h^{OutletHot}) + F_{sol}^{InletHot} \times (h_{sol}^{InletHot} - h_{sol}^{OutletHot}) \quad \text{(A.68)}$$

Balanço de energia para o lado frio

$$Q = F^{InletCold} \times (h^{OutletCold} - h^{InletCold}) + F_{sol}^{InletCold} \times (h_{sol}^{OutletCold} - h_{sol}^{InletCold}) \quad \text{(A.69)}$$

$$Q = U \times A \times \theta_{CM2} \quad \text{(A.70)}$$

Aproximação da diferença de temperatura média logarítmica

$$2 \times \theta_{CM2}^{0.3275} = \theta_1^{0.3275} + \theta_2^{0.3275} \quad \text{(A.71)}$$

Temperatura de saída da corrente quente

$$T^{OutletHot} = THot \quad \text{(A.72)}$$

Temperatura de saída da corrente fria

$$T^{OutletCold} = TCold \quad \text{(A.73)}$$

Balanços de massa para o lado quente

$$F^{InletHot} = F^{OutletHot} \quad \text{(A.74a)}$$
$$F_{sol}^{InletHot} = F_{sol}^{OutletHot} \quad \text{(A.74b)}$$

Balanços de massa para o lado frio

$$F^{InletCold} = F^{OutletCold} \quad \text{(A.75a)}$$
$$F_{sol}^{InletCold} = F_{sol}^{OutletCold} \quad \text{(A.75b)}$$

Balanços de massa por componente para o lado quente

$$z^{InletHot} = z^{OutletHot} \tag{A.76a}$$
$$z_{sol}^{InletHot} = z_{sol}^{OutletHot} \tag{A.76b}$$

Balanços de massa por componente para o lado frio

$$z^{InletCold} = z^{OutletCold} \tag{A.77a}$$
$$z_{sol}^{InletCold} = z_{sol}^{OutletCold} \tag{A.77b}$$

Perda de carga para o lado quente

$$P^{OutletHot} = P^{InletHot} - \Delta P^{Hot} \tag{A.78}$$

Perda de carga para o lado frio

$$P^{OutletCold} = P^{InletCold} - \Delta P^{Cold} \tag{A.79}$$

ExchangerType = "Counter Flow"

$$\theta_1 = T^{InletHot} - T^{OutletCold} \tag{A.80a}$$
$$\theta_2 = T^{OutletHot} - T^{InletCold} \tag{A.80b}$$

ExchangerType = "Cocurrent Flow"

$$\theta_1 = T^{InletHot} - T^{InletCold} \tag{A.81a}$$
$$\theta_2 = T^{OutletHot} - T^{OutletCold} \tag{A.81b}$$

A.2.8 Trocador de calor entre corrente sólida e de água – *MWheatex*

Modelo de um trocador de calor com duas correntes. O modelo realiza os balanços de massa e energia para as duas correntes e também calcula a troca de calor utilizando uma equação simplificada para a diferença de temperatura média logarítmica (CHEN, 1987). A aproximação é dada por $\theta_{CM2}^{0.3275} = 0.5 \times (\theta_1^{0.3275} + \theta_2^{0.3275})$. Onde θ_{CM2} é a aproximação para o *lmtd*, θ_1 e θ_2 são as diferenças de temperatura entre as duas correntes na entrada e na saída do trocador. Tanto a operação em contra-corrente quanto em concorrente são possíveis nesse modelo. O modelo também inclui o cálculo do custo do equipamento usando a regra dos 6/10.

Hipóteses:

- Operação em estado estacionário;
- Sem perda de calor para o ambiente;

- O custo do equipamento é baseado no custo do equipamento de certo tamanho e considerando um fator de escala.

Deve-se especificar:

- As correntes de entrada;
- A temperatura de uma das correntes de saída;
- As quedas de pressão ou pressões das correntes de saída;
- A área de troca ou o coeficiente de troca térmica.

Deve-se definir os seguintes parâmetros:

- O tipo de operação do trocador de calor: paraledo ou contra-corrente;
- O tipo de processo que o trocador de calor realiza, do ponto de vista da corrente sólida: aquecimento ou resfriamento;
- Se o custo do equipamento deverá ser calculado ou não;
- O fator de escala;
- O fator de instalação;
- A área que servirá de base para o cálculo do custo;
- O custo base do equipamento;
- A área máxima que o trocador poderá ter.

Parâmetros

propterm *Plug-in* que calcula as propriedades físicas da água pura.

HEType Tipo de processo realizado no trocador de calor, do ponto de vista da corrente sólida. Estados válidos = [*"heater"*,*"cooler"*].

ExchangerType Tipo de trocador de calor: paralelo ou contracorrente. Estados válidos = [*"Counter flow"*,*"Cocurrent flow"*].

Variáveis

in InletS solidStream

in InletW waterStream

out OutletS solidStreamPH

out OutletW waterStreamEq

Q Calor trocado [kW]

TS Temperatura de saída da corrente sólida

TW Temperatura de saída da corrente de água

U Coeficiente global de transferência de calor [kJ/K/m^2]

A Área de troca [m^2]

θ**1** Média aritmética das temperaturas [K]

θ**2** Média aritmética das temperaturas [K]

$\theta_{\mathbf{CM2}}$ Aproximação da diferença de temperatura média logarítmica [K] (CHEN, 1987).

$\mathbf{\Delta P^S}$ Perda de carga no trocador para a corrente sólida [kPa]

$\mathbf{\Delta P^W}$ Perda de carga no trocador para a corrente de água [kPa]

Equações

Cálculo do calor trocado

$$Q = U \times A \times \theta_{CM2} \tag{A.82}$$

Aproximação da diferença de temperatura média logarítmica

$$2 \times \theta_{CM2}^{0.3275} = \theta_1^{0.3275} + \theta_2^{0.3275} \tag{A.83}$$

Temperatura de saída da corrente sólida

$$T^{OutletS} = TS \tag{A.84}$$

Temperatura de saída da corrente de água

$$T^{OutletW} = TW \tag{A.85}$$

Balanços de massa para a corrente sólida

$$F^{InletS} = F^{OutletS} \tag{A.86a}$$

$$F_{sol}^{InletS} = F_{sol}^{OutletS} \tag{A.86b}$$

Balanços de massa para a corrente de água

$$F^{InletW} = F^{OutletW} \tag{A.87a}$$

$$F_{sol}^{InletW} = F_{sol}^{OutletW} \tag{A.87b}$$

Balanços de massa por componente para a corrente sólida

$$z^{InletS} = z^{OutletS} \tag{A.88a}$$

$$z_{sol}^{InletS} = z_{sol}^{OutletS} \tag{A.88b}$$

Balanços de massa por componente para a corrente de água

$$z^{InletW} = z^{OutletW} \tag{A.89a}$$

$$z_{sol}^{InletW} = z_{sol}^{OutletW} \tag{A.89b}$$

Perda de carga para a corrente sólida

$$P^{OutletS} = P^{InletS} - \Delta P^{S} \tag{A.90}$$

Perda de carga para a corrente de água

$$P^{OutletW} = P^{InletW} - \Delta P^{W} \tag{A.91}$$

HEType = “heater”

$$Q = F^{InletS} \times (h^{OutletS} - h^{InletS}) + F_{sol}^{InletS} \times (h_{sol}^{OutletS} - h_{sol}^{InletS}) \tag{A.92a}$$

$$Q = F^{InletW} \times (H^{InletS} - H^{OutletS}) \tag{A.92b}$$

ExchangerType = “Counter Flow”

$$\theta_1 = T^{InletW} - T^{OutletS} \tag{A.92c}$$

$$\theta_2 = T^{OutletW} - T^{InletS} \tag{A.92d}$$

ExchangerType = “Cocurrent Flow”

$$\theta_1 = T^{InletW} - T^{InletS} \tag{A.92e}$$

$$\theta_2 = T^{OutletW} - T^{OutletS} \tag{A.92f}$$

HEType = “cooler”

$$Q = F^{InletS} \times (h^{InletS} - h^{OutletS}) + F_{sol}^{InletS} \times (h_{sol}^{InletS} - h_{sol}^{OutletS}) \tag{A.93a}$$

$$Q = F^{InletW} \times (H^{OutletS} - H^{InletS}) \tag{A.93b}$$

ExchangerType = “Counter Flow”

$$\theta_1 = T^{InletS} - T^{OutletW} \tag{A.93c}$$
$$\theta_2 = T^{OutletS} - T^{InletW} \tag{A.93d}$$

ExchangerType = “Cocurrent Flow”

$$\theta_1 = T^{InletS} - T^{InletW} \tag{A.93e}$$
$$\theta_2 = T^{OutletS} - T^{OutletW} \tag{A.93f}$$

A.2.9 Trocador de calor entre correntes de água – *WWheatex*

Modelo de um trocador de calor com duas correntes. O modelo realiza os balanços de massa e energia para as duas correntes e também calcula a troca de calor utilizando uma equação simplificada para a diferença de temperatura média logarítmica (CHEN, 1987). A aproximação é dada por $\theta_{CM2}^{0.3275} = 0.5 \times (\theta_1^{0.3275} + \theta_2^{0.3275})$. Onde θ_{CM2} é a aproximação para o *lmtd*, θ_1 e θ_2 são as diferenças de temperatura entre as duas correntes na entrada e na saída do trocador. Tanto a operação em contra-corrente quanto em concorrente são possíveis nesse modelo. O modelo também inclui o cálculo do custo do equipamento usando a regra dos 6/10.

Hipóteses:

- Operação em estado estacionário;
- Sem perda de calor para o ambiente;
- O custo do equipamento é baseado no custo do equipamento de certo tamanho e considerando um fator de escala.

Deve-se especificar:

- As correntes de entrada;
- A temperatura de uma das correntes de saída;
- As quedas de pressão ou pressões das correntes de saída;
- A área de troca ou o coeficiente de troca térmica.

Deve-se definir os seguintes parâmetros:

- O tipo de operação do trocador de calor: paralelo ou contra-corrente;
- Se o custo do equipamento deverá ser calculado ou não;
- O fator de escala;
- O fator de instalação;
- A área que servirá de base para o cálculo do custo;
- O custo base do equipamento;
- A área máxima que o trocador poderá ter.

Parâmetros

ExchangerType Tipo de trocador de calor: paralelo ou contracorrente. Estados válidos = [“*Counter flow*”,“*Cocurrent flow*”].

Variáveis

in InletHot waterStream

in InletCold waterStream

out OutletHot waterStreamEq

out OutletCold waterStreamEq

Q Calor trocado [kW]

THot Temperatura de saída da corrente quente

TCold Temperatura de saída da corrente fria

U Coeficiente global de transferência de calor [kJ/K/m^2]

A Área de troca [m^2]

θ**1** Média aritmética das temperaturas [K]

$\theta 2$ Média aritmética das temperaturas [K]

$\theta_{\mathbf{CM2}}$ Aproximação da diferença de temperatura média logarítmica [K] (CHEN, 1987).

$\mathbf{\Delta P^{Hot}}$ Perda de carga no trocador para a corrente quente [kPa]

$\mathbf{\Delta P^{Cold}}$ Perda de carga no trocador para a corrente fria [kPa]

Equações

Balanço de energia para o lado quente

$$Q = F^{InletHot} \times (H^{InletHot} - H^{OutletHot}) \tag{A.94}$$

Balanço de energia para o lado frio

$$Q = F^{InletCold} \times (H^{OutletCold} - H^{InletCold}) \tag{A.95}$$

$$Q = U \times A \times \theta_{CM2} \tag{A.96}$$

Aproximação da diferença de temperatura média logarítmica

$$2 \times \theta_{CM2}^{0.3275} = \theta_1^{0.3275} + \theta_2^{0.3275} \tag{A.97}$$

Temperatura de saída da corrente quente

$$T^{OutletHot} = THot \tag{A.98}$$

Temperatura de saída da corrente fria

$$T^{OutletCold} = TCold \tag{A.99}$$

Balanços de massa para o lado quente

$$F^{InletHot} = F^{OutletHot} \tag{A.100a}$$

$$F_{sol}^{InletHot} = F_{sol}^{OutletHot} \tag{A.100b}$$

Balanços de massa para o lado frio

$$F^{InletCold} = F^{OutletCold} \tag{A.101a}$$

$$F_{sol}^{InletCold} = F_{sol}^{OutletCold} \tag{A.101b}$$

Perda de carga para o lado quente

$$P^{OutletHot} = P^{InletHot} - \Delta P^{Hot} \tag{A.102}$$

Perda de carga para o lado frio

$$P^{OutletCold} = P^{InletCold} - \Delta P^{Cold} \tag{A.103}$$

ExchangerType = “Counter Flow”

$$\theta_1 = T^{InletHot} - T^{OutletCold} \tag{A.104a}$$

$$\theta_2 = T^{OutletHot} - T^{InletCold} \tag{A.104b}$$

ExchangerType = “Cocurrent Flow”

$$\theta_1 = T^{InletHot} - T^{InletCold} \tag{A.105a}$$

$$\theta_2 = T^{OutletHot} - T^{OutletCold} \tag{A.105b}$$

A.3 Misturadores e separadores

A.3.1 Misturador da corrente sólida – *solidMixer*

Modelo de um misturador simples da corrente solidStream.

Hipóteses:

- Operação em estado estacionário;
- Sem perda de calor para o ambiente.

Deve-se especificar:

- As correntes de entrada.

Variáveis

in Inlet$_1$ solidStream

in Inlet$_2$ solidStream

out Outlet solidStreamPH

Equações

Balanço de massa para a fase fluida

$$F^{Inlet_1} + F^{Inlet_2} = F^{Outlet} \tag{A.106}$$

Balanço de massa para a fase fluida

$$F_{sol}^{Inlet_1} + F_{sol}^{Inlet_2} = F_{sol}^{Outlet} \tag{A.107}$$

Balanço de massa por componente para a fase fluida

$$F^{Inlet_1} \times z^{Inlet_1}(i) + F^{Inlet_2} \times z^{Inlet_2}(i) = F^{Outlet} \times z^{Outlet}(i) \tag{A.108}$$

Balanço de massa por componente para a fase sólida

$$F_{sol}^{Inlet_1} \times z_{sol}^{Inlet_1}(i) + F_{sol}^{Inlet_2} \times z_{sol}^{Inlet_2}(i) = F_{sol}^{Outlet} \times z_{sol}^{Outlet}(i) \tag{A.109}$$

Balanço de energia

$$\begin{aligned} F^{Inlet_1} \times h^{Inlet_1} + F_{sol}^{Inlet_1} \times h_{sol}^{Inlet_1} + F^{Inlet_2} \times h^{Inlet_2} + F_{sol}^{Inlet_2} \times h_{sol}^{Inlet_2} \\ = F^{Outlet} \times h^{Outlet} + F_{sol}^{Outlet} \times h_{sol}^{Outlet} \end{aligned} \tag{A.110}$$

Equilíbrio mecânico

$$P^{Outlet} = min([P^{Inlet_1}, P^{Inlet_2}]) \tag{A.111}$$

A.3.2 Separador da corrente sólida – *solidSplitter*

Modelo de um separador simples da corrente solidStream.

Hipóteses:

- Operação em estado estacionário;
- Sem perda de calor para o ambiente.

Deve-se especificar:

- A corrente de entrada;
- A fração de separação.

Variáveis

in Inlet solidStream

out Outlet$_1$ solidStream

out Outlet$_2$ solidStream

frac fração da *Inlet* que vai para a $Outlet_1$

Equações

Balanço de massa para a fase fluida

$$F^{Inlet} = F^{Outlet_1} + F^{Outlet_2} \tag{A.112}$$

Balanço de massa para a fase sólida

$$F_{sol}^{Inlet} = F_{sol}^{Outlet_1} + F_{sol}^{Outlet_2} \tag{A.113}$$

Composições das correntes de saída (fase fluida)

$$z^{Outlet_1}(i) = z^{Inlet}(i) \tag{A.114a}$$
$$z^{Outlet_2}(i) = z^{Inlet}(i) \tag{A.114b}$$

Composições das correntes de saída (fase sólida)

$$z_{sol}^{Outlet_1}(i) = z_{sol}^{Inlet}(i) \tag{A.115a}$$
$$z_{sol}^{Outlet_2}(i) = z_{sol}^{Inlet}(i) \tag{A.115b}$$

Fração da corrente *Inlet* desviada para a corrente $Outlet_1$

$$F_{mass}^{Outlet_1} = F_{mass}^{Inlet} \times frac \tag{A.116a}$$
$$F_{sol\_mass}^{Outlet_1} = F_{sol\_mass}^{Inlet} \times frac \tag{A.116b}$$

Temperatura das correntes de saída

$$T^{Outlet_1} = T^{Inlet} \tag{A.117a}$$
$$T^{Outlet_2} = T^{Inlet} \tag{A.117b}$$

Pressão das correntes de saída

$$P^{Outlet_1} = P^{Inlet} \tag{A.118a}$$
$$P^{Outlet_2} = P^{Inlet} \tag{A.118b}$$

Entalpia molar das correntes de saída (fase fluida)

$$h^{Outlet_1} = h^{Inlet} \tag{A.119a}$$
$$h^{Outlet_2} = h^{Inlet} \tag{A.119b}$$

Entalpia molar das correntes de saída (fase sólida)

$$h_{sol}^{Outlet_1} = h_{sol}^{Inlet} \tag{A.120a}$$
$$h_{sol}^{Outlet_2} = h_{sol}^{Inlet} \tag{A.120b}$$

Título das correntes de saída

$$v^{Outlet_1} = v^{Inlet} \tag{A.121a}$$
$$v^{Outlet_2} = v^{Inlet} \tag{A.121b}$$

A.3.3 Misturador de água – *waterMixer*

Modelo de um misturador simples da corrente waterStream.

Hipóteses:

- Operação em estado estacionário;
- Sem perda de calor para o ambiente.

Deve-se especificar:

- As correntes de entrada.

Parâmetros

propterm *Plug-in* que calcula as propriedades físicas da água pura.

Variáveis

in Inlet$_1$ waterStream

in Inlet$_2$ waterStream

out Outlet waterStreamEq

Equações

Balanço de massa

$$F^{Inlet_1} + F^{Inlet_2} = F^{Outlet} \tag{A.122}$$

Balanço de energia

$$F^{Inlet_1} \times H^{Inlet_1} + F^{Inlet_2} \times H^{Inlet_2} = F^{Outlet} \times H^{Outlet} \tag{A.123}$$

Equilíbrio mecânico

$$P^{Outlet} = min([P^{Inlet_1}, P^{Inlet_2}]) \tag{A.124}$$

A.3.4 Separador de água – *waterSplitter*

Modelo de um separador simples da corrente waterStream.

Hipóteses:

- Operação em estado estacionário;
- Sem perda de calor para o ambiente.

Deve-se especificar:

- A corrente de entrada;
- A fração de separação.

Parâmetros

propterm *Plug-in* que calcula as propriedades físicas da água pura.

Variáveis

in Inlet waterStream

out Outlet$_1$ waterStream

out Outlet$_2$ waterStream

frac fração da *Inlet* que vai para a $Outlet_1$

Equações

Vazão da corrente $Outlet_1$

$$F^{Outlet_1} = F^{Inlet} \times frac \tag{A.125}$$

Vazão da corrente $Outlet_2$

$$F^{Outlet_2} = F^{Inlet} \times (1 - frac) \tag{A.126}$$

Temperatura das correntes de saída

$$T^{Outlet_1} = T^{Inlet} \tag{A.127a}$$
$$T^{Outlet_2} = T^{Inlet} \tag{A.127b}$$

Pressão das correntes de saída

$$P^{Outlet_1} = P^{Inlet} \tag{A.128a}$$
$$P^{Outlet_2} = P^{Inlet} \tag{A.128b}$$

Entalpia mássica das correntes de saída

$$H^{Outlet_1} = H^{Inlet} \tag{A.129a}$$
$$H^{Outlet_2} = H^{Inlet} \tag{A.129b}$$

Entropia mássica das correntes de saída

$$S^{Outlet_1} = S^{Inlet} \tag{A.130a}$$
$$S^{Outlet_2} = S^{Inlet} \tag{A.130b}$$

Título das correntes de saída

$$v^{Outlet_1} = v^{Inlet} \tag{A.131a}$$
$$v^{Outlet_2} = v^{Inlet} \tag{A.131b}$$

A.3.5 Separador de calor – *heatSplitter*

Modelo de um separador simples da corrente heatStream.

Hipóteses:

- Operação em estado estacionário;
- Sem perda de calor para o ambiente.

Deve-se especificar:

- A corrente de entrada;
- A fração de separação.

Variáveis

in InletQ heatStream

out OutletQ$_1$ heatStream

out OutletQ$_2$ heatStream

frac fração da *InletQ* que vai para a $OutletQ_1$

Equações

$$Q^{InletQ} = Q^{OutletQ_1} + Q^{OutletQ_2} \tag{A.132}$$

$$Q^{OutletQ_1} = Q^{InletQ} \times frac \tag{A.133}$$

A.3.6 Separador de trabalho – *workSplitter*

Modelo de um separador simples da corrente workStream.

Hipóteses:

- Operação em estado estacionário;

- Sem perda de calor para o ambiente.

Deve-se especificar:

- A corrente de entrada;
- A fração de separação.

Variáveis

in InletQ workStream

out OutletQ$_1$ workStream

out OutletQ$_2$ workStream

frac fração da *InletQ* que vai para a $OutletQ_1$

Equações

$$Q^{InletQ} = Q^{OutletQ_1} + Q^{OutletQ_2} \tag{A.134}$$

$$Q^{OutletQ_1} = Q^{InletQ} \times frac \tag{A.135}$$

A.4 Bombas e turbinas

A.4.1 Bomba para a corrente sólida – *Pump*

Modelo simplificado de uma bomba para a corrente solidStream.

Hipóteses:

- Operação em estado estacionário;
- Só a fase líquida e sólida existem;
- Sem perda de calor para o ambiente.

Deve-se especificar:

- A corrente de entrada;
- A pressão da corrente de saída ou o incremento de pressão;
- A eficiência da bomba.

Deve-se definir os seguintes parâmetros:

- Se o custo do equipamento deverá ser calculado ou não;
- A densidade da corrente.

Parâmetros

density Densidade média da corrente

Variáveis

in Inlet solidStream

out Outlet solidStreamPH

in InletW workStream

ΔP Aumento de pressão na bomba [kPa]

η Eficiência da bomba

Equações

Balanço de massa (fase fluida)

$$F^{Inlet} = F^{Outlet} \tag{A.136}$$

Balanço de massa (fase sólida)

$$F_{sol}^{Inlet} = F_{sol}^{Outlet} \tag{A.137}$$

Balanço de massa por componente (fase fluida)

$$z^{Inlet} = z^{Outlet} \tag{A.138}$$

Balanço de massa por componente (fase sólida)

$$z_{sol}^{Inlet} = z_{sol}^{Outlet} \tag{A.139}$$

Diferença de pressão

$$P^{Outlet} = P^{Inlet} + \Delta P \tag{A.140}$$

Balanço de energia

$$W^{InletW} = F^{Inlet} \times (h^{Outlet} - h^{Inlet}) + F^{Inlet}_{sol} \times (h^{Outlet}_{sol} - h^{Inlet}_{sol}) \tag{A.141}$$

Trabalho necessário

$$W^{InletW} = \frac{(F^{Inlet}_{mass} + F^{Inlet}_{sol\_mass}) \times \Delta P}{\eta \times \rho} \tag{A.142}$$

A.4.2 Bomba para a corrente de água – *WPump*

Modelo simplificado de uma bomba para a corrente waterStream.

Hipóteses:

- Operação em estado estacionário;
- Só a fase líquida e sólida existem;
- Sem perda de calor para o ambiente.

Deve-se especificar:

- A corrente de entrada;
- A pressão da corrente de saída ou o incremento de pressão;
- A eficiência da bomba.

Deve-se definir os seguintes parâmetros:

- Se o custo do equipamento deverá ser calculado ou não;
- A densidade da corrente.

Parâmetros

density Densidade média da corrente

propterm *Plug-in* que calcula as propriedades físicas da água pura

Variáveis

in Inlet waterStream

out Outlet waterStreamVapFrac

in InletW workStream

ΔP Aumento de pressão na bomba [kPa]

η Eficiência da bomba

Equações

Balanço de massa

$$F^{Inlet} = F^{Outlet} \tag{A.143}$$

Diferença de pressão

$$P^{Outlet} = P^{Inlet} + \Delta P \tag{A.144}$$

Balanço de energia

$$W^{InletW} = F^{Inlet} \times (H^{Outlet} - H^{Inlet}) \tag{A.145}$$

Entalpia e entropia mássica da corrente de saída *Outlet*

$$[S^{Outlet}, H^{Outlet}] = propterm.propPH(P^{Outlet}, H^{Outlet}) \tag{A.146}$$

Trabalho necessário

$$W^{InletW} = \frac{F^{Inlet} \times \Delta P}{\eta \times \rho} \tag{A.147}$$

A.4.3 Turbina a vapor – *turbine*

Modelo de uma turbina a vapor baseada em eficiência isoentrópica para a corrente waterStream.

Hipóteses:

- Operação em estado estacionário;
- Sem perda de calor para o ambiente.

Deve-se especificar:

- A corrente de entrada;
- A pressão da corrente de saída ou a queda de pressão;
- A eficiência isoentrópica da turbina.

Parâmetros

density Densidade média da corrente

propterm *Plug-in* que calcula as propriedades físicas da água pura

Variáveis

in Inlet waterStream

out Outlet waterStreamVapFrac

out OutletW workStream

$\mathbf{H_{IS}}$ Entalpia isoentrópica da corrente de saída [kJ/kg]

ΔP Queda de pressão na turbina [atm]

η_{term} Eficiência térmica da turbina

η_{mech} Eficiência mecânica da turbina

Equações

Balanço de massa

$$F^{Inlet} = F^{Outlet} \tag{A.148}$$

Diferença de pressão

$$P^{Inlet} = P^{Outlet} + \Delta P \tag{A.149}$$

Cálculo da entalpia mássica isoentrópica

$$H_{IS} = propterm.propPS(P^{Outlet}, S^{Inlet}) \tag{A.150}$$

Cálculo da entalpia mássica real da corrente de saída $Outlet$

$$H^{Outlet} = (H_{IS} - H^{Inlet}) \times \eta_{term} + H^{Inlet} \tag{A.151}$$

Entalpia e entropia mássica da corrente de saída $Outlet$

$$[S^{Outlet}, H^{Outlet}] = propterm.propPH(P^{Outlet}, H^{Outlet}) \tag{A.152}$$

Trabalho produzido

$$W^{OutletW} = F^{Inlet} \times (H^{Inlet} - H^{Outlet}) \times \eta_{mech} \tag{A.153}$$

A.5 Reatores

A.5.1 Biodigestor anaeróbico – *anaerobic_digester*

Modelo de um digestor anaeróbico. As reações especificadas devem representar a remoção da demanda química de oxigênio (DQO) sem ter produtos. A biomassa e o biogás produzidos são baseados na quantidade de DQO na corrente de entrada e na DQO removida.

Hipóteses:

- Todas as três fases podem estar presentes;
- Operação em estado estacionário;
- As temperaturas de saída são iguais as da entrada.

Deve-se especificar:

- A corrente de entrada;
- A conversão de cada reação, baseada nos respectivos reagentes limitantes;
- O tempo de retenção hidráulica (*HRT*), o tempo de retenção de células (*CRT*) ou a taxa de alimentação (*LoadRate*);
- A umidade do lodo;
- A produção de células (*Yxs*) ou de metano (*Yps*).

Deve-se definir os seguintes parâmetros:

- A demanda química de oxigênio de cada componente (*COD*);
- O número de reações;
- A matriz estequiométrica;
- O reagente limitante de cada reação;
- A posição dos componentes “água”, “células”, “dióxido de carbono” e “metano” no vetor de componentes;
- A fração molar de metano no biogás;

- A densidade da corrente de entrada;
- A densidade da corrente de saída;
- A densidade do lodo.

Parâmetros

COD(NComp) Demanda química de oxigênio (DQO) de cada composto [kg/kmol]

NReac Número de reações

stoic(NComp+NCompS,NReac) Matriz de coeficientes estequiométricos das reações

limit(NReac) Posição do reagente limitante de cada reação no vetor de componentes

NCell Posição do componente "Biomassa" no vetor de componentes

NWater Posição do componente "água" no vetor de componentes

NCO2 Posição do componente "CO_2" no vetor de componentes

NCH4 Posição do componente "Metano" no vetor de componentes

CH4frac Fração de metano na corrente de biogás

$dens_{in}$ Densidade da corrente de entrada $Inlet$

$dens_{out}$ Densidade da corrente de saída $Outlet$

$dend_{sludge}$ Densidade da corrente de lodo $OutletSolid$

Variáveis

in Inlet solidStream

out Outlet solidStreamEq

out OutletGas solidStreamEq

out OutletSolid solidStreamEq

Inter solidStreamEq

r(NComp+NCompS,NReac) Reação

conv(NReac) Conversão do reator em remover o DQO

COD_{in} Demanda química de oxigênio da corrente de entrada – $VinasseNature$ [kg/m^3]

COD_{out} Demanda química de oxigênio da corrente de saída – $VinasseOutlet$ [kg/m^3]

$COD_{removed}$ Demanda química de oxigênio removida [kg/h]

HRT Tempo de retenção hídrica [h]

CRT Tempo de retenção de células [h]

OrganicRate Carga orgânica volumétrica [kg/m^3/h]

sludgeRate Carga de lodo (Carga de DQO por massa de células) [1/h]

$V_{reactor}$ Volume do biodigestor [m^3]

C_{micro} Concentração de microorganismos [kg/m^3]

$Y_{x/s}$ Rendimento de biomassa

$Y_{p/s}$ Rendimento de metano [m^3/kg]

sludgeHumidity Umidade do lodo

Equações

Balanço de massa

$$F^{Inlet}_{total\_mass} = F^{Outlet}_{total\_mass} + F^{OutletSolid}_{total\_mass} + F^{OutletGas}_{total\_mass} \tag{A.154}$$

Reação ($i = [1 : NComp + NCompS]$, $j = [1 : NReac]$)

$$r(i,j) = stoic(i,j) \times conv(i,j) \times z^{Inlet}_{total}(limit(j)) \tag{A.155}$$

Soma das frações molares (fase sólida)

$$\sum_{i=1}^{NCompS} z^{Outlet}_{sol} = 1 \tag{A.156}$$

Soma das frações molares (fase fluida)

$$\sum_{i=1}^{NCompS} z^{Outlet} = 1 \tag{A.157}$$

Nenhuma célula é perdida na corrente $Outlet$

$$z^{Outlet}_{sol}(NCell) = 0 \tag{A.158}$$

Soma das frações molares (fase sólida)

$$\sum_{i=1}^{NCompS} z^{Inter}_{sol} = 1 \tag{A.159}$$

Soma das frações molares (fase fluida)

$$\sum_{i=1}^{NCompS} z^{Inter} = 1 \tag{A.160}$$

Composição do biogás $OutletGas$ (fase sólida)

$$z_{sol}^{OutletGas} = z_{sol}^{Inlet} \tag{A.161}$$

Vazão de sólidos na corrente de biogás – $OutletGas$

$$F_{sol}^{OutletGas} = 1E-6[kmol/h] \tag{A.162}$$

Produção de metano

$$F^{OutletGas} \times z^{OutletGas}(NCH4) = \frac{Y_{p/s} \times COD_{removed}}{22.7[l/mol]} \tag{A.163}$$

Umidade do lodo

$$sludgeHumidity \times F_{total\_mass}^{OutletSolid} = F_{mass}^{OutletSolid} \tag{A.164}$$

Tempo de retenção hídrica

$$HRT \times F_{total\_mass}^{Inlet} = V_{reactor} \times dens_{in} \tag{A.165}$$

Tempo de retenção de células

$$CRT \times F_{total\_mass}^{OutletSolid} = V_{reactor} \times dens_{sludge} \tag{A.166}$$

Demanda química de oxigênio da corrente de entrada $Inlet$

$$COD_{in} \times F_{total\_mass}^{Inlet} = \sum_{i=1}^{NComp+NCompS} \left(COD \times z_{total}^{Inlet}\right) \times F_{total}^{Inlet} \times dens_{in} \tag{A.167}$$

Demanda química de oxigênio da corrente de entrada $Outlet$

$$COD_{out} \times F_{total\_mass}^{Outlet} = \sum_{i=1}^{NComp+NCompS} \left(COD \times z_{total}^{Outlet}\right) \times F_{total}^{Outlet} \times dens_{out} \tag{A.168}$$

Demanda quimica de oxigênio removida

$$COD_{removed} = \frac{COD_{in} \times F_{total\_mass}^{Inlet}}{dens_{in}} - \frac{COD_{out} \times F_{total\_mass}^{Outlet}}{dens_{out}} \tag{A.169}$$

Carga orgânica volumétrica

$$OrganicRate \times V_{reactor} \times dens_{in} = F_{total\_mass}^{Inlet} \times COD_{in} \tag{A.170}$$

Carga de lodo (carga biológica)

$$sludgeRate \times C_{micro} \times V_{reactor} \times dens_{in} = F^{Inlet}_{total\_mass} \times COD_{in} \tag{A.171}$$

Concentração de microorganismos no reator

$$C_{micro} \times \left(\frac{F^{OutletSolid}_{total\_mass}}{dens_{sludge}} + \frac{F^{OutletL}_{total\_mass}}{dens_{out}} \right) = F^{OutletS}_{sol\_mass} \tag{A.172}$$

Equilíbrio térmico

$$T^{Inter} = T^{Inlet} \tag{A.173a}$$
$$T^{Inter} = T^{OutletL} \tag{A.173b}$$
$$T^{Inter} = T^{OutletSolid} \tag{A.173c}$$
$$T^{Inter} = T^{OutletGas} \tag{A.173d}$$

Equilíbrio mecânico

$$P^{Inter} = P^{Inlet} \tag{A.174a}$$
$$P^{Inter} = P^{OutletL} \tag{A.174b}$$
$$P^{Inter} = P^{OutletSolid} \tag{A.174c}$$
$$P^{Inter} = P^{OutletGas} \tag{A.174d}$$

Balanço molar por componente para a corrente intermediária – $Inter$ (fase fluida)

$$F^{Inter} \times z^{Inter}(i) = F^{Inlet} \times z^{Inlet}(i) + F^{Inlet}_{total} \times \sum_{j=1}^{NReac} r(i,j) \tag{A.175}$$

Balanço molar por componente para a corrente intermediária – $Inter$ (fase sólida)

$$F^{Inter}_{sol} \times z^{Inter}_{sol}(i) = F^{Inlet}_{sol} \times z^{Inlet}_{sol}(i) + F^{Inlet}_{total} \times \sum_{j=1}^{NReac} r(i,j) \tag{A.176}$$

Se $i = NWater$ então:

Balanço molar por componente (fase fluida)

$$F^{Inter} \times z^{Inter}(i) = F^{OutletL} \times z^{OutletL}(i) + F^{OutletSolid} \times z^{OutletSolid}(i) \tag{A.177a}$$

$$z^{OutletSolid}(i) = 1 \tag{A.177b}$$

Senão:

Balanço molar por componente (fase fluida)

$$F^{Inter} \times z^{Inter}(i) = F^{OutletL} \times z^{OutletL}(i) \tag{A.178a}$$

$$z^{OutletSolid}(i) = 0 \tag{A.178b}$$

Se $i = NCell$ então:

Crescimento celular

$$F^{Inter}_{sol\_mass} \times z^{Inter}_{sol}(i) + \frac{Y_{x/s} \times COD_{in} \times F^{Inlet}_{total\_mass}}{dens_{in}} = F^{OutletSolid}_{sol\_mass} \times z^{OutletSolid}_{sol\_mass}(i) \tag{A.179a}$$

$$z^{OutletSolid}_{sol}(i) = 1 \tag{A.179b}$$

Senão:

Crescimento celular

$$F^{Inter}_{sol\_mass} \times z^{Inter}_{sol}(i) = F^{OutletL}_{sol\_mass} \times z^{OutletL}_{sol\_mass}(i) \tag{A.180a}$$

$$z^{OutletSolid}_{sol}(i) = 0 \tag{A.180b}$$

Se $i = NCH4$ então:

Composição do biogás

$$z^{OutletG}(i) = CH4frac \tag{A.181}$$

Se $i = NCO2$ então:

Composição do biogás

$$z^{OutletG}(i) = 1 - CH4frac \tag{A.182}$$

Senão:

Composição do biogás

$$z^{OutletG}(i) = 0 \tag{A.183}$$

A.5.2 Caldeira – *boiler*

Modelo de uma caldeira baseada em reações estequiométricas de combustão. A conversão das reações devem ser especificadas com relação ao reagente limitante. Além disso, o reagente limitante deve ter coeficiente estequiométrico igual a -1.

O poder calorífico superior (PCS) foi definido no modelo como o calor de combustão a 298.15 K, como definido pelo Instituto Americano de Petróleo (*American Petroleum*

Institute - API). O poder calorífico inferior (PCI), por outro lado, foi definido da forma mais comumente usada na indústria de açúcar e etanol. Essa definição assume que todos os produtos da combustão (água e dióxido de carbono) estão presentes na fase gasosa a 298.15 K. É importante notar que essa definição considera não somente a água produzida pela combustão, mas também a água já presente nas correntes de entrada (ar e combustível).

Hipóteses:

- Todas as três fases podem estar presentes;
- Operação em estado estacionário;
- Combustão completa; somente água e dióxido de carbono são produzidos.

Deve-se especificar:

- As correntes de entrada: Ar e Combustível;
- A corrente de entrada de água, exceto sua vazão;
- A conversão de cada reação, baseada nos respectivos reagentes limitantes;
- A temperatura do gás de escape;
- A eficiência da caldeira, tanto baseada no PCI quanto no PCS;
- A fração de excesso de ar;
- A queda de pressão no lado da água/vapor;
- A fração de calor que é perdida para o ambiente (baseada no PCS).

Deve-se definir os seguintes parâmetros:

- O número de reações;
- A matriz estequiométrica;
- O reagente limitante de cada reação;
- O calor de reação para cada reação;
- A posição dos componentes “água” e “oxigênio” no vetor de componentes.

O modelo fornece as seguintes informações adicionais:

- A produção específica de vapor (baseada na vazão mássica de combustível úmido);
- O podere calorífico superior em base seca e úmida;
- O poder calorífico inferior;
- A umidade do ar;
- A eficiência da caldeira (baseada no PCI e no PCS).

Parâmetros

***outer* PP** Chamada para o plugin externo *VRTherm* que calcula as propriedades físicas da fase fluida

***outer* PPS** Chamada para o plugin externo *VRTherm* que calcula as propriedades físicas da fase sólida item[*outer* NComp] Número de compostos na fase fluida

***outer* NCompS** Número de compostos na fase sólida

M(NComp) Vetor de tamanho "NComp" contendo os pesos moleculares dos compostos da fase fluida [kg/kmol]

MS(NCompS) Vetor de tamanho "NCompS" contendo os pesos moleculares dos compostos da fase sólida [kg/kmol]

NReac Número de reações

stoic(NComp+NCompS,NReac) Matriz de coeficientes estequiométricos das reações

limit(NReac) Posição do reagente limitante de cada reação no vetor de componentes

h(NReac) Entalpia de reação para cada reação [kJ/kmol]

NWater Posição do componente "água" no vetor de componentes

NO2 Posição do componente "O_2" no vetor de componentes

Variáveis

in Fuel solidStream

in Air solidStream

in Water waterStream

in InletQ heatStream

out Steam waterStreamVapFrac

out Gas solidStreamEq

out Ash solidStreamEq

FGas Vazão estequiométrica de ar [kmol/h]

zGas(NComp) Fração molar na corrente de gás estequiométrico

F Vazão molar total da entrada [kmol/h]

z Composição molar total da entrada

ΔP Perda de carga na lado da água/vapor [atm]

T Temperatura de saída do vapor [K]

η_{HHV} Eficiência da transferência de calor com base do poder calorífico superior

η_{LHV} Eficiência da transferência de calor com base do poder calorífico inferior

$\mathbf{q_{losses}}$ Perdas de calor [kW]

$\mathbf{f_{losses}}$ Fração de calor perdido

$\mathbf{q_{ex}}$ Calor trocado [kW]

$\mathbf{q_{HHV}}$ Calor gerado (baseado no poder calorífico superior) [kW]

$\mathbf{q_{LHV}}$ Calor gerado (baseado no poder calorífico inferior) [kW]

$\mathbf{q_{comb}}$ Calor gerado (baseado no calor de combustão) [kW]

$\mathbf{v_{spec}}$ Produção específica de vapor (kg de vapor / kg de combustível]

$\mathbf{HHV_{dry}}$ Poder calorífico superior do combustível (base seca) [kJ/kg]

$\mathbf{HHV_{wet}}$ Poder calorífico superior do combustível (base úmida) [kJ/kg]

LHV Poder calorífico inferior do combustível (base úmida) [kJ/kg]

r Reações

conv Conversão para cada reação em relação ao reagente limintante

Ex_Air Fração de excesso de ar

humidity Umidade do ar

$\mathbf{h_{gas}}$ Entalpia molar do gás [kJ/kmol]

$\mathbf{h_{ash}}$ Entalpia molar das cinzas [kJ/kmol]

$\mathbf{h_{air}}$ Entalpia molar do ar [kJ/kmol]

$\mathbf{h_{fuel\_sol}}$ Entalpia molar do bagaço (fase sólida) [kJ/kmol]

$\mathbf{h_{fuel\_fluid}}$ Entalpia molar do bagaço (fase fluida) [kJ/kmol]

x_gas_1(NComp) Fração de líquidos no gás de escape na condição de referência

y_gas_1(NComp) Fração de gases no gás de escape na condição de referência

v_gas_1(NComp) Fração de vapor no gás de escape na condição de referência

x_gas_2(NComp) Fração de líquidos no gás de escape na condição de saída

y_gas_2(NComp) Fração de gases no gás de escape na condição de saída

v_gas_2(NComp) Fração de vapor no gás de escape na condição de saída

x_air_1(NComp) Fração de líquidos no ar de entrada na condição de referência

y_air_1(NComp) Fração de gases no ar de entrada na condição de referência

v_air_1(NComp) Fração de vapor no ar de entrada na condição de referência

x_air_2(NComp) Fração de líquidos no ar de entrada na condição de saída

y_air_2(NComp) Fração de gases no ar de entrada na condição de saída

v_air_2(NComp) Fração de vapor no ar de entrada na condição de saída

Equações

Balanço de massa global para o lado da água/vapor

$$F^{Water} = F^{Steam} \tag{A.184}$$

Temperatura de saída do vapor

$$T^{Steam} = T \tag{A.185}$$

Equilíbrio térmico no lado das cinzas/ar de escape

$$T^{Gas} = T^{Ash} \tag{A.186}$$

Perda de carga no lado da água/vapor

$$P^{Steam} = P^{Water} - \Delta P \tag{A.187}$$

Equilíbrio mecânico no lado do combustível

$$P^{Gas} = \min(P^{Fuel}, P^{Air}) \tag{A.188a}$$

$$P^{Gas} = P^{Ash} \tag{A.188b}$$

Entropia e entalpia mássicas do vapor

$$[S^{Steam}, H^{Steam}] = propterm.propPTv(P^{Steam}, T^{Steam}) \tag{A.189}$$

Calor trocado

$$(H^{Steam} - H^{Water}) \times F^{Water} = q_{ex} + Q^{InletQ} \tag{A.190}$$

Reação

$$r(i,j) = stoic(i,j) \times conv(j) \times z(limit(j)) \tag{A.191}$$

Soma das frações molares das correntes de saída

$$\sum_{i=1}^{NComp} (z^{Gas}) = 1 \tag{A.192a}$$

$$\sum_{i=1}^{NCompS} (z_{sol}^{Ash}) = 1 \tag{A.192b}$$

$$\sum_{i=1}^{NComp} (zGas) = 1 \tag{A.192c}$$

Quantidade de oxigênio estequiométrica na corrente $FGas$

$$zGas(NO2) = 0 \tag{A.193}$$

Cálculo flash para o gás de escape na temperatura de referência (298.15 [K] e 1 [atm])

$$[v\_gas\_1, x\_gas\_1, y\_gas\_1] = PP.Flash(298.15[K], 1[atm], z^{Gas}) \tag{A.194}$$

Cálculo flash para o gás de escape na temperatura de saída

$$[v\_gas\_1, x\_gas\_1, y\_gas\_1] = PP.Flash(T^{Gas}, P^{Gas}, z^{Gas}) \tag{A.195}$$

Diferença de entalpia para o gás de escape entre a temperatura de referência e a temperatura do gás

$$\begin{aligned} h^{Gas} &= v\_gas\_2 \times PP.VapourEnthalpy(T^{Gas}, P^{Gas}, y\_gas\_2) \\ &+ (1 - v\_gas\_2) \times PP.VapourEnthalpy(T^{Gas}, P^{Gas}, x\_gas\_2) \\ &- v\_gas\_1 \times PP.VapourEnthalpy(298.15[K], 1[atm], y\_gas\_1) \\ &+ (1 - v\_gas\_1) \times PP.VapourEnthalpy(298.15[K], 1[atm], x\_gas\_1) \end{aligned} \tag{A.196}$$

Cálculo flash para o ar na temperatura de referência (298.15 [K] e 1 [atm])

$$[v\_air\_1, x\_air\_1, y\_air\_1] = PP.Flash(298.15[K], 1[atm], z^{Air}) \tag{A.197}$$

Cálculo flash para o ar na temperatura de entrada

$$[v\_air\_1, x\_air\_1, y\_air\_1] = PP.Flash(T^{Air}, P^{Air}, z^{Air}) \tag{A.198}$$

Diferença de entalpia para o ar entre a temperatura de referência e a temperatura do ar

$$\begin{aligned} h^{Air} &= v\_air\_2 \times PP.VapourEnthalpy(T^{Air}, P^{Air}, y\_air\_2) \\ &+ (1 - v\_air\_2) \times PP.VapourEnthalpy(T^{Air}, P^{Air}, x\_air\_2) \\ &- v\_air\_1 \times PP.VapourEnthalpy(298.15[K], 1[atm], y\_air\_1) \\ &+ (1 - v\_air\_1) \times PP.VapourEnthalpy(298.15[K], 1[atm], x\_air\_1) \end{aligned} \tag{A.199}$$

Diferença de entalpia para as cinzas entre a temperatura de referência e a temperatura de saída

$$\begin{aligned} h^{Ash} &= PP.VapourEnthalpy(T^{Air}, P^{Air}, z_{sol}^{Ash}) \\ &- PP.VapourEnthalpy(298.15[K], 1[atm], z_{sol}^{Ash}) \end{aligned} \tag{A.200}$$

Diferença de entalpia para o combustível entre a temperatura de referência e a temperatura de entrada (fase sólida)

$$\begin{aligned} h^{Fuel} &= PP.VapourEnthalpy(T^{Fuel}, P^{Fuel}, z_{sol}^{Fuel}) \\ &- PP.VapourEnthalpy(298.15[K], 1[atm], z_{sol}^{Fuel}) \end{aligned} \tag{A.201}$$

Diferença de entalpia para o combustível entre a temperatura de referência e a temperatura de entrada (fase fluida)

$$\begin{aligned} h^{Ash} &= PP.LiquidEnthalpy(T^{Fuel}, P^{Fuel}, z_{sol}^{Fuel}) \\ &- PP.LiquidEnthalpy(298.15[K], 1[atm], z_{sol}^{Fuel}) \end{aligned} \tag{A.202}$$

Balanço de energia

$$q_{comb} = q_{ex} + q_{losses} \tag{A.203}$$

Perdas de calor

$$q_{losses} = q_{HHV} \times f_{losses} \tag{A.204}$$

Calor de combustão na temperatura de operação da caldeira

$$\begin{aligned} -q_{comb} &= F^{Air} \times h^{Air} + F_{sol}^{Fuel} \times h_{fuel\_sol} + F \times \sum_{i=1}^{NReac} (h(i) \times conv(i) \times z(limit(i)) \\ &+ F^{Fuel} \times h_{fuel\_fluid} + F^{Gas} \times h^{Gas} + F_{sol}^{Ash} \times h^{Ash} \end{aligned} \tag{A.205}$$

Calor gerado baseado no poder calorífico superior

$$-q_{HHV} = F \times \sum_{i=1}^{NReac} (h(i) \times conv(i) \times z(limit(i))) \tag{A.206}$$

Calor gerado baseado no poder calorífico superior

$$-q_{LHV} = q_{HHV} - F^{Fuel}_{total\_mass} \times z^{Gas}_{mass}(NWater) \times 2442.1[kJ/kg] \tag{A.207}$$

Poder calorífico superior (base úmida)

$$HHV_{wet} \times F^{Fuel}_{total\_mass} = q_{HHV} \tag{A.208}$$

Poder calorífico superior (base seca)

$$HHV_{wet} \times (F^{Fuel}_{total\_mass} - F^{Fuel}_{mass} \times z^{Fuel}(NWater)) = q_{HHV} \tag{A.209}$$

Poder calorífico inferior (base úmida)

$$LHV_{wet} \times F^{Fuel}_{total\_mass} = q_{LHV} \tag{A.210}$$

Produção específica de vapor

$$v_{spec} \times F^{Fuel}_{total\_mass} = F^{Steam} \tag{A.211}$$

Eficiência de tranferência de calor (baseado no poder calorífico inferior)

$$\eta_{LHV} \times q_{LHV} = q_{ex} \tag{A.212}$$

Eficiência de tranferência de calor (baseado no poder calorífico superior)

$$\eta_{HHV} \times q_{HHV} = q_{ex} \tag{A.213}$$

Umidade do ar

$$humidity \times (F^{Air}_{mass} - F^{Air}_{mass} \times z^{Air}_{mass}(NWater)) = F^{Air}_{mass} \times z^{Air}_{mass}(NWater) \tag{A.214}$$

Composição total da corrente de combustível – $Fuel$ (fase fluida)

$$F \times z(i) = F^{Fuel} \times z^{Fuel}(i) + F^{Air} \times z^{Air}(i) \tag{A.215}$$

Composição total da corrente de combustível – $Fuel$ (fase sólida)

$$F \times z(i) = F^{Fuel}_{sol} \times z^{Fuel}_{sol}(i) + F^{Air}_{sol} \times z^{Air}_{sol}(i) \tag{A.216}$$

A.5.3 Reator estequiométrico – *stoic_reactor*

Modelo de um reator estequiométrico. A conversão das reações devem ser especificadas com relação ao reagente limitante. Além disso, o reagente limitante deve ter coeficiente estequiométrico igual a -1.

Hipóteses:

- Todas as três fases podem estar presentes;
- Operação em estado estacionário.

Deve-se especificar:

- A corrente de entrada;
- A conversão de cada reação, baseada nos respectivos reagentes limitantes;
- A temperatura do reator;
- O tempo de residência ou volume do reator.

Deve-se definir os seguintes parâmetros:

- O número de reações;
- A matriz estequiométrica;
- O reagente limitante de cada reação;
- O calor de reação para cada reação;
- A densidade da mistura no reator (para o cálculo do volume do reator ou tempo de residência).

Parâmetros

NReac Número de reações

stoic(NComp+NCompS,NReac) Matriz de coeficientes estequiométricos das reações

limit(NReac) Posição do reagente limitante de cada reação no vetor de componentes

h(NReac) Entalpia de reação para cada reação [kJ/kmol]

density Densidade da mistura dentro do reator [kg/m^3]

Variáveis

in Inlet solidStream

out Outlet solidStreamPH

F Vazão molar total da entrada [kmol/h]

z Composição molar total da entrada

Q Calor trocado no reator

r Reações

conv Conversão para cada reação em relação ao reagente limintante

V Volume do reator [m^3]

τ Tempo de residência no reator [h]

T Temperatura do reator [K]

Equações

Reação ($i = [1 : NComp + NCompS]$, $j = [1 : NReac]$)

$$r(i,j) = stoic(i,j) \times conv(i,j) \times z_{total}^{Inlet}(limit(j)) \tag{A.217}$$

Soma das frações molares (fase sólida)

$$\sum_{i=1}^{NCompS} z_{sol}^{Outlet} = 1 \tag{A.218}$$

Soma das frações molares (fase fluida)

$$\sum_{i=1}^{NCompS} z^{Outlet} = 1 \tag{A.219}$$

Balanço de energia

$$F^{Outlet} \times h^{Outlet} + F_{sol}^{Outlet} \times h_{sol}^{Outlet} = F^{Inlet} \times h^{Inlet} + F_{sol}^{Inlet} \times h_{sol}^{Inlet} + Q - F \times \sum_{i=1}^{NReac} (h \times conv(i) \times z(limit(i))) \tag{A.220}$$

Vazão molar total da entrada

$$F = F^{Inlet} + F_{sol}^{Inlet} \tag{A.221}$$

Composição total da entrada (fase fluida)

$$F \times z = F^{Inlet} \times z^{Inlet} \tag{A.222}$$

Composição total da entrada (fase sólida)

$$F \times z = F_{sol}^{Inlet} \times z_{sol}^{Inlet} \tag{A.223}$$

Equilíbrio mecânico

$$P^{Inlet} = P^{Outlet} \tag{A.224}$$

Temperatura do reator

$$T^{Outlet} = T \tag{A.225}$$

Volume do reator

$$V = \frac{F_{total\_mass}^{Inlet} \times \tau}{density} \tag{A.226}$$

Balanço molar por componente (fase fluida)

$$F^{Outlet} \times z^{Outlet}(i) = F^{Inlet} \times z^{Inlet}(i) + F \times \sum_{j=1}^{NReac} r(i,j) \tag{A.227}$$

Balanço molar por componente (fase sólida)

$$F_{sol}^{Outlet} \times z_{sol}^{Outlet}(i) = F_{sol}^{Inlet} \times z_{sol}^{Inlet}(i) + F \times \sum_{j=1}^{NReac} r(i,j) \tag{A.228}$$

A.6 Separadores

A.6.1 Coluna de adsorção – *adsorptionTower*

Modelo de uma coluna de adsorção.

Hipóteses:

- Operação em estado estacionário;
- Só o componente alvo é transferido entre as fases;
- Sem perda de calor para o ambiente.

Deve-se especificar:

- A corrente de entrada de gás;
- A corrente de entrada de líquido, exceto a vazão;
- O fator de recuperação;
- O fator de partição;
- A razão entre o líquido e o gás.

Deve-se definir os seguintes parâmetros:

- A posição do componente alvo no vetor de componentes.

Parâmetros

Target Posição do componente de interesse no vetor de componentes

Variáveis

in InletG solidStream

in InletL solidStream

out OutletG solidStreamEq

out OutletL solidStreamEq

R Fator de recuperação

f Razão entre as vazões mássicas de gás e líquido

T Temperatura de operação da coluna [K]

P Preção de operação da coluna [atm]

m Inclinação da curva de equilíbrio

Equações

Razão entre as vazões mássicas de gás e líquido

$$F^{OutletL} = m \times F^{InletG} \times f \tag{A.229}$$

Balanço de massa global (fase fluida)

$$F^{InletL} + F^{InletG} = F^{OutletG} + F^{OutletL} \tag{A.230}$$

Soma das frações molares (fase fluida) das correntes de saída *OutletL* e *OutletG*

$$\sum_{i=1}^{NComp} z^{OutletG} = \sum_{i=1}^{NComp} z^{OutletL} \tag{A.231}$$

Balanço de massa global (fase sólida)

$$F_{sol\_mass}^{InletL} + F_{sol\_mass}^{InletG} = F_{sol\_mass}^{OutletL} \tag{A.232a}$$
$$F_{sol\_mass}^{OutletG} = 0[kmol/h] \tag{A.232b}$$

Especificação da fração mássica (fase sólida) da corrente *OutletG*

$$z_{sol\_mass}^{OutletG} = z_{sol\_mass}^{OutletL} \tag{A.233}$$

Equilíbrio térmico

$$T^{OutletL} = T \tag{A.234a}$$
$$T^{OutletG} = T \tag{A.234b}$$

Equilíbrio mecânico

$$P^{OutletL} = P \tag{A.235a}$$
$$P^{OutletG} = P \tag{A.235b}$$

Balanço de massa por componente (i) para a fase fluida
Se $i = Target$ então:

$$F^{InletL} \times z^{InletL}(i) + F^{InletG} \times z^{InletG}(i) = F^{OutletL} \times z^{OutletL}(i) + F^{OutletG} \times z^{OutletG}(i) \tag{A.236a}$$
$$F^{OutletL} \times z^{OutletL}(Target) = R \times z^{InletG}(Target) \times F^{InletG} \tag{A.236b}$$

Senão:

$$F^{InletL} \times z^{InletL}(i) = F^{OutletL} \times z^{OutletL}(i) \tag{A.236c}$$
$$F^{OutletG} \times z^{OutletG}(i) = F^{OutletG} \times z^{OutletG}(i) \tag{A.236d}$$

Balanço de massa por componente (i) para a fase sólida
Se $F_{sol\_mass}^{OutletL} < 1E-6[kg/h]$ então:

$$z_{sol}^{OutletL} = z_{sol}^{InletL} \tag{A.237a}$$

Senão:

$$F_{sol}^{OutletL} \times z_{sol}^{OutletL} = F_{sol}^{InletL} \times z_{sol}^{InletL} + F_{sol}^{InletG} \times z_{sol}^{InletG} \tag{A.237b}$$

A.6.2 Centrífuga – *centrifuge*

Modelo de uma centrífuga com correntes de filtrado e torta de filtro.

Hipóteses:

- Operação em estado estacionário;
- Sem perda de calor para o ambiente.

Deve-se especificar:

- A corrente de entrada;
- A fração de separação das fases fluida e sólida;
- O número de centrífugas;
- A potência de uma centrífuga.

Parâmetros

density Densidade da mistura [kg/m^3]

f$_{vol_cent}$ Vazão volumétrica por centrífuga [m^3/h]

NWater Posição do componente "água" no vetor de componentes

Variáveis

in Inlet solidStream

in InletW workStream

out FilterCake solidStream

out Filtrate solidStream

frac$_{sol}$ Eficiência de separação para a fase sólida

frac$_{liq}$ Eficiência de separação para a fase líquida

humidity Fração de água na torta de filtro

impurity Fração de sólidos no filtrado

Power Demanda de potência de uma centrífuga individual [kW]

Nunits Número de centrífugas necessárias

Equações

Balanço de massa global (fase fluida)

$$F^{Inlet} = F^{FilterCake} + F^{Filtrate} \tag{A.238}$$

Eficiência de separação para a fase líquida

$$F^{Filtrate}_{mass} = F^{Inlet}_{mass} \times frac_{liq} \tag{A.239}$$

Balanço de massa global (fase sólida)

$$F^{Inlet}_{sol} = F^{FilterCake}_{sol} + F^{Filtrate}_{sol} \tag{A.240}$$

Eficiência de separação para a fase sólida

$$F^{FilterCake}_{sol\_mass} = F^{Inlet}_{sol\_mass} \times frac_{sol} \tag{A.241}$$

Composição das correntes de saída: $Filtrate$ e $FilterCake$
Fase fluida

$$z^{Filtrate} = z^{Inlet} \tag{A.242a}$$
$$z^{FilterCake} = z^{Inlet} \tag{A.242b}$$

Fase sólida

$$z^{Filtrate}_{sol} = z^{Inlet}_{sol} \tag{A.242c}$$
$$z^{FilterCake}_{sol} = z^{Inlet}_{sol} \tag{A.242d}$$

Umidade da torta de filtro

$$z^{FilterCake}_{total\_mass}(NWater) = humidity \tag{A.243}$$

Impureza no filtrado

$$F^{Filtrate}_{sol\_mass} = impurity \times (F^{Filtrate}_{mass} + F^{Filtrate}_{sol\_mass}) \tag{A.244}$$

Entalpia das correntes de saída: $Filtrate$ e $FilterCake$
Fase fluida

$$h^{Filtrate} = h^{Inlet} \tag{A.245a}$$
$$h^{FilterCake} = h^{Inlet} \tag{A.245b}$$

Fase sólida

$$h_{sol}^{Filtrate} = h_{sol}^{Inlet} \tag{A.245c}$$
$$h_{sol}^{FilterCake} = h_{sol}^{Inlet} \tag{A.245d}$$

Equilíbrio térmico (isotérmico)

$$T^{Filtrate} = T^{Inlet} \tag{A.246a}$$
$$T^{FilterCake} = T^{Inlet} \tag{A.246b}$$

Equilíbrio mecânico

$$P^{Filtrate} = P^{Inlet} \tag{A.247a}$$
$$P^{FilterCake} = P^{Inlet} \tag{A.247b}$$

Fração de vapor nas correntes de saída

$$v^{Filtrate} = v^{Inlet} \tag{A.248a}$$
$$v^{FilterCake} = v^{Inlet} \tag{A.248b}$$

Demanda total de energia elétrica

$$W^{InletW} = Power \times Nunits \tag{A.249}$$

Número de centrífugas

$$f_{vol\_cent} \times density \times Nunits = F_{total\_mass}^{Inlet} \tag{A.250}$$

A.6.3 Lavagem da cana-de-açúcar – *cleaning*

Modelo da etapa de lavagem da cana-de-açúcar, onde água é utilizada para diminuir a quantidade de impurezas presentes na cana-de-açúcar.

Hipóteses:

- Operação em estado estacionário;
- A água usada na limpeza da cana não é absorvida por ela;
- Sem perda de calor para o ambiente.

Deve-se especificar:

- A corrente de entrada de cana-de-açúcar;

- A corrente de entrada de água, exceto a vazão;
- A proporção entre as vazões das correntes de entrada: cana-de-açúcar e água;
- A eficiência de limpeza;
- A fração de açúcar perdida;
- A fração de sólidos que segue na corrente de cana-de-açúcar.

Deve-se definir os seguintes parâmetros:

- A posição do componente “água”, “impurezas”, “celulose”, “hemicelulose” e “lignina” no vetor de componentes.

Parâmetros

NWater Posição do componente “água” no vetor de componentes

NDirt Posição do componente “Terra” no vetor de componentes

NCell Posição do componente “Celulose” no vetor de componentes

NHemi Posição do componente “Hemicelulose” no vetor de componentes

NLignin Posição do componente “Lignina” no vetor de componentes

Variáveis

in CrudeCane solidStream

in Water solidStream

out SugarCane solidStreamEq

out Dirt solidStreamEq

Separation Eficiência de separação

Efficiency Eficiência de limpeza

SugarLosses Fração de açúcares perdidas do lodo

humidity Fração de água na cana-de-açúcar

impurity Fração de impurezas na cana-de-açúcar

WFPTC Tonelada de água utilizada por tonelada de cana-de-açúcar

Fiber Fração de fibras na entrada de cana-de-açúcar

Equações

Balanço de massa global (fase fluida)

$$F^{CrudeCane} + F^{Water} = F^{SugarCane} + F^{Dirt} \tag{A.251}$$

Balanço de massa global (fase sólida)

$$F_{sol}^{CrudeCane} + F_{sol}^{Water} = F_{sol}^{SugarCane} + F_{sol}^{Dirt} \tag{A.252}$$

Tonelada de água utilizada por tonelada de cana-de-açúcar

$$F_{mass}^{Water} = (F_{mass}^{CrudeCane} + F_{sol\_mass}^{CrudeCane}) \times WFPTC \tag{A.253}$$

Soma das frações molares (fase fluida)

$$\sum_{i=1}^{NComp} z^{SugarCane} = \sum_{i=1}^{NComp} z^{Dirt} \tag{A.254}$$

Soma das frações molares (fase sólida)

$$\sum_{i=1}^{NCompS} z_{sol}^{SugarCane} = \sum_{i=1}^{NCompS} z_{sol}^{Dirt} \tag{A.255}$$

Umidade do lodo

$$F_{sol\_mass}^{Dirt} = humidity \times (F_{sol\_mass}^{Dirt} + F_{mass}^{Dirt}) \tag{A.256}$$

Impurezas sólidas na corrente $SugarCane$

$$F_{sol\_mass}^{SugarCane} \times z_{sol\_mass}^{SugarCane}(NDirt) = impurity \times (F_{mass}^{SugarCane} + F_{sol\_mass}^{SugarCane}) \tag{A.257}$$

Equilíbrio térmico

$$T^{SugarCane} = T^{CrudeCane} \tag{A.258a}$$

$$T^{Dirt} = T^{CrudeCane} \tag{A.258b}$$

Equilíbrio mecânico

$$P^{SugarCane} = P^{CrudeCane} \tag{A.259a}$$

$$P^{Dirt} = P^{CrudeCane} \tag{A.259b}$$

Teor de fibras na cana-de-açúcar

$$Fiber \times (F_{mass}^{CrudeCane} + F_{sol\_mass}^{CrudeCane}) = F_{sol\_mass}^{CrudeCane} \times (z_{sol\_mass}^{CrudeCane}(NCell) + z_{sol\_mass}^{CrudeCane}(NHemi) + z_{sol\_mass}^{CrudeCane}(NLignin)) \quad \text{(A.260)}$$

Balanço molar por componente (fase fluida)
Se i = NWater

$$F^{CrudeCane} \times z^{CrudeCane}(i) = F^{SugarCane} \times z^{SugarCane}(i) \quad \text{(A.261a)}$$

$$F^{Water} \times z^{Water}(i) = F^{Dirt} \times z^{Dirt}(i) \quad \text{(A.261b)}$$

Senão

$$F^{CrudeCane} \times z^{CrudeCane}(i) \times (1 - SugarLosses) = F^{SugarCane} \times z^{SugarCane}(i) \quad \text{(A.261c)}$$

$$F^{Water} \times z^{Water}(i) \times SugarLosses = F^{Dirt} \times z^{Dirt}(i) \quad \text{(A.261d)}$$

Balanço molar por componente (fase sólida)
Se i = NDirt

$$F_{sol}^{SugarCane} \times z_{sol}^{SugarCane}(i) = (F_{sol}^{CrudeCane} \times z_{sol}^{CrudeCane}(i) + F_{sol}^{Water} \times z_{sol}^{Water}(i)) \times (1 - Efficiency) \quad \text{(A.262a)}$$

$$F_{sol}^{Dirt} \times z_{sol}^{Dirt}(i) = (F_{sol}^{CrudeCane} \times z_{sol}^{CrudeCane}(i) + F_{sol}^{Water} \times z_{sol}^{Water}(i)) \times Efficiency \quad \text{(A.262b)}$$

Senão

$$F_{sol}^{SugarCane} \times z_{sol}^{SugarCane}(i) = (F_{sol}^{CrudeCane} \times z_{sol}^{CrudeCane}(i) + F_{sol}^{Water} \times z_{sol}^{Water}(i)) \times Separation \quad \text{(A.262c)}$$

$$F_{sol}^{Dirt} \times z_{sol}^{Dirt}(i) = (F_{sol}^{CrudeCane} \times z_{sol}^{CrudeCane}(i) + F_{sol}^{Water} \times z_{sol}^{Water}(i)) \times (1 - Separation) \quad \text{(A.262d)}$$

A.6.4 Coluna de destilação do etanol hidratado – *column*

Modelo do trem de colunas de destilação responsável por purificar o vinho delevedurado e produzir etanol hidratado. Esse modelo utiliza uma tabela de inspeção multidimensional com as principais informações necessárias para descrever a operação da coluna de destilação. Essas informações foram obtidas por simulação rigorosa do trem de colunas no simulador Aspen Plus.

Hipóteses:

- Operação em estado estacionário;

- Sem perda de calor para o ambiente;
- Todos os sólidos da corrente de entrada deixam a coluna na corrente de vinhaça;
- Somente etanol e água estão presentes nas correntes de etanol hidratado e flegmassa.

Deve-se especificar:

- A corrente de entrada de vinho.

Deve-se definir os seguintes parâmetros:

- O vetor que indica se o componente (exceto etanol e água) deixará a coluna na corrente de vinhaça ou de etanol de segunda;
- A posição dos componentes "água" e "etanol".

Parâmetros

IntLiquid *plug-in* interpolador com os dados do trem de colunas de destilação para o etanol hidratado líquido

IntVapour *plug-in* interpolador com os dados do trem de colunas de destilação para o etanol hidratado vapor

***outer* PP** Chamada para o plugin externo *VRTherm* que calcula as propriedades físicas da fase fluida

***outer* PPS** Chamada para o plugin externo *VRTherm* que calcula as propriedades físicas da fase sólida

***outer* NComp** Número de compostos na fase fluida

***outer* NCompS** Número de compostos na fase sólida

frac(NComp) Indica se o componente i vai deixar o trem de coluna na corrente $Vinasse$ (0) ou na corrente $SecGrad$ (1)

NEthanol Posição do componente "etanol" no vetor de componentes

NWater Posição do componente "água" no vetor de componentes

HydrOutletPhase Fase em que o etanol hidratado deixa a coluna. Estados válidos = ["*Liquid*","*Vapour*"]

Variáveis

in Wine solidStream

in QAA1 heatStream

in QBB1 heatStream

out Vinasse solidStreamEq

out Phlegm solidStreamEq

out HydrEth solidStream

out SecGrad solidStreamEq

out CD heatStream

out CBB1 heatStream

TWine Temperatura da corrente de entrada $Wine$ [K]

SecGradz Fração de etanol na corrente de etanol de segunda

Winez Fração de etanol na corrente de vinho $Wine$

VinF Vazão molar da vinhaça – $Vinasse$ (considerando somente etanol e água) [kmol/h]

SecF Vazão molar do etanol de segunda – $SecGrad$ (considerando somente etanol e água) [kmol/h]

WineF Vazão molar do vinho – $Wine$ (considerando somente etanol e água) [kg/h]

Equações

Balanço molar global (fase fluida)

$$F^{Wine} = F^{Vinasse} + F^{Phlegm} + F^{HydrEth} + F^{SecGrad} \tag{A.263}$$

Balanço molar global (fase sólida)

$$F_{sol}^{Wine} = F_{sol}^{Vinasse} \tag{A.264a}$$

Nenhum sólido segue para as correntes $SecGrad$, $HydrEth$ e $Phlegm$

$$F_{sol}^{SecGrad} = 0[kmol/h] \tag{A.264b}$$
$$F_{sol}^{HydrEth} = 0[kmol/h] \tag{A.264c}$$
$$F_{sol}^{Phlegm} = 0[kmol/h] \tag{A.264d}$$

Composição das correntes de saída (fase sólida)

$$z_{sol}^{Wine} = z_{sol}^{Vinasse} \tag{A.265a}$$
$$z_{sol}^{Wine} = z_{sol}^{Phlegm} \tag{A.265b}$$
$$z_{sol}^{Wine} = z_{sol}^{HydrEth} \tag{A.265c}$$
$$z_{sol}^{Wine} = z_{sol}^{SecGrad} \tag{A.265d}$$

Soma das frações molares (fase fluida)

$$\sum_{i=1}^{NComp} z^{Vinasse} = \sum_{i=1}^{NComp} z^{SecGrad} \tag{A.266}$$

Vazão mássica da corrente $Wine$ considerando somente etanol e água

$$WineF = F_{mass}^{Wine} \times (z_{mass}^{Wine}(NEthanol) + z_{mass}^{Wine}(NWater)) \tag{A.267}$$

Fração de etanol na corrente $Wine$ considerando somente etanol e água

$$WineF \times Winez = F_{mass}^{Wine} \times z_{mass}^{Wine}(NEthanol) \tag{A.268}$$

Entalpia molar da fase sólida da corrente $HydrEth$

$$h_{sol}^{HydrEth} = PP.VapourEnthalpy(T^{HydrEth}, P^{HydrEth}, z_{sol}^{HydrEth}) \tag{A.269}$$

Temperatura do vinho – $Wine$

$$TWine = T^{Wine} \tag{A.270}$$

Se $i = NEthanol$:

Fração de etanol na corrente $Vinasse$

$$F^{Vinasse} \times z^{Vinasse}(NEthanol) = 7.82E-5 \times VinF \tag{A.271a}$$

Fração de etanol na corrente $SecGrad$

$$F^{SecGrad} \times z^{SecGrad}(NEthanol) = SecGradz \times SecF \tag{A.271b}$$

Fração de etanol na corrente $HydrEth$

$$z^{HydrEth}(NEthanol) = 0.849 \tag{A.271c}$$

Fração de etanol na corrente $Phlegm$

$$z^{Phlegm}(NEthanol) = 7.82E-5 \tag{A.271d}$$

Senão, se $i = NWater$:

Fração de água na corrente $Vinasse$

$$F^{Vinasse} \times z^{Vinasse}(NWater) = 0.9999218 \times VinF \tag{A.272a}$$

Fração de água na corrente $SecGrad$

$$F^{SecGrad} \times z^{SecGrad}(NWater) = (1 - SecGradz) \times SecF \tag{A.272b}$$

Fração de água na corrente $HydrEth$

$$z^{HydrEth}(NWater) = 0.151 \tag{A.272c}$$

Fração de água na corrente $Phlegm$

$$z^{Phlegm}(NWater) = 0.9999218 \tag{A.272d}$$

Senão:

Fração de etanol na corrente $Vinasse$

$$F^{Vinasse} \times z^{Vinasse}(i) = (1 - f(i)) \times F^{Wine} \times z^{Wine}(i) \tag{A.273a}$$

Fração de etanol na corrente $SecGrad$

$$F^{SecGrad} \times z^{SecGrad}(i) = f(i) \times F^{Wine} \times z^{Wine}(i) \tag{A.273b}$$

Fração de etanol na corrente $HydrEth$

$$z^{HydrEth}(i) = 0 \tag{A.273c}$$

Fração de etanol na corrente $Phlegm$

$$z^{Phlegm}(i) = 0 \tag{A.273d}$$

Se $HydrOutletPhase$ ="$Liquid$":

Chamada para o interpolador

$$[\frac{QAA1}{WineF}, \frac{QBB1}{WineF}, \frac{-Q^{CD}}{WineF}, \frac{-Q^{CBB1}}{WineF}, SecGradz, \frac{VinF}{WineF}, \frac{SecF}{WineF}, \frac{F^{Phlegm}}{WineF}, \frac{F^{HydrEth}}{WineF}] = intLiquid.interpola(TWine, Winez) \tag{A.274a}$$

Entalpia molar da corrente $HydrEth$ (fase fluida)

$$h^{HydrEth} = PP.LiquidEnthalpy(T^{HydrEth}, P^{HydrEth}, z^{HydrEth}) \tag{A.274b}$$

Fração de vapor da corrente $HydrEth$

$$v^{HydrEth} = 0 \tag{A.274c}$$

Se $HydrOutletPhase$ ="$Vapour$":

Chamada para o interpolador

$$[\frac{QAA1}{WineF}, \frac{QBB1}{WineF}, \frac{-Q^{CD}}{WineF}, \frac{-Q^{CBB1}}{WineF}, SecGradz, \frac{VinF}{WineF}, \frac{SecF}{WineF}, \frac{F^{Phlegm}}{WineF}, \frac{F^{HydrEth}}{WineF}] = intVapour.interpola(TWine, Winez) \tag{A.275a}$$

Entalpia molar da corrente $HydrEth$ (fase fluida)

$$h^{HydrEth} = PP.VapourEnthalpy(T^{HydrEth}, P^{HydrEth}, z^{HydrEth}) \quad \text{(A.275b)}$$

Fração de vapor da corrente $HydrEth$

$$v^{HydrEth} = 1 \quad \text{(A.275c)}$$

A.6.5 Decantador – *decanter*

Modelo de um decantador simplificado com uma razão de separação entre as fases sólida e fluida especificada pelo usuário.

Hipóteses:

- Operação em estado estacionário;
- Sem perda de calor para o ambiente.

Deve-se especificar:

- A corrente de entrada;
- A fração de separação entre as fases sólida e fluida;
- A entrada de calor;

Deve-se definir os seguintes parâmetros:

- Os compostos que participam no cálculo do Brix, pelo parâmetro *Brix(NComp)* (1 se participa e 0 se não participa).

Parâmetros

***outer* PP** Chamada para o plugin externo *VRTherm* que calcula as propriedades físicas da fase fluida

***outer* PPS** Chamada para o plugin externo *VRTherm* que calcula as propriedades físicas da fase sólida

***outer* NComp** Número de compostos na fase fluida

***outer* NCompS** Número de compostos na fase sólida

M(NComp) Vetor de tamanho "NComp" contendo os pesos moleculares dos compostos da fase fluida [kg/kmol]

MS(NCompS) Vetor de tamanho "NCompS" contendo os pesos moleculares dos compostos da fase sólida [kg/kmol]

Brix(NComp) Indica se o componente i participa do cálculo do Brix da corrente (1 - se participa, 0 - se não participa)

NWater Posição do componente "água" no vetor de componentes

Variáveis

in Inlet solidStream

out Sludge solidStreamEq

out Clarified solidStreamEq

$\mathbf{frac_{sol}}$ Eficiência de separação para a fase sólida

$\mathbf{frac_{liq}}$ Eficiência de separação para a fase líquida

humidity Fração de água no lodo

impurity Fração de sólidos no sobrenadante

$\mathbf{Outlet_{Brix}}$ Fração de sólidos solúveis totais na corrente de saída $Clarified$

Q Calor perdido [kW]

Equações

Balanço molar global (fase fluida)

$$F^{Inlet} = F^{Sludge} + F^{Clarified} \tag{A.276}$$

Fração de partição (fase fluida)

$$F^{Clarified} = F^{Inlet} \times frac_{liq} \tag{A.277}$$

Composição molar da corrente $Clarified$ (fase fluida)

$$z^{Clarified} = z^{Inlet} \tag{A.278}$$

Composição molar da corrente $Sludge$ (fase fluida)

$$z^{Sludge} = z^{Inlet} \tag{A.279}$$

Balanço molar global (fase sólida)

$$F_{sol}^{Inlet} = F_{sol}^{Sludge} + F_{sol}^{Clarified} \tag{A.280}$$

Fração de partição (fase sólida)

$$F_{sol}^{Sludge} = F_{sol}^{Inlet} \times frac_{sol} \tag{A.281}$$

Composição molar da corrente $Clarified$ (fase sólida)

$$z_{sol}^{Clarified} = z_{sol}^{Inlet} \tag{A.282}$$

Composição molar da corrente $Sludge$ (fase sólida)

$$z_{sol}^{Sludge} = z_{sol}^{Inlet} \tag{A.283}$$

Umidade do lodo – $Sludge$

$$z_{total\_mass}^{Sludge}(NWater) = humidity \tag{A.284}$$

Impurezas no clarificado – $Clarified$

$$F_{sol\_mass}^{Clarified} = impurity \times (F_{mass}^{Clarified} + F_{sol\_mass}^{Clarified}) \tag{A.285}$$

Sólidos solúveis totais na corrente $Clarified$

$$Outlet_{Brix} = \sum_{i=1}^{NComp} z_{mass}^{Clarified} \times Brix \tag{A.286}$$

Balanço de energia

$$\begin{aligned} &F^{Sludge} \times z^{Sludge} + F_{sol}^{Sludge} \times z_{sol}^{Sludge} + F^{Clarified} \times z^{Clarified} \\ &+ F_{sol}^{Clarified} \times z_{sol}^{Clarified} + Q = F^{Inlet} \times z^{Inlet} + F_{sol}^{Inlet} \times z_{sol}^{Inlet} \end{aligned} \tag{A.287}$$

Equilíbrio térmico

$$T^{Clarified} = T^{Sludge} \tag{A.288}$$

Equilíbrio mecânico

$$P^{Sludge} = P^{Inlet} \tag{A.289a}$$

$$P^{Clarified} = P^{Inlet} \tag{A.289b}$$

A.6.6 Coluna de desidratação do etanol – *dehydration*

Modelo do trem de colunas de destilação responsável pela desidratação do etanol. Esse modelo utiliza uma tabela de inspeção multidimensional com as principais informações necessárias para descrever a operação da coluna de destilação. Essas informações foram obtidas por simulação rigorosa do trem de colunas de destilação extrativa empregando monoetilenoglicol (MEG) no simulador Aspen Plus.

Hipóteses:

- Operação em estado estacionário;
- Sem perda de calor para o ambiente;
- Todos os sólidos da corrente de entrada deixam a coluna na corrente de água;
- Somente etanol e água estão presentes nas correntes de etanol hidratado e flegmassa.

Deve-se especificar:

- A corrente de entrada de etanol hidratado.

Deve-se definir os seguintes parâmetros:

- A posição dos componentes "água", "MEG" e "etanol".

Parâmetros

Int *plug-in* interpolador com os dados do trem de colunas de destilação para o etanol anidro

***outer* PP** Chamada para o plugin externo *VRTherm* que calcula as propriedades físicas da fase fluida

***outer* PPS** Chamada para o plugin externo *VRTherm* que calcula as propriedades físicas da fase sólida

***outer* NComp** Número de compostos na fase fluida

***outer* NCompS** Número de compostos na fase sólida

NEthanol Posição do componente "etanol" no vetor de componentes

NWater Posição do componente "água" no vetor de componentes

NMEG Posição do componente "MEG" no vetor de componentes

Variáveis

in HydrEth solidStream

in MEG solidStream

in QREXT heatStream

in QRREC heatStream

out AnhyEth solidStreamEq

out RecMEG solidStreamEq

out Water solidStreamEq

out QCEXT heatStream

out QCREC heatStream

zEth_Anh Fração molar de etanol na corrente $AnhyEth$

zEth_RMEG Fração molar de etanol na corrente $RecMEG$

zEth_Water Fração molar de etanol na corrente $Water$

zMEG_Anh Fração molar de MEG na corrente $AnhyEth$

zMEG_RMEG Fração molar de MEG na corrente $RecMEG$

zMEG_Water Fração molar de MEG na corrente $Water$

WaterF Vazão molar da corrente de água ($Water$) considerando somente água, etanol e MEG [kmol/h]

HydroF Vazão molar da corrente de etanol hidratado ($HydrEth$) considerando somente água, etanol e MEG [kmol/h]

SolventRation Razão entre as vazões mássicas de MEG e etanol hidratado

Equações

Balanço molar global (fase fluida)

$$F^{HydrEth} + F^{MEG} = F^{Water} + F^{AnhyEth} + F^{RecMEG} \tag{A.290}$$

Balanço molar global (fase sólida)

$$F_{sol}^{HydrEth} + F_{sol}^{MEG} = F_{sol}^{Water} \tag{A.291a}$$

$$F_{sol}^{RecMEG} = 0[kmol/h] \qquad F_{sol}^{AnhyEth} = 0[kmol/h] \tag{A.291b}$$

Balanço molar por componente (fase sólida)

$$F_{sol}^{HydrEth} \times z_{sol}^{HydrEth} + F_{sol}^{MEG} \times z_{sol}^{MEG} = F_{sol}^{Water} \times z_{sol}^{Water} \tag{A.292a}$$

$$z_{sol}^{AnhyEth} = z_{sol}^{HydrEth} \tag{A.292b}$$

$$z_{sol}^{RecMEG} = z_{sol}^{HydrEth} \tag{A.292c}$$

Balanço molar por componente (fase fluida)

$$F^{HydrEth} \times z^{HydrEth} + F^{MEG} \times z^{MEG} = F^{Water} \times z^{Water} + F^{AnhyEth} \times z^{AnhyEth} + F^{RecMEG} \times z^{RecMEG} \tag{A.293}$$

Vazão mássica de etanol hidratado considerando somente etanol, água e MEG

$$HydroF = F^{HydrEth} \times (z^{HydrEth}(NEthanol) + z^{HydrEth}(NWater) + z^{HydrEth}(NMEG)) \tag{A.294}$$

Vazão de água

$$HydroF + F^{MEG} - WaterF = F^{AnhyEth} + F^{RecMEG} \tag{A.295}$$

Razão entre as vazões mássicas de etanol hidratado e MEG

$$SolventRation \times F_{total\_mass}^{HydrEth} = F_{total\_mass}^{MEG} \tag{A.296}$$

Chamada para o interpolador

$$[\frac{Q^{QREXT}}{HydroF}, \frac{Q^{QRREC}}{HydroF}, \frac{-Q^{QCEXT}}{HydroF}, \frac{-Q^{QCREC}}{HydroF}, \frac{F^{AnhyEth}}{HydroF}, \frac{F^{RecMEG}}{HydroF}, T^{AnhyEth}, T^{Water}, T^{RecMEG}, zEth\_Anh, zEth\_Water, zEth\_RMEG, zMEG\_Anh, zMEG\_Water, zMEG\_RMEG] = Int.Interpola(SolventRatio) \tag{A.297}$$

Se $i = NEthanol$ então:

Fração de etanol na corrente $AnhyEth$

$$z^{AnhyEth}(i) = zEth\_Anh \tag{A.298a}$$

Fraçao de etanol na corrente $RecMEG$

$$z^{Phlegm}(i) = zEth\_RMEG \tag{A.298b}$$

Se $i = NMEG$ então:

Fração de etanol na corrente $AnhyEth$

$$z^{AnhyEth}(i) = zMEG\_Anh \tag{A.299a}$$

Fraçao de etanol na corrente $RecMEG$

$$z^{Phlegm}(i) = zMEG\_RMEG \tag{A.299b}$$

Se $i = NWater$ então:

Fração de etanol na corrente $AnhyEth$

$$z^{AnhyEth}(i) = 1 - zEth\_Anh - zMEG\_Anh \tag{A.300a}$$

Fraçao de etanol na corrente $RecMEG$

$$z^{Phlegm}(i) = 1 - zEth\_RMEG - zMEG\_Anh \tag{A.300b}$$

Senão:

Fração de etanol na corrente $AnhyEth$

$$z^{AnhyEth}(i) = 0 \tag{A.301a}$$

Fraçao de etanol na corrente $RecMEG$

$$z^{Phlegm}(i) = 0 \tag{A.301b}$$

A.6.7 Evaporador – *evaporator*

Modelo de um evaporador para concentração de açúcar, com cálculo da elevação do ponto de ebulição baseado na fração de sólidos solúveis totais (Brix) da mistura.

Hipóteses:

- Operação em estado estacionário;
- Sem perda de calor para o ambiente;
- A corrente de vapor que deixa o evaporador é constituída somente de água (corrente waterStreamEq);
- O vapor de aquecimento deixa o evaporador como líquido saturado.

Deve-se especificar:

- A corrente de entrada de caldo;
- A corrente de entrada de vapor, exceto a vazão;
- A pressão de operação do evaporador
- O Brix de saída.

Deve-se definir os seguintes parâmetros:

- A posição do componente "água" no vetor de componentes;
- Os compostos que participam no cálculo do Brix, pelo parâmetro *Brix(NComp)* (1 se participa e 0 se não participa).

Parâmetros

propterm *Plug-in* que calcula as propriedades físicas da água pura

***outer* PP** Chamada para o plugin externo *VRTherm* que calcula as propriedades físicas da fase fluida

***outer* PPS** Chamada para o plugin externo *VRTherm* que calcula as propriedades físicas da fase sólida

***outer* NComp** Número de compostos na fase fluida

***outer* NCompS** Número de compostos na fase sólida

M(NComp) Vetor de tamanho "NComp" contendo os pesos moleculares dos compostos da fase fluida [kg/kmol]

MS(NCompS) Vetor de tamanho "NCompS" contendo os pesos moleculares dos compostos da fase sólida [kg/kmol]

Brix(NComp) Indica se o componente *i* participa do cálculo do Brix da corrente (1 - se participa, 0 - se não participa)

NWater Posição do componente "água" no vetor de componentes

$\mathbf{Brix_{max}}$ Brix máximo na corrente de saída

Variáveis

in Inlet solidStream

in InletS waterStream

out OutletL solidStreamEq

out OutletS waterStreamVapFrac

out OutletV waterStreamEq

Q Calor trocado no evaporador [kW]

vfrac fração da entrada que é vaporizada

Tsat Temperatuda de saturação da água pura na pressão de operação do evaporador [K]

P Pressão de operação do evaporador [atm]

$\mathbf{Inlet_{Brix}}$ Fração de sólidos solúveis totais na corrente de entrada $Inlet$

$\mathbf{Outlet_{Brix}}$ Fração de sólidos solúveis totais na corrente de saída $OutletL$

BPE Elevação do ponto de ebulição [K]

Hv Entalpia mássica da corrente $OutletV$ no estado de referência [kJ/kg]

Sv Entropia mássica da corrente $OutletV$ no estado de referência [kJ/kg/K]

hl1 Entalpia molar da corrente $Inlet$ (fase fluida) no estado de referência [kJ/kg]

hlsol1 Entalpia molar da corrente $Inlet$ (fase sólida) no estado de referência [kJ/kg]

hl2 Entalpia molar da corrente $OutletL$ (fase fluida) no estado de referência [kJ/kg]

hlsol2 Entalpia molar da corrente $OutletL$ (fase sólida) no estado de referência [kJ/kg]

Equações

Balanço de massa global (Vapor de aquecimento)

$$F^{InletS} = F^{OutletS} \tag{A.302}$$

Balanço de massa global (fase sólida)

$$F_{sol}^{Inlet} = F_{sol}^{OutletL} \tag{A.303}$$

Balanço de massa por componente (fase sólida)

$$z_{sol}^{Inlet} = z_{sol}^{OutletL} \tag{A.304}$$

Brix na corrente de entrada

$$Inlet_{Brix} = \sum_{i=1}^{NComp} z_{mass}^{Inlet} \times Brix \tag{A.305}$$

Entropia e entalpia mássicas da corrente $OutletS$

$$[S^{OutletS}, H^{OutletS}] = propterm.propPTl(P^{OutletS}, propterm.Tsat(P^{OutletS})) \tag{A.306}$$

Entropia e entalpia mássicas da corrente de água pura na condição de referência

$$[Sv, Hv] = propterm.propPTl(P^{InletS}, 300[K]) \tag{A.307}$$

Entalpia molar da corrente $Inlet$ na condição de referência

$$hl1 = PP.LiquidEnthalpy(300[K], P^{Inlet}, z^{Inlet}) \tag{A.308a}$$
$$hl1_{sol} = PPS.VapourEnthalpy(300[K], P^{Inlet}, z_{sol}^{Inlet}) \tag{A.308b}$$

Entalpia molar da corrente $OutletL$ na condição de referência

$$hl2 = PP.LiquidEnthalpy(300[K], P^{OutletL}, z^{OutletL}) \tag{A.309a}$$
$$hl2_{sol} = PPS.VapourEnthalpy(300[K], P^{OutletL}, z_{sol}^{OutletL}) \tag{A.309b}$$

Equilíbrio mecânico

$$P^{OutletV} = P \tag{A.310a}$$
$$P^{OutletL} = P \tag{A.310b}$$
$$P^{OutletS} = P^{InletS} \tag{A.310c}$$

Temperatura de saída da corrente $OutletS$

$$T^{OutletS} = propterm.Tsat(P^{InletS}) \tag{A.311}$$

Se $\text{Inlet}_{\text{Brix}} > \text{Brix}_{\text{max}}$ então:

Balanço de massa global (fase fluida)

$$F_{mass}^{Inlet} = F_{mass}^{OutletL} \tag{A.312a}$$

Balanço de massa por componente (fase fluida)

$$z^{Inlet} = z^{OutletL} \tag{A.312b}$$

Fração da entrada $Inlet$ que é vaporizada

$$vfrac = 1E-6 \tag{A.312c}$$

Calor trocado

$$Q = F^{InletS} \times (H^{InletS} - H^{OutletS}) \tag{A.312d}$$

Brix na corrente de saída

$$Outlet_{Brix} = Inlet_{Brix} \tag{A.312e}$$

Temperatura de saturação da água pura na pressão de operação do evaporador

$$Tsat = propterm.Tsat(P^{OutletV}) \tag{A.312f}$$

Elevação do ponto de ebulição

$$BPE = 1[K] \tag{A.312g}$$

Equilíbrio térmico

$$T^{OutletL} = T^{Inlet} \tag{A.312h}$$

$$T^{OutletV} = Tsat + BPE \tag{A.312i}$$

Equilíbrio mecânico

$$P^{OutletL} = 1[atm] \tag{A.312j}$$

Senão: Balanço de massa global (fase fluida)

$$F^{Inlet}_{mass} = F^{OutletL}_{mass} + F^{OutletV} \tag{A.313a}$$

Se $i = NWater$ então:

Balanço de massa por componente (fase fluida)

$$F^{Inlet}_{mass} \times z^{Inlet}_{mass}(i) = F^{OutletL}_{mass} \times z^{OutletL}_{mass}(i) + F^{OutletV} \tag{A.313ba}$$

Senão:

Balanço de massa por componente (fase fluida)

$$F^{Inlet}_{mass} \times z^{Inlet}_{mass}(i) = F^{OutletL}_{mass} \times z^{OutletL}_{mass}(i) \tag{A.313bb}$$

$$z^{Inlet} = z^{OutletL} \tag{A.313c}$$

Fração da entrada $Inlet$ que é vaporizada

$$F^{OutletV} = F^{Inlet}_{mass} \times vfrac \tag{A.313d}$$

Calor trocado

$$Q = F^{InletS} \times (H^{InletS} - H^{OutletS}) \tag{A.313e}$$

Brix na corrente de saída

$$Outlet_{Brix} = \sum_{i=1}^{NComp} z^{OutletL}_{mass} \times Brix \tag{A.313f}$$

Temperatura de saturação da água pura na pressão de operação do evaporador

$$Tsat = propterm.Tsat(P^{OutletV}) \tag{A.313g}$$

Elevação do ponto de ebulição

$$BPE = \frac{Outlet_{Brix} \times (0.3 + Outlet_{Brix}) \times (0.22[K] + 0.0078 \times (Tsat - 273.15[K]))}{0.355 \times (1.036 - Outlet_{Brix})} \tag{A.313h}$$

Equilíbrio térmico

$$T^{OutletL} = T^{OutletV} \tag{A.313i}$$

$$T^{OutletV} = Tsat + BPE \tag{A.313j}$$

Balanço de energia

$$\begin{aligned} Q = {} & (H^{OutletV} - Hv) \times F^{OutletV} + (h^{OutletL} - hl2) \times F^{OutletL} \\ & + (h^{OutletL}_{sol} - hl2_{sol}) \times F^{OutletL}_{sol} + (h^{Inlet} - hl1) \times F^{Inlet} \\ & - (h^{Inlet}_{sol} - hl1_{sol}) \times F^{Inlet}_{sol} \end{aligned} \tag{A.313k}$$

A.6.8 Filtro – *filter*

Modelo de um filtro com correntes de filtrado e torta de filtro.

Hipóteses:

- Operação em estado estacionário;
- Sem perda de calor para o ambiente.

Deve-se especificar:

- A corrente de entrada;
- A fração de separação das fases fluida e sólida.

Parâmetros

NWater Posição do componente "água" no vetor de componentes

Variáveis

in Inlet solidStream

out FilterCake solidStream

out Filtrate solidStream

$frac_{insol}$ Eficiência de separação dos sólidos insolúveis

$frac_{sol}$ Eficiência de separação dos sólidos solúveis

$frac_{water}$ Eficiência de separação da água

humidity Fração de água no lodo

impurity Fração de sólidos no sobrenadante

Equações

Balanço molar global (fase fluida)

$$F^{Inlet} = F^{FilterCake} + F^{Filtrate} \tag{A.330}$$

Soma das frações molares (fase fluida)

$$\sum_{i=1}^{NComp} z^{FilterCake} = \sum_{i=1}^{NComp} z^{Filtrate} \tag{A.331}$$

Balanço molar global (fase sólida)

$$F_{sol}^{Inlet} = F_{sol}^{Filtrate} + F_{sol}^{FilterCake} \tag{A.332}$$

Fração de partição dos sólidos insolúveis

$$F_{sol}^{FilterCake} = F_{sol}^{Inlet} \times frac_{insol} \tag{A.333}$$

Composição molar da corrente $Filtrate$ (fase fluida)

$$z^{Filtrate} = z^{Inlet} \tag{A.334}$$

Composição molar da corrente $FilterCake$ (fase fluida)

$$z^{FilterCake} = z^{Inlet} \tag{A.335}$$

Umidade da torta de filtro – $FilterCake$

$$z^{FilterCake}_{total\_mass}(NWater) = humidity \tag{A.336}$$

Impurezas no filtrado – $Filtrate$

$$F^{Filtrate}_{sol\_mass} = impurity \times (F^{Filtrate}_{mass} + F^{Filtrate}_{sol\_mass}) \tag{A.337}$$

Entalpia molar das correntes de saída

$$h^{Filtrate} = PP.LiquidEnthalpy(T^{Filtrate}, P^{Filtrate}, z^{Filtrate}) \tag{A.338a}$$
$$h^{FilterCake} = PP.LiquidEnthalpy(T^{FilterCake}, P^{FilterCake}, z^{FilterCake}) \tag{A.338b}$$
$$h^{Filtrate}_{sol} = PP.VapourEnthalpy(T^{Filtrate}, P^{Filtrate}, z^{Filtrate}_{sol}) \tag{A.338c}$$
$$h^{FilterCake}_{sol} = PP.VapourEnthalpy(T^{FilterCake}, P^{FilterCake}, z^{FilterCake}_{sol}) \tag{A.338d}$$

Equilíbrio térmico

$$T^{Filtrate} = T^{Inlet} \tag{A.339a}$$
$$T^{FilterCake} = T^{Inlet} \tag{A.339b}$$

Fração de vapor das correntes de saída

$$v^{Filtrate} = v^{Inlet} \tag{A.340a}$$
$$v^{FilterCake} = v^{Inlet} \tag{A.340b}$$

Equilíbrio mecânico

$$P^{Filtrate} = P^{Inlet} \tag{A.341a}$$
$$P^{FilterCake} = P^{Inlet} \tag{A.341b}$$

Se $i = NWater$ então:

$$F^{Filtrate} \times z^{Filtrate}(i) = F^{Inlet} \times z^{Inlet}(i) \times frac_{water} \tag{A.342a}$$
$$F^{FilterCake} \times z^{FilterCake}(i) = F^{Inlet} \times z^{Inlet}(i) \times (1 - frac_{water}) \tag{A.342b}$$

Senão:

$$F^{Filtrate} \times z^{Filtrate}(i) = F^{Inlet} \times z^{Inlet}(i) \times frac_{sol} \tag{A.343a}$$
$$F^{FilterCake} \times z^{FilterCake}(i) = F^{Inlet} \times z^{Inlet}(i) \times (1 - frac_{sol}) \tag{A.343b}$$

A.6.9 Tanque flash – *flash*

Modelo de um tanque flash para a corrente solidStream.

Hipóteses:

- Operação em estado estacionário;
- Sem perda de calor para o ambiente;
- As duas fases tem mistura perfeita;
- Nenhum sólido é arrastado na corrente de vapor.

Deve-se especificar:

- A corrente de entrada;
- A pressão de saída (OutletV.P);
- A temperatura de saída ou a quantidade de calor fornecida.

Parâmetros

***outer* PP** Chamada para o plugin externo *VRTherm* que calcula as propriedades físicas da fase fluida

***outer* PPS** Chamada para o plugin externo *VRTherm* que calcula as propriedades físicas da fase sólida

***outer* NComp** Número de compostos na fase fluida

***outer* NCompS** Número de compostos na fase sólida

Variáveis

in Inlet solidStream

out OutletLiquid solidStreamEq

out OutletVapour solidStreamEq

Q Calor trocado [kW]

vfrac Fração de vaporização

h Entalpia total da mistura [kJ/kmol]

$\mathbf{P_{Ratio}}$ Razão entre as pressões de entrada e de saída

ΔP Queda de pressão [kPa]

Equações

Balanço molar global (fase fluida)

$$F^{Inlet} = F^{OutletLiquid} + F^{OutletVapour} \tag{A.344}$$

Vazão de sólidos na corrente de vapor $OutletVapour$

$$F_{sol}^{OutletVapour} = 1E-6[kmol/h] \tag{A.345}$$

Vazão de sólidos na corrente de vapor $OutletLiquid$

$$F_{sol}^{OutletLiquid} = F_{sol}^{Inlet} \tag{A.346}$$

Composição das correntes de saída (fase sólida)

$$z_{sol}^{OutletVapour} = z_{sol}^{Inlet} \tag{A.347}$$

$$z_{sol}^{OutletLiquid} = z_{sol}^{Inlet} \tag{A.348}$$

Fração de vapor

$$F^{OutletVapour} = vfrac \times F^{Inlet} \tag{A.349}$$

Balanço de energia

$$F^{Inlet} \times (h - h^{Inlet}) = Q \tag{A.350}$$

Entalpia da mistura de saída

$$h = (1 - vfrac) \times h^{OutletLiquid} + vfrac \times h^{OutletVapour} \tag{A.351}$$

Equilíbrio térmico

$$T^{OutletVapour} = T^{OutletLiquid} \tag{A.352}$$

Equilíbrio mecânico

$$P^{OutletVapour} = P^{OutletLiquid} \tag{A.353}$$

Queda de pressão

$$P^{OutletLiquid} = P^{Inlet} - \Delta P \tag{A.354}$$

Razão entre as pressões

$$P^{OutletLiquid} = P^{Inlet} \times P_{Ratio} \tag{A.355}$$

Se $vfrac > 0$ e $vfrac < 1$ então: Cálculo flash

$$[vfrac, z^{OutletLiquid}, z^{OutletVapour}] = PP.Flash(T^{OutletVapour}, P^{OutletVapour}, z^{Inlet}) \tag{A.356a}$$

Equilíbrio de fases

$$[vfrac, z^{OutletLiquid}, z^{OutletVapour}] = PP.FlashPH(P^{OutletVapour}, h, z^{Inlet}) \tag{A.356b}$$

A.6.10 Tanque flash para a corrente de água – *flashW*

Modelo de um tanque flash para a corrente waterStream.

Hipóteses:

- Operação em estado estacionário;
- Sem perda de calor para o ambiente;
- As duas fases tem mistura perfeita;
- Nenhum sólido é arrastado na corrente de vapor.

Deve-se especificar:

- A corrente de entrada;
- A pressão de saída (OutletV.P);
- A temperatura de saída ou a quantidade de calor fornecida.

Parâmetros

propterm *Plug-in* que calcula as propriedades físicas da água pura

Variáveis

in Fin waterStream

out FoutV waterStream

out FoutL waterStream

Q Calor trocado no flash [kW]

v Fração de vaporização no flash

P Pressão no flash [atm]

T Temperatura no flash [K]

Hl Entalpia mássica de saturação da água líquida na pressão de operação [kJ/kg]

Hv Entalpia mássica de saturação do vapor de água na pressão de operação [kJ/kg]

Hl Entropia mássica de saturação da água líquida na pressão de operação [kJ/kg/K]

Hv Entropia mássica de saturação do vapor de água na pressão de operação [kJ/kg/K]

Equações

Balanço de massa global

$$F^{Fin} = F^{FoutV} + F^{FoutL} \tag{A.357}$$

Balanço de energia

$$F^{Fin} \times H^{Fin} + Q = F^{FoutV} \times H^{FoutV} + F^{FoutL} \times H^{FoutL} \tag{A.358}$$

Equilíbrio mecânico

$$P^{FoutV} = P \tag{A.359a}$$
$$P^{FoutL} = P \tag{A.359b}$$

Equilíbrio térmico

$$T^{FoutV} = T \tag{A.360a}$$
$$T^{FoutL} = T \tag{A.360b}$$

Fração de vaporização

$$F^{FoutV} = v \times F^{Fin} \tag{A.361}$$

Entropia e entalpia mássicas do vapor saturado na pressão de operação

$$[Sv, Hv] = propterm.PTv(P, T) \tag{A.362}$$

Entropia e entalpia mássicas da água líquida saturada na pressão de operação

$$[Sl, Hl] = propterm.PTl(P, T) \tag{A.363}$$

Fração de vapor das correntes de saída

$$v^{FoutL} = 0 \tag{A.364a}$$
$$v^{FoutV} = 1 \tag{A.364b}$$

Entropia e entalpia mássicas da corrente $FoutV$

$$[S^{FoutV}, H^{FoutV}] = propterm.PTv(P, T) \tag{A.365}$$

Entropia e entalpia mássicas da corrente $FoutL$

$$[S^{FoutL}, H^{FoutL}] = propterm.PTl(P, T) \tag{A.366}$$

Temperatura de saturação

$$T = propterm.Tsat(P) \tag{A.367}$$

A.6.11 Moenda – *mill*

Modelo simplificado de uma moenda com a potência de acionamento calculada baseada na quantidade de fibra na entrada.

Hipóteses:

- Operação em estado estacionário;
- Sem perda de calor para o ambiente.

Deve-se especificar:

- A corrente de entrada de cana-de-açúcar;
- A corrente de entrada de água, exceto a vazão;
- A proporção entre as vazões das duas correntes de entrada;
- A umidade de saída do bagaço;

- A fração de impurezas sólidas (insolúveis) no caldo;
- A demanda específica de potência (por tonelada de fibra).

Deve-se definir os seguintes parâmetros:

- A posição do componente "água", "celulose", "hemicelulose" e "lignina" no vetor de componentes;
- Os compostos que participam no cálculo do Brix, pelo parâmetro *Brix(NComp)* (1 se participa e 0 se não participa).

Parâmetros

***outer* PP** Chamada para o plugin externo *VRTherm* que calcula as propriedades físicas da fase fluida

***outer* PPS** Chamada para o plugin externo *VRTherm* que calcula as propriedades físicas da fase sólida

***outer* NComp** Número de compostos na fase fluida

***outer* NCompS** Número de compostos na fase sólida

M(NComp) Vetor de tamanho "NComp" contendo os pesos moleculares dos compostos da fase fluida [kg/kmol]

MS(NCompS) Vetor de tamanho "NCompS" contendo os pesos moleculares dos compostos da fase sólida [kg/kmol]

Brix(NComp) Indica se o componente *i* participa do cálculo do Brix da corrente (1 - se participa, 0 - se não participa)

NWater Posição do componente "água" no vetor de componentes

NCell Posição do componente "Celulose" no vetor de componentes

NHemi Posição do componente "Hemicelulose" no vetor de componentes

NLignin Posição do componente "Lignina" no vetor de componentes

Variáveis

in Cane solidStream

in Water solidStream

out MixedJuice solidStreamEq

out Bagasse solidStreamEq

$frac_{sol}$ Eficiência de separação para a fase sólida

humidity Fração de água no bagaço

impurity Fração de sólidos no caldo misto

Duty Potência da moenda por tonelada de fibra [kW*h/t]

Work Potência total da moenda [kW]

WFPTC Tonelada de água por tonelada de fibra

Fiber Fração de fibras na entrada

$Outlet_{Brix}$ Sólidos solúveis totais na corrente de caldo misto

Extract Fração de açúcares extraído

Equações

Tonelada de água por tonelada de cana-de-açúcar

$$F_{mass}^{Water} = F_{total\_mass}^{Cane} \times Fiber \times WFPTC \tag{A.368}$$

Balanço molar global (fase fluida)

$$F^{Cane} + F^{Water} = F^{MixedJuice} + F^{Bagasse} \tag{A.369}$$

Soma das frações molares (fase fluida)

$$\sum_{i=1}^{NComp} z^{MixedJuice} = \sum_{i=1}^{NComp} z^{Bagasse} \tag{A.370}$$

Balanço molar global (fase sólida)

$$F_{sol}^{Cane} + F_{sol}^{Water} = F_{sol}^{Juice} + F_{sol}^{Bagasse} \tag{A.371}$$

Soma das frações molares (fase sólida)

$$\sum_{i=1}^{NComp} z_{sol}^{MixedJuice} = \sum_{i=1}^{NComp} z_{sol}^{Bagasse} \tag{A.372}$$

Balanço molar por componente (fase sólida)

$$F_{sol}^{MixedJuice} \times z_{sol}^{MixedJuice} = (F_{sol}^{Cane} \times z_{sol}^{Cane} + F_{sol}^{Water} \times z_{sol}^{Water}) \times (1 - frac_{sol}) \tag{A.373}$$

$$F_{sol}^{Bagasse} \times z_{sol}^{Bagasse} = (F_{sol}^{Cane} \times z_{sol}^{Cane} + F_{sol}^{Water} \times z_{sol}^{Water}) \times frac_{sol} \tag{A.374}$$

Impurezas no caldo misto – $MixedJuice$

$$F_{sol\_mass}^{MixedJuice} = impurity \times F_{total\_mass}^{MixedJuice} \tag{A.375}$$

Sólidos solúveis totais na corrente $MixedJuice$

$$Outlet_{Brix} = \sum_{i=1}^{NComp} z_{mass}^{MixedJuice} \times Brix \tag{A.376}$$

Balanço de energia

$$\begin{aligned} &F^{Bagasse} \times h^{Bagasse} + F_{sol}^{Bagasse} \times h_{sol}^{Bagasse} + F^{MixedJuice} \times h^{MixedJuice} \\ &+ F_{sol}^{MixedJuice} \times h_{sol}^{MixedJuice} = F^{Cane} \times h^{Cane} + F_{sol}^{Cane} \times h_{sol}^{Cane} \\ &+ F^{Water} \times h^{Water} + F_{sol}^{Water} \times h_{sol}^{Water} \end{aligned} \tag{A.377}$$

Equilíbrio térmico

$$T^{MixedJuice} = T^{Bagasse} \tag{A.378}$$

Equilíbrio mecânico

$$P^{MixedJuice} = P^{Cane} \tag{A.379}$$

$$P^{Bagasse} = P^{Cane} \tag{A.380}$$

Cálculo da fração de fibras

$$\begin{aligned} Fiber &= z_{total\_mass}^{Cane}(NComp + NCell) + z_{total\_mass}^{Cane}(NComp + NHemi) \\ &+ z_{total\_mass}^{Cane}(NComp + NLignin) \end{aligned} \tag{A.381}$$

Cálculo da demanda de potência

$$Work = F_{total\_mass}^{Cane} \times Duty \times Fiber \tag{A.382}$$

Se $i = NWater$ então:

Umidade do bagaço

$$z_{total\_mass}^{Bagasse}(i) = humidity \tag{A.383a}$$

Balanço molar por componente (fase fluida)

$$F^{Juice} \times z^{Juice}(i) + F^{Bagasse} \times z^{Bagasse}(i) = F^{Cane} \times z^{Cane}(i) + F^{Water} \times z^{Water}(i) \quad \text{(A.383b)}$$

Senão:

Balanço molar por componente (fase fluida)

$$F^{Juice} \times z^{Juice}(i) + F^{Bagasse} \times z^{Bagasse}(i) = F^{Cane} \times z^{Cane}(i) + F^{Water} \times z^{Water}(i) \quad \text{(A.384a)}$$

$$F^{Bagasse} \times z^{Bagasse}(i) = F^{Cane} \times z^{Cane}(i) \times (1 - Extract) \quad \text{(A.384b)}$$

A.6.12 Peneira – *sieve*

Modelo de uma peneira com correntes de filtrado e torta de filtro.

Hipóteses:

- Operação em estado estacionário;
- Sem perda de calor para o ambiente.

Deve-se especificar:

- A corrente de entrada;
- A fração de separação das fases fluida e sólida.

Parâmetros

NWater Posição do componente "água" no vetor de componentes

Parâmetros

NWater Posição do componente "água" no vetor de componentes

Variáveis

in Inlet solidStream

out FilterCake solidStream

out Filtrate solidStream

$\mathbf{frac_{sol}}$ Eficiência de separação para a fase sólida

$\mathbf{frac_{liq}}$ Eficiência de separação para a fase líquida

humidity Fração de água no lodo

impurity Fração de sólidos no sobrenadante

Equações

Balanço molar global (fase fluida)

$$F^{Inlet} = F^{FilterCake} + F^{Filtrate} \tag{A.385}$$

Fração de partição (fase fluida)

$$F^{Filtrate} = F^{Inlet} \times frac_{liq} \tag{A.386}$$

Composição molar da corrente $Filtrate$ (fase fluida)

$$z^{Filtrate} = z^{Inlet} \tag{A.387}$$

Composição molar da corrente $FilterCake$ (fase fluida)

$$z^{FilterCake} = z^{Inlet} \tag{A.388}$$

Balanço molar global (fase sólida)

$$F_{sol}^{Inlet} = F_{sol}^{Filtrate} + F_{sol}^{FilterCake} \tag{A.389}$$

Fração de partição (fase sólida)

$$F_{sol}^{FilterCake} = F_{sol}^{Inlet} \times frac_{sol} \tag{A.390}$$

Composição molar da corrente $Filtrate$ (fase sólida)

$$z_{sol}^{Filtrate} = z_{sol}^{Inlet} \tag{A.391}$$

Composição molar da corrente $FilterCake$ (fase sólida)

$$z_{sol}^{FilterCake} = z_{sol}^{Inlet} \tag{A.392}$$

Umidade do lodo – $FilterCake$

$$z_{total\_mass}^{FilterCake}(NWater) = humidity \tag{A.393}$$

Impurezas no clarificado – $Filtrate$

$$F_{sol\_mass}^{Filtrate} = impurity \times (F_{mass}^{Filtrate} + F_{sol\_mass}^{Filtrate}) \tag{A.394}$$

Entalpia molar das correntes de saída

$$h^{Filtrate} = h^{Inlet} \tag{A.395a}$$
$$h^{FilterCake} = h^{Inlet} \tag{A.395b}$$
$$h_{sol}^{Filtrate} = h_{sol}^{Inlet} \tag{A.395c}$$
$$h_{sol}^{FilterCake} = h_{sol}^{Inlet} \tag{A.395d}$$

Equilíbrio térmico

$$T^{Filtrate} = T^{Inlet} \tag{A.396a}$$
$$T^{FilterCake} = T^{Inlet} \tag{A.396b}$$

Fração de vapor das correntes de saída

$$v^{Filtrate} = v^{Inlet} \tag{A.397a}$$
$$v^{FilterCake} = v^{Inlet} \tag{A.397b}$$

Equilíbrio mecânico

$$P^{Filtrate} = P^{Inlet} \tag{A.398a}$$
$$P^{FilterCake} = P^{Inlet} \tag{A.398b}$$

A.7 *Plug-ins*

A.7.1 Interpolador

O *plug-in* do interpolador possui somente um método, chamado *interpola*. Porém, o número de argumentos que esse método aceita (e retorna) é variável. Esse número é dado pelo arquivo de texto contendo a tabela de inspeção contendo os dados a serem interpolados. Assim, na declaração do plugin, deve-se especificar o endereço para esse arquivo de texto, como no exemplo abaixo:

(No ambiente "*PARAMETERS*" do EMSO)
Int as Plugin (Type = "*nome com que o plugin foi adicionado no EMSO*", file = "*endereço (relativo ou absoluto) para o arquivo de texto da tabela de inspeção*");

O arquivo de texto deve conter as seguintes informações, na ordem descrita:

Nofinputs: <*número de argumentos a serem especificados pelo usuário*>
Lowerbounds: <*limite inferior para os argumentos de entrada, separados por espaço*>

Increments: <*distância entre os pontos da malha, separados por espaço*>
Nofpoints: <*número de pontos em cada dimensão da malha, separados por espaço*>
InputUnits: <*unidades dos argumentos de entrada, separados por espaço*>
Nofoutputs: <*número de argumentos de retorno*>
OutputUnits: <*unidades dos argumentos de retorno, separados por espaço*>
Output: <*dados utilizados para a interpolação*>

Sobre a organização dos dados utilizados para a interpolação, estes devem conter somente os argumentos de retorno em cada ponto. A ordenação dos dados segue a sequência (x - argumentos de entrada, y - argumentos de saída):

$$
\begin{array}{cccccccc}
x_1 & x_2 & \cdots & x_n & y_{1,1} & y_{1,2} & \cdots & y_{1,m} \\
x_1 & x_2 & \cdots & x_n + \Delta x_n & y_{2,1} & y_{2,2} & \cdots & y_{2,m} \\
x_1 & x_2 & \cdots & x_n + 2 \times \Delta x_n & y_{3,1} & y_{3,2} & \cdots & y_{3,m} \\
\vdots & \ddots & & \vdots & \vdots & \vdots & \ddots & \vdots \\
x_1 & \cdots & x_{n-1} + \Delta x_{n-1} & x_n & y_{d_{n+1},1} & y_{d_{n+1},2} & \cdots & y_{d_{n+1},m} \\
\vdots & & \vdots & \vdots & \vdots & \vdots & \ddots & \vdots \\
x_1 + d_1 \times \Delta x_1 & x_2 + d_2 \times \Delta x_2 & \cdots & x_n + d_n \times \Delta x_n & y_{\prod_{i=1}^{n} d_i,1} & y_{\prod_{i=1}^{n} d_i,2} & \cdots & y_{\prod_{i=1}^{n} d_i,m}
\end{array}
$$

A.7.2 *Propterm*

Esse *plug-in* implementa as funções apresentadas na tabela 1.

A.7.3 Pacote de propriedades termodinâmicas – *VRTherm*

Métodos

As Tabelas 2, 3 e 4 foram adaptadas das tabelas apresentadas no manual do pacote *VRTherm*, disponível em: http://www.enq.ufrgs.br/alsoc/download/emso/docs/EMSOQuickRefTherm.pdf

Tabela 1 – Métodos implementados pelo plugin *propterm* para o cálculo das propriedades da água pura.

Nome da função	Descrição	Argumentos
propPTv	Retorna a entalpia e a entropia específicas mássicas do vapor de água na pressão e temperatura especificados	P, T
propPTl	Retorna a entalpia e a entropia específicas mássicas da água líquida na pressão e temperatura especificados	P, T
Tsat	Retorna a temperatura de saturação na pressão especificada	P
propPH	Retorna a entropia específica mássica e a temperatura água na pressão e com a entalpia específica mássica especificados	P, H
propPS	Retorna a entalpia específicas mássicas e a temperatura da água na pressão e entropia específica mássica especificadas	P, S

Tabela 2 – Métodos para cálculo de propriedades para componentes puros

Nome da função	Descrição	Argumentos
NormalBoilingPoint	Ponto de ebulição normal	-
VapourPressure	Pressão de vapor	T
CriticalTemperature	Temperatura crítica	-
CriticalPressure	Pressão crítica	-
CriticalVolume	Volume crítico	-
NormalFreezingPoint	Ponto de fusão normal	-
MolecularWeight	Peso molecular	-

Tabela 3 – Cálculos *Flash*

Nome da função	Descrição	Argumentos	Retorna
VapourFraction	Fração de vapor	T, P, z	v_{frac}
Flash	Cálculo flash a T e P	T, P, z	v_{frac}, z_l, z_v
FlashPH	Cálculo flash a P e H	P, h, z	v_{frac}, x, y

Tabela 4 – Métodos para cálculo de propriedades para componentes puros

Nome da função	**Descrição**	**Argumentos**
NumberOfComponents	Número de componentes	-
LiquidCpCv	C_p/C_v da fase líquida	T, P, z_l
VapourCpCv	C_p/C_v da fase vapor	T, P, z_v
LiquidCp	C_p da fase líquida	T, P, z_l
VapourCp	C_p da fase vapor	T, P, z_v
LiquidCv	C_v da fase líquida	T, P, z_l
VapourCv	C_v da fase vapor	T, P, z_v
LiquidCompressibilityFactor	Fator de compressibilidade do líquido	T, P, z_l
VapourCompressibilityFactor	Fator de compressibilidade do líquido	T, P, z_l
LiquidEnthalpy	Entalpia do líquido	T, P, z_l
VapourEnthalpy	Entalpia do vapor	T, P, z_v
LiquidEntropy	Entropia do líquido	T, P, z_l
VapourEntropy	Entropia do vapor	T, P, z_v
LiquidGibbsFreeEnergy	Energia livre de Gibbs do líquido	T, P, z_l
VapourGibbsFreeEnergy	Energia livre de Gibbs do vapor	T, P, z_v
LiquidVolume	Volume do líquido	T, P, z_l
VapourVolume	Volume do vapor	T, P, z_v
LiquidDensity	Densidade do líquido	T, P, z_l
VapourDensity	Densidade do vapor	T, P, z_v
LiquidThermalConductivity	Condutividade térmica do líquido	T, P, z_l
VapourThermalConductivity	Condutividade térmica do vapor	T, P, z_v
LiquidViscosity	Viscosidade do líquido	T, P, z_l
VapourViscosity	Viscosidade do vapor	T, P, z_v
LiquidFugacityCoefficient	Coeficiente de fugacidade do líquido	T, P, z_l
VapourFugacityCoefficient	Coeficiente de fugacidade do vapor	T, P, z_v

ANEXO A – Otimização do processo de produção de etanol 2G

O artigo intitulado *Assessing the production of first and second generation bioethanol from sugarcane through the integration of global optimization and process detailed modeling*, publicado no periódico *Computers and Chemical Engineering* (v. 43, p. 1–9, 2012) foi produzido durante o mestrado utilizando o interpolador multilinear para aproximar o trem de colunas de destilação para produção de etanol hidratado.

Computers and Chemical Engineering 43 (2012) 1–9

Contents lists available at SciVerse ScienceDirect

Computers and Chemical Engineering

journal homepage: www.elsevier.com/locate/compchemeng

Assessing the production of first and second generation bioethanol from sugarcane through the integration of global optimization and process detailed modeling

Felipe Fernando Furlan[a], Caliane Bastos Borba Costa[a], Gabriel de Castro Fonseca[a], Rafael de Pelegrini Soares[b], Argimiro Resende Secchi[c], Antonio José Gonçalves da Cruz[a], Roberto de Campos Giordano[a,*]

[a] Department of Chemical Engineering, Federal University of São Carlos, UFSCar, Via Washington Luiz, km 235, São Carlos, São Paulo 13565-905, Brazil
[b] Department of Chemical Engineering, Federal University of Rio Grande do Sul, Brazil
[c] Chemical Engineering Program, COPPE, Federal University of Rio de Janeiro, Brazil

ARTICLE INFO

Article history:
Received 1 September 2011
Received in revised form 28 March 2012
Accepted 4 April 2012
Available online xxx

Keywords:
Sugarcane bioethanol
Global optimization
Equation based simulator
Energy integration
Biorefinery
Lignocellulosic feedstock

ABSTRACT

There is a worldwide effort to make economically feasible the use of lignocellulosic biomass for production of biofuels. In sugarcane industry, cane juice (sucrose) is fermented for bioethanol production. Sugarcane bagasse is used as fuel in cogeneration systems, to produce steam and electric power to the plant, and the surplus of electric power may be delivered to the grid. The hydrolysis of bagasse to produce second generation ethanol poses a challenge: how much bagasse can be diverted, since the process must continue energetically self-sufficient. This work presents a computational tool developed within an equation-oriented process simulator that couples the simulation of first and second generation bioethanol production with a global optimization algorithm. The tool was robust, optimizing the steady state process in any economic scenario and for different process configurations. Four case studies are presented, and their implications on process internal demands and on the surplus electrical power are discussed.

1. Introduction

Engineering research has dedicated great efforts recently to enable a more sustainable, less oil/fossil-based energetic matrix to humankind. Amongst several alternatives, lignocellulosic biomass-based fuels are a promising one. Biofuels have the advantage of the availability of their renewable feedstock, thus assisting the development of a sustainable industrial society. They contribute for the energetic independence of societies and decrease greenhouse gas emissions (Cherubini & Stromman, 2010; FitzPatrick, Champagne, Cunningham, & Whitney, 2010; Lynd, Wyman, & Gerngross, 1999; Ng, 2010). Besides these benefits, biomass-based energy generation can use agricultural residues, thus avoiding competition with food crops.

Ethanol is expected to be one of the most important renewable liquid biofuels within the next couple of decades (Hahn-Hagerdal, Galbe, Gorwa-Grauslund, Liden, & Zacchi, 2006) and is one of the keystones of the future biobased chemical industry (Kamm & Kamm, 2007). Nowadays, ethanol is produced in large scale from sucrose or starch in some countries. Nevertheless, the world production capacity of this fuel can increase considerably by using lignocellulosic material as feedstock for second generation ethanol. Besides, in the case of sugarcane, the use of bagasse (a lignocellulosic residue) for bioethanol production may contribute for the increase of the ratio biofuel/land area, thus indirectly reducing the land demand for crop fuels. The world effort to turn second generation bioethanol economically viable has been intense during the last decade. The biochemical route, based on the enzymatic hydrolysis of biomass followed by fermentation of hexoses (and maybe also pentoses) is one of the promising alternatives. Currently, many groups are researching biomass pretreatment, hydrolysis and fermentation of the resulting sugars. The sources of biomass that are considered is diversified: wood, wheat or rice straw, sugarcane bagasse, corn stover and vegetative grasses are some examples (Demirbas, 2009).

The carbohydrate portion of lignocellulosic material is comprised by cellulose ($(C_6H_{10}O_5)_n$), a homopolymer of β-linked glucose which has cellobiose as its constitutive unit; and by hemicellulose ($(C_5H_8O_4)_n$), a heteropolymer containing mainly the pentoses xylose and arabinose. Cellulose may present in a highly ordered crystalline structure with amorphous fragments in

* Corresponding author. Tel.: +55 16 3351 8708; fax: +55 16 3351 8266.
E-mail address: roberto@ufscar.br (R.d.C. Giordano).

0098-1354/$ – see front matter © 2012 Elsevier Ltd. All rights reserved.
http://dx.doi.org/10.1016/j.compchemeng.2012.04.002

Nomenclature

Variables

c_1, c_2	cognitive and social acceleration factors, respectively
F_i	mass flow of stream i
$gbest_g$	the overall best position out of all the particles in the population
Glucose	total amount of glucose (including glucose produced by sucrose hydrolysis) inside the fermenter
m	number of decision variables for the optimization problem
M_i	molar mass of component i
n	number of particles in the swarm
$pbest_{j,g}$	gth component of the best fitness of particle j
r_1, r_2	random numbers uniformly distributed in the range [0, 1]
$v_{j,g}^{(k)}$	gth component of the velocity of particle j at iteration k
w	inertia weight factor
$x_{j,g}^{(k)}$	gth component of the position of particle j at iteration k
$yield_i$	stoichiometric yield of reaction i
z_i^j	mass fraction of component j in stream i
$\$_i$	market price for product of raw material i

Greek letters

Φ	objective function for the optimization problem
$\Phi_{\min}$	minimum value for the objective function
$\Phi_{\max}$	maximum value for the objective function

between, while hemicellulose is a relatively amorphous component that is easier to break down with chemicals and/or heat. The non-carbohydrate part of the lignocellulosic biomass is mainly lignin ($C_9H_{10}O_2(OCH_3)_n$), a complex aromatic heteropolymer that completes the rigid structure of plants and trees cell walls. In minor contents, lignocellulosic biomass also contains inorganics, as silica, potassium and sodium, and soluble substances, named extractives (Cherubini & Stromman, 2010; Lynd et al., 1999).

One of the major obstacles for the cost-effective exploitation of cellulosic biomass is its recalcitrance. The thermochemical route tries to circumvent this problem via gasification of the solid biomass, but several technological challenges still remain – for instance, cleaning the off gas before it gets in contact with Fisher–Tropsch catalysts. The biochemical route, on its turn, requires pretreatment processes, which make cellulose fibers accessible to be hydrolyzed into its glucose monomers. Strong acid hydrolysis might be an alternative, but it generates byproducts that are toxic for the fermentative microorganisms, and detoxification may be a costly process.

Lynd and co-workers stressed a decade ago that coproduction of multiple products in a biorefinery would be essential for economic viability of the exploitation of a biomass-based matrix (Lynd et al., 1999). A biorefinery is a facility that integrates biomass conversion technologies to produce a variety of goods, such as fuels, power and chemicals (Demirbas, 2009). Biomass composition is more heterogeneous than petroleum's, due to the difference between possible feedstocks. This fact poses a technological challenge. Hahn-Hagerdal et al. (2006) enumerated features that biomass processing technologies must exhibit in order to turn second generation ethanol industrially viable: efficient hydrolysis and fermentation of hexoses and pentoses, advanced process integration, and cost-efficient use of lignin. Furthermore, the optimization of the integrated process is mandatory for implementation of biomass conversion (Lyko, Deerberg, & Weidner, 2009).

The literature describes developments on biorefineries modeling and simulation for different feedstocks. Huang, Lin, Ramaswamy, and Tschirner (2009) simulated a forest biorefinery integrated to pulp and paper production and concluded that an pre-existing infrastructure is an important factor for the biorefinery feasibility. Several authors (Arifeen, Wang, Kookos, Webb, & Koutinas, 2007a; Arifeen, Kookos, Wang, Koutinas, & Webb, 2009, Sadhukhan et al., 2008) considered the use of wheat to produce ethanol and other by-products such as gluten, arabinoxylan and bran-rich pearling. These authors stressed the importance of commercializing added-value by-products in order to decrease ethanol production costs and achieve viable commercial operation. Grisi, Yusta, and Khodr (2011) presented a linear model of a biorefinery using sugarcane and sugarcane bagasse as feedstock. The authors considered several economical conditions representing the Brazilian market and the results showed that ethanol and sugar production were economically more important than biogas and electric energy production for the scenario considered. Dias et al. (2011) compared the economical viability of electric energy and second generation ethanol for the case of industrial plants using sugarcane as raw material. With the available technology, electric energy generation obtained gave the best results, while second generation ethanol could compete with the first when sugarcane trash is used, and technologies yet to be developed to increase the yields are applied. An economic study of the production of second generation ethanol from sugarcane, sugarcane bagasse and trash was performed by Dias et al. (2012). The authors compared the stand-alone second generation ethanol production with the first generation and the integrated first and second generation. The main result showed that the integrated process presented several advantages over the stand-alone process, including larger ethanol production, best economical results and best environmental indicators. The authors also concluded that energy and mass integration plays an important role in the economical advantage of the former over the last.

On the field of process design and optimization, several authors presented different tools and approaches for the biorefinery problem. Arifeen, Wang, Kookos, Webb, and Koutinas (2007b) presented a continuous process integrating the liquefaction and saccharification of wheat in a single step as a cost-optimized process for ethanol feedstock production. The exergetic analysis of the second generation ethanol production, considering different pretreatments, was performed by Ojeda, Avila, Suarez, and Kafarov (2011). The exergy analysis showed a negative net value for all cases, indicating the need for subsequent studies regarding thermal integration for the pretreatments considered. The thermal integration of a sugarcane and sugarcane bagasse biorefinery was performed by Dias et al. (2009), which considered the sugarcane trash and lignin replacing bagasse as boiler fuel. The use of multi-pressure distillation columns besides the thermal integration was reported as responsible for a great increase of bagasse surplus. Alvarado-Morales et al. (2010) presented a set o tools for process and control design. The tools were applied to the bioethanol production and were able to find more controllable and less sensitive conditions for the ethanol production reactor, using integrated process design and control (IPDC). The process-group contribution tool (PGC) was used to generate a set of feasible solutions for the ethanol purification and chose the most promising one for further analysis. Several different process flowsheets for bioethanol production from lignocellulosic materials were proposed by Morales-Rodriguez, Mayer, Gernaey, and Sin (2011). The authors used a benchmark criteria considering ethanol yield, ethanol concentration and number of unit operations to choose between fed-batch/continuous operation, separated hydrolysis and fermentation (SHF)/simultaneous

saccharification and co-fermentation (SSCF) and recycles/no recycle. SSCF with recycle of the reactor effluent had the best productivity among the proposed configurations.

Since many technologies for biomass processing are available, many combinations of them are, at first sight, possible. Nevertheless, process viability must be assessed, which includes not solely optimization of process conditions (in order to increase conversions and efficiencies), but also energetic integration of the process, in order to improve economics. In this way, the availability of an integrated tool that makes use of process systems engineering in order to optimize process and to indicate process viability is essential in the analysis of alternatives and in decision making.

In this work, the concept of biorefinery is applied to sugarcane biomass (bagasse and juice) in order to produce biofuel (first and second generation bioethanol), steam, electric power, and possibly valued residues (like yeast and surplus bagasse). The paper main contribution is on developing a tool that joins global optimization with the detailed modeling of the whole integrated biorefinery, in order to evaluate process demands and indicate optimal process configurations. The optimal configuration can be defined with the most suitable metric to the user: it can be translated in terms of profitability of the process configuration, techno-economic or environmental metrics. Impacts on the demands and economics of the process caused by changes in process parameters, in the prices of raw material and/or market prices of products can be easily evaluated. An important application of process engineering involves the decision of the amount of bagasse that should be diverted from steam/electric energy to second generation bioethanol production, depending on the prevailing economical scenario. Within the tool, Particle Swarm (Kennedy & Eberhart, 1995) is the optimization algorithm used and EMSO (Environment for Modeling Simulation and Optimization) software (Soares & Secchi, 2003) is the platform for the whole process modeling, simulation and optimization.

2. Biorefinery

The biorefinery put forth here makes use of the infrastructure already established for first generation sugarcane industry in Brazil. The fundamental processing steps for first generation bioethanol production from sugarcane are well-known and were described in details by Dias et al. (2010). The biorefinery was modeled for a sugarcane input of 500 metric ton of cane (TC) per hour, whose composition is presented in Table 1. The composition of dry sugarcane bagasse is considered to be 39% in mass of cellulose, 37% of hemicelluloses, 21% of lignin and 3% of ash. The most important data for first generation ethanol production is presented in Table 2.

Table 1
Sugarcane composition used in the biorefinery.

Component	wt%
Dirt	0.60
Glucose	0.62
Cellulose	4.77
Lignin	2.62
Hemicellulose	4.53
K_2O	0.20
Aconitic acid	1.79
Sucrose	13.30
Water	71.57

Table 2
Operational conditions for the modeled biorefinery.

Variable	Value	Unit
Sugarcane crushing rate	500	TC/h
Sugarcane sugars content	13.92	wt%
Dirt removal after sugarcane cleaning	70	%
Sugar losses after sugarcane cleaning	0.5	%
Sugar recovery in the mills	97.5	%
Sugarcane bagasse water content	50.0	wt%
Glucose fermentation yield	90.0	%
Distillation column plate efficiency	0.72	

The models involved in the biorefinery were mostly stoichiometric, except when a rigorous model was essential. That was the case of the train of multiple effect evaporators, responsible for the concentration of sugars both from sugarcane juice and from the hydrolysis of cellulose (glucose solution). This process has an important influence on the thermal demand of the biorefinery and is strongly affected by the amount of bagasse diverted to production of second generation ethanol. Appendix 1 shows stoichiometric and mass balance equations for the main steps of the biorefinery.

In a solely first generation sugarcane biorefinery, bagasse is burnt, producing steam and electric power. However, for the integrated first and second generation bioethanol production, part of bagasse is diverted to second generation ethanol production, and must undergo pretreatment, hydrolysis of carbohydrates polymers (cellulose and/or hemicelluloses) and fermentation of the resulting sugars. Pretreatment steps and considered yields are based on the work of Wolf (2011). A block diagram of the considered second generation process is presented in Fig. 1. Initially, the diverted

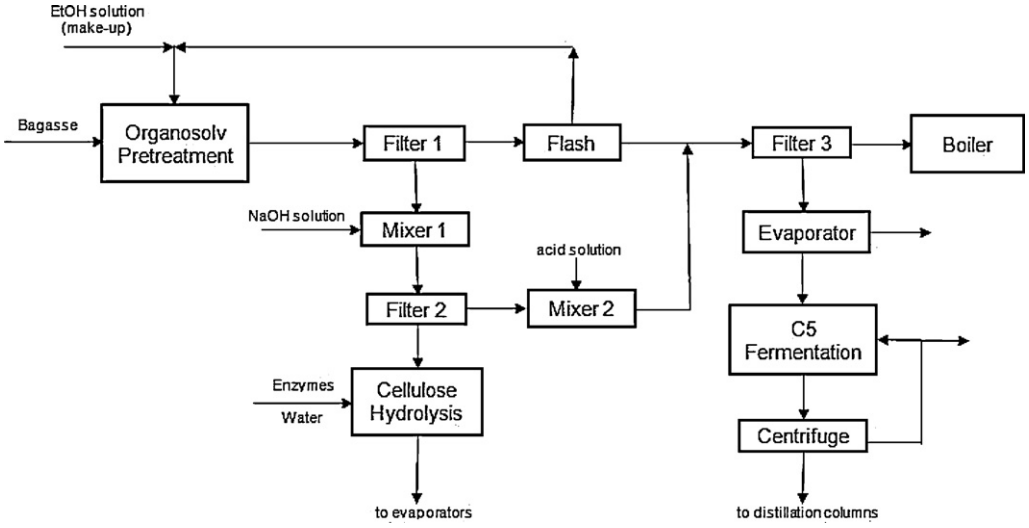

Fig. 1. Block diagram for the second generation part of the biorefinery.

sugarcane bagasse is pretreated using the organosolv process (using a 50 wt% aqueous ethanol solution), followed by filtration (in Filter 1), responsible for separating the cellulose-rich stream (solid) from the lignin-rich stream (liquid). The solid stream is washed with a 1 wt% NaOH aqueous solution, to remove the remaining lignin (in Filter 2), then diluted with water at the mass ratio 1:10 (cellulose/water), and finally hydrolyzed by a pool of enzymes. The resulting sugar-rich stream is then mixed with sugarcane juice and follows to the concentration step. Liquid stream that comes out from Filter 1 is rich in lignin and hemicellulose. This stream is sent to a flash tank for solvent recovery. The solvent extraction causes lignin precipitation. Liquid stream that comes out from Filter 2 is neutralized, in order to precipitate lignin, and this stream is joined to the suspension that comes out from the flash tank. Hemicellulose is then separated from lignin by another filtration step (Filter 3). Lignin is burnt in the boiler, while hemicellulose pentoses can be concentrated and fermented by *Pichia stipitis*. It is possible to choose not to consider ethanol production from the hemicellulose fraction, and, in this case, the concentration and fermentation steps just mentioned are not included into the calculations. Within the biorefinery concept, there are many options for aggregating value to the C5 fraction, besides the fermentation route (production of ethanol or xylitol). As an example, this fraction can be used in the production of xylooligomers or in the production of hydrogen. These options must be fully integrated to the current process, but this approach is not the purpose of this paper and other uses for C5 fraction were not considered for now. In this way, in the modeled biorefinery, second generation ethanol is obtained by enzymatic hydrolysis and fermentation of the resulting sugars by *Saccharomyces cerevisiae* (hexoses) and possibly *Pichia stipitis* (pentoses). Table 3 presents the main data used in the simulation of the production of second generation ethanol.

The cogeneration system is comprised by a boiler (fed with bagasse and lignin from the second generation ethanol production), a high pressure, a medium pressure and a condensing turbine. The condensing turbine allows the operation of the biorefinery as a thermoelectric power plant by decoupling the electric power generation from the thermal demand of the biorefinery. All streams of live steam condensate were re-compressed to the boiler pressure and returned to the cogeneration system with the water from the condensing turbine. Efficiencies of turbines and boiler depend on the steam flow. Relevant data for the cogeneration system are presented in Table 4.

Table 3
Specifications for second generation processes in the sugarcane biorefinery.

Variable	Value	Unit
Organosolv solid/liquid ratio	1/10	(wt/wt)
Hydrolysis solid/liquid ratio	1/10	(wt/wt)
Cellulose hydrolysis yield	80.0	%
Hemicellulose to xylose yield	20.4	%
Xylose fermentation yield	65.0	%
Organosolv temperature	170	°C
Organosolv pressure	22.15	bar
Hydrolysis temperature	50.0	°C
Enzyme/cellulose ratio	0.01	(wt/wt)
Cellulose losses after pre-treatment	13.4	%
Lignin recovery	95.5	%

Table 4
Operational conditions for the cogeneration process.

Variable	Value	Unit
Boiler outlet vapor pressure	90	bar
Boiler outlet vapor temperature	520	°C
Boiler efficiency	0.84–0.86	
High pressure turbine outlet pressure	22	bar
Medium pressure turbine outlet pressure	2.5	bar
High pressure turbine efficiency[a]	0.68–0.72	
Medium pressure turbine efficiency[a]	0.77–0.81	
Condensing turbine efficiency[a]	0.66–0.70	
Bagasse lower heating value[b]	7.52	MJ/kg
Lignin lower heating value[c]	12.20	MJ/kg

[a] For 62–100% of the nominal flow.
[b] Dias et al. (2009).
[c] Manninen (2010).

EMSO software (Environment for Modeling, Simulation and Optimization (Soares & Secchi, 2003)) was used to perform the simulations and optimizations described in this work. It solves all models equations simultaneously, since it is an equation-oriented simulator (Rodrigues, Soares, & Secchi, 2010), and not a

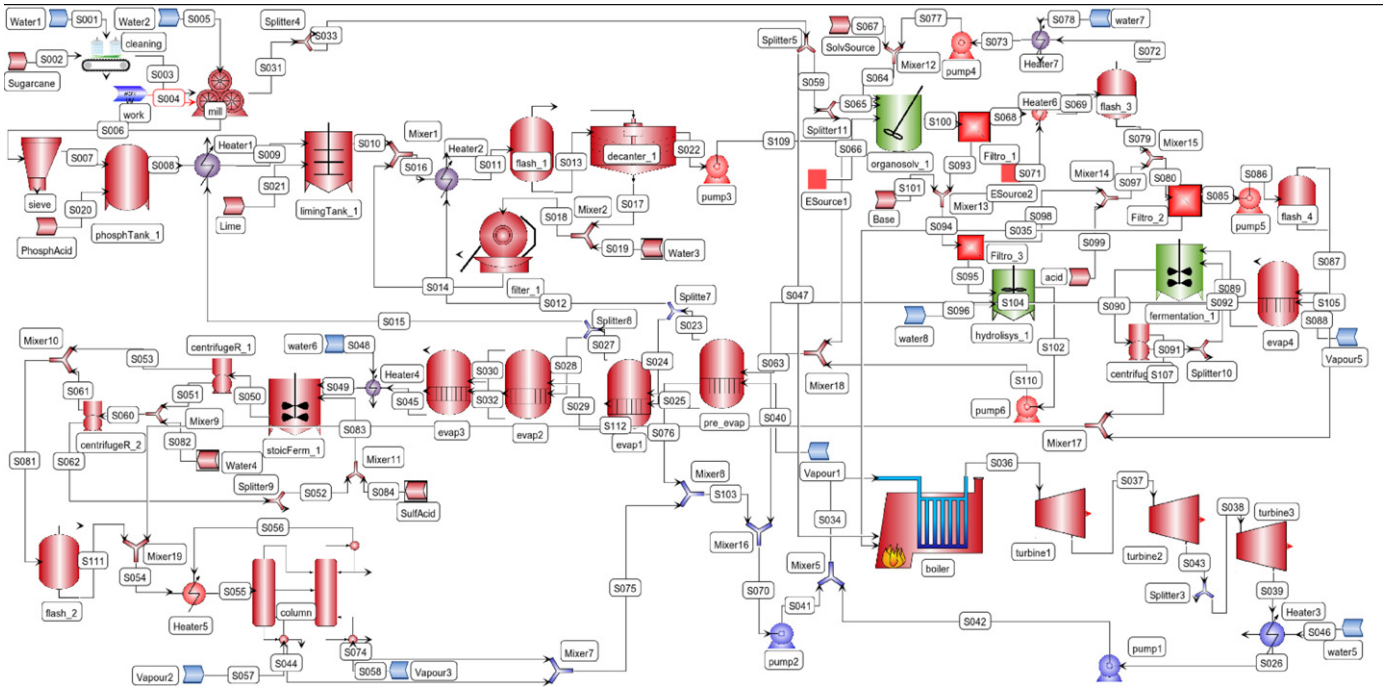

Fig. 2. Sugarcane biorefinery in EMSO software.

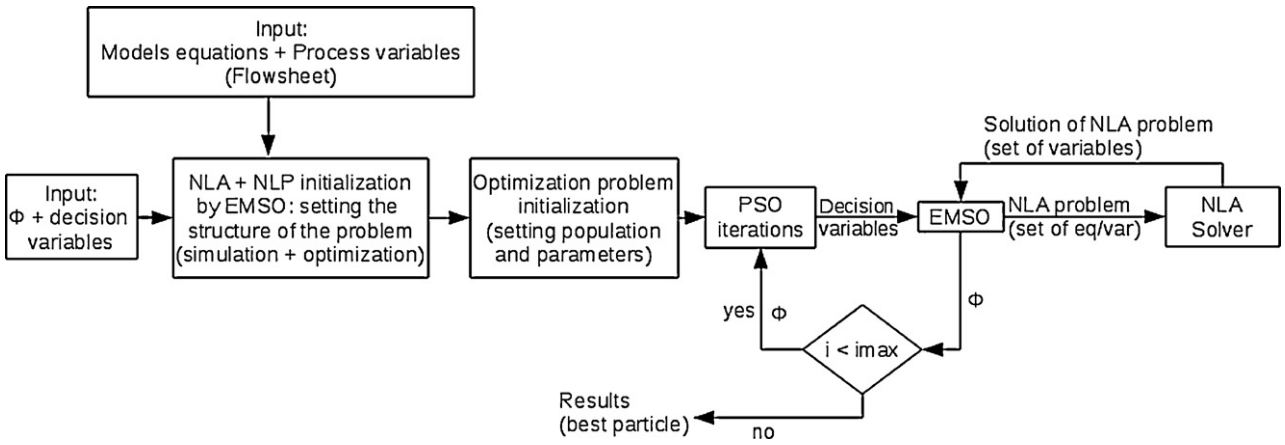

Fig. 3. EMSO + PSO integration: structure of the computational algorithm. Φ stands for the considered objective function.

modular one. The software is in continuous development by the ALSOC project (http://www.eng/ufrgs/br/alsoc) and has its own modeling language, implementing the object-oriented concepts of inheritance and composition. Inheritance makes possible to build complex models from simpler ones and the composition feature enables the creation of complex models from several other models (Soares & Secchi, 2003). All built-in models are open for user inspection and extension. The software comes with many numeric solvers for resolution of algebraic and differential-algebraic equation systems, as well as for optimization and parameter estimation problems. Users can also add their own numeric packages to the simulator, using the provided template. The simulator also supports the use of external routines, in C, C++ and FORTRAN (Rodrigues et al., 2010). Physical and thermodynamic properties of many substances, including water, are already part of the adjoining routines/packages that come with the software. The user can insert new properties whenever necessary.

Fig. 2 depicts the biorefinery entirely modeled in EMSO. The entire process is comprised of 3909 variables, 3458 equations and 451 specifications. All equations are solved simultaneously during the process simulation. The developed tool turns possible the optimization of the whole process for a fixed structure with a global optimizer, which is an important issue, considering that the modeled process is comprised of nonlinear functions. In this way, any optimization problem would be classified as a nonlinear programming (NLP) one. In optimization studies, the fraction of bagasse diverted to second generation production can be defined as a decision variable. It is important to draw attention to the fact that the fraction of bagasse diverted to second generation ethanol production is not an unconstrained variable, since it is possible that energy requirements of the plant might not be fulfilled solely by the burning of surplus bagasse. This situation is attenuated by the burn of lignin extracted from the biomass. Nevertheless, the entire process must always be self-sufficient in terms of energetic demands (constraint imposed to the decision of the maximal fraction of bagasse that can be diverted to second generation production).

The developed biorefinery is coupled in this work to the Particle Swarm Optimization (PSO) algorithm, in order to solve general optimization problems, turning possible the assessment of the integrated process under different scenarios. The next item briefly describes PSO concepts, while Section 4 analyses some results extracted from the developed tool.

3. PSO algorithm

Since the biorefinery model is comprised of nonconvex functions (e.g. the model of the evaporators), local deterministic optimization methods tend to fail in the search for the global optimal solution. Besides inherent convergence issues, local search algorithms are highly sensitive with respect to the chosen initial guess. Nondeterministic optimization methods, on the other hand, do not exhibit these disadvantages, since they do not require manipulation of the mathematical structure of the objective function and/or constraints (Mariano, Costa, Vasco de Toledo, Melo, & Maciel Filho, 2011). On the other hand, they are computationally intensive. Particle Swarm Optimization (PSO), initially proposed by Kennedy and Eberhart (1995), emulates social behavior of individuals, called particles within the algorithm. Each particle moves in the search space looking for the optimal position. The velocity of this movement is calculated according to both the experience of each particular particle and to the experience of the whole group of particles. Furthermore, particles have inertia, so as their previous velocities also influence the new velocities (Eq. (1)). Particles positions are updated at each iteration of the algorithm, according to Eq. (2) (Kennedy & Eberhart, 1995):

$$v_{j,g}^{(k+1)} = w \cdot v_{j,g}^{(k)} + c_1 \cdot r_1 \cdot \left(pbest_{j,g} - x_{j,g}^{(k)} \right) + c_2 \cdot r_2 \cdot \left(gbest_g - x_{j,g}^{(k)} \right) \quad (1)$$

$$x_{j,g}^{(k+1)} = x_{j,g}^{(k)} + v_{j,g}^{(k+1)} \quad \text{with} \quad j = 1, 2, \ldots, n \quad \text{and} \quad g = 1, 2, \ldots, m \quad (2)$$

It is noteworthy that PSO (as any other global optimization method) can only handle a limited number of variables (usually less than 100) and is not well-suited for solving problems with nonlinear equality constraints. In the present work, these deficiencies were circumvented by exposing to PSO only the decision variables. This strategy is also known as feasible path approach, as opposed to infeasible path approach (Biegler, Grossmann, & Westerberg, 1997). Only a small subset (actually, two) of the 451 model specifications were chosen as decision variables to be manipulated by the global optimization method and no equality constraints were handled directly by the algorithm. At each objective function evaluation, a very efficient non-linear algebraic (NLA) solver for sparse systems, available in EMSO, was called. Fig. 3 shows the flux of information between the main structures of the tool. A potential issue with this strategy is the convergence failure in the NLA solution. Nevertheless, the experience in this work has confirmed that PSO is very robust as long as a large objective function value is returned if there is a convergence problem with the underlying NLA or if an infeasible operating point is reached. The inequality constraints,

Table 5
Case studies considered in this work.

Case study	Process scenario
Case 1 (base case)	Production of 1st generation bioethanol only, all sugarcane bagasse is burnt, in order to produce surplus electric power to be sold.
Case 2	Production of 1st generation bioethanol only, just the sugarcane bagasse necessary to fulfill the demand of energy of the process is burnt, the remaining is sold.
Case 3	Production of 1st and 2nd generation bioethanol, but hemicellulose (C5) fraction is not used for 2nd generation fuel production; lignin is burnt.
Case 4	Production of 1st and 2nd generation bioethanol, using both hemicellulose (C5) and cellulose (C6) fractions; lignin is burnt.

on the other hand, were handled as penalizations for the objective function.

4. Results and discussion

In order to demonstrate the potential of the developed tool, four process scenarios were considered, as depicted in Table 5. PSO, with 20 particles, during 20 iterations and parameters c_1 and c_2 equal to 2.0, was used in order to find bagasse optimal partition for Cases 2–4. The inertia factor was changed linearly from 1.0 to 0.5 in order to initially provide a global search and turn it into a local one as the optimization process approaches the end, as described by Shi and Eberhart (1998). PSO particles were randomly initialized, taking into account the boundaries of the decision variables (which are fractions of the bagasse stream, thus constrained between 0 and 1).

Case 1 required no optimization and serves as the base case, standard situation. Case 2 exemplifies what happens to process demands when bagasse is burnt only in the amount required for energetic fulfill of the plant itself. This amount is found by maximizing bagasse fraction to be sold. Optimal partition of bagasse in Cases 3 and 4 are translated as the ones that maximize the objective function (Φ), which takes into account the sale prices of ethanol, electric power surplus, bagasse and yeast, and the costs of enzyme and sugarcane (Eq. (3)).

$$\begin{aligned}\Phi = {} & (\text{Ethanol Flow rate}\,(\text{kg/h}))\cdot \$_1 \\ & + (\text{Surplus of Electricity}\,(\text{MWh/h}))\cdot \$_2 + (\text{Bagasse sold}\,(\text{kg/h}))\cdot \$_3 \\ & + (\text{Yeast}\,(\text{kg/h}))\cdot \$_4 - (\text{Enzyme}\,(\text{kg/h}))\cdot \$_5 \\ & - (\text{Sugarcane}\,(\text{kg/h}))\cdot \$_6 \end{aligned} \quad (3)$$

In Eq. (3), $\$_1$, $\$_2$, $\$_3$ and $\$_4$ stand for the sale prices of, respectively, ethanol, electric energy, bagasse and yeast, while $\$_5$ and $\$_6$ represent the purchasing prices of, respectively, enzyme and sugarcane. Table 6 presents the prices used in the simulations and optimizations.

All equations involved in the simulation of the biorefinery are considered as constraints to the optimization problem, particularly

Table 6
Unit price for each product of the biorefinery.

Product or raw material	Price	Unit
Ethanol	1.50	US$/kg
Electric energy	25.00–75.00[a]	US$/MWh
Bagasse	20.00	US$/t
Yeast	100.00	US$/t
Enzyme	0.60–1.20[b]	US$/kg
Sugarcane	32.10	US$/t

[a] Cases 3 and 4, respectively.
[b] Cases 4 and 3, respectively.

Table 7
Values of decision variables for Cases 2, 3 and 4.

Case study	Splitter1	Splitter2
Case 2	0.70	0.00
Case 3	0.73	1.00
Case 4	0.89	1.00

the steam demand for production of first and second generation ethanol. This steam has to be provided by the burning of bagasse and lignin in the boiler.

Fig. 4 depicts the decision variables that PSO manipulates in order to optimize Eq. (3). The first decision variable is named "Splitter1" and represents the fraction of sugarcane bagasse that is sent to be burnt in the boiler (Eq. (4)). The other decision variable (named "Splitter2") is the fraction of the bagasse surplus that is sent to pretreatment and subsequent steps (Eq. (5)). Table 7 presents the configuration for the decision variables for Cases 2, 3 and 4. The decision variables for Cases 2–4 were obtained by the search performed by PSO algorithm. Cases 3 and 4 show that, when second generation fuel production is considered, a great amount of bagasse still needs to be burnt, in order to provide the steam and electric power to support the energetic demand of the process.

$$Splitter1 = \frac{bagasse\_to\_boiler}{total\_bagasse\_flow} \quad (4)$$

$$Splitter2 = \frac{bagasse\_to\_second\_generation}{bagasse\_surplus} \quad (5)$$

Bagasse partition and objective function values for all PSO particles were stored in order to allow the construction of contour plots of the objective functions for Cases 3 and 4. In order to facilitate the comparison among cases, normalized objective function values were calculated: $(\Phi - \Phi_{min})/(\Phi_{max} - \Phi_{min})$. Figs. 5 and 6 present the contour plot of the dimensionless objective function for Cases 3 and 4 respectively. The white region in the left of the diagram in Fig. 6 is an infeasible region, where the burn of bagasse and lignin in the boiler does not provide the necessary steam to meet the thermal demand of the industrial plant. The slope of the curve that separates the feasible region from the infeasible one (Fig. 6), leads to the conclusion that the burning of the lignin is not enough to supply the energy demand for the second generation ethanol production. The slope is less visible in Case 3 (without C5 fermentation,

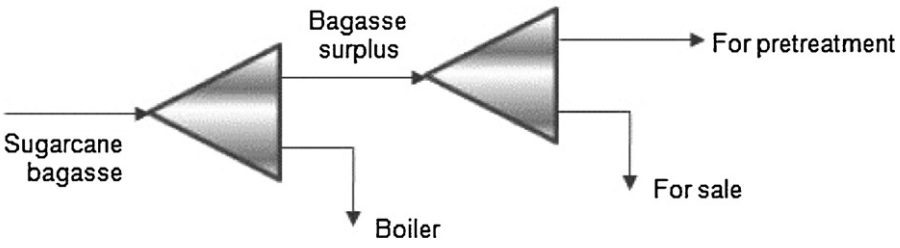

Fig. 4. Bagasse partition in the biorefinery.

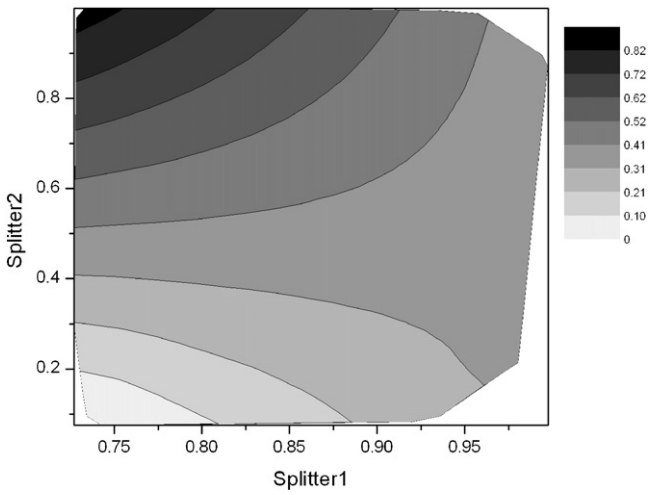

Fig. 5. Contour plot for Case 3.

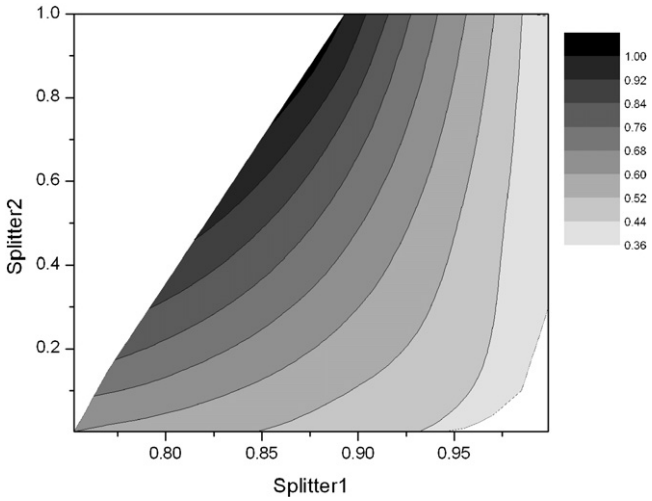

Fig. 6. Contour plot for Case 4.

Fig. 5), which suggests that the step of concentration of pentoses has great impact on the thermal demand of the biorefinery.

The behavior mentioned in the previous paragraph is confirmed by the comparison of thermal demands of Cases 3 and 4 with the standard case (Case 1), presented in Table 8, and the steam demand of each section of the biorefinery, presented in Table 9.

Table 8
Process thermal demand and surplus electric power for Cases 2–4 – comparison to Case 1 (base case).

Case study	Extra thermal demand	Electric power surplus
Case 2	0.0%	−42.1%
Case 3	+25.2%	−65.4%
Case 4	+33.7%	−31.0%

Table 9
Partition of steam demand among process sectors for each case study.

Case	Evaporation train (broth)	Distillation	Evaporation (C5 hydrolysate)
Case 1	52.0%	48.0%	0.0%
Case 2	52.0%	48.0%	0.0%
Case 3	43.6%	56.4%	0.0%
Case 4	39.8%	41.2%	19.0%

Table 10
Percentage of electric power production among turbines for Cases 1–4.

Case	High pressure	Medium pressure	Condensing
Case 1	41.6%	53.8%	4.6%
Case 2	43.3%	56.7%	0.0%
Case 3	43.7%	56.3%	0.0%
Case 4	43.7%	56.3%	0.0%

Steam demand is greatly increased by the inclusion of second generation ethanol production. Case 3 leads to an increase in steam demand of 25.2%, but has a great impact in electric surplus (−65.4%), due to a large amount of bagasse that is diverted from burning. It is interesting to note that when both C5 and C6 are used for ethanol production (Case 4) the steam demand is even greater than that of Case 3 (33.7%), mainly due to C5 concentration step, which is responsible for 19.0% of the total thermal demand in this case. This elevated steam demand of Case 4 leads to a larger amount of bagasse diverted to the cogeneration production system, which consequently causes higher fluxes of high pressure steam through the turbines. In this way the decrease of electric power production is not so pronounced in Case 4 as it is in Case 3.

The percentage of electric power generated in each turbine can be viewed in Table 10. While the condensing turbine does not provide a significant amount of electric power, it is important to the process by decoupling the electric power production from the thermal demand of the biorefinery, allowing the plant to be operated as a thermoelectric one, as in Case 1. Except for Case 1, the condensing turbine does not operate because the amount of bagasse burnt is only the necessary to support the energy demand of the plant, which is accounted for by the steam that leaves the medium pressure turbine.

5. Conclusions

In this work, first and second generation bioethanol production from sugarcane is modeled in an equation-oriented simulator and the process simulator is linked to a global optimization algorithm. Four case studies were considered and the results demonstrated the important role of precise partition of bagasse for the process energetic self-sufficiency. Sugarcane bagasse is already used mainly for supplying electric and thermal energy to the process itself. The production of second generation ethanol increases thermal demands in at least 25%, which narrows the decision feasible range on how much bagasse can be diverted to production of second generation fuel. Furthermore, electric power surplus is diminished in at least 31%, which may have a great impact on process economics, since it is sold as part of industry products portfolio.

Thus, coupling of a process simulator to a global optimization algorithm demonstrated to be a powerful tool to assess process demands and feasibility, which is essential for guiding decisions and further research efforts in order to make biomass exploitation for fuel production commercially viable.

Acknowledgments

The authors would like to thank to the São Paulo State Research Funding Agency (Fundação de Amparo à Pesquisa do Estado de São Paulo, FAPESP) and Brazilian National Council for Scientific and Technological Development (Conselho Nacional de Desenvolvimento Científico e Tecnológico, CNPq) for the financial support.

Appendix 1.

In this section it is presented the stoichiometric and mass balance equations for the main biochemical steps used in the simulations and optimizations.

Fermenter

Stoichiometry

Sucrose to glucose:

$$C_{12}H_{22}O_{11} + H_2O \rightarrow 2C_6H_{12}O_6 \quad (a1)$$

Glucose to ethanol:

$$C_6H_{12}O_6 \rightarrow 2C_2H_6O + 2CO_2 \quad (a2)$$

Glucose to glycerol:

$$C_6H_{12}O_6 + 4H^+ + 4e^- \rightarrow 2C_3H_8O_3 \quad (a3)$$

Glucose to succinic acid:

$$C_6H_{12}O_6 + 2H_2O \rightarrow 2C_4H_6O_4 + 2CO_2 + 10H^+ + 10e^- \quad (a4)$$

Glucose to acetic acid:

$$C_6H_{12}O_6 + 2H_2O \rightarrow 2C_2H_4O_2 + CO_2 + 8H^+ + 8e^- \quad (a5)$$

Yeast growth:

$$0.1485C_6H_{12}O_6 + 0.145NH_4^+ + 0.1087CO_2 \rightarrow CH_{1.8}O_{0.9} + 0.2087H_2O + 0.145H^+ \quad (a6)$$

Mass balances

$$F_{out} \times z_{out}^{sucrose} = F_{in} \times z_{in}^{sucrose} \times (1 - yield_{a1}) \quad (a7)$$

$$Glucose = F_{in} \times \left[z_{in}^{glucose} + z_{in}^{sucrose} \times yield_{a1} \times \frac{2 \times M_{glucose}}{M_{sucrose}} \right] \quad (a8)$$

$$F_{out} \times z_{out}^{glucose} = Glucose \times (1 - yield_{a2-a6}) \quad (a9)$$

$$F_{out} \times z_{out}^{ethanol} = F_{in} \times z_{in}^{ethanol} + Glucose \times yield_{a2} \times \frac{2 \times M_{ethanol}}{M_{glucose}} \quad (a10)$$

$$F_{out} \times z_{out}^{glycerol} = F_{in} \times z_{in}^{glycerol} + Glucose \times yield_{a3} \times \frac{2 \times M_{glycerol}}{M_{glucose}} \quad (a11)$$

$$F_{out} \times z_{out}^{succinic} = F_{in} \times z_{in}^{succinic} + Glucose \times yield_{a4} \times \frac{2 \times M_{succinic}}{M_{glucose}} \quad (a12)$$

$$F_{out} \times z_{out}^{acetic} = F_{in} \times z_{in}^{acetic} + Glucose \times yield_{a5} \times \frac{2 \times M_{acetic}}{M_{glucose}} \quad (a13)$$

$$F_{out} \times z_{out}^{yeast} = F_{in} \times z_{in}^{yeast} + Glucose \times yield_{a6} \times \frac{M_{yeast}}{0.1485 \times M_{glucose}} \quad (a14)$$

$$F_{out} \times z_{out}^{water} = F_{in} \times z_{in}^{water} + Glucose \times (0.2087 \times yield_{a6} - yield_{a1} - 2 \times yield_{a4} - 2 \times yield_{a5}) \times \frac{M_{water}}{M_{glucose}} \quad (a15)$$

$$F_{out} \times z_{out}^{CO2} = F_{in} \times z_{in}^{CO2} + Glucose \times (2 \times yield_{a2} + 2 \times yield_{a4} + yield_{a5} - 0.1087 \times yield_{a6}) \times \frac{M_{CO2}}{M_{glucose}} \quad (a16)$$

C5 hydrolysis

Stoichiometry

Hemicellulose to xylose (neglecting ramifications and terminations):

$$[C_5H_8O_4]_n + nH_2O \rightarrow nC_5H_{10}O_5 \quad (a17)$$

Mass balances

$$F_{out} \times z_{out}^{hemicellulose} = F_{in} \times z_{in}^{hemicellulose} \times (1 - yield_{a17}) \quad (a18)$$

$$F_{out} \times z_{out}^{xylose} = F_{in} \times \left[z_{in}^{xylose} + z_{in}^{hemicellulose} \times (1 - yield_{a17}) \times \frac{M_{xylose}}{M_{hemicellulose}} \right] \quad (a19)$$

$$F_{out} \times z_{out}^{water} = F_{in} \times \left[z_{in}^{water} + z_{in}^{hemicellulose} \times yield_{a17} \times \frac{M_{water}}{M_{hemicellulose}} \right] \quad (a20)$$

C6 hydrolysis

Stoichiometry

Cellulose to glucose:

$$C_6H_{10}O_5 + H_2O \rightarrow C_6H_{12}O_6 \quad (a21)$$

$$F_{out} \times z_{out}^{cellulose} = F_{in} \times z_{in}^{cellulose} \times (1 - yield_{a21}) \quad (a22)$$

$$F_{out} \times z_{out}^{glucose} = F_{in} \times \left[z_{in}^{glucose} + z_{in}^{cellulose} \times (1 - yield_{a21}) \times \frac{M_{glucose}}{M_{cellulose}} \right] \quad (a23)$$

$$F_{out} \times z_{out}^{water} = F_{in} \times \left[z_{in}^{water} + z_{in}^{cellulose} \times yield_{a21} \times \frac{M_{water}}{M_{cellulose}} \right] \quad (a24)$$

References

Alvarado-Morales, M., Hamid, M. K. A., Sin, G., Gernaey, K. V., Woodley, J. M., & Gani, R. (2010). A model-based methodology for simultaneous design and control of a bioethanol production process. *Computers and Chemical Engineering*, *34*, 2043–2061.

Arifeen, N., Kookos, I. K., Wang, R., Koutinas, A. A., & Webb, C. (2009). Development of novel wheat biorefining: Effect of gluten extraction from wheat on bioethanol production. *Biochemical Engineering Journal*, *43*, 113–121.

Arifeen, N., Wang, R., Kookos, I., Webb, C., & Koutinas, A. A. (2007). Optimization and cost estimation of novel wheat biorefining for continuous production of fermentation feedstock. *Biotechnology Progress*, *23*, 872–880.

Arifeen, N., Wang, R., Kookos, I. K., Webb, C., & Koutinas, A. A. (2007). Process design and optimization of novel wheat-based continuous bioethanol production system. *Biotechnology Progress*, *23*, 1394–1403.

Biegler, L. T., Grossmann, I. E., & Westerberg, A. W. (1997). *Systematic methods of chemical process design*. Prentice Hall.

Cherubini, F., & Stromman, A. H. (2010). Production of biofuels and biochemicals from lignocellulosic biomass: Estimation of maximum theoretical yields and efficiencies using matrix algebra. *Energy & Fuels*, *24*, 2657–2666.

Demirbas, M. F. (2009). Biorefineries for biofuel upgrading: A critical review. *Applied Energy*, *86*, S151–S161.

Dias, M. O. S., Junqueira, T. L., Cavalett, O., Cunha, M. P., Jesus, C. D. F., Rossell, C. E. V., et al. (2012). Integrated versus stand-alone second generation ethanol production from sugarcane bagasse and trash. *Bioresource Technology*, *103*, 152–161.

Dias, M. O. S., Cunha, M. P., Jesus, C. D. F., Rocha, G. J. M., Pradella, J. G. C., Rossell, C. E. V., et al. (2011). Second generation ethanol in Brazil: Can it compete with electricity production? *Bioresource Technology*, *102*, 8964–8971.

Dias, M. O. S., Cunha, M. P., Jesus, C. D. F., Scandiffio, M. I. G., Rossell, C. E. V., Maciel Filho, R., et al. (2010). Simulation of ethanol production from sugarcane in Brazil: Economic study of an autonomous distillery. *Computer Aided Chemical Engineering*, *28*, 733–738.

Dias, M. O. S., Ensinas, A. V., Nebra, S. A., Maciel, R., Rossell, C. E. V., & Maciel, M. R. W. (2009). Production of bioethanol and other bio-based materials from sugarcane bagasse: Integration to conventional bioethanol production process. *Chemical Engineering Research & Design*, *87*, 1206–1216.

FitzPatrick, M., Champagne, P., Cunningham, M. F., & Whitney, R. A. (2010). A biorefinery processing perspective: Treatment of lignocellulosic materials for the production of value-added products. *Bioresource Technology*, *101*, 8915–8922.

Grisi, E. F., Yusta, J. M., & Khodr, H. M. (2011). A short-term scheduling for the optimal operation of biorefineries. *Energy Conversion and Management*, *52*, 447–456.

Hahn-Hagerdal, B., Galbe, M., Gorwa-Grauslund, M. F., Liden, G., & Zacchi, G. (2006). Bio-ethanol – The fuel of tomorrow from the residues of today. *Trends in Biotechnology*, *24*, 549–556.

Huang, H. J., Lin, W. L., Ramaswamy, S., & Tschirner, U. (2009). Process modeling of comprehensive integrated forest biorefinery – An integrated approach. *Applied Biochemistry and Biotechnology*, *154*, 205–216.

Kamm, B., & Kamm, M. (2007). Biorefineries – Multi product processes. *White Biotechnology*, *105*, 175–204.

Kennedy, J., & Eberhart, R. C. (1995). Particle Swarm Optimization. In *IEE international conference on neural networks (ICNN)* (pp. 1942–1948).

Lyko, H., Deerberg, G., & Weidner, E. (2009). Coupled production in biorefineries – Combined use of biomass as a source of energy, fuels and materials. *Journal of Biotechnology*, *142*, 78–86.

Lynd, L. R., Wyman, C. E., & Gerngross, T. U. (1999). Biocommodity engineering. *Biotechnology Progress*, *15*, 777–793.

Manninen, K. (2010). *Effect of forest-based biofuels production on carbon footprint, case: Integrated LWC paper mill*. Master Thesis, Lappeenranta University of Technology.

Mariano, A. P., Costa, C. B. B., Vasco de Toledo, E. C., Melo, D. N. C., & Maciel Filho, R. (2011). Analysis of the particle swarm algorithm in the optimization of a three-phase slurry catalytic reactor. *Computers and Chemical Engineering*, *35*, 2741–2749.

Morales-Rodriguez, R., Mayer, A. S., Gernaey, K. V., & Sin, G. (2011). Dynamic model-based evaluation of process configurations for integrated operation of hydrolysis and co-fermentation for bioethanol production from ligoncellulose. *Bioresource technology*, *102*, 1174–1184.

Ng, D. K. S. (2010). Automated targeting for the synthesis of an integrated biorefinery. *Chemical Engineering Journal*, *162*, 67–74.

Ojeda, K., Avila, O., Suarez, J., & Kafarov, V. (2011). Evaluation of technological alternatives for process integration of sugarcane bagasse for sustainable biofuels production – Part 1. *Chemical Engineering Research & Design*, *89*, 270–279.

Rodrigues, R., Soares, R. P., & Secchi, A. R. (2010). Teaching chemical reaction engineering using EMSO simulator. *Computer Applications in Engineering Education*, *18*, 607–618.

Sadhukhan, J., Mustafa, M. A., Misailidis, N., Mateos-Salvador, F., Du, C., & Campbell, G. M. (2008). Value analysis tool for feasibility studies of biorefineries integrated with value added production. *Chemical Engineering Science*, *63*, 503–519.

Shi, Y., & Eberhart, R. (1998). A modified particle swarm optimizer. In *IEEE World Congress on Computational Intelligence (WCCI)* (pp. 69–73).

Soares, R. P., & Secchi, A. R. (2003). EMSO: A new environment for modelling, simulation and optimisation. *Computer Aided Chemical Engineering*, *14*, 947–952.

Wolf, L. D. (2011). *Organosolv pretreatment of sugarcane bagasse for the production of ethanol and xylo-oligomers*. Master Thesis, Federal University of São Carlos (in Portuguese).